Chapter 13: Sea Level Change

Coordinating Lead Authors: John A. Church (Australia), Peter U. Clark (USA)

Lead Authors: Anny Cazenave (France), Jonathan Gregory (UK), Svetlana Jevrejeva (UK), Anders Levermann (Germany), Mark Merrifield (USA), Glenn Milne (Canada), R. Steven Nerem (USA), Patrick Nunn (Australia), Antony Payne (UK), W. Tad Pfeffer (USA), Detlef Stammer (Germany), Alakkat Unnikrishnan (India)

Contributing Authors: David Bahr (USA), Jason E. Box (USA), David H. Bromwich (USA), Mark Carson (Germany), William Collins (UK), Xavier Fettweis (Belgium), Piers Forster (UK), Alex Gardner (USA), Peter Good (UK), Rune Grand Graversen (Sweden), Ralf Greve (Japan), Stephen Griffies (USA), Edward Hanna (UK), Mark Hemer (Australia), Regine Hock (USA), Simon J. Holgate (UK), John Hunter (Australia), Philippe Huybrechts (Belgium), Gregory Johnson (USA), Ian Joughin (USA), Georg Kaser (Austria), Caroline Katsman (Netherlands), Leonard Konikow (USA), Gerhard Krinner (France), Jan Lanaerts (Netherlands), Ben Marzeion (Austria), Kathleen L. McInnes (Australia), Sebastian Mernild (USA), Didier Monselesan (Australia), Ruth Mottram (Denmark), Tavi Murray (UK), Gunnar Myhre (Norway), J.P. Nicholas (USA), David Pollard (USA),Valentina Radić (Canada), Jamie Rae (UK), Christian Schoof (Canada), Aimée Slangen (Netherlands), Jan H. van Angelen (Netherlands), Willem Jan van de Berg (Netherlands), Michiel van den Broeke (Netherlands), Miren Vizcaíno (Netherlands), Yoshihide Wada (Netherlands), Jianjun Yin (USA), Masakazu Yoshimori (Japan)

Review Editors: Jean Jouzel (France), Roderik van de Wal (Netherlands), Philip L. Woodworth (UK), Cunde Xiao (China)

Date of Draft: 5 October 2012

Notes: TSU Compiled Version

Table of Contents

Executive Summary **3**
13.1 Components and Models of Sea Level Change **6**
13.1.1 Introduction and Chapter Overview *6*
13.1.2 Fundamental Definitions and Concepts *7*
13.1.3 Sea Level Change Caused by Contemporary Climate Change *8*
13.1.4 Sea Level Change Not Caused by Contemporary Climate Change *9*
13.1.5 Models Used to Interpret Past and Project Future Changes in Sea Level *9*
13.2 Past Sea Level Change **12**
13.2.1 The Geological Record *12*
13.2.2 The Instrumental Record (~1700–2010) *13*
FAQ 13.1: Why Does Local Sea Level Change Differ from the Global Average? **14**
13.3 Contributions to Global Mean Sea Level Rise During the Instrumental Period **16**
13.3.1 Thermosteric Contribution *16*
13.3.2 Glaciers *17*
13.3.3 Greenland and Antarctic Ice Sheets *17*
13.3.4 Contributions from Water Storage on Land *21*
13.3.5 Ocean Mass Observations from GRACE (2002–2010) *22*
13.3.6 Budget of GMSL Rise *23*
Box 13.1: The Global Energy Budget **24**
13.4 Projected Contributions to Global Mean Sea Level **26**
13.4.1 Ocean Heat Uptake and Thermosteric Sea Level Rise *26*
13.4.2 Glaciers *27*
13.4.3 Greenland Ice Sheet *29*
13.4.4 Antarctic Ice Sheet *35*

Box 13.2: History of the Marine Ice Sheet Instability Hypothesis 41
FAQ 13.2: Will the Greenland and Antarctic Ice Sheets Contribute to Sea Level Change Over the Rest of the Century? 42
13.4.5 Anthropogenic Intervention in Water Storage on Land 44
13.5 Projections of Global Mean Sea Level Rise 44
13.5.1 Projections for the 21st Century 45
13.5.2 Projections Beyond the 21st Century 51
13.6 Regional Sea Level Changes 54
13.6.1 Regional Sea Level Changes, Climate Modes and Forced Sea Level Response 55
13.6.2 CMIP5 GCM Projections/Predictions on Decadal to Centennial Time Scales 55
13.6.3 Response to Atmospheric Pressure Changes 56
13.6.4 Response to Freshwater Forcing 57
13.6.5 Net Regional Sea Level Changes 58
13.6.6 Uncertainties and Sensitivity to Ocean/Climate Model Formulations and Parameterizations 59
13.6.7 Summary Assessment 60
13.7 21st Century Projections of Sea Level Extremes and Waves 60
13.7.1 Changes in Sea Level Extremes 61
13.7.2 Projections of Extreme Sea Levels 61
13.7.3 Projections of Ocean Waves 62
13.7.4 Summary Assessment 64
13.8 Synthesis and Key Uncertainties 64
References 66
Appendix 13.A: Methods of Sea Level Projections for the 21st Century 83
Figures 85

Executive Summary

Changes in sea level represent an integration of many aspects of climate change, and thus occur over a broad range of temporal and spatial scales. The primary contributors to global averaged sea level change are the expansion/contraction of the ocean as it warms/cools and the transfer of water to/from the ocean/land, particularly from glaciers and ice sheets. The amount of sea level change at any given location depends on global aspects of the climate system as well as on regional and local phenomena. As a result, regional sea level change may differ from the global average. We consider sea level measured with respect to the surface of the solid Earth which itself may be moving (relative sea level), and also sea level relative to the Earth's centre of mass (geocentric sea level). We also consider changes in extreme sea level events and surface waves as these may also impact coastal and island communities and ecosystems.

Sea Level Observations

Paleo sea level records from warm periods during the last 3 million years provide *medium-to-high confidence* that global mean sea level was more than 6 m higher than present when global temperature was 2°C–3°C warmer than present. During the Last Interglacial Period, for the time interval in which global mean sea level was above present, the maximum 1000-year average rate of global mean sea level rise *very likely* exceeded 2.0 m kyr^{-1}, *likely* exceeded 4.1 m kyr^{-1}, and was *unlikely* to have exceeded 5.8 m kyr^{-1}. Faster rates lasting less than a millennium cannot be ruled out. Because these periods give only a limited analogy for future anthropogenic climate change, we do not consider that they provide upper bounds for global mean sea level rise during the 21st century. [Chapter 5, 13.2.1, Figure 13.3]

It is *very likely* that the rate of global mean sea level rise has increased during the last two centuries. Paleo sea level data from many locations around the globe indicate low rates of sea level change during the late Holocene (order tenths of mm yr^{-1}) and modern rates (order mm yr^{-1}) during the 20th century. It is *very likely* that global mean sea level has risen ~1.7 [1.5 to 1.9] mm yr^{-1} during the 20th century, and between 2.8 and 3.6 mm yr^{-1} since 1993. It is *likely* that global mean sea level has accelerated since the early 1900s, with estimates ranging from 0.000 to 0.013 [–0.002 to 0.019] mm yr^{-2}. [Chapter 3, Chapter 5, 13.2.1–2, Figure 13.3].

Understanding of Sea Level Change

Since the early 1970s, ocean warming and expansion and glacier melting have been the dominant contributors to global mean sea level rise, together explaining about 80% of the observed rise. Both the Greenland and Antarctic ice sheets have made only small contributions to global mean sea level since the early 1970s. However, their rate of contribution has increased since the early 1990s, partly due to increased outflow caused by warming of the immediately adjacent ocean, and has been of a similar magnitude to thermosteric and glacier contributions since 2005. Reservoir impoundment exceeded groundwater depletion for the majority of the 20th century but the rate of groundwater depletion has increased and now exceeds the rate of impoundment. The closure of the observational budget for recent periods within uncertainties represents an advance since the AR4 in physical understanding of the causes of past global mean sea level change, and provides an improved basis for critical evaluation of models used for projecting sea level change. [Chapter 3; Chapter 4; 13.3.6; Figures 13.4 and 13.5; Table 13.1]

AOGCM-based estimates of the thermal expansion and glacier contributions, and the estimated change in land water storage, which is relatively small, together account for about 70% of the observed rate of Global Mean Sea Level rise for 1901–1990, and over 80% for 1971–2010 and 1993–2010. The difference between the observed rate of global mean sea level and the sum of the modelled terms and the contribution from land water storage prior to 1970 is consistent with zero, but is potentially explained by long-term contributions from ice sheets, the possible underestimate in modelled thermal expansion from not including preindustrial volcanic forcing, or greater mass loss from glaciers during the 1930s due to unforced climate variability. Model-based estimates of ocean thermal expansion and glacier contributions increase from 1990, in agreement with the global mean sea level record. Increasing ocean thermal expansion and glacier loss are the largest contributions but loss of mass by the ice sheets, not included in the models, also contributes to the observed increase in rate. This simulation of past global mean sea level rise is a further scientific advance relative to the AR4, and is a reason for increased confidence in

using these same process-based models and methods for projections. The evidence now available gives a clearer account than in previous IPCC assessments of 20th century sea level change. Progress in ice sheet modelling since the AR4 has enabled an assessment to be made of the contribution to sea level rise from ice sheet dynamics. [Chapter 3; Chapter 4; 13.3.6; Figures 13.4 and 13.5; Table 13.1]

The Earth's Energy Budget

The largest increase in the storage of heat in the climate system over recent decades has been in the oceans, and thus sea level rise from ocean warming is a central part of the Earth's response to increasing greenhouse gas concentrations. Independent estimates of radiative forcing of the Earth by greenhouse gases, volcanic and anthropogenic aerosols, the observed heat storage and surface warming combine to give an energy budget for the Earth that is *very likely* closed, and is consistent with our best estimate of climate sensitivity. [Box 13.1]

Global Mean Sea Level Rise Projections

It is *very likely* that the rate of global mean sea level rise during the 21st century will exceed the rate observed during 1971–2010 for all RCP scenarios. For the period 2081 to 2100, compared to 1986 to 2005, global mean sea level rise is *likely* to be in the range 0.29–0.55 m for RCP2.6, 0.36–0.63 m for RCP4.5, 0.37–0.64 m for RCP6.0, and 0.48–0.82 m (0.56–0.96 m by 2100 with a rate of rise 8–15 mm yr^{-1} over the last decade of the 21st century) for RCP8.5. Unlike in the AR4, these projections include a contribution from changes in ice-sheet outflow, for which the central projection is 0.11 m. There is only *medium confidence* in these ranges of projected global mean sea level rise, because there is only *medium confidence* in the likely range of projected contributions from models of ice sheet dynamics, and because there is no consensus about the reliability of semi-empirical models, which give higher projections than process-based models. Larger values cannot be excluded, but current scientific understanding is insufficient for evaluating their probability. [13.5.1, Table 13.5, Figures 13.8 and 13.9]

Global mean sea level rise will *very likely* continue beyond 2100, with ocean thermosteric sea level rise to continue for centuries to millennia, unless global temperatures decline. Longer-term sea level rise depends on future emissions. The amount of ocean thermal expansion increases with global warming (0.2–0.6 $m°C^{-1}$) but the glacier contribution decreases over time as their volume (currently ~0.6 m sea level equivalent) decreases. Currently available information indicates that the dynamical contribution of the ice sheets will continue beyond 2100, but confidence in projections is low. The few available model results indicate global mean sea level rise by 2300 is *likely* to be less than 1 m for greenhouse gas concentrations below 500 ppm CO_2-equivalent scenario but rise as much as 1–3 m for concentrations above 700 ppm CO_2-equivalent. [13.5.2, Figures 13.10 and 13.11]

With its present topography, surface melting of the Greenland ice sheet is projected to exceed accumulation for global mean surface air temperature over 3.1 [1.9–4.6]°C above preindustrial, leading to ongoing decay of the ice sheet. The reduction in surface elevation as ice is lost increases the vulnerability of the ice sheet; taking this into account, one study estimated a lower threshold of 1.6 [0.8–3.2]°C. The loss of the ice sheet is not inevitable because surface melting has long time scales and it might re-grow to its original volume or some fraction thereof if global temperatures decline. However, a significant decay of the ice sheet may be irreversible on millennial time scales. In the 21st century surface melting is projected to remain small on the Antarctic ice sheet, while we have *medium confidence* that snowfall will increase. On longer timescales and with higher greenhouse gas scenarios, the increase in surface melting could exceed the increase in accumulation. [13.3.3, 13.4.3, 13.4.4,Figure 13.11]

Regional Sea Level Change Projections

It is *very likely* (*high confidence*) that in the 21st century and beyond sea level change will have a strong regional pattern, with many places experiencing significant deviations of local and regional sea level change from the global mean change. This regional sea level change will result from a combination of dynamical ocean change, mass changes of the ocean from contributions from glaciers and ice sheets, including the regional patterns from both contemporary and past changes in land ice, and regional changes in atmospheric pressure. Over decadal periods, the rates of regional sea level change as a result of climate

variability can differ from the global average rate by more than 100% of the global average rate. By the end of the 21st century, it is *very likely* (*high confidence*) that over about 95% of the ocean will experience regional sea level rise, but less than about 5%, mostly high latitude regions near current and former ice sheets and melting glaciers, will experience a sea level fall. About 75% and 80% of the global coastlines are projected to experience a sea level change within 20% of the global mean sea level change, for RCP4.5 and 8.5, respectively. In both cases the maximum of the probability density function is larger than the global mean sea level, however, the arithmetic mean is lower than the global mean (0.3 m versus 0.37 m for RCP4.5; 0.56 m versus 0.68 m for RCP8.5, respectively). [Section 13.6.5, Figures 13.15–13.17].

Projections of Extreme Events and Surface Waves

It is *very likely* that there will be an increase in the occurrence of future extreme sea level and flooding events. The combined effects of mean sea level rise and changes in storminess will determine future extremes. There is *high confidence* that extremes will increase with global mean sea level rise, however, there is *low confidence* in region-specific projections in storminess and storm surges. The impact on the return period for exceeding given threshold levels is *likely* to be high, for example with current 100-year return period events decreasing to 10-year and possibly 1-year events by the end of the 21st century. [13.7.2, Figure 13.19]

Wave projections are presented with *low confidence*. This reflects the challenge of down-scaling future wind states from coarse resolution climate models into regional and global wave model projections. The regions with the largest projected changes in surface wave height are the Southern Ocean, associated with the projected strengthening of the westerlies, and the tropical South Pacific, associated with a projected strengthening of austral winter easterly trade winds. A consistent mean decrease in surface wave height is projected for all other ocean basins. [13.7.3; Figure 13.20].

13.1 Components and Models of Sea Level Change

13.1.1 Introduction and Chapter Overview

Changes in sea level occur over a broad range of temporal and spatial scales, with the many factors contributing make it an integral measure of climate change (Church et al., 2010; Milne et al., 2009). The primary contributors to contemporary sea level change are the expansion of the ocean as it warms and the transfer of water currently stored on land, particularly from glaciers and ice sheets (Church et al., 2011b). Observations (Chapter 3) indicate the largest increase in the storage of heat in the climate system over recent decades has been in the oceans and thus sea level rise from ocean warming is a central part of the Earth's response to increasing greenhouse gas concentrations.

The First IPCC Assessment (Warrick and Oerlemans, 1990) laid the groundwork for much of our current understanding of sea level change. This included the recognition that sea level had risen during the 20th century, that the rate of rise had increased compared to the 19th century, that ocean-thermal expansion and the mass loss from glaciers were likely the main contributors to the 20th century rise, that during the 21st century the rate of rise was projected to be faster than during the 20th century, and that sea level would continue to rise well after greenhouse gas emissions were reduced. They also concluded that no major dynamic response of the ice sheets was expected during the 21st century, leaving ocean-thermal expansion and the melting of glaciers as the most likely main contributors to the 21st century rise. The Second Assessment Report (Warrick et al., 1996) came to very similar conclusions.

By the time of the Third Assessment Report (Church et al., 2001) , coupled atmosphere-ocean general circulation models (AOGCMs) and ice sheet models largely replaced energy-balance climate models as the primary techniques supporting the interpretation of observations and the projections of sea level. This approach allowed consideration of the regional distribution of sea level change in addition to the global averaged change. By the time of the Fourth Assessment Report (AR4; Solomon et al., 2007), there were more robust observations of the variations in the rate of global average sea level rise for the 20th century (rather than just mean trends over the 20th century), some understanding of the variability in the rate of rise, and the satellite altimeter record was long enough to reveal the complexity of the time-variable spatial distribution of sea level. Nevertheless, three central issues remained. First, the observed sea level rise over decades was larger than the sum of the individual contributions estimated from observations or with models (Rahmstorf et al., 2007; submitted), although in general the uncertainties were large enough that there was no significant contradiction. Second, it was not possible to make confident projections of the regional distribution of sea level rise. Third, there was insufficient understanding of the potential contributions from the ice sheets. In particular, the AR4 recognised that existing ice sheet models were unable to represent the recent observations of ice sheet accelerations and that understanding of ice sheet dynamics was too limited to assess the likelihood of continued acceleration or to provide a best estimate or an upper bound for their future contributions.

Despite changes in the scenarios between the four Assessments, the projections for 2100 (compared to 1990) for the full range of scenarios were remarkably similar, with the reduction in the upper end in more recent reports likely reflecting the smaller increase in radiative forcing in recent scenarios due to smaller GHG emissions and the inclusion of aerosols: 15 to 110 cm in the FAR, 13 to 94 cm in the SAR, 9 to 88 cm in the TAR, and 18 to about 80 cm or more in AR4 (when extended to 2100 and when including an allowance for a dynamic ice sheet response).

Results since the AR4 show that for recent decades, sea level has continued to rise (Chapter 3). Improved and new observations of the ocean (Chapter 3) and the cryosphere (Chapter 4) and their representation in models have resulted in better understanding of 20th century sea level rise and its components (this chapter). Paleo records of past sea level changes constrain glacier and ice sheet response to warmer climates as well as extend the observational record to provide a longer context for current sea level rise (Chapter 5).

This chapter provides a synthesis of past and contemporary sea level change at global and regional scales. Drawing on the published refereed literature, including as summarised in earlier chapters of this Assessment, we explain the reasons for contemporary change, and assess and provide projections of sea level change for the 21st century and beyond. We emphasize that the amount of sea level change at any given location

depends not only on global aspects of the climate system but also on regional and local phenomena that may strongly modulate the global rise (Milne et al., 2009). We discuss the primary factors that cause regional sea level to differ from the global average and how these may change in the future. In addition, we address projected changes in surface waves and the consequences of sea level and climate change for extreme sea level events.

In the remainder of Section 13.1, we introduce the major causes of sea level change and summarize the models used to understand and project sea level change (both those associated with anthropogenic climate change and those that are not). Building on Chapters 3 (Oceans) and 5 (Paleoclimate), the record of past sea level changes is summarised in Section 13.2. Section 13.3 discusses our understanding of the causes of sea level change over recent decades. This understanding underpins projections of global averaged sea level change. In Section 13.4, we assess an ensemble of climate, ice sheet and glacier model contributions, including the dynamic response of the ice sheets, and bring these together to assess sea level change for the 21st century and beyond in Section 13.5. Section 13.5 also assesses semi-empirical models developed using historical data to provide an additional approach for projecting 21st century sea level change. Section 13.5 also discusses the potential for crossing critical thresholds that could result in large, sustained responses and essentially irreversible commitments.

In Section 13.6, we assess all aspects of regional sea level change that are a result of both past and future climate change. However, we do not address several aspects of local relative sea level change that are not climate related but which may be important for assessing its impacts. For example, we do not consider local relative sea level rise resulting from vertical land motion associated with the compaction of soil or the withdrawal of water or petroleum products.

Extreme sea level events at the coast occur as a result of natural variability in climate, oceans, storm surges and waves. We assess projections of these extreme events for a number of regions based on the current literature (Section 13.7). Our observations and understanding of sea level change remain incomplete and we synthesize current understanding and identify key uncertainties throughout the chapter and in Section 13.8.

13.1.2 Fundamental Definitions and Concepts

The height of the ocean surface at any given location, or sea level, is measured either with respect to the surface of the solid Earth (relative sea level) or a geocentric reference such as the reference ellipsoid (geocentric sea level). The former is the more relevant quantity when considering the coastal impacts of sea level change. Relative sea level has been measured using tide gauges during the past few centuries (Section 13.2.2 and Chapter 3) and estimated for longer time spans from geological records (Section 13.2.1 and Chapter 5). Geocentric sea level has been measured over the past two decades using satellite altimetry (Section 13.2.2 and Chapter 3).

The temporal average, known as Mean Sea Level (MSL; see Glossary), is used to remove the effects of tides, storms and waves. Apart from Section 13.7, which considers high frequency changes in ocean surface height, the use of 'sea level' elsewhere in this chapter refers to MSL. It is common to average MSL spatially to define Global Mean Sea Level (GMSL; see Glossary). Integrated over the ocean, relative sea level change (or GMSL) gives the change in ocean water volume, which is directly related to the processes that dominate climate-driven sea level change (ocean warming and land ice melting). In contrast, integrating geocentric sea level change over ocean area does not result in ocean volume change due to changes in ocean basin volume caused, largely, by the on-going deformation of the Earth to the most recent global deglaciation (Mitrovica and Peltier, 1991). A small correction (–0.15 to –0.5 mm yr^{-1}) is required to estimate ocean volume change (Tamisiea, 2011). Note that local relative sea level change differs, in general, from the globally integrated value because of spatial variability in both the sea surface and ocean floor height change (see FAQ 13.1).

Any process that causes vertical motion of the ocean surface or ocean floor will result in relative sea level change. Height changes of the ocean surface can be affected by flow within the atmosphere and oceans, changes in ocean volume, and changes in the Earth's gravity field. The latter is influenced by tides, changes in Earth rotation, and mass redistribution that can occur within or between the various components of the Earth System (e.g., solid Earth, atmosphere, hydrosphere, cryosphere). Height changes of the ocean floor are driven by tectonics, isostatic deformation of the solid Earth, erosion/deposition, sediment compaction, body

tides, and changes in Earth rotation. Note that height changes of the ocean surface and ocean floor are not independent. For example, changes in ocean-floor height can lead to changes in ocean-surface height through perturbations to the gravity field and the volume of the ocean basins. Conversely, height changes of the ocean surface that relate to a redistribution of ocean mass will influence the height of the ocean floor through isostatic adjustment.

13.1.3 Sea Level Change Caused by Contemporary Climate Change

Contemporary climate change influences sea level through changes in the ocean and atmosphere, ice grounded on land (glaciers and ice sheets), the hydrological cycle, and the climatic responses to volcanic activity (Figure 13.1). Figure 13.2 is a navigation aid for the different sections of this chapter and sections of other chapters that are relevant to sea level change.

[INSERT FIGURE 13.1 HERE]
Figure 13.1: Climate sensitive processes and components that can influence sea level and are considered in this chapter. Changes in any one of the components or processes shown will result in a sea level change. The term 'ocean properties' refers to ocean temperature, salinity and density, which influence and are dependent on ocean circulation.

[INSERT FIGURE 13.2 HERE]
Figure 13.2: Schematic representation of key processes and components that contribute to sea level change and are considered in this report. Colouring of individual boxes indicates the types of models and approaches used in projecting the contribution of each process or component to future sea level change. The diagram also serves as an index to the sections in this report that are relevant to the assessment of sea level projections via the section numbers given at the bottom of each box. Note gravity and solid Earth effects change the shape of the ocean floor hence global mean sea level.

Atmosphere-ocean momentum transfer (through surface winds) as well as heat and mass (freshwater) exchange result in ocean currents which cause the sea surface to deviate from an equipotential of the Earth's gravity field (the geoid). These ocean currents advect changes in temperature and salinity at the ocean surface into the ocean interior and therefore, together with ocean mixing, determine the temperature and salinity structure of the ocean. Changes in temperature and salinity affect sea level through the associated changes in ocean water density (thermosteric and halosteric effects, respectively). As a result, changes in ocean currents, ocean density and sea level are all tightly coupled such that changes at one location impact both local sea level and sea level far from the initial change. While both temperature and salinity changes can contribute significantly to regional sea level change (Church et al., 2010), only the thermosteric component produces a significant contribution to global average ocean volume (Gregory and Lowe, 2000). Regional atmospheric pressure anomalies also cause sea level to vary through atmospheric loading (Wunsch and Stammer, 1997). All of these processes cause sea level to vary on a broad range of space and time scales, some of which can be relatively short lived, such as waves and storm surges, while some are sustained over several decades or centuries and may be associated with atmospheric and ocean modes of climate variability (Miller and Douglas, 2007; White et al., 2005).

Water mass exchange between the terrestrial cryosphere, land, and the oceans will lead to a change in GMSL by the simple addition/subtraction of water mass to/from the ocean basins. This signal of added mass to the ocean propagates rapidly around the globe such that all regions experience a sea level rise within days of the mass being added (Lorbacher et al., 2012). In addition, an influx of freshwater changes ocean temperature and salinity and hence changes ocean currents and local sea level (Stammer, 2008; Yin et al., 2009). The coupled atmosphere-ocean system can also adjust to temperature anomalies associated with surface freshwater anomalies through air-sea feedbacks, which can result in dynamical adjustments of sea level (Okumura et al., 2009; Stammer et al., 2011). Water mass exchange between land and the ocean also results in contemporary sea level change due to vertical movement of the ocean floor associated with visco-elastic Earth deformation and change in the gravity field as a consequence of this deformation and the ice water surface mass redistribution (Farrell and Clark, 1976). These changes affect the Earth's inertia tensor and therefore rotation, which produces an additional sea level response (Milne and Mitrovica, 1998). This short-term response is captured in so-called 'sea level fingerprints' (Clark and Lingle, 1977; Conrad and Hager, 1997; Mitrovica et al., 2001).

13.1.4 Sea Level Change Not Caused by Contemporary Climate Change

There are a number of processes that occur independently of contemporary climate change that have contributed to past sea level changes and hence are important for understanding the observational record and projecting sea level change (Section 13.2). Five processes fall under this category: deformation of the Earth in response to past (as opposed to current) surface mass redistribution; the ongoing response of ice sheets to past climate change (see Section 13.1.5.1); changes in the hydrological cycle and ground subsidence associated with anthropogenic activity; tectonic processes; and coastal processes.

Surface mass transfer from land ice to oceans during the most recent global deglaciation contributes significantly to present-day sea level change due to the on-going visco-elastic deformation of the Earth and the corresponding changes ocean floor height and gravity (glacial isostatic adjustment, GIA; Lambeck and Nakiboglu, 1984; Peltier and Tushingham, 1991).

Anthropogenic processes that influence the amount of water stored in the ground or on its surface in lakes and reservoirs, or cause changes in land-surface characteristics that influence runoff or evapotranspiration rates, will perturb the hydrological cycle and potentially cause a sea level change (Sahagian, 2000). Such processes include water impoundment (dams, reservoirs), irrigation schemes and ground water extraction (Section 13.4). In some coastal locations, the subsidence caused by anthropogenic processes, such as ground water extraction, can dominate the total sea level change. However, due to the highly localised extent of this subsidence, these processes are not explicitly considered in this chapter.

Sea level changes due to tectonic and coastal processes are not considered in this chapter. Deformation of the solid Earth due to convective flow of the mantle or tectonic processes cause, on average, relatively low rates of sea level change (<O[0.1 mm yr^{-1}]; Moucha et al., 2008), with the exception of earthquakes, which can cause rapid local changes and tsunamis (Broerse et al., 2011) and significant secular relative sea level changes due to post-seismic deformation (Watson et al., 2010). Coastal processes can result in sea level change directly through changes in ocean-floor height due to sediment transfer and compaction (Ericson et al., 2006) and indirectly through the associated isostatic response of the solid Earth (Watts, 2001). These changes in turn influence the regional gravity field, which causes further sea level change. Coastal processes are particularly important in areas that experience high rates of sedimentation or erosion, most notably deltaic regions (Blum and Roberts, 2009; Syvitski et al., 2009). While they can dominate sea level change in these localised areas, they are less important as a source of sea level change at regional and global scales. Estimates of sediment delivery to the oceans (Syvitski and Kettner, 2011) suggest a contribution to GMSL of order 0.01 mm yr^{-1}.

13.1.5 Models Used to Interpret Past and Project Future Changes in Sea Level

Atmosphere-ocean general circulation models (AOGCMs) have components representing the ocean, atmosphere, land and cryosphere and simulate the MSL change resulting from the natural forcings of volcanic eruptions and changes in solar irradiance, and anthropogenic increases in greenhouse gases and aerosols (Chapter 9). AOGCMs also exhibit internally generated climate variability, including such modes as the El Nino Southern Oscillation (ENSO), the Pacific Decadal Oscillation (PDO), the North Atlantic Oscillation (NAO), and others which affect sea level (White et al., 2005). Critical components for global and regional changes in sea level are changes in surface wind stress and air-sea heat and freshwater fluxes (Lowe and Gregory, 2006; Suzuki and Ishii, 2011; Timmermann et al., 2010) and the resultant changes in ocean density and circulation, for instance in the strength of the Atlantic meridional overturning circulation (Lorbacher et al., 2010; Pardaens et al., 2011a; Yin et al., 2009). As in the real world, ocean density, circulation, and sea level are dynamically connected in AOGCMs and evolve together.

Geodynamic surface-loading models are used to simulate the relative sea level response to past and contemporary changes in surface water and land-ice mass redistribution and contemporary atmospheric pressure changes. The sea surface height component of the calculation is based solely on perturbations to the geoid, so there are no considerations of ocean dynamic effects. Application of these models tends to fall into two categories: those that focus on interannual and annual variability driven by contemporary changes in the hydrological cycle and atmospheric loading (Clarke et al., 2005; Tamisiea et al., 2010), and those that consider secular trends associated with past and contemporary changes in the cryosphere and land hydrology

(Lambeck et al., 1998; Mitrovica et al., 2001; Peltier, 2004; Riva et al., 2010). These models typically have four components: a model of space-time changes in the surface load of interest (e.g., land ice, terrestrial water storage), a model of the Earth to simulate the deformational response to the surface load (Peltier, 1974; Zhong et al., 2003), an algorithm to compute the static redistribution of ocean mass (Farrell and Clark, 1976; Kendall et al., 2005; Mitrovica and Milne, 2003), and an algorithm to compute changes in Earth rotation and the sea level changes associated with this feedback mechanism (Milne and Mitrovica, 1998; Mitrovica et al., 2005).

More recently, semi-empirical models based on statistical relationships between observed GMSL and global mean temperature (Grinsted et al., 2010; Rahmstorf, 2007b; Vermeer and Rahmstorf, 2009) or total radiative forcing (Jevrejeva et al., 2009; Jevrejeva et al., 2010) have been used to project sea level. The form of this relationship is motivated by physical considerations, whereas the parameters are determined from observational data – hence the term 'semi-empirical' (Rahmstorf et al., 2011). Although these models do not explicitly simulate the underlying processes, they assume that sea level rise is caused primarily by changes in global ice volume and global ocean heat content in response to changes in global temperature or radiative forcing with a characteristic response time. This response time could be infinite (Rahmstorf, 2007b) or explicitly determined by the model with a wide range of time scales (Grinsted et al., 2010).

Storm-surge and wave projection models are used to assess how changes in storminess and global and regional MSL change impact extreme sea levels and wave climates. The two main approaches involve dynamical (Lowe et al., 2010) and statistical models (Wang et al., 2010). The dynamical models are forced by near-surface wind and atmospheric pressure fields derived from regional or global climate models (Lowe et al., 2010).

In this chapter, we use the term 'process-based models' (see Glossary) to refer to sea level and cryosphere models (13.1.5.1) that simulate the relevant processes and interactions, in contrast to semi-empirical models which do not attempt to simulate the individual underlying processes. While these two approaches are distinct, it is important to note that semi-empirical methods are often employed in components of the process-based models (e.g., glacier models in which surface mass balance is determined by a Degree Day method, or in which calving rate is determined by water depth).

13.1.5.1 Models Used to Project Changes in Ice Sheets and Glaciers

The representation of glaciers and ice sheets within AOGCMs is not yet at a stage where projections of their changing mass are routinely available. Additional process models (as described here) use output from AOGCMs to evaluate the consequences of projected climate change on these ice masses.

The overall contribution of an ice mass to sea level involves changes to either its surface mass balance (SMB) or changes in the dynamics of ice flow that affect outflow (i.e., solid ice discharge) to the ocean. SMB is primarily the difference between snow accumulation and the melt of snow and ice (ablation). The contemporary ice sheets are close to a steady state that has taken several thousands of years to evolve in which SMB and outflow are nearly in balance (Huybrechts, 2002), and it is therefore very likely that their net contribution is much smaller than the magnitude of either of these terms. Although some ice sheet models used in projections incorporate both effects, most studies have focussed on either SMB or flow dynamics. It is assumed that the overall contribution can be found by summing the contributions calculated independently for these two sources, which is valid if they do not interact significantly. While this may be acceptable for the ice sheet projections over the next century, it may become an issue on longer time scales when, for example, changes in ice sheet topography may significantly affect SMB or dynamics. For instance, in an experiment with CO_2 initially increasing at 1% yr^{-1} and then stabilising after 140 years at $4 \times CO_2$, Vizcaíno et al. (2010) found that SMB changes were not discernibly affected by the changing geometry of the ice sheets until about year 150 in Antarctic and about year 250 in Greenland, at which point the lowered surface elevation contributed to SMB changes.

To project the sea level contribution of land ice, it is necessary to compare the model results with a base state that assumes no significant sea level contribution. This base state is taken to be either the preindustrial period or, because of our scant knowledge of the ice sheets before the advent of satellites, the late 20th century. In reality, even in these base states, the ice sheets are likely to have been contributing to sea level change (Box,

submitted-b; Huybrechts et al., 2011) and this contribution, although difficult to quantify, should be included in the observed sea level budget (Gregory et al., submitted) and the projections.

The two steps required for making a projection of future sea level with ice sheet SMB and dynamical models are simulating the local climate forcing affecting change of the ice sheet, and simulating the response of the ice sheet in terms of mass fluxes. For example, projecting Greenland's SMB relies on the simulation of regional climate change over the ice sheet and the ice sheet model's ability to simulate how these regional changes affect SMB. Similar issues exist for Antarctica, where simulations of changing mass outflow rely on the ability to simulate regional oceanographic change and ice flow dynamics. Where changes in outflow are associated with changes in grounding line position, one must account for the volume of ocean water occupying the space formerly covered by ice, which reduces the associated sea level rise (SLR).

Regional climate models (RCMs), which incorporate or are coupled to sophisticated representations of the mass and energy budgets associated with snow and ice surfaces, are now the primary source of projections of ice sheet SMB. A major source of uncertainty lies in the ability of these schemes to adequately represent the process of internal refreezing of melt water within the snowpack (Bougamont et al., 2007; Fausto et al., 2009). These models require information on the state of the atmosphere and ocean at their lateral boundaries, which are derived from reanalysis data sets or AOGCMs for past climate, or from AOGCM projections of future climate.

Because of limited understanding, the AR4 was unable to quantify the SLR that may be caused by ice sheet dynamical change on decadal timescales. Since the publication of the AR4, there has been substantial progress in understanding the relevant processes as well as in developing new ice sheet models that are capable of simulating them, such that a quantitative assessment of SLR due to ice sheet dynamics for the next century is now possible. However, these efforts are still in their infancy, and the published literature does not yet offer a sufficient basis for a time-dependent or scenario-dependent assessment. Moreover, there are still challenges to fully understanding the mechanisms as well as in modelling them, with associated uncertainties.

Ice sheet dynamics (see Chapter 4) rely on coupling mechanisms with the rest of the climate system that have not traditionally been included in models of the Earth system. There are reasonably clear links between ice dynamics and climate forcing in the case of potential surface melt water affecting basal lubrication in Greenland (Bartholomew et al., 2010) and ice shelf collapse in Antarctica (Vaughan, 2008). In addition, changes in the coastal seas surrounding Greenland and Antarctica are now recognised as being important in causing ice dynamical changes. The most likely links are between water temperature at depth and iceberg calving in Greenland (Holland et al., 2008a), and submarine melt experienced by ice shelves in Antarctica, leading to grounding line retreat (Holland et al., 2008b; Jacobs et al., 2011; Thoma et al., 2008). Detailed regional ocean models are needed to simulate the flow in sub-ice shelf cavities (Hellmer et al., 2012; Thoma et al., 2008) and the melt rates experienced by these shelves, and confidence in the ability of global Earth system models to adequately represent these regional oceanic phenomena is low. This will clearly affect the predictability of the SLR contribution from ice dynamics. Models of ice dynamics require a fairly complete representation of stresses within an ice mass in order to represent the response of ice flow to changes at the marine boundary and the governing longitudinal stresses (Schoof, 2007a). For Antarctica, there is also a need to employ high spatial resolution (<1 km) to capture the dynamics of grounding-line migration robustly so that results do not depend to an unreasonable extent on model resolution (Durand et al., 2009; Goldberg et al., 2009; Morlighem et al., 2010). One alternative approach is to parameterise grounding line physics in a coarser-resolution model (Gladstone et al., 2010b; Pollard and DeConto, 2009; Schoof, 2007b) but because grounding line migration is likely to be the primary control of the SLR contribution from Antarctica (Vaughan, 2008), rigorous efforts are needed to validate any such parameterizations. Another approach is to use models with adaptable spatial resolution (Gladstone et al., 2010a; Goldberg et al., 2009; Schoof, 2007a).

One-dimensional flowline models have been developed to the stage that modelled iceberg calving is in agreement with many observations (Nick et al., 2009). The success of this modelling approach relies on the ability of the model's computational grid to evolve to continuously track the migrating calving front. Although this is relatively straightforward in a one-dimensional model, this technique is difficult to incorporate into three-dimensional ice sheet models that typically employ a computational grid that is fixed in time. Progress is being made in this area (Amundson et al., 2010; Benn et al., 2007; Nick et al., 2010;

Pfeffer, 2007) but many challenges remain in basic process understanding and the need to ensure sufficient spatial resolution in models.

The main challenge faced by models attempting to assess sea level change from glaciers is the very large number of glaciers (the World Glacier Inventory contains more than 120,000) in comparison to the number for which mass budget observations are available (~300; Radic and Hock, 2010). Statistical techniques are used to derive relations between observed SMB and climate variables for the small sample of surveyed glaciers, and then these relations are used to upscale to regions of the world. These techniques often include volume-area scaling to estimate glacier volume from their more readily observable areas. Although tidewater glaciers are also likely to be affected by changes in outflow related to calving, the complexity of the associated processes means that most studies limit themselves to assessing the effects of SMB changes.

13.2 Past Sea Level Change

13.2.1 The Geological Record

Records of past sea level change provide critical context for understanding current changes and evaluating projected changes. In addition to establishing a longer term reference for placing current rates of sea level rise in the context of natural variability, these records provide insight into the sensitivity of sea level to past climate change. Since the AR4, important progress has been made in understanding the amplitude and variability of warm-climate sea level largely through better understanding of and accounting for the effects of GIA on coastal sequences. Here we summarize the assessment by Chapter 5 on the constraints provided by the record of paleo-sea level variations during times when global temperature was similar to or warmer than today.

13.2.1.1 The Middle Pliocene

During the Middle Pliocene (3.3 to 3.0 Ma), there is medium confidence that global mean surface temperatures were approximately 2°C–3°C warmer than for pre-industrial climate (Chapter 5). Multiple lines of evidence suggest that global mean sea level was above modern levels during warm intervals of the mid-Pliocene, implying reduced volume of polar ice sheets. The best estimates from the various methods used imply that sea level was 10 ± 10 m above present during the warmest periods of the Pliocene (medium confidence), and there is low confidence that sea level was more than 20 m above present. Direct geological evidence, together with ice sheet simulations, suggest that most of the variation in ice volume occurred in the Greenland and West Antarctic ice sheets with only a slightly reduced East Antarctic ice sheet compared to today.

13.2.1.2 Marine Isotope Stage 11

Published studies of the magnitude of emergent shorelines attributed to marine isotope stage (MIS) 11 (~400 ka) have generated highly divergent estimates. Since the AR4, studies have accounted for GIA effects or reported elevations from sites where the GIA effects are small. From the limited evidence, the assessment by Chapter 5 is that MIS 11 GMSL reached 5–15 m higher than present (medium confidence), requiring a loss of most or all of the present Greenland and West Antarctic Ice Sheets plus a reduction in the EAIS of up to 5 m equivalent sea level.

13.2.1.3 The Last Interglacial

Data syntheses suggest that during the Last Interglacial (LIG, ~130–116 ka), peak global warmth was 1°C–2°C above pre-industrial temperatures (Chapter 5). There is robust evidence and high agreement that under this warmer climate, sea level was higher than present. There have been a large number of estimates of the magnitude of LIG GMSL rise from localities around the globe, but they are generally form a small number of relative sea level reconstructions , and do not consider GIA effects, which can be substantial (Chapter 5). Since the AR4, two approaches have addressed GIA effects in order to infer LIG sea level from observations of relative sea level at coastal sites. Kopp et al. (2009) obtained a probabilistic estimate of global mean sea level (GMSL) based on a large and geographically broadly distributed database of LIG sea level indicators. Their analysis accounted for GIA effects as well as uncertainties in geochronology, the interpretation of sea

level indicators, and regional tectonic uplift and subsidence. They concluded that GMSL was very likely +6.6 m (95% probability) and likely +8.0 m (67% probability), relative to present, and that it is unlikely to have exceeded +9.4 m (33% probability). The other approach, taken by Dutton and Lambeck (2012), used data from far-field sites that are tectonically stable. Their estimate of 5.5–9 m LIG GMSL is consistent with the probabilistic estimates made by Kopp et al. (2009). There is thus high confidence that during the LIG, GMSL was more than 6 m higher than current values and less than 10 m above current values (Chapter 5). Of this sea level rise, there is medium confidence that contributions from thermosteric and glacier changes are $\leq$1 m, and ~2 m can be attributed to melting of Greenland, indicating that at least 3–4 m of sea level rise can be attributed to mass loss from Antarctica (Chapter 5).

There is medium confidence that local LIG sea levels experienced a meter-scale fluctuation sometime between 126 and 120 ka. Regional sea level variability and uncertainties in sea level proxies and their ages, however, cause differences in the timing and amplitude of the reported fluctuation. Based on the probabilistic assessment of LIG sea level by Kopp et al. (2009), for the time interval in which GMSL was above present, the 1000-year average rate of GMSL rise very likely exceeded 2.0 m kyr^{-1} (95% probability), likely exceeded 4.1 m kyr^{-1} (67% probability), and was unlikely to have exceeded 5.8 m kyr^{-1}. Faster rates lasting less than a millennium could not be ruled out by their data. By having integrated a large number of observations within a probabilistic framework, the estimate by Kopp et al. currently provides the most robust evidence for the rates of sea level change during the LIG.

13.2.1.4 The Late Holocene

Since the AR4, there has been significant progress in resolving the sea level history of the last 7000 years. From ~7 to 2 ka, interpretations of relative sea level records indicates GMSL rose 2–3 m to near present-day levels. Local sea level records spanning the last 2000 years provide high confidence that fluctuations in GMSL during this interval have not exceeded ~ ±25 cm on time scales of a few hundred years (Figure 13.3; Chapter 5). The most robust signal captured in the sea level records from both northern and southern hemispheres supports the AR4 conclusion for high confidence in an acceleration that is widely interpreted to mark the transition from relatively low rates of change during the late Holocene (order tenths of mm yr^{-1}) to modern rates (order mm yr^{-1}). There is variability in the magnitude and the timing (1840–1920) of this acceleration, however, as is also the case with tide gauge records (Chapter 3). By combining proxy sea level records with tide gauge records at the same localities, Gehrels and Woodworth (submitted) concluded that sea level began to rise above the late Holocene background rate between 1905 and 1945 CE.

[INSERT FIGURE 13.3 HERE]

Figure 13.3: (a) Paleo sea level data from salt-marsh reconstructions from two sites in North Carolina (purple symbols is Sand Point, magenta symbols is Tump Point), with corrections for long-term subsidence attributed to glacial isostatic adjusment (Kemp et al., 2011). Values are relative to a preindustrial average for AD 1400–1800. **(b)** Tide gauge reconstructions from Ray and Douglas (2011) (twilight blue), Church and White (2011) (autumn orange), and Jevrejeva et al. (submitted) (light green line), relative to the mean for 1900–1905. Uncertainties are one standard deviation as reported by the authors. **(c)** Altimetry data sets from five groups (CU, NOAA, GSFC, AVISO, CSIRO) with mean of the five shown as black line. **(d)** Comparison of the paleo, tide gauge, and altimetry data sets (same symbol and line colors as in panels a-c. All tide gauge time series have been centered so that their individual mean is zero over their common period (1900–2007). The altimeter time series has been shifted so that is mean value over the 1993–2007 period is equal to the mean value of the average of all three tide gauge time series over the same period. The tide gauge and altimeter time series were then shifted vertically up by 150 mm in order to align with the paleo data.

13.2.2 The Instrumental Record (~1700–2010)

The instrumental record of sea level change is mainly comprised of tide-gauge measurements over the past 2–3 centuries and, since the early 1990s, of satellite-based radar altimeter measurements. The number of tide gauges has increased since the first sites at some Northern Europe ports were installed in the 18th century. However, Southern Hemisphere measurements only started in the late 19th century. Chapter 3 assesses 20th century sea level rise estimates from various groups (e.g., Church and White, 2006; Church and White, 2011; Douglas, 2001; Holgate, 2007; Jevrejeva et al., 2006; 2008; Ray and Douglas, 2011), and concludes that even though different strategies were developed to account for inhomogeneous tide gauge data coverage in space and time, and to correct for vertical crustal motions (also sensed by tide gauges, in addition to sea level change and variability), long-term trend estimates in GMSL are very similar (~1.7 ± 0.2 mm yr^{-1} between

1900 and 2010). Interannual and decadal-scale variability is superimposed on the long-term mean sea level trend, but Chapter 3 noted that discrepancies between the various published mean sea level records are present at these shorter time scales.

Chapter 3 also assesses the significance of the sea level acceleration since the beginning of the instrumental record reported by a number of studies. Because of the presence of low-frequency oscillations (e.g., 60-year oscillations; Chambers et al., submitted; in some tide gauge records), sea level acceleration results are sensitive to the choice of the analysis time span. Chapter 3 concludes that the rate of sea level rise has increased since the late 19th century and has continued during the 20th century. When a 60-year oscillation is modeled along with an acceleration term, the estimated acceleration in GMSL since 1900 ranges from: 0.000 [–0.002 to 0.002] mm yr^{-2} (90% confidence) in the Ray and Douglas (2011) record, 0.013 [0.007 to 0.019] mm yr^{-2} in the Jevrejeva et al. (2008) record, and 0.012 [0.009 to 0.015] mm yr^{-2} (90% confidence) in the Church and White (2011) record. For comparison, (Church and White, 2011) estimated the acceleration term to be 0.009 ± 0.003 mm yr^{-2} over the 1880–2009 time span when the 60-year cycle is not considered.

The high-precision satellite altimetry record started in 1992. Although there are slight differences at interannual time scales in the altimetry based GMSL time series produced by different groups (e.g., Masters et al., submitted), there is very good agreement on the 20-year long GMSL trend. After accounting for the ~ –0.3 mm yr^{-1} correction related to the increasing size of the global ocean basins due to GIA (Peltier, 2009), a GMSL rate of 3.2 ± 0.4 mm yr^{-1} over 1993–2010 is found by the different altimetry data processing groups. The current 0.4 mm yr^{-1} level of precision is derived from assessments of all source of errors affecting the altimetric measurements (Ablain et al., 2009) and from tide gauge comparisons (Beckley et al., 2010; Nerem et al., 2010). Chapter 3 discusses the significance of this higher GMSL trend since 1993 compared to mean rates over previous decades. It concludes that there is high confidence that this higher rate, which is also seen in tide gauge data over the same period, is real but does not necessarily reflect a recent acceleration, considering the previously reported multi-decadal oscillations of the mean sea level.

[START FAQ 13.1 HERE]

FAQ 13.1: Why Does Local Sea Level Change Differ from the Global Average?

Shifting surface winds, the expansion of warming ocean water, and the addition of melting ice can alter ocean currents which, in turn, lead to changes in sea level that vary from place to place. Past and present variations in the distribution of land ice affect the shape and gravitational field of the Earth, which also cause regional fluctuations in sea level. Additional variations in sea level are cause by the influence of highly localised processes such as sediment compaction.

Along any coast, vertical motion of either the sea or land surface can cause changes in sea level relative to the land (known as relative sea level). For example, a local rise can be caused by an increase in sea surface height, or by a decrease in land height. Over relatively short time spans (seconds to years), the influence of tides, storms and climatic variability—such as El Niño—dominates sea level variations. Earthquakes and landslides can also have an effect by causing changes in land height and, sometimes, tsunamis. Over longer time spans (decades to centuries), the influence of climate warming—with consequent expansion of ocean water and melting of land ice—is the main contributor to sea level change. Over these longer time scales, various processes cause vertical motion of the land surface, which can also result in substantial changes in relative sea level.

Since 1992, satellites have measured the height of the ocean surface relative to the center of the Earth (known as geocentric sea level). These measurements show differing rates of geocentric sea level rise around the world during the past few decades (see FAQ 13.1, Figure 1a). For example, in the western Pacific Ocean, rates were about three times greater than the global mean value of about three millimeters a year. In contrast, those in the eastern Pacific Ocean are lower than the global mean value, with much of the west coast of the Americas experiencing a fall in sea surface height during this period.

Much of the spatial variation shown in FAQ 13.1, Figure 1 is a result of natural climate variability—such as El Niño and the Pacific Decadal Oscillation—over time scales from about a year to several decades. These climate variations alter surface winds, ocean currents, temperature and salinity, and hence affect sea level.

The influence of these processes will continue during the 21st century, and will be superimposed on the spatial pattern of sea level change associated with longer-term climate change, which also arises through changes in surface winds, ocean currents, temperature and salinity, as well as ocean volume.

Tide gauges measure relative sea level, and so they include any changes resulting from vertical land motion. Over many coastal regions, this motion is small, and so the long-term rate of sea level change recorded by coastal and island tide gauges is similar to the global mean value (see records at San Francisco and Pago Pago in FAQ 13.1, Figure 1a). The relatively large, short-term oscillations in sea level—seen in the tide gauge plots as grey lines—are due to the natural climate variability described above. For example, the large, regular deviations at Pago Pago are associated with the El Niño-Southern Oscillation.

Changes in relative sea level over the past ~50 years have varied from place to place, due to spatial patterns in both sea surface and land-height change. In some regions, vertical land motion has had an important influence. For example, the steady fall in sea level recorded at Stockholm (FAQ 13.1, Figure 1a) is caused by uplift of this region after the melting of a large (>1 km thick) continental ice sheet at the end of the last Ice Age, between ~20,000 and ~9,000 years ago. Such on-going land deformation as a response to the melting of ancient ice sheets is a significant contributor to regional sea level changes in North America and northwest Eurasia, which were covered by large continental ice sheets during the peak of the last Ice Age.

In other regions, this process can also lead to land subsidence, which elevates sea levels, as it has at Charlottetown, where a relatively large increase has been observed, compared to the global mean rate (FAQ 13.1, Figure 1a). Vertical land motion due to movement of the Earth's tectonic plates can also cause departures from the global mean sea level trend in some areas – most significantly, those located near active subduction zones, where one tectonic plate slips beneath another, causing steady land uplift and therefore relative sea level fall at Antofagasta (FAQ 13.1, Figure 1a).

In addition to regional influences of vertical land motion on relative sea level change, some processes lead to land motion that is rapid, but highly localised. For example, the greater rate of rise relative to the global mean at Manila (FAQ 13.1, Figure 1a) is due to sediment slumping and compaction. This is common in many river deltas due to both natural and anthropogenic processes—such as the extraction of ground water or hydrocarbons.

It is commonly assumed that melting ice from glaciers, or the Greenland and Antarctic ice sheets, would cause globally uniform sea level rise, much like filling a bath tub with water. In fact, such melting actually results in spatial variations in sea level due to a variety of processes, including changes in ocean currents, winds, the Earth's gravity field, and land height. For example, a computer model that simulates these latter two processes predicts a regional fall in relative sea level around the melting ice sheets, because the land tends to rise as the ice melts, and the gravitational attraction between ice and ocean water is smaller (FAQ 13.1, Figure 1b).

However, further away from the melting, sea level rise is enhanced, compared to the global average value. Thus, if only the Greenland ice sheet was melting, many parts of North America and northwest Europe would experience a sea level fall or a modest rise, compared to the global average. If either, or both, of the ice sheets were melting, equatorial regions would experience a sea level rise larger than the global average, with falls in sea level nearer the ice sheets (FAQ 13.1, Figure 1b).

In summary, a variety of processes drive height changes of the ocean surface and ocean floor, resulting in distinct spatial patterns of sea level change at local to regional scales. The combination of these processes produces a complex pattern of total sea level change, which varies through time as the relative contribution of each process changes. The global average change is a useful single value which reflects the contribution of climatic processes—land-ice melting and ocean warming, and represents a good estimate of sea level change at many coastal locations. At the same time, however, where the various regional processes result in a strong signal, there can be large departures from the global average value.

[INSERT FAQ 13.1, FIGURE 1 HERE]

FAQ13.1, Figure 1: (a) Mean rates of change in sea surface height (geocentric sea level) for the period 1993–2010 from satellite altimetry. Also shown are relative sea level changes (grey lines) from selected tide gauge stations for the

period 1950–2010. For comparison, an estimate of global mean sea level change is also shown (red lines) with each tide gauge time series. (b) Model output, showing relative sea level change due to melting of the Greenland ice sheet and the West Antarctic ice sheet at rates of 0.5 mm yr^{-1} each (giving a global mean value of 1 mm yr^{-1}).

[END FAQ 13.1 HERE]

13.3 Contributions to Global Mean Sea Level Rise During the Instrumental Period

13.3.1 Thermosteric Contribution

13.3.1.1 Observational

Important progress has been realized since AR4 in quantifying the thermosteric component of sea level rise. This progress reflects (1) the detection of systematic depth-varying biases affecting historical XBT data (Gouretski and Koltermann, 2007; Chapter 3), (2) the newly available Argo ocean (temperature and salinity) data with almost global coverage of the oceans down to 2000 m since 2004–2005, and (3) estimates of the deep-ocean contribution using ship-based data collected during the World Ocean Circulation Experiment (WOCE) and revisit cruises (Johnson and Gruber, 2007; Johnson et al., 2007; Kouketsu et al., 2011; Purkey and Johnson, 2010).

For the period 1971–2010, the thermosteric rate for the 0–700 m depth range is 0.6 [0.4–0.8] mm yr^{-1} (Chapter 3). Accounting for the deep-ocean contribution, this value increases to 0.8 [0.5–1.1] mm yr^{-1} for that same period (Figure 13.4a). Over the altimetry operating period (1993–2010), the thermosteric rate for the 0–700 m depth range is 0.7 [0.4–1.0] mm yr^{-1} and 1.0 [0.7–1.3] mm yr^{-1} when accounting for the deep ocean (Chapter 3). For the period 2005–2010, estimates of the thermosteric component 0.9 [0.6–1.2] mm yr^{-1} (Chapter 3, Figure 13.5).

13.3.1.2 Modelled

GMSL rise due to thermal expansion is approximately proportional to the increase in ocean heat content (Körper et al., submitted; Russell et al., 2000), and both of these can be calculated from AOGCM simulations (Section 13.5.1). Experiments have been carried out with CMIP3 and CMIP5 AOGCMs forced with historical time-dependent anthropogenic change in atmospheric composition since the late 19th century, in most cases also including natural forcing due to volcanic aerosols and variations in solar irradiance. These experiments provide the basis for the statistical detection of climate change and its attribution to forcing agents (Chapter 10). Domingues et al. (2008) compared GMSL due to thermal expansion of the upper 700 m of the ocean in observations with CMIP3 historical experiments. For 1961–1999, the simulations with natural forcing as well as anthropogenic forcing had substantially smaller increasing trends than those without the natural forcing, because the natural volcanic forcing tends to cool the climate system and reduce ocean heat uptake (Levitus et al., 2001). The models including natural forcing are closer to observations, though with a tendency to underestimate the trend by about 10% (Section 10.4.1).

Historical GMSL rise due to thermal expansion simulated by CMIP5 models is shown in Table 13.1 and Figure 13.4a. The rate of thermal expansion increases during the 20th century because the ocean takes up heat more rapidly as the climate warms. The model-mean rate for 1971–2010 is close to observations (Figure 13.4a, Figure 13.5a). For 1993–2010, the model-mean rate exceeds that observed, probably because ocean warming in the AOGCMs during the first decade of the 21st century is at least as large as in the late 1990s, whereas in observations (Chapter 3) there has been a decreased rate of ocean warming and hence thermal expansion, possibly due in part to increased negative tropospheric aerosol and other radiative forcings (Church et al., 2011b) not included in the model simulations. Following the major volcanic eruptions in 1963, 1982 and 1991, the modelled rate of expansion is substantially larger than the 20th century average, as the ocean recovers from the cooling caused by the volcanic forcing (Church et al., 2005; Gregory et al., 2006).

Gregory (2010) suggested that because AOGCMs are usually spun up without volcanic forcing, they may underestimate ocean heat uptake in historical simulations. Imposition of volcanic forcing in models during the 20th century therefore represents a net negative forcing relative to the control climate, whereas in reality

volcanic eruptions should give zero long-term forcing, because they are a normal part of the system. The hypothesis is that the apparent long persistence of the oceanic cooling following the 1883 eruption of Krakatau in the CMIP3 historical simulations (Delworth et al., 2005; Gleckler et al., 2006a; Gleckler et al., 2006b; Gregory et al., 2006) is a consequence of spin-up without volcanoes. Comparison of CMIP3 historical experiments with and without volcanic forcing indicates that this effect could lead to an underestimate of 0.16 mm yr^{-1} of thermal expansion on average during the 20th century. If this hypothesis is correct, the results in Table 13.1 and Figures 13.4a and 13.5 are underestimated by this amount (see Appendix for the implication for projections).

13.3.2 Glaciers

13.3.2.1 Observational

The aggregate volume and mass changes of global glaciers, defined here as all glacier ice exclusive of the Greenland and Antarctic ice sheets, but including the peripheral glaciers surrounding the ice sheets, has conventionally been determined by compilation and upscaling of a limited set of direct observations of mass balance terms and by various methods of repeat mapping of surface elevation to detect elevation (and thus volume) change. GRACE gravity methods have only recently been adapted to mass change detection for the world's glaciers. The details of observational methods are described in Chapter 4.

Overall, the combined records suggest that the net decline of global glacier volume began in the 19th century before significant anthropogenic radiative forcing had started, and was probably the result of natural climatic variability (Crowley, 2000; Gregory et al., 2006; Gregory et al., submitted). As assessed in Chapter 4, observations, combined with improved methods of analysis and a new, globally complete inventory, indicate that global glaciers, including those around the ice sheet peripheries, are very likely continuing to be significant contributors to sea level (at more than 50% of the cryospheric total since about 1990), but are also highly variable on annual to decadal time scales. From the assessment in Chapter 4, the global glacier contribution to sea level was 0.87 [0.36–1.38] mm yr^{-1} SLE during 1900–1990, 0.86 [0.64–1.07] mm yr^{-1} SLE during 1971–2009, 1.04 [0.85–1.23] mm yr^{-1} SLE during 1993–2009, and 1.03 [0.89–1.17] mm yr^{-1} SLE during 2005–2009 (Table 13.1, Figure 13.4b, Figure 13.5a).

13.3.2.2 Modelled

Global glacier mass balance models have been constructed on the basis of models of the small sample of well-observed glaciers. Confidence in global glacier mass balance models used for projections of global changes (Section 13.4.2) thus arises from the ability of the models of the well-observed glaciers to reproduce time series of historical changes of those glaciers using observed climate input. Because the model parameters are mainly derived from or calibrated against observed glacier changes (Bahr et al., 2009; Marzeion et al., 2011; Marzeion et al., submitted; Meier et al., 2007; Radic and Hock, 2011; Raper and Braithwaite, 2005), the models cannot be independently evaluated against glacier observations.

Confidence that the AOGCM multi-model mean simulation of climate change provides accurate input for glacier simulations can be gained by comparing results from a global glacier model using AOGCM simulations of historical climate change with the same model using observed climate change. For the model of Marzeion et al. (submitted), the simulated historical glacier changes in the two cases are very similar to each other and to other observational glacier estimates since the 1970s (Figure 13.4b). In the 1930s, the simulation using observational input shows a larger rate of glacier mass loss than the simulations using AOGCM input. This arises from an episode of warming in Greenland, which was associated with unforced variability of regional climate (Chylek et al., 2004), rather than with radiative forcing of the climate system, and is therefore not reproduced by AOGCM experiments (Section 10.2). In our analysis of the budget of GMSL rise (Section 13.3.6), we take the difference between the simulations using AOGCM input and the simulation using observed input as an estimate of the influence of unforced climate variability on global glacier mass balance (Figure 13.4e).

13.3.3 Greenland and Antarctic Ice Sheets

13.3.3.1 Observational

Knowledge of the contribution of the Greenland and Antarctic ice sheets to sea level changes over the last two decades comes primarily from satellite and airborne surveys. Three main techniques are employed (Chapter 4): the mass budget method, repeat altimetry, and temporal variation in the Earth's gravity field. The strengths and weaknesses of these methods are discussed in Section 4.4.1. The Greenland ice sheet's mass budget comprises its surface mass budget (the sum of ablation which is primarily ice and snow melt and subsequent runoff, and accumulation primarily snowfall) and outflow (the flow over the grounding lines). Antarctica's mass budget is dominated by accumulation and outflow in the form of calving and ice flow into floating (and therefore sea level neutral) ice shelves.

Observations indicate that Greenland is very likely to be experiencing a net loss of mass, and this rate of loss is likely to have increased over the last two decades. Drawn from the assessment made in Chapter 4 (Section 4.4.2.2), Greenland's contribution was 0.34 ± 0.06 mm yr^{-1} SLR between 1993 and 2009, and 0.61 ± 0.18 mm yr^{-1} between 2005 and 2009. Antarctica is also likely to be in a state of net mass loss and its contribution to sea level is also likely to be increasing through time (4.4.2.3). The associated rate of sea level rise was an average of 0.24 ± 0.09 mm yr^{-1} between 1993 and 2009, and 0.40 ± 0.19 mm yr^{-1} over the period 2005–2009. The contribution of both ice sheets is 0.42 ± 0.11 mm yr^{-1} over 1993–2009 and 0.73 ± 0.26 mm yr^{-1} over 2005–2009. For context, the AR4's assessment was 0.21 ± 0.07 mm yr^{-1} for Greenland and 0.21 ± 0.35 mm yr^{-1} for Antarctica, over the period 1993–2003.

13.3.3.2 Modelled Surface Mass Balance

Projections of future changes in the SMB of the Antarctic and Greenland ice sheets are obtained from regional climate models (RCMs) of the future, or by computing it by various methods from downscaled AOGCM or RCM simulations of future climate (Sections 13.4.3.1 and 13.4.4.1). A spatial resolution of a few 10s km or finer is required in order to resolve the strong gradients in SMB across the steep slopes of the ice sheet margins. Table 13.2 compares results derived using methods to simulate Greenland SMB in recent decades on the basis of climate input from observations that are similar to those employed for projections. The average and standard deviation of accumulation (precipitation minus sublimation) estimates for 1961–1990 is 589 ± 77 Gt yr^{-1} from these models. This agrees with published observation-based accumulation maps, for example 513 ± 41 Gt yr^{-1} by Bales et al. (2009) and 591 ± 83 Gt yr^{-1} by Burgess et al. (2010). For SMB (shown in Table 13.2, accumulation minus runoff; drifting snow erosion is small over the Greenland ice sheet), the same set of models give 333 ± 96 Gt yr^{-1} for 1961–1990.

All the models indicate that Greenland ice sheet SMB showed no significant trend from the 1960s to the 1980s, then started decreasing in the early 1990s, on average by 3% yr^{-1}. This results in a statistically significant and increasing contribution to the rate of GMSL rise (SMB trend column of Table 13.1, Figure 13.6). The largest trends are found in models with coupled snow and atmosphere simulations (RACMO2 and MAR). Van den Broeke et al. (2009) concluded that the mass loss during 2000–2008 is equally split between SMB and dynamical change. Rignot et al. (2011) evaluated trends in Greenland SMB and ice outflow since 1992, when the ice sheets are assumed to be near balance; their results indicate that dynamics accounts for ~60% of the total mass loss. Sasgen et al. (2012) showed that SMB change, simulated by RACMO2 (Ettema et al., 2009, an earlier version of the model in Table 13.2), accounts for about 60% of the observed net rate of mass loss during 2002–2010, and an observational estimate of the increase in ice outflow for the remainder, for the entire ice sheet and its individual drainage basins. This satisfactory agreement gives confidence in SMB simulations of the past, and hence also in the similar models used for projections of future SMB changes (Section 13.4.3.1).

The recent trend towards increasingly negative SMB is caused almost entirely by increased melting and subsequent runoff, with variability in accumulation being comparatively small (Sasgen et al., 2012); Figure 13.6). This tendency is related to pronounced regional warming, which may be attributed to a combination of anomalous regional variability in recent years, for instance associated with the NAO or AMO, and anthropogenic climate change (Hanna et al., 2008; Fettweis et al., submitted; Mernild et al., submitted; Section 10.5.2.1). However, Greenland SMB models forced by boundary conditions from AOGCM historical simulations (Rae et al., submitted; Fettweis et al., submitted) do not show statistically significant trends towards increasing contributions to GMSL. The same is true of Greenland SMB changes calculated

from AOGCM historical simulations of global-mean SAT change, which are the same methods used for projections (Section 13.5.3.1, Appendix 13.A, Table 13.1, Figure 13.4e). It is possible that these models do not simulate SMB trends as large as those observed because of the important contribution of regional climate variability, which is not expected to be reproduced by AOGCM historical simulations (Section 10.2). There is not yet sufficient evidence to evaluate how realistically AOGCMs simulate anthropogenic regional climate change in Greenland, because the signal is relatively small. However, we have high confidence in projections of future warming in Greenland because of the qualitative agreement of models in predicting amplified warming at high northern latitudes (Section 12.4.3.1) for well-understood physical reasons, and we have high confidence in projections of increasing surface melting because of the sensitivity to warming demonstrated by SMB models.

All Greenland SMB simulations for the first half of the 20th century depend on reconstructions of meteorological variability over the ice sheet made using empirical relationships dependent on observations from coastal stations and estimates of accumulation from ice cores. Despite the similar input datasets in all cases, the various climate reconstruction and SMB methods employed have led to a range of results (Box, submitted-a; Box, submitted-b; Box et al., submitted; Fettweis et al., 2008; Hanna et al., 2011; Wake et al., 2009). Hanna et al. (2011) have a substantial positive anomaly with respect to assumed balance in 1961–1990, giving a GMSL contribution of –0.3 mm yr^{-1} in the time-mean of 1901–1990, while Box (submitted-b) has a weakly positive contribution and the others are about zero. In all cases, there is substantial variability associated with regional climate fluctuations, in particular the warm episode in the 1930s, during which glaciers retreated in south-east Greenland (Bjork et al., 2012). It has been argued that this episode was connected with the NAO (e.g., Chylek et al., 2004), rather than with global climate change.

Accumulation (precipitation minus sublimation) approximates SMB in Antarctica, since surface melting and runoff are negligible in the present climate. There are model uncertainties in Antarctic accumulation because drifting snow processes, which remove an estimated 7% of the accumulated snow (Lenaerts et al., 2012), and snow hydrology are not accounted for by global models, and the ice sheet's steep coastal slopes are not well captured by coarse-resolution models. There are also uncertainties in observation-based estimates of Antarctic SMB, which rely on sparse accumulation measurements with very little coverage in high-accumulation areas. Observation-based SMB estimates of the Antarctic ice sheet, for example 1768 ± 49 Gt yr^{-1} in Arthern et al. (2006), are generally lower than model-based SMB estimates, for example 1923 ± 184 Gt yr^{-1} for the average of results from the regional climate model RACMO2 of Lenaerts et al. (2012), and the four global reanalysis models of Bromwich et al. (2011).

For the Antarctic ice sheets, interannual variability in accumulation is dominated by changes in precipitation. However, global reanalysis data have been shown to contain spurious trends in the Southern Hemisphere related to changes in the observing systems, for example the introduction of new satellite observations (Bromwich et al., 2007; Bromwich et al., 2011). This problem also potentially affects RCMs that are forced at the boundaries of their limited-area domain by global reanalyses. In the models in which the temporal variability is deemed most reliable, no significant trend is present in accumulation over recent decades (see also Section 4.4.2.3). This agrees with observation-based studies (Anschütz et al., 2009; Monaghan et al., 2006; Chapter 4) and implies that Antarctic SMB change has not contributed significantly to changes in the rate of GMSL rise. Likewise, CMIP3 historical simulations do not exhibit any systematic trend in Antarctic precipitation during the late 20th century (Uotila et al., 2007). Nothing is known observationally about variability in Antarctic mass balance earlier in the 20th century, or about its long-term mean (Chapter 4).

GCM and RCM projections consistently indicate significant Antarctic warming and concomitant increase in precipitation. We have high confidence in expecting a relationship between these quantities, on physical grounds (Section 13.4.4.1) and from ice core evidence (Lemieux-Dudon et al., 2010; Stenni et al., 2011; Van Ommen et al., 2004). The absence of a significant trend in Antarctic precipitation up to the present is not inconsistent with the expected relationship, because observed temperature trends over the majority of the continent are weak (Section 10.5.2.1) and trends in Antarctic precipitation simulated for recent decades are much smaller than interannual variability (Uotila et al., 2007; van den Broeke et al., 2006). Based on limited observational coverage, there is medium confidence that anthropogenic influence has made a significant contribution to warming in Antarctica (Section 10.3.1.1.4). Ozone recovery, through its influence on atmospheric circulation at high southern latitudes (Section 10.3.3.5), may offset some effects of greenhouse gas increase in the 21st century, but Antarctic precipitation is nonetheless projected to increase (Polvani et

al., 2011). Taking all these considerations together, we have medium confidence in model projections of future Antarctic SMB increase, but we note that, if these projections are incorrect, it implies an underestimate in projections of GMSL rise (Section 13.5.1.3).

[INSERT FIGURE 13.4 HERE]

Figure 13.4: Modeled and observed global-mean sea level contributions and total sea level from 1900 to 2008. All curves have an arbitrary offset and are set to zero in the time-mean of 1986–2005 (the reference period for the projections). The grey lines are derived from individual AOGCM simulations and the black line from the average of the AOGCM-based results. **(a)** Thermal expansion, with the observations since 1971 in blue and the 5–95% uncertainty shaded. **(b)** Glacier melting, with the observations of Marzeion et al. (submitted), Leclercq et al. (2011) and Cogley (2009). **(c)** Estimated changes in land water storage due to human intervention. **(d)** Observed sea level (blue - tide gauges; red - altimeter) and modeled sea level (black, the sum of terms in a to c, and black dashed also including the terms in e). **(e)** Additional terms: modeled Greenland SMB changes since 1900 (dashed green, the average of four individual estimates in dotted green, and for comparison the modeled Greenland SMB changes from the results shown in Figure 13.5 in black), a possible long term Antarctic ice sheet contribution (dashed blue), the possible underestimate of thermal expansion due to AOGCM preindustrial simulations not including volcanic forcing (orange), and the possible greater mass loss by glaciers in high northern latitudes prior to 1950. The two ice sheet series are joined to the observed changes in Greenland and Antarctica (from Chapter 4) in 1992. **(f)** The residual (black, observed GMSL rise – modelled expansion – modelled glaciers – land water, the difference between blue and black in d), and the sum of the additional terms (purple, from e). **(g)** Trends in sea level calculated over 18 year periods (the length of the altimeter record), from tide-gauges (blue; Church and White, 2011), altimetry (red dot), and models (black and dashed black, as in d); also the observed rates of the contributions from the Greenland (green dashed) and Antarctic (blue dashed) ice sheets and their sum (blue dots) since 1992.

[INSERT FIGURE 13.5 HERE]

Figure 13.5: Observed global-mean sea level contributions and observed and projected total sea level from 1993 to 2010. **(a)** Observed contributions to GMSL from 1993 (ocean thermal expansion, red, Chapter 3; Glaciers, dark blue and Ice Sheets, light blue and green, Chapter 4; Land water storage, brown, Section 13.4). **(b)** Observed GMSL from satellites (light blue dashed) and estimated from tide gauges (dark blue solid) and the sum of contributions from (a, red). The shading indicates 5–95% confidence limits. The mean sea level from modeled thermal expansion, modeled glaciers and land water storage from Figure 13.4 is shown in black. **(c)** The projected sea level rise (Section 13.5) relative to the 1986–2005 average (black and coloured lines for the four scenarios, with shading indicating the likely range). Also shown is the observed sea level from (b), set to have the same value as the projections over 1993 to 2001.

[INSERT FIGURE 13.6 HERE]

Figure 13.6: Annual-mean surface mass balance (accumulation minus ablation) for the Greenland Ice Sheet, simulated by regional climate models for the period 1960–2010.

Table 13.1: Global mean sea level budget (mm yr^{-1}) over different time intervals from observations and from model-based contributions. Uncertainties are 5–95%. The AOGCM historical integrations end in 2005; projections for RCP4.5 are used for 2006–2010. The thermosteric, glacier and ice sheet SMB contributions are computed from the CMIP5 results.

Source	1901–1990	1971–2010	1993–2010	2005–2010
Observed Contributions to GMSL Rise				
Expansion		0.8 [0.5 to 1.1]	1.0 [0.7 to 1.3]	0.9 [0.6 to 1.2]
Glaciers	0.87 [0.36 to 1.38]	0.86 [0.64 to 1.07]	1.04 [0.85 to 1.23]	0.30 [0.27 to 0.34][a]
Greenland			0.34 [0.28 to 0.40]	0.63 [0.48 to 0.78]
Antarctica			0.18 [0.09 to 0.27]	0.31 [0.15 to 0.47]
Land Water	–0.11 [–0.16 to –0.06]	0.12 [0.03 to 0.22]	0.38 [0.26 to 0.49]	–0.33 [–0.54 to –0.10][b]
Total			2.9 [2.5 to 3.2]	1.8 [1.4 to 2.2]
Observed GMSLR	1.5 [1.3 to 1.7]	2.0 [1.7 to 2.3]	3.2 [2.8 to 3.6]	2.3 [1.7 to 2.9]
Modelled Contributions to GMSL Rise				
Expansion	0.25 [–0.06 to 0.56]	0.83 [0.36 to 1.30]	1.42 [0.94 to 1.91]	
Glaciers	0.88 [0.47 to 1.28]	0.87 [0.57 to 1.18]	1.18 [0.63 to 1.73]	
Total incl Land Water	1.0 [0.5 to 1.5]	1.8 [1.3 to 2.4]	3.0 [2.2 to 3.7]	
Residual[c]	0.5 [–0.1 to 1.0]	0.2 [–0.5 to 0.8]	0.2 [–0.6 to 1.1]	

Notes:
(a) For 2005–2010 the figure for glaciers refers only to the glaciers on Greenland and Antarctica, peripheral to the ice sheets. The other glaciers in the world are included in the figure for land water for this period.
(b) For 2005–2010 the figure for land water is from GRACE observations of water mass change on all land areas except Greenland and Antarctica, and includes both liquid water storage and glaciers.
(c) Observed GMSL rise – modelled expansion – modelled glaciers – land water.

Table 13.2: Surface mass balance and rates of change for the Greenland Ice Sheet calculated from ice sheet surface mass balance models. The sea level equivalent is shown for the model-average SMB anomaly. A negative SMB anomaly of 360 Gt yr^{-1} means an increase of 1 mm yr^{-1} in the Greenland contribution to sea level rise. Uncertainties are one standard deviation. Note that a negative SMB anomaly means that SMB has decreased, but not that SMB has become negative. It can be seen that SMB remains positive in nearly all cases, by comparing the first and last columns. Uncertainty in individual model results reflects temporal variability, that is one standard deviation of annual time series; the uncertainty in the model average is one standard deviation of the various model averages.

Reference and Model[a]	**Mean SMB 1961–1990 Gt yr^{-1}**	**SMB Trend 1991–2010 Gt yr^{-2}**	**Mean SMB Anomaly (with Respect to 1961–1990 Mean SMB)[b] Gt yr^{-1}**		
			1971–2010	**1993–2010**	**2005–2010**
RACMO2, Van Angelen et al. (2012), 11 km RCM	410 ± 110	–12.7 ± 3.5	–25 ± 118	–82 ± 110	–170 ± 86
MAR, Fettweis et al. (2011), 25 km RCM	423 ± 112	–16.9 ± 3.4	–42 ± 138	–130 ± 120	–231 ± 79
PMM5, Box et al. (2009), 25 km RCM	357 ± 65	–8.9 ± 3.1	–1 ± 70	–38 ± 80	–82 ± 76
ECMWFd, Hanna et al. (2011), 5 km PDD	279 ± 99	–7.3 ± 3.7	–8 ± 102	–43 ± 97	–86 ± 68
SnowModel, Mernild and Liston (submitted), 5 km EBM	194 ± 77	–9.4 ± 2.6	–32 ± 90	–68 ± 88	–129 ± 85
Model Average	333 ± 96	–11.0 ± 3.8	–22 ± 17	–72 ± 37	–140 ± 62
Model Average SLE (mm yr^{-1})			0.06 ± 0.05	0.20 ± 0.10	0.39 ± 0.17

Notes:
(a) The approximate spatial resolution is stated and the model type denoted by PDD = positive degree day, EBM = energy balance model, RCM = regional climate model.
(b) Difference from the mean SMB of 1961–1990 in the models of Table 13.2. This difference equals the sea level contribution from Greenland SMB changes if the ice sheet is assumed to have been near zero mass balance during 1961–1990 (Hanna et al., 2005; Sasgen et al., 2012).

13.3.4 Contributions from Water Storage on Land

Changes in water storage on land in response to climate change and variability (i.e., water stored in rivers, lakes, wetlands, the vadose zone, aquifers, and snow pack at high latitudes and altitudes) and from direct human-induced effects (i.e., storage of water behind dams and groundwater pumping) have the potential to contribute to sea level change. Estimates of climate-related changes in land water storage over the past two decades rely on global hydrological models because corresponding observations are deemed inadequate. In assessing the relation between terrestrial water storage and climate, Milly et al. (2003) and Ngo-Duc et al. (2005) found no long-term climatic trend in total water storage, but rather large interannual to decadal fluctuations, equivalent to several millimetres of sea level. Recent studies have shown that interannual variability in observed GMSL is correlated with ENSO indices (Nerem et al., 2010) and is inversely related to ENSO-driven changes of terrestrial water storage, especially in the tropics (Llovel et al., 2011). During El Niño events, sea level (and ocean mass) tends to be higher because ocean precipitation increases and land precipitation decreases (Cazenave et al., accepted), whereas the reverse happens during La Niña events, as seen during the 2010–2011 La Niña event (Boening et al., submitted).

Direct human interventions on land water storage also induce sea level changes (Gornitz, 2001; Huntington, 2008; Lettenmaier and Milly, 2009; Sahagian, 2000). The largest contributions come from reservoir filling behind dams and groundwater withdrawal (for agricultural, industrial, and municipal use). Over the past

half-century, tens of thousands of dams have been constructed to create artificial reservoirs, with the resultant storage offsetting some of the sea level rise that would otherwise have occurred. Chao et al. (2008) reconstructed the history of water impoundment in the nearly 30,000 reservoirs built during the 20th century and estimated the resulting nominal reservoir storage up to 2007 of ~23 mm of sea level fall (mostly since 1940), with a stabilization in recent years. Chao et al. further assumed the reservoirs were 85% full, and by including seepage into groundwater, estimated from a model, they obtained a total of 30 mm of sea level fall (equivalent to a rate of sea level fall of 0.55 mm yr^{-1} from 1950 to 2000). Their seepage estimate is unrealistically large because it assumes aquifers are infinite and have no interfering boundary conditions (Konikow, submitted; Lettenmaier and Milly, 2009). Chao et al. argued that sedimentation of reservoirs does not reduce their sea level contribution, but this argument is disputed (Gregory et al., submitted). Based primarily on observational data, Lettenmaier and Milly (2009) suggested a smaller contribution, because of a loss of capacity to sedimentation at 1% yr^{-1}. Given these concerns, we disregard both the seepage, and the smaller effect of sedimentation, and in our budget calculation (Section 13.3.6) we assume the (negative) sea level contribution from reservoir storage to be 85% [70–100%], with the lower limit coming from Pokhrel et al. (2012), of the nominal capacity, or –0.2 mm yr^{-1} over 1971–2010.

Human-induced groundwater depletion partly cancels the effect of reservoir storage. For example, Konikow (2011) estimated this contribution to be 0.26 ± 0.07mm yr^{-1} over 1971–2008 and 0.34 ± 0.07 mm yr^{-1} over 1993–2008 (based mostly on observational methods to estimate change in water storage), whereas Wada et al. (2012) estimated values of 0.42 ± 0.08 mm yr^{-1} over 1971–2008 and 0.54 ± 0.09 mm yr^{-1} over 1993–2008 (based on modelling of water fluxes). We use the average of these two series with the difference as a measure of the uncertainty. Pokhrel et al. (2012) also estimated groundwater depletion, but Konikow (submitted) argued that their underlying assumptions of defining depletion as equivalent to groundwater use, and allowing unlimited extraction to meet water demand, leads to substantial overestimates of depletion.

Accounting for reservoir impoundment, Wada et al. (2012) proposed that the net contribution of changes in human-induced land water storage to sea level is 0.15 ± 0.09 mm yr^{-1} for 1971–2008 and 0.25 ± 0.09 mm yr^{-1} for 1990–2000.

Additional information on global terrestrial water storage is provided by temporal changes in satellite gravity measurements from the GRACE satellite mission since 2002. GRACE cannot separate the contribution of individual water reservoirs nor distinguish between climate and anthropogenic effects. The GRACE-based total water volume trend in the world's largest river basins since 2002 is small and not significantly different from zero (Llovel et al., 2010a; Ramillien et al., 2008). However, given the short time span of GRACE observations, this short-term trend is mostly the result of interannual variability and any long-term trend is not detectable, in agreement with model-based studies. GRACE results also suffer from low spatial resolution and contamination by GIA (Lettenmaier and Milly, 2009). For example, in some river basins adjacent to mountain ranges (e.g., Indus, Ganges, Brahmaputra), GRACE cannot clearly separate land hydrology from glacier mass changes (Matsuo and Heki, 2010), whereas at high latitudes, estimates of GRACE-based water storage change are affected by GIA uncertainty.

In summary, model-based estimates of climate-related changes in water storage on land do not show significant long-term trends for the past decades. On the other hand, human-induced changes (reservoir impoundment and groundwater depletion) have each contributed at least several tenths of mm yr^{-1} SLE. Reservoir impoundment exceeded groundwater depletion for the majority of the 20th century but groundwater depletion has increased and now exceeds current rates of impoundment. Their combined net contribution for the 20th century is estimated to be small.

13.3.5 Ocean Mass Observations from GRACE (2002–2010)

As discussed in Chapter 3, it is now possible to directly estimate the ocean mass change using space gravimetry data from GRACE since 2002 (Cazenave et al., 2009; Chambers, 2006; Chambers et al., 2004; Chambers et al., 2010; Leuliette and Miller, 2009; Llovel et al., 2010b). These measurements represent the sum of total land-ice plus land-water components, and thus provide an independent assessment of these contributions. However, GRACE is also sensitive to mass redistribution associated with GIA and requires that this effect (on the order of –1 to –1.3 mm yr^{-1}; Chambers et al., 2010; Paulson et al., 2007; Peltier, 2009; Tamisiea, 2011) be removed before estimating the ocean mass component. Most recent estimates (e.g.,

Leuliette and Willis, 2011; von Schuckmann and Le Traon, 2011) report a global mean ocean mass increase of 1.2 ± 0.4 mm yr^{-1} over 2005–2010 after correcting of the GIA factor. The associated error results from the low signal-to-noise ratio over the oceanic domain and uncertainty in model-based GIA correction (Quinn and Ponte, 2010). Chapter 3 notes that the GRACE-based ocean mass increase is compatible, within error, with the altimetry based GMSL minus steric trends over the same time span. While the GRACE-based ocean mass is somewhat lower than observed estimates of the total land ice plus land water contributions over 2005–2010, the difference remains compatible with quoted uncertainties (see Section 13.4.6 and Table 13.1).

The simultaneous availability of altimeter, GRACE, and Argo measurements provides a means of testing these relatively new observation systems. In terms of global averages, the sum of global ocean mass from GRACE and global thermosteric sea level change from Argo should roughly equal the total sea level change observed by satellite altimetry, although there is still a missing contribution from the deep ocean below 2000 m. As longer data time series from these observing systems become available, they will provide more powerful constraints on closure of the sea level budget.

13.3.6 Budget of GMSL Rise

Drawing on Sections 13.1–13.5, the budget of GMSL rise (Table 13.1) is analysed for the periods 1901–1990 (the 20th century, excluding the period after 1990 when ice sheet contributions to GMSL rise are likely to have increased; Sections 4.4 and 13.3.1.1), since 1971 (when significantly more ocean data became available and systematic glacier reconstructions began), since 1993 (when satellite sea level altimetry began), and since 2005 (during which ARGO and GRACE data are available). Other contributions, including runoff from melted permafrost, change in atmospheric moisture content, and sedimentation in the ocean, are not considered in the budget because they are negligible compared with the uncertainties.

The observational budget cannot be rigorously assessed for 1901–1990 or 1971–2010 because there is insufficient observational information to estimate ice sheet contributions with high confidence before the 1990s, and ocean data sampling is too sparse to permit an estimate of global mean thermal expansion before the 1970s. For land water storage (Figure 13.4c), we use the GRACE observational estimate for 2005–2010 and the estimated effect of human intervention for the earlier periods, for which global observations are not available. Over the periods 1993–2010 and 2005–2010, allowing for uncertainties, the observed GMSL rise (Sections 3.7 and 13.2.2) is consistent with the sum of the observationally estimated contributions (Table 13.1, Figure 13.4 and 13.5). The two dominant terms are ocean thermal expansion (accounting for about 30% and 40% of the observed GMSL rise for the two periods, respectively, Figure 13.4a and 13.5) and glacier melting (accounting for a further 30% and 45%, Figure 13.4b and 13.5). The closure of the observational budget for recent periods within uncertainties represents a significant advance since the AR4 in physical understanding of the causes of past GMSL change, and provides an improved basis for critical evaluation of models of these contributions (introduced in Section 13.2) in order to assess their reliability for making projections (Sections 13.4 and 13.5.1.1).

Using similar methods to those used in projecting future sea level rise (Sections 13.4, 13.5.1.1), AOGCM-based estimates of the thermal expansion and glacier contributions can be made from the start of the 20th century (Sections 13.3.1.2 and 13.3.2.2, Table 13.1). The sum of these process-based model contributions, and the estimated change in land water storage (Figure 13.4c), which is relatively small, accounts for about 70% of the observed rate of GMSL rise for 1901–1990, and over 80% for 1971–2010 and 1993–2010 (Figure 13.4d and 13.5). Model-based attribution of sea level change to radiative forcings is discussed in Section 10.4.3. We do not consider model-based estimates for 2005–2010, because it is a short period during which interannual climate variability has had a strong effect on GMSL change, notably through the influence of ENSO on ocean mass (Nerem et al., 2010) and heat content (Landerer et al., 2008) and regional variability affecting Greenland warming (Sections 10.5.2 and 13.3.3.2). Such variability is not externally forced and therefore not expected to be reproduced in AOGCM historical experiments.

AOGCM-based models for the ice sheet contributions are not available for the past (Section 13.3.3.2). There is particular uncertainty about the contribution from ice sheet dynamical change, which has not been modelled on the basis of AOGCM input although when calibrated appropriately, dynamical ice sheet models (Section 13.2.3) can reproduce the observed rapid changes in ice sheet outflow for example Graversen et al. (2011) for Greenland, Gladstone et al. (2012) for Pine Island Glacier in Antarctica. If increasing ice sheet

outflow explains half the contribution from Greenland during 1993–2010 and all of that from Antarctica (Section 13.3.3.2), it would amount to about 6 mm, which is about 10% of the GMSL rise during that period, and about 3% of the GMSL rise during 1901–2010 (Chapter 4). Thus, this contribution has also been relatively small up to now. Nonetheless, the omission of ice sheet models, especially of dynamics, from the model budget of the past means that we cannot place the same level of confidence in them as in other contributions.

Within the uncertainties, the residual during 1971–2010 and 1993–2010 (observed rate of GMSL change minus the sum of the modelled terms and the contribution from land water storage; Table 13.2, Figure 13.4f) is consistent with zero. The residual for 1993–2010 (0.2 [–0.6 to 1.1] mm yr^{-1}) is also consistent with the sum of the observed ice sheet contributions (0.5 [0.4 to 0.6] mm yr^{-1}). The sum of model-based contributions shows an increase in rate from 1990, as also observed in the GMSL record estimated from tide gauges (Figure 13.4f). Increasing loss of mass by the ice sheets (Figure 13.4g), not included in the models, also contributes to the observed increase in rate. This improved explanation of past GMSL rise is a further scientific advance relative to the AR4, and is a reason for confidence in using these same process-based models and methods for projections.

The residual of 0.5 [–0.1 to 1.0] mm yr^{-1} for 1901–1990 is also consistent with zero, but is the largest as a fraction of observed GMSL rise for any of the periods considered. We quantify four potential contributions to this residual (Figure 13.4e). Firstly, we consider modelled SMB for Greenland for the 20th century (Section 13.3.3.2) and since 1960 (Table 13.2, Figure 13.6), since observational data are not available. The model data show considerable spread and variability for most of the period, and a positive tendency since 1990. Secondly, there could be a relatively constant contribution from the Antarctic ice sheet (Gregory et al., submitted; Huybrechts et al., 2011) due to long-term adjustment to climate change in previous millennia. Geological evidence constrains such a contribution not to exceed ~0.2 mm yr^{-1} (Section 13.2.1), and we show an illustrative value of 0.1 mm yr^{-1}. Thirdly, part of the residual could also arise from the possible underestimate of 0.16 mm yr^{-1} in thermal expansion due to AOGCM preindustrial simulations not including volcanic forcing (Section 13.3.1.2). Fourthly, the unusually warm conditions in the Arctic during the 1930s, attributed to unforced climate variability and not simulated by AOGCMs, likely produced a greater mass loss by glaciers in high northern latitudes (Section 13.3.2.2).

The sum of these four additional terms captures much of the trend and some of the variability in the residual time series (Figure 13.4f). We add these terms to the modelled thermal expansion and glacier terms and the estimate of land water storage (Figure 13.4d). The rate of GMSL rise from the sum is similar to the observed rate of rise (Figure 13.4g). Both have a minimum in the 1960s and larger values over the last few decades. While the uncertainties in the contributions are larger for the 20th century as a whole than for recent decades, we consider that the evidence now available gives a clearer account than in previous IPCC assessments of 20th century sea level change. The projections (see Sections 13.4 and 13.5, but with the Marzeion et al. (submitted) glacier model only as the other models are not available for this period) from 1996 are also consistent with the satellite and *in situ* observations of GMSL change (Figure 13.5c).

[START BOX 13.1 HERE]

Box 13.1: The Global Energy Budget

A fundamental aspect of the Earth's climate system is the global energy balance, which is dependent on many phenomena of the system. The ocean has stored over 90% of the increase in energy in the climate system over recent decades (Box 3.1), resulting in ocean thermal expansion and hence sea level rise (Chapter 9, Section 13.4). Thus the energy and sea level budgets are linked and must be consistent (Church et al., 2011b).

At the top of the atmosphere (TOA), the boundary of the climate system, the balance involves shortwave radiation received from the sun, shortwave radiation reflected and long-wave radiation emitted by the Earth (Chapter 1). The rate of storage of energy in the Earth system must be equal to the net downward radiative flux at the TOA, this flux being the difference between radiative forcing, due to changes imposed on the system, and the radiative response of the system. There are also significant transfers of energy between components (atmosphere, Chapter 2; ocean, Chapter 3; cryosphere, Chapter 4) of the climate system

(Trenberth et al., 2009) and from one location to another. All of these transfers impact the global energy budget.

Tracking the Earth's energy budget over years to decades and longer is a critical element in understanding climate variability and change (Trenberth, 2009; 2010; Trenberth and Fasullo, 2010). Here we focus on the Earth's global energy budget since 1970, when better global observational data coverage is available.

The radiative forcing of the climate system (Chapter 8) has increased as a result of a increase in solar irradiance, increases in well-mixed (long-lived) greenhouse gas concentrations and contributions from changes in short-lived greenhouse gases (tropospheric and stratospheric ozone and stratospheric water vapour; Box 13.1, Figure 1a). Volcanic eruptions (two major eruptions since 1970, El Chichón in Mexico in 1982 and Mount Pinatubo in the Philippines in 1991, and other smaller eruptions) have injected aerosols into the stratosphere, reflecting some of the incoming solar radiation, and thus give a negative radiative forcing, which persists for a couple of years, temporarily offsetting the increased forcing from greenhouse gases. Changes in the surface albedo from land use change have led to a greater reflection of short-wave radiation back to space. Tropospheric aerosols have a greater influence; they predominantly reflect sunlight and enhance brightness of clouds which reflects more sunlight, reinforcing their negative radiative forcing. Black carbon, including that on snow and ice, is a small positive radiative forcing but is not included here. The integrated impact of these forcings is an energy gain over this period (Box 13.1, Figure 1).

[INSERT BOX 13.1, FIGURE 1 HERE]

Box 13.1, Figure 1: The Earth's energy budget from 1970 through 2010. **(a)** The cumulative energy flux into the Earth system from changes in solar forcing, well-mixed and short-lived greenhouse gases, changes in surface albedo, volcanic forcing and tropospheric aerosol forcing are shown by the coloured lines and these are added to give the total energy changes (dashed black line). **(b)** The cumulative total energy change from (a), with an expanded scale, is balanced by the warming of the Earth system (energy absorbed in the melting of ice and warming the atmosphere, the land and the ocean) and an increase in outgoing radiation inferred from temperature change of a warming Earth. These terms are represented by the time-varying thicknesses of the coloured regions. The residuals in the cumulative energy budget are indicated by the difference between the red lines and the horizontal zero line. The full-drawn line is for a climate feedback parameter α of 1.23 W m^{-2} ºC^{-1}, equivalent to a radiative forcing for a doubled CO_2 concentration of 3.7 W m^{-2} (Forster et al., Chapter 2, AR4) combined with an equilibrium climate sensitivity of 3.0°C (assessed in Box 12.1 to be the most likely value). Following Box 12.1, the climate feedback parameter α is likely to be in the range from 0.82 W m^{-2} ºC^{-1} (corresponding to an equilibrium climate sensitivity of 4.5ºC) to 1.85 W m^{-2} ºC^{-1} (corresponding to an equilibrium climate sensitivity of 2.0 ºC).

As the climate system warms, energy is lost to space through increased outgoing radiation. This radiative response by the system is predominantly due to increased thermal grey-body radiation, but is modified by climate feedbacks, such as changes in water vapour, surface albedo and cloud, which affect both outgoing long-wave and reflected shortwave radiation. The TOA fluxes (Chapter 2) have been measured by the Earth Radiation Budget Experiment (ERBE) satellites from 1985 to 1999 (Wong et al., 2006) and the Cloud and the Earth's Radiant Energy System (CERES) satellites from March 2000 to the present. The TOA radiative flux measurements are highly precise, allowing identification of changes in the Earth's net energy budget from year to year within the ERBE and CERES missions (Kato, 2009; Stackhouse Jr et al., 2010), but the absolute calibration of the instruments is not sufficiently accurate to allow determination of the absolute TOA energy flux or to provide continuity across missions (Loeb et al., 2009). Following Murphy et al. (2009), Box 13.1, Figure 1b relates the cumulative total energy change of the Earth system to the change in energy storage and the cumulative outgoing radiation. Calculation of the latter is based on the observed globally averaged surface temperature ΔT, which is multiplied by the climate feedback parameter α, which in turn is related to the equilibrium climate sensitivity (see Section 9.7.2.1). The mid-range value for α of 1.23 W m^{-2} ºC^{-1} is equivalent to a radiative forcing for a doubled CO_2 concentration of 3.7 W m^{-2} (Forster et al., 2007) combined with an equilibrium climate sensitivity of 3.0°C (assessed in Box 12.1 to be the most likely value). Following Box 12.1, the climate feedback parameter α is likely to be in the range from 0.82 W m^{-2} ºC^{-1} (corresponding to an equilibrium climate sensitivity of 4.5ºC) to 1.85 W m^{-2} ºC^{-1} (corresponding to an equilibrium climate sensitivity of 2.0ºC).

If the radiative forcing were fixed, the climate system would eventually warm sufficiently that the radiative response would balance the radiative forcing, and there would be zero net heat flux into the system. However, the forcing is increasing and the ocean's large capacity to store heat means the climate system is

not in radiative equilibrium (Hansen et al., 2005), and has stored energy (Box 13.1, Figure 1b; Box 3.1). This storage provides strong evidence of a changing climate. The majority of this additional heat is in the upper 750 m of the ocean but there is also warming in the deep and abyssal ocean (Box 3.1). The associated thermal expansion of the ocean has contributed about 40% of the observed sea level rise since 1970 (Section 13.4.2.2.6; Church et al., 2011b). A small amount of additional heat has been used to warm the continents, warm and melt glacial and sea ice, and warm the atmosphere (See Box 3.1 and Box 13.1, Figure 1b).

The magnitude of the residual in the energy budget in 2010 (Box 13.1, Figure 1b, red line) is about 10% of the total energy accumulated for the central value of climate sensitivity of 3°C. A positive residual would mean that the cumulative forcing is apparently greater than the heat lost and stored by the system. Over the period from 1970 to 2012, this residual is small, less than 0.2 W m^{-2}, and is consistent with a climate sensitivity well within the range of climate sensitivities of 2.0°C–4.5°C (Chapter 10.9 and Box 12.1). Most of this residual occurs in the last 15 years and would imply a small unaccounted negative forcing of the climate system or a climate sensitivity slightly less than 3.0°C but within the range of accepted values. Nevertheless, with any of these choices, the residual is smaller than the uncertainties and confirms our understanding of climate change and provides evidence that no major forcings of climate are omitted in current climate assessments (see also Footnote 13.1).

In addition to these forced variations in Earth's energy budget, there is also internal variability on decadal time scales. Observations and models indicate that (because of the very small heat capacity of the atmosphere) a decade of steady or even decreasing surface temperature can occur in a warming world (Easterling and Wehner, 2009; Palmer et al., 2011). GCM simulations indicate these periods are associated with a transfer of heat from the upper to the deeper ocean, of order 0.1 W m^{-2} (Katsman and van Oldenborgh, 2011; Meehl et al., 2011), with a near steady (Meehl et al., 2011) or an increased radiation to space (Katsman and van Oldenborgh, 2011), again of order 0.1 W m^{-2}. While these natural fluctuations represent a large amount of heat, they are significantly smaller than the anthropogenic forcing of the Earth's energy budget (Huber and Knutti, 2012).

These independent estimates of radiative forcing, observed heat storage and surface warming combine to give an energy budget for the Earth that is very likely closed, and is consistent with our best estimate of climate sensitivity. Changes in the Earth's energy storage are thus a powerful observation for the detection and attribution of climate change (Gleckler et al., 2012; Huber and Knutti, 2012).

[INSERT FOOTNOTE 13.1 HERE]

Footnote 13.1: The geothermal heat flux is small (less than 2×10^{21} J from 1970 to 2010; Pollack et al., 1993) and changes little over the period considered. Although increasing rapidly, the energy released by the burning of fossil fuels is also small.

[END BOX 13.1 HERE]

13.4 Projected Contributions to Global Mean Sea Level

13.4.1 Ocean Heat Uptake and Thermosteric Sea Level Rise

Over 90% of the net energy increase of the climate system on multiannual timescales is stored in the ocean (Box 3.1). GMSL rise due to thermal expansion is approximately proportional to the increase in ocean heat content. Because the expansion of sea water per degree of warming is greater at higher temperature and higher pressure, the constant of proportionality depends on the distribution of warming in the ocean, and thus varies among models (Körper et al., submitted; Russell et al., 2000).

In projections of the early decades of the 21st century, the upper ocean dominates the heat uptake, and heat content rises roughly linearly with global mean surface air temperature (SAT; Körper et al., submitted; Pardaens et al., 2011b). On multidecadal timescales under scenarios of steadily increasing radiative forcing, the global mean rate of ocean heat uptake is approximately proportional to the global mean SAT change from equilibrium (Gregory, 2000; Gregory and Forster, 2008; Rahmstorf, 2007b), with the constant of proportionality (in W m^{-2} K^{-1}) being the ocean heat uptake efficiency κ.Thus, the rate of ocean heat uptake is projected to increase while the radiative forcing increases, and heat uptake can be scaled with reasonable

accuracy to radiative forcing or SAT change in order to make an estimate for one scenario, based on model results for another scenario, at a particular time in the future, provided that the scenarios have a sufficiently similar time profile (Gregory and Forster, 2008; Katsman et al., 2008; Meehl et al., 2007).

The ocean heat uptake efficiency quantifies the effect of ocean heat uptake on moderating time-dependent climate change (Raper et al., 2002). In the model average of CMIP3 and CMIP5 AOGCMs, κ is about half the magnitude of the climate feedback parameter α. Neglecting the small fraction of heat stored other than in the ocean, the transient climate response can be approximated as $F_{2\times}/(\alpha+\kappa)$, where $F_{2\times}$ is the radiative forcing due to doubling CO_2 (Raper et al., 2002). The CMIP3 and CMIP5 spread in α is about twice as large as that in κ; the former dominates the spread in projections of surface warming for a given forcing scenario, but their contributions to the spread in projections of ocean heat uptake are more similar (Dufresne and Bony, 2008; Geoffroy et al., submitted-b; Gregory and Forster, 2008; Knutti and Tomassini, 2008; Kuhlbrodt and Gregory, submitted). On timescales of many decades or in scenarios of constant or decreasing radiative forcing, a constant κ is an inadequate assumption (Rahmstorf, 2007b), and a good representation of AOGCM behaviour is obtained by distinguishing an upper layer associated with surface temperature from a lower layer which has the majority of the heat capacity (Bouttes et al., submitted; Geoffroy et al., submitted-a; Held et al., 2010).

In the ocean interior, heat is transported by large-scale motion, eddies and turbulent mixing, the last of which is parametrised as thermal diffusion. Observed thermal expansion in the upper 700 m is well matched by an upwelling-diffusion model with observationally determined parameters by Marčelja (2010); using AR4 global SAT projections, this model gives thermal expansion projections in the lower half of the AR4 range for each SRES scenario. Observed ocean heat uptake has been used in conjunction with observed global SAT change to constrain the ocean thermal diffusivity and hence projections of thermal expansion in EMICs (Knutti and Tomassini, 2008; Sokolov et al., 2010). For scenario A1B, Sokolov et al. (2010) obtained a range of thermal expansion projections which was lower than the AR4 range when using the observational dataset of Levitus et al. (2005) as a constraint, and greater than AR4 when using Domingues et al. (2008). Kuhlbrodt and Gregory (submitted) demonstrate a significant correlation between κ and the vertical temperature profile in the ocean model in CMIP5 AOGCMs. From these studies, it appears that observations of heat uptake could have the potential to constrain significantly the representation of relevant ocean heat transport processes in AOGCMs.

Because the ocean integrates the surface heat flux, thermal expansion projections following different scenarios do not significantly diverge for several decades. Scenarios assuming strong mitigation of greenhouse gas emissions begin to show a reduced rate of thermal expansion beyond about 2040; the amount by 2100 is about one-third less than in a typical non-mitigation scenario (Körper et al., submitted; Pardaens et al., 2011b; Washington et al., 2009), and half as much in RCP2.6 as in RCP8.5 (Yin, submitted; Section 13.5.1.1). The integrating effect also means that annual time series of thermosteric sea level rise show less interannual variability than time series of global SAT.

Ocean heat uptake and thermal expansion take place not only while atmospheric GHG concentrations are rising, but continue for many centuries after stabilization of radiative forcing, at a rate which declines only slowly (Figure 13.6; Meehl et al., 2007; Meehl et al., 2005; Solomon et al., 2009). This is because the timescale for warming the deep ocean is much longer than for the shallow ocean (Gregory, 2000; Held et al., 2010). While the approximation that the rate of thermosteric sea level rise increases with the temperature elevation above preindustrial is valid for initial periods of increasing temperature, the rate is reduced when temperature stabilization begins (Schewe et al., 2011). The rate and the stabilization timescale for thermal expansion depend on the GHG stabilization level. For the highest scenarios RCP8.5 thermosteric sea level rise can reach up to 2 m in the year 2500. Nonlinear changes in ocean circulation, particularly due to a reduction in deep water formation, can also have a large effect on global ocean heat uptake (Fluckiger et al., 2006; Levermann et al., 2005; Vellinga and Wood, 2008).

13.4.2 Glaciers

The 21st century sea level contribution from glaciers presented in the AR4 assessment (Meehl et al., 2007) ranged from 0.06 to 0.15 m SLE by 2100 across a range of scenarios. Some subsequent estimates, published between 2007 and 2009, ranged from 0.08 to 0.55 m SLE by 2100. These analyses, not based on direct,

scenario-dependent SMB models forced by AOGCMs, used a variety of methods of projecting future losses from glaciers, and were developed in response to two significant handicaps, now to a large degree eliminated: the absence of a global compilation of contemporary glacier loss rates after 2005 to provide initial conditions, and the absence of a complete global glacier inventory to provide area and hypsometric boundary conditions for mass balance modeling. The alternate approaches included extrapolation from contemporary observed rates (Meier et al., 2007; Bahr et al., 2009; Pfeffer et al., 2008). Extrapolation permits partial accounting of calving losses, while accumulation area ratio (AAR) equilibration has fairly strong physical and theoretical underpinnings. These strengths partially offset the weaknesses of these models, which include, in the case of extrapolation, an assumption of statistical stationarity that may not be valid, while the AAR equilibration approach gives only a final steady-state value so that rates or cumulative losses at any intermediate time must be estimated by other means, such as area-response time scaling. Most significantly, however, neither of these methods use future climate forcing as inputs, so there is no opportunity to use knowledge obtained from atmospheric modelling or other sources of information about future relevant conditions to adjust these projections. Refinements of these methods are nevertheless still used to advantage.

Two crucial developments in 2011 improved the prospects for assessing present-day glacier contributions to sea level and making improved projections. The first was the compilation and analysis of mass balance data for the 2005–2010 pentad, as discussed in 13.4.2.1 and in Chapter 4. The second was the creation and publication of the Randolph Glacier Inventory (RGI; Arendt et al., 2012), the first globally complete glacier inventory, assembled as a minimal outline inventory specifically for assessment and mass balance modelling for AR5. The details of the evolution of the RGI, and aggregate area and derived volume estimates are discussed in Chapter 4. As a consequence of these developments, several scenario-dependent SMB model projections have been produced in late 2011 and early 2012, including those by Slangen et al. (submitted), Marzeion et al. (submitted) and Radic et al. (submitted). Projections using these models are summarized in Table 13.3. Glacier contributions at 2100, expressed as SLE, range between 0.08 and 0.21 m for RCP2.6, between 0.06 and 0.24 m for RCP4.5, between 0.12 and 0.24 m for RCP6.0, and between 0.10 and 0.30 m for RCP8.5.

Table 13.3: Process-based projection model results using new inventory data for global glaciers and forcing scenarios RCP2.6, 4.5, 6.0, and 8.5. Five non-AOGCM models projections are shown for comparison.

AOGCM-driven models

Source	Year	Projected SLR (m)	Source	Year	Projected SLR (m)
RCP 2.6			**RCP 6.0**		
Marzeion	2100	0.15 [0.08 to 0.21]	Marzeion	2100	0.18 [0.12 to 0.24]
RCP 4.5			**RCP 8.5**		
Radic	2100	0.13 [0.06 to 0.20]	Radic	2100	0.18 [0.10 to 0.25]
Slangen	2090	0.13 [0.01 to 0.15]	Slangen	2090	0.20 [0.16 to 0.23]
Marzeion	2100	0.16 [0.08 to 0.24]	Marzeion	2100	0.21 [0.12 to 0.30]
		0.14 [0.06 to 0.24]			***0.19 [0.10 to 0.30]***

Non-AOGCM Models

Source	Year	Projected SLR (m)	Model Type
NRC	2100	0.14 [0.13 to 0.16]	extrapolation, variable rate
Meier at al. 2007	2100	0.10 [0.08 to 0.13]	extrapolation, fixed rate
	2100	0.24 [0.11 to 0.37]	extrapolation, variable rate
Bahr et al, 2009	Final equilibrium value	0.18 [0.15 to 0.22]	AAR equilibration, fixed AAR
	Final equilibrium value	0.38 [0.35 to 0.39]	AAR equilibration, variable AAR
Mernild et al, submitted	Final equilibrium value	0.23 [0.18 to 0.27]	AAR equilibration, variable AAR
Pfeffer et al, 2008	2100	0.17	Low range projection
	2100	0.24	High range projection

In addition to AOGCM-driven mass balance modelling, two earlier post-AR4 non-processed-based models and two recent projections are available. The Pfeffer et al. (2008) projection, based on a modified type of extrapolation, is described in Section 13.4.4.2. The National Research Council's (Committee on Sea Level Rise in California et al., 2012) report includes global mean sea level projections broken down into components, including steric, ice sheets, and glaciers; the cryospheric components are projected into the future by extrapolation using an uncertainty-weighted scheme that accounts for the quality of the data determining the initial rate conditions. Bahr et al. (2009) and Mernild et al. (submitted) calculate the glacier volume loss required to re-establish equilibrium with climate based on fundamental assumptions about the glacier's AAR at equilibrium. The AAR method is based on simple and robust theory but only gives a final steady state value and is thus an upper bound at intermediate times.

The non-processed based models provide independent checks on the AOGCM-driven mass balance models, and the extrapolation models provide information on future dynamic response to a limited degree. While the non-processed based model do not have the same level of reliability that processed based models have, being founded (with the exception of AAR equilibration models) on far more qualitative assumptions, their correspondence (or lack of correspondence) with process based model provides a check on aspects of the process-based models such as the potential consequence of neglecting calving discharge and dynamic effects. The mean and range of the non-processed based models listed here is 0.21 [0.13–0.29] m SLE, consistent with the process-based models.

[INSERT FIGURE 13.7 HERE]

Figure 13.7: Modeled glacier contributions to sea level from glaciers (including peripheral glaciers surrounding the Greenland and Antarctic ice sheets), from models of Marzeion et al. (submitted), Radic et al. (submitted), and Slangen et al. (submitted).

Further unresolved uncertainties include the potential for near-term dynamic response from marine-ending glaciers. While the discharge from many glacier regions includes a large calving fraction, dynamic discharge from glaciers is limited in comparison to potential discharge from the ice sheets because of the limited ice volume held in upstream reservoirs. On decadal time scales, however, dynamic losses may be an important component of total sea level rise. In Alaska, 14% of the total glacier area drains through tidewater outlets; the fraction of the region's loss rate through calving is unknown at this point, but the potential for significant dynamic losses is evident. Completion of the global inventory at even a very basic level has allowed large improvements in assessment and modelling, but further uncertainties related to the inventory remain to be resolved, including those arising from the size cutoff decided for the inventory (Bahr and Radic, 2012). Another source of uncertainty is interception of glacier runoff by land hydrology. Despite rapidly growing knowledge of the significance of changing groundwater in sea level rise, especially with the growing reliability of GRACE gravity analyses, glacier mass losses rates are generally assumed to flow directly to the ocean, with no delay or interception by surface or aquifer storage. While discharge from glaciers located near coasts (e.g., Canadian Arctic, Patagonia, Alaska, ice sheet peripheries) has little potential for interception by terrestrial reservoirs, but runoff from regions in continental interiors (e.g., Alps, High Mountain Asia) may be significantly depleted before reaching the ocean. Whether terrestrial interception has any significant effect on net glacier contributions to sea level rise is undetermined at this time.

13.4.3 Greenland Ice Sheet

13.4.3.1 Surface Mass Balance Change

Greenland SMB is positive in the present climate but shows a decreasing trend (Section 13.3.3.2), which implies an increasing contribution to GMSL rise. Like the AR4, all recent studies have indicated that the future sea level contribution from Greenland SMB change will be increasingly positive, because the increase in ablation (mostly runoff) outweighs that in accumulation (mostly snowfall), and that scenarios of greater radiative forcing lead to a larger sea level contribution (for instance RCP8.5 compared with RCP4.5).

Precipitation is projected to increase at about 5% per °C of annual-mean warming over Greenland, but the increase in snowfall is smaller because the fraction of rain increases as temperature rises (Fettweis et al., submitted; Gregory and Huybrechts, 2006). Ablation is computed using either a surface energy balance

model (EBM), which may be stand-alone or part of a regional climate model, or from surface air temperature using an empirical temperature-index method, mostly commonly the positive-degree-day (PDD) method, in which melting is proportional to the time-integral of temperature above freezing point. Fettweis et al. (2008) and Franco et al. (2011) followed a hybrid approach, in which they derived a regression relationship from RCM simulations of the recent past between annual anomalies in climate and in Greenland SMB, then applied it to project future Greenland SMB from projected future climate anomalies. This method depends on the assumption that a relationship derived from past variability will also hold for future forced climate change.

Several post-AR4 studies of the 21st century can be readily compared with one another and the AR4 because they are all based on CMIP3 AOGCM results for scenario SRES A1B, and there is a similarly comparable group of results based on CMIP5 AOGCM results for scenario RCP4.5 (see Table 13.4). Most of these studies carried out time-dependent simulations, thus removing the need to scale the results, as was necessary with the time-slice simulations available at the time of the AR4. For these two scenarios, results lie in the range 0.00–0.13 m. In studies of Greenland SMB change, the time-integral of the Greenland SMB anomaly with respect to a reference period is interpreted as a contribution to GMSL rise, on the assumption that the ice sheet was in approximate mass balance during the reference period (see discussion in Section 13.1.5.1 and 13.3.3.2); such an assumption can be avoided only if ice sheet outflow is also modelled.

Most of the studies in Table 13.4 give ranges of results, derived from sets of AOGCMs; it is evident that the spread in the magnitude and patterns of Greenland climate change projected by the AOGCMs causes a large spread in the projected contribution to GMSL rise. Yoshimori and Abe-Ouchi (2012) found that the inter-model spread in global SAT change accounts for about 60% of the spread in the change of projected Greenland ablation. Two important contributions to the remaining spread are the weakening of the Atlantic meridional overturning circulation, which affects the magnitude of warming over Greenland, and the SAT of Greenland in the model control climate, which affects the sensitivity of melting to warming (Fettweis et al., submitted; Yoshimori and Abe-Ouchi, 2012).

The treatments of melting and meltwater refreezing differ among models and are an important source of uncertainty in SMB simulations. Bougamont et al. (2007) found that a PDD method gave larger ablation and smaller refreezing than an EBM, resulting in almost twice as large an increase in runoff. Other authors have also reported sensitivity to choice of parameters in the PDD method (Graversen et al., 2011). A comparison of four different RCMs forced by the same AOGCM results (Rae et al., submitted) showed that the simulated SMB was particularly sensitive to the snow-albedo parameterisations of melting and on the allowance for refreezing. From analysis of RCM results, van Angelen et al. (2012) reported that the fraction of meltwater that refreezes decreases from about 50% to about 30% during the 21st century, with a consequent increase in runoff, on account of warming of the firn and reduction of pore space due to greater penetration of liquid water from rain and melting. Fettweis et al. (submitted) showed that the meltwater runoff increases faster than linearly with temperature increase because of reduced albedo and refreezing due to expansion of the area of bare ice.

Another source of model spread is the representation of topography. Bengtsson et al. (2011) found that precipitation and ablation are both larger when simulated at lower horizontal resolution because of its associated lower topography. This allows precipitation to spread further inland because of reduced topographic barriers, and enhances ablation because there is more area at lower, warmer altitudes. Seddik et al. (2012) obtained different SMB results from the same climate input and PDD scheme in two thermomechanical ice sheet models; the one with higher surface altitude and consequently colder surface conditions at the ice sheet margins gave smaller mass loss. Most of the models in Table 13.4 use a fixed Greenland topography, and thus cannot simulate the positive feedback on ablation which can be expected as the ice sheet surface becomes lower; to include this, dynamical models are required.

Fettweis et al. (submitted) ran their RCM with boundary conditions from three AOGCMs and two scenarios, and from these results fitted a polynomial function for the Greenland SMB change in terms of global mean SAT change. In Table 13.4, we show the range they obtained by applying this formula to the CMIP5 ensemble of global mean SAT change projections under RCP4.5, and the range computed from the same input with the set of polynomials (Gregory and Huybrechts, 2006) used in the AR4. This comparison with the same reference period (the AR4 used the late 19th century for the reference period) indicates that the

formulae derived from the PDD model of Gregory and Huybrechts (2006) predict a smaller SMB change than the RCM of Fettweis et al. (submitted). However, other studies using temperature index methods (Graversen et al., 2011; Yoshimori and Abe-Ouchi, 2012) have ranges extending to higher values than Fettweis et al. (submitted), so there does not appear to be a dominant bias resulting from the SMB method.

Table 13.4: Contribution to sea level rise from change in the surface mass balance of the Greenland ice sheet during the 21st century. Where given, ranges are 5–95% estimated from the published results and indicate the uncertainty due to the climate change modelling by AOGCMs, except where noted otherwise.

Reference	Model[a]	Contribution to Global Mean Sea Level Rise			
		starting from	up to	amount (m)[b]	rate (mm yr^{-1})[b]
Scenario SRES A1B, CMIP3 AOGCMs					
AR4 (Meehl et al., 2007)	20 km PDD[c]	1990	2090–2099	0.01–0.08[d]	0.3–1.9[d]
Bengtsson et al. (2011)[e]	60 km (T213) EBM	1959–1989	2069–2099	—	1.4
Fettweis et al. (2008)	TI from 25 km EBM	1970–1999	2090–2099	0.03–0.05	0.3–1.0
Graversen et al. (2011)	10 km PDD	2000	2100	0.02–0.08 0.00–0.17[f]	 0.0–2.1[f]
Mernild et al. (2010)	25 km EBM	1980–1999	2070–2079	0.02	0.5
Rae et al. (submitted)[g]	25 km EBM	1980–1999	2090–2099	0.01, 0.04, 0.06	0.3,1.2,1.5
Seddik et al., (2012)[h]	10 km[e] PDD	2004	2104	0.02, 0.04	—
Yoshimori and Abe-Ouchi (2012)	1–2 km TI	1980–1999	2100	0.02–0.13	0.2–2.0
Scenario RCP4.5, CMIP5 AOGCMs					
Fettweis et al.(submitted)	25 km RCM[c]	1980–1999	2100	0.01–0.08	0.1–1.2 in 2080–2099
Gregory and Huybrechts (2006)[j]	20 km PDD[c]	1980–1999	2100	0.00–0.06	0.0–0.8 in 2080–2099
Van Angelen et al. (2012)[i]	11 km RCM	1990–2010	2100	0.07	1.4 in 2069–2098
Yoshimori and Abe-Ouchi (2012)[j]	1–2 km TI	1980–1999	2090–2099	0.00–0.11	0.0–1.8

Notes:
(a) The spatial resolution is stated and the SMB method denoted by TI = temperature index, PDD = positive degree day, EBM = energy balance model.
(b) The amount of sea level rise is the time-integral of the SMB anomaly from the period or date labelled 'starting from' to the one labelled 'up to'. Unless otherwise indicated, the SMB anomaly is calculated relative to the mean SMB for the 'starting from' period, and the rate of sea level rise is the SMB anomaly in the 'up to' period.
(c) These results are estimated from global mean SAT change, using formulae fitted to results from a Greenland SMB model.
(d) The SMB anomaly is relative to the late 19th century.
(e) This experiment used time-slices, with boundary conditions from the ECHAM5 GCM, rather than a simulation of the complete century, so results are not available for the amount.
(f) Range including uncertainty in choice of emission scenario (B1, A1B or A2), SMB modelling and ice sheet dynamical modelling, as well as uncertainty in climate modelling.
(g) Results are given for the HadRM3P, HIRHAM5 and MAR RCMs driven with boundary conditions from the ECHAM5/MPI-OM AOGCM.
(h) Results are given for two ice sheet models (Elmer/Ice, SICOPOLIS) using the same AOGCM climate boundary conditions. The resolution given is for SICPOLIS; Elmer/Ice has variable resolution.
(i) Boundary conditions from the HadGEM2-ES AOGCM.
(j) Results calculated from CMIP5 AOGCMs by the same method as used in the paper.

On multi-centennial to millennial time scales feedbacks between the regional climate and the ice sheets become increasingly relevant, especially under strong climate change scenarios. Thus beyond the year 2100, coupled climate ice sheet models are used to capture potential feedbacks. These models apply a reduced spatial resolution in order to be computationally efficient enough to compute longer time scales and to combine the different climatic components. Consistent with regional climate models for the 21st century, these models project an increasingly negative surface mass balance (SMB) for the Greenland ice sheet for all warming scenarios (Driesschaert et al., 2007; Mikolajewicz et al., 2007b; Ridley et al., 2005; Swingedouw et al., 2008; Vizcaino et al., 2008; Vizcaino et al., 2010; Winguth et al., 2005; Goelzer et al., submitted;

Huybrechts et al., 2011). A nonlinear increase in ice loss from Greenland with increasing regional radiative forcing is found across different scenarios (Driesschaert et al., 2007). The nonlinearity arises from the increase in both the length of the ablation season and the daily amount of melting.

Surface mass balance on Greenland is controlled by regional climate which is influenced by interactions with sea ice distribution and atmospheric and oceanic circulation. On multi-centennial time scales, Swingedouw et al. (2008) found enhanced ice loss from Greenland in a coupled simulation in which ice topography and melt water flux influence the ocean and atmospheric circulation as well as sea ice distribution. They also found that interactive changes of the Antarctic ice sheet results in reduced ice loss from Antarctica. Vizcaino et al. (2010) found the opposite effect, mainly due to the effect of topographic changes on the surface temperature, but less pronounced in amplitude.

Due to reduced regional temperature on Greenland, Mikolajewicz et al. (2007b) and Vizcaino et al. (2008) found strongly reduced ice loss from Greenland in scenarios with a cessation of the Atlantic meridional overturning circulation (AMOC). Also the most recent model version (Vizcaino et al., 2010) shows a strong weakening of the AMOC (~60% reduction in 560 ppm scenario; ~80% for 1120ppm). The GIS sea level contribution including this effect after 600 years of integration is ~1m (corresponding to an average rate of 1.7 mm yr^{-1}) for 560 ppm CO_2equ and ~3 m (5 mm yr^{-1}) for 1120 ppm CO_2equ. Even though the AMOC weakening in the model by Huybrechts et al. (2011) is less pronounced (10–25%), the ice loss through melting is significantly weaker in this model. During the first 1000 years of integration, GIS contributes 0.35 m (corresponding to an average rate of 0.35 mm yr^{-1}) for 560 ppm CO_2equ and (2.5 mm yr^{-1}) for 1120 ppm CO_2equ. These differences are likely due to differences in the coarse representation of the regional climate.

Using the same model as Huybrechts et al. (2011), Goelzer et al. (submitted) computed the SRES scenarios B1, A1B and A2 with subsequent GHG stabilization after the year 2100. As in Huybrechts et al. (2011), the ice sheet evolution is dominated by the SMB. They find sea level contributions of 1.4, 2.6 and 4.2 m in the year 3000 for the scenarios B1, A1B and B2. The sea level commitment with fixed GHG concentrations at the level of the year 2000 is 0.7 m in their model.

In summary, coupled climate-ice sheet models consistently show an increasingly negative SMB under warming scenarios beyond 2100. Some models find a threshold temperature/increase beyond which the melting of the Greenland Ice Sheet self-amplifies and the ice volume is reduced to less than 30% of its present volume. This threshold behaviour is detailed in Section 13.5.3.2.

13.4.3.2 Dynamical Change

Observations suggest two main mechanisms by which climate change can directly affect the dynamics of ice flow in Greenland (4.4.3 and 4.4.4): by affecting ice loss (outflow) through the calving of ice bergs and marine melt from marine-terminating outlet glaciers (MTOGs), and by altering basal sliding through the interaction surface melt water with the glacier bed. The interaction between SMB and ice flow is a third means by which dynamical change may be indirectly affected by climate change.

Two estimates of the effect of dynmical change in Greenland's contribution to SLR by 2100 have been made on the basis of physical intuition. Pfeffer et al. (2008) developed a low scenario assuming a first-decade doubling of outlet glacier velocity throughout the ice sheet that equates to 93 mm SLR, while a high scenario assumes an order of magnitude increase on the same time scale that contributes 467 mm. Katsman et al. (2011) used a similar methodology. They assumed a doubling of discharge to 2050 (followed by a rapid slowdown to original values) for MTOGs in the east and south, while in the north and for Jakobshavn Isbrae, they assumed a quadrupling by 2100. Their final estimate is 100 mm SLR. These estimates provide a useful context for the following discussion of process-based projections and set an extreme limit of 467 mm but a more plausible one of 100 mm.

Observations provide some constraints on projections of future outflow. Between 2005 and 2010, widespread dynamic thinning of the Greenland ice sheet that expanded from southeastern Greenland up much of western coast (Khan et al., 2010; Luthcke et al., 2006; Wouters et al., 2008). The spatial pattern of thinning is linked predominantly to MTOGs, suggesting that accelerated flow triggered calving-based retreat (Pritchard et al., 2009; Sole et al., 2008). This thinning has been linked to the migration of subtropical water

masses around the coast of Greenland (Holland et al., 2008a) and its occupation of coastal fjords (Christoffersen et al., 2011; Straneo et al., 2010). Yin et al. (2011) assessed output from 19 AOGCMs under scenario A1B. They showed warming of 1.7–2.0°C around Greenland over the course of the 21st century, which suggests that the trend towards increased outflow triggered by warming coastal waters will continue.

Projections of outflow are at a fairly earlier stage. However an expanding literature is now becoming available. Price et al. (2011) modelled the response of the ice sheet to observed recent retreat of its three main MTOGs (Jakobshavn Isbræ, and Helheim and Kangerdlugssuaq Glaciers). At 2100, the projected SLR associate with the three modelled glaciers is 1 ± 0.4 mm. Price et al. (2011) generalise this estimate by scaling to observations of all outlet glaciers (van den Broeke et al., 2009), the resultant SLR is 4 to 8 mm. Total projected SLR then varies between 10 and 45 mm at 2100, if successive retreats are specified with a repeat interval between 50 and 10 years, however these intervals are notional.

Flow-line modelling of MTOGs has shown considerable success in simulating the retreat and associated acceleration of Helheim and Petermann Glaciers (Nick et al., 2012; Nick et al., 2009), as well as Jakobshavn Isbræ (Vieli and Nick, 2011). The same model has been used to project mass loss from the same glaciers (Nick et al., submitted), as well as Kangerdlugssuaq Glacier, using ocean and atmosphere forcing based on scenario A1B. At 2100, projected SLR is 6 to 10 mm, which generalises to 36 to 60 mm with the scaling of Price et al. (2011). This scaling is approximate because it ignores the contribution of outlying glaciers in Greenland, which are not included in van den Broeke et al. (2009), and is employed to scale up from the four glaciers of Nick et al. (submitted) as opposed to the three of Price et al. (2011). Other issues associated with this scaling are discussed below.

The Nick et al. (submitted) retreat chronology is implemented within a 5 km resolution ice sheet model by Goelzer et al. (submitted) as an enhanced SMB term. They introduce their own generalization to include MTOGs not sampled by Nick et al. (submitted) which approximately doubles overall mass loss (likely to be a resolution-dependent underestimate based on the spatial coverage shown in Goelzer et al. (submitted). Associated SLR at 2100 varies between 4 and 12 mm depending which scenario is chosen from Nick et al. (submitted). Two effects are identified which reduce the overall effect of outflow change when introduced into the full ice sheet system. The first is the depletion effect of retreating MTOGs loosing contact with the ocean (and therefore ceasing to experience outflow). The four glaciers sampled by Nick et al. (submitted) all occupy amongst the longest and deepest bedrock troughs in Greenland and so do not exhibit this effect, whereas the many smaller MTOGs not sampled by Nick et al. (submitted) are more likely to lose contact with the ocean. The second is the competition effect of mass loss at the ice sheet margin, which is generated by increased future ablation (and margin retreat) removing ice before it can be subject to outflow.

Two projections from ice sheet models that attempt to capture the effect of increased outflow by enhancing basal sliding generate SLR at 2100 of 9–24 mm (Graversen et al., 2011) and 0–20 mm (Fürst et al., submitted). The latter uses sliding enhancement that is a function of projected coastal water temperature but may have a low bias in comparison to observations (Rignot et al., 2011).

Bindschadler et al. (submitted) and Nowicki et al. (submitted) report an extensive model inter-comparison exercise in which standardised experiments are used to assess the effects of ice shelf melting (in the absence of ice shelves implemented as loss from the grounded marine boundary) on the Greenland ice sheet. A five-model ensemble generates SLR at 2100 of 27, 135 and 249 mm for increases in melt rate of 2, 20 and 200 m yr^{-1} applied uniformly. The most extreme scenario is incompatible with the results assessed thus far (with the exception of the high scenario of Pfeffer et al., 2008) and the imposed forcing is very likely to be unrealistically high (it equates to a constant, sustained calving ~2 km yr^{-1} in a 10 km resolution model). Interestingly, mass loss continues after 500 years even in the most extreme scenario which suggests continued contact with the ocean along a small number of bedrock troughs (Nowicki, submitted).

Observations of basal sliding as a consequence of interactions between surface meltwater with the glacier bed (Bartholomew et al., 2010; Das et al., 2008; Joughin et al., 2008; Sundal et al., 2011) suggest that surface melt water penetrates to the bed of the ice sheet, however its effect on basal sliding is likely to be complex and dependent on details of the subglacial hydrological system (Schoof, 2010). Process-based modelling of these interactions shows great potential (e.g., Hewitt, 2011), however is not yet at stage where it can be used in projections. These effects therefore have to be parameterized in ice sheet models.

Bindschadler et al. (submitted) and Nowicki et al. (submitted) reported a second suite of experiments in which basal sliding is uniformly increased by factors of 2.0, 2.5 and 3.0, with resultant mean SLR at 2100 of 69, 105 and 146 mm from an eight-model ensemble. Shannon et al. (submitted) assessed this effect by developing a parameterization between surface melt and sliding based observations (Bartholomew et al., 2011; van de Wal et al., 2008), in which sliding is only altered if melt is locally present and which acknowledges uncertainty in the form of the relation between melt and basal sliding. Their projected SLR at 2100 is much smaller and varies between –0.5 and 2 mm for a four-model ensemble (sharing two members with Bindschadler et al., submitted). Changes in ice flow merely redistribute mass within the ice sheet, leading to local thinning and compensatory thickening. However, for mass to be lost, and for there to be a SLR contribution, these changes must be linked to either reduced SMB or increased outflow. Shannon et al. (submitted) omitted the former in their experiment but make an additional assessment using the Goelzer et al. (submitted) model of ~0.6 mm, suggesting that this is not the reason for the discrepancy. One potential reason is the uniform use of a large (in comparison to observations) increase in sliding which generates changes where there is no local surface melt and may have an exaggerated effect on SMB. These two studies can not readily be reconciled; however, the work of Shannon et al. (submitted) appears to employ the more realistic forcing. Neither study incorporates the effects that may be triggered by the release of latent heat from increased quantities of melt water within the ice sheet (Phillips et al., 2010) and for which no projections are available.

Finally, we assess the level of interaction between SMB and ice flow. This arises because of the effect that changing ice sheet topography will have on SMB during the 21st century, which is however rarely included in the RCMs used in Section 13.4.3.1 to project SMB. Few studies explicitly determine this effect, however Goelzer et al. (submitted) report that it amounts to an increase of less than 10% over the course of the 21st century with estimates varying according to the type of SMB model used. This figure is similar to the assessment used in the TAR (p 817) of 0 ± 10% (one standard deviation).

Most available projections for outflow in Greenland are consistent with SLR at 2100 below our 60 mm generalization of Nick et al. (submitted). In many cases, projections are substantially lower (in particular Goelzer et al., submitted) and the generalization likely introduces an over estimate because it ignores depletion and competition effects; however all projections omit contributions from outlying glaciers in Greenland which may partially compensate these effects. It is also lies between the two more plausible experiments reported by Bindschadler et al. (submitted) and Nowicki et al. (submitted). This number is regarded as the upper limit of the likely range rather than very likely range because our ability to project ice berg calving is still hampered by inadequate understanding of the links between climate change and ice berg production (in particular the role of fjord water temperature and calving processes) and poor knowledge of the subglacial bedrock topography underlying many outlet glaciers. The lower limit of the likely range is assessed using the lower estimate of Nick et al. (submitted) with the generalization of Goelzer et al. (submitted) and is 12 mm. A likely range for the effect of altered basal lubrication is –1 to 2 mm (Shannon et al., submitted). Issues related to both the lack of projections of the effects latent-heat release on ice flow and the mismatch between Bindschadler et al. (submitted) and Shannon et al. (submitted) prevent the assessment of a very likely range. A likely range for the effects of interaction between SMB and ice flow is assessed as 5–6 mm based on Goelzer et al. (submitted) and the SMB range identified in Section 13.4.3.1.

In summary, dynamic change within the Greenland ice sheet will lead to SLR during the next century with a likely range of 16–68 mm for RCP6.0 (and A1B). We are also unable to assess the equivalent SLR in other scenarios; however a dependency of SLR on scenario is likely to exist. All the available literature suggests that this dynamical contribution to sea level rise will continue well beyond 2100.

13.4.3.3 Possible Irreversibility of Greenland Ice Loss and Associated Temperature Threshold

Model results suggest that, like other climatic subsystems (see Section 12.6.4.4), the Greenland Ice Sheet exhibits a strongly nonlinear and potentially irreversible response to surface warming. These models show a critical threshold in surface warming beyond which self-amplifying feedbacks result in a near complete ice loss on Greenland (Charbit et al., 2008; Driesschaert et al., 2007; Greve, 2000; Ridley et al., 2010; Robinson et al., 2012). If a greater warming is maintained over a multi-millennial time period, the majority of the Greenland Ice Sheet will be lost via changes in SMB over many centuries or millennia. This nonlinear

behaviour is caused by a combination of the surface-elevation feedback (because lower elevations experience more melt) and the surface-albedo feedback (because darker surfaces such as debris-covered ice experience more melt), both of which tend to speed deglaciation.

In assuming that this threshold lies at the temperature at which the overall SMB of Greenland becomes negative Gregory and Huybrechts (2006) estimated the threshold global mean temperature to be 3.1 [1.9 to 4.6]°C above pre-industrial. In a coupled ice sheet-climate model of intermediate complexity Huybrechts et al. (2011) find this threshold at 2.5°C. This is consistent with simulations with the regional climate model MAR (Fettweis et al., submitted). Although the exact regional temperature on Greenland depends on the global climate model projection that supplies the boundary conditions, they find that at around 2.5°C the SMB becomes negative. In their simulations, this threshold is not exceeded in the 21st century under the RCP4.5 scenario and is reached around 2070 under the RCP8.5 scenario. Fettweis et al. (submitted) argue that due to the lack of feedbacks between ice topography and regional climate their projections are likely to underestimate SMB changes.

Comparing three regional climate models, Rae et al. (submitted) find a strong dependence of the threshold on the model formulation of the surface mass balance. Using the high-resolution regional climate model RACMO including a snow model, van Angelen et al. (submitted) find that latent heat release and loss of pore space in the firn layer reduces refreezing of melt water and thereby enhances runoff to the ocean. In their simulation the SMB becomes negative around the year 2050 under the RCP4.5 scenario which represents a significantly stronger sensitivity compared to other studies.

Robinson et al. (2012) find that the sufficient condition of a negative SMB is likely to result in an overestimate of the threshold temperature. While changes in the average SMB over Greenland will be strongly influenced by southern Greenland, this region does not determine the initiation of the self-amplifying feedback. Constraining simulations with a dynamic ice sheet model to changes during the last interglacial, they estimate the threshold to lie between 0.8°C and 3.2°C above pre-industrial with a best estimate at 1.6°C.

The loss of the ice sheet is not inevitable because it has a long timescale. If the CO_2 concentration declines before the ice sheet is eliminated, the ice sheet might regrow. In the light of future GHG emissions, the time scale of ice loss is competing with the time scale of temperature decline after a reduction of GHG emissions (Allen et al., 2009; Solomon et al., 2009; Zickfeld et al., 2009). The outcome therefore depends on both the CO_2 concentration and on how long it is sustained. Charbit et al. (2008) found that loss of the ice sheet is inevitable for cumulative emissions above about 3000 GtC, but a partial loss followed by regrowth occurs for cumulative emissions less than 2500 GtC. Ridley et al. (2010) identified three steady states of the ice sheet. If the CO_2 concentration is returned to pre-industrial when more than 20–40% of the ice sheet has been lost, it will regrow only to 80% of its original volume due to a local climate feedback in one region; if 50% or more, it regrows to 20–40% of the original. Similar states with ice volume around 20, 60–80 and 100% of the initial ice volume are also found in other models (Langden et al., 2012; Robinson et al., 2012).

13.4.4 Antarctic Ice Sheet

13.4.4.1 Surface Mass Balance Change

Projections of Antarctic SMB changes over the 21st century indicate a negative contribution to sea level because of the projected widespread increase in snowfall associated with warming air temperatures (Bracegirdle et al., 2008; Krinner et al., 2007; Uotila et al., 2007). Several studies (Bengtsson et al., 2011; Krinner et al., 2007; Uotila et al., 2007) have shown that the precipitation increase is directly linked to atmospheric warming via the increased moisture holding capacity of warmer air, and is therefore larger for scenarios of greater warming. The relationship is exponential, resulting in an increase of SMB as a function of Antarctic SAT change evaluated in various recent studies with high-resolution (~60 km) models as 3.7% $°C^{-1}$ (Bengtsson et al., 2011), 4.8% $°C^{-1}$ (Ligtenberg et al., submitted) and ~7% $°C^{-1}$ (Krinner et al., 2007). These agree well with the sensitivity of 5.1 ± 1.5$°C^{-1}$ (one standard deviation) of CMIP3 AOGCMs (Gregory and Huybrechts, 2006). In the 21st century, ablation is projected to remain small on the Antarctic ice sheet, because low surface temperatures inhibit surface melting, except near the coast and on the

Antarctic Peninsula, and meltwater and rain continue to freeze in the snowpack (Ligtenberg et al., submitted).

The effect of atmospheric circulation changes on continental-mean SMB is an order of magnitude smaller than the effect of warming, but circulation changes can have a large influence on regional changes in accumulation, particularly near the ice sheet margins (Uotila et al., 2007) where they might induce additional ice flow across the grounding line (Winkelmann et al., accepted). Simulated SMB is strongly and non-linearly influenced by ocean surface temperature and sea ice conditions (Swingedouw et al., 2008). This dependence means that the biases in the model-control climate may distort the SMB sensitivity to climate change, suggesting that more accurate predictions may be obtained from regional models by using boundary conditions constructed by combining observed present-day climate with projected climate change (Krinner et al., 2007). There is a tendency for higher resolution models to simulate a stronger future precipitation increase because of better representation of coastal and orographic precipitation processes (Genthon et al., 2009; Agosta et al., submitted).

For multicentennial to millennial projections, feedbacks between the ice sheet and regional climate need to be accounted for. This is done by use of coupled climate-ice sheet models of intermediate complexity. These models capture the increase in snowfall under future warming, but the regional distribution is represented less accurately. In idealized scenarios of 1% increase per year up to 560 and 1120 ppm CO_2equ with subsequent stabilization, Vizcaino et al. (2010) and Huybrechts et al. (2011) find an initial increase of ice volume due to the additional snowfall during the first 600 years of integration for the 560-ppm stabilization. In both models, the changes in SMB dominate the mass changes during and beyond the first 100 years. After 600 years of integration, Vizcaino et al. (2010) finds a mass gain in the equivalent of 0.15 m of sea level fall (–0.25 mm yr^{-1} on average) when GHGs are stabilized at 560 ppm CO_2equ. For the same experiment and the same period, Huybrechts et al. find a negative sea level contribution of 0.08 m (–0.13 mm yr^{-1} on average). When GHG concentrations are stabilized at 1120 ppm CO_2equ, both models show a net positive sea level contribution after 600 years of integration. Huybrechts et al. find long-term average rate of 2 mm yr^{-1} with a contribution of ~4 m after 3000 years of integration. Vizcaino et al. (2010) find 1.6 m sea level equivalent after 600 years (average rate of about 2.7 mm yr^{-1}). In both models, the ice sheets are not equilibrated with the surrounding climate after the integration period under the 1120 ppm CO_2equ forcing. Though GHG concentrations were stabilized after 120 years of integration, the Antarctic ice sheet continues to contribute to sea level rise at a relatively constant rate for another 480 years in Vizcaino et al. (2010) and 2880 years in Huybrechts et al. (2011). The same model as in Huybrechts et al. (2011) was applied to the three SRES scenarios B1, A1B and A2 with stabilization in the year 2100 by Goelzer et al. (submitted). While they find some grounding line retreat due to basal ice shelf melt, the multi-centennial evolution of the ice sheet is again dominated by the changes in the SMB. For the B1 scenario they find a slightly negative contribution to sea level in the year 3000. Under the A1B scenario, the AIS contributes 0.26 m and under the A2 scenario 0.94 m to global sea level in the year 3000. While surface melting never exceeds snowfall during the 1000 years of integration, the mass flux imbalance that leads to the ice loss is dominated by surface melt while the solid ice discharge after an initial increase shows a significant decrease during the scenario. These simulations include a negative feedback on the regional climate by ice sheet melt through which summer temperatures can be significantly reduced over Antarctica (Swingedouw et al., 2008). Regional climate models with a significantly higher spatial resolution but without climate-ice sheet feedbacks included show a net ice gain until the year 2200 (Agosta et al., submitted; Ligtenberg et al., submitted). For the A1B scenario the average rates of ice gain cover an interval of 1.4 and 1.7 mm yr^{-1} for 2200. For the lower emission scenario E1 values lie within 0.29 and 0.43 mm yr^{-1}.

In summary, both coupled ice sheet-climate models show consistently that the surface melt overcompensates for the increased snowfall and leads to an ice loss for higher GHG concentrations on multi-centennial time scales. The long time period over which AIS continues to lose mass indicates an important role of the feedback between climate and ice sheet. Consistent with regional climate models for the 21st and 22nd centuries, both coarse-resolution coupled models show a positive SMB change for most of the first 100 years of climate change. Due to the inertia in the climate system, regional temperatures continue to rise after that. Together with enhanced solid ice discharge, this results in mass loss of AIS. The corresponding decline in surface elevation increases the surface temperature and leads to further ice loss. Without this feedback regional climate models show a negative contribution of Antarctic SMB change to GMSL.

13.4.4.2 Dynamical Change

The Antarctic ice sheet represents the largest potential source of future SLR (West Antarctica alone has the potential to raise sea level by 3.3 m; Bamber et al., 2009). The rate at which this reservoir will be depleted (and hence sea level rises), however, is not easily quantifiable. SLR is affected by increases in the flux of ice across the grounding line (or outflow) that separates ice resting on bedrock (some of which is not currently displacing ocean water) from the ice shelves (which are floating and therefore already displace their weight in ocean water). Issues associated with the inability of models to reproduce observed changes in the dynamics of the Antarctic ice sheet prevented the AR4 to fully quantify the effect of these changes on future sea level. Since the AR4, progress has been made in understanding the observations (Sections 4.4.3 and 4.4.4), and projections are becoming available. It must, however, be stressed that this field has yet to reach the same level of development of projections as exist for many other components of the Earth system. There is an underlying concern that observations presage the onset of large-scale grounding line retreat in what is termed the Marine Ice Sheet Instability (MISI; Box 13.2) and much of the research assessed here attempts to understand the applicability of this theoretical concept to projected SLR from Antarctica. The following discussion limits itself to quantifying SLR contributions by 2100 because of the relative immaturity of the research area. We pay particular attention to whether projections of ice dynamics can be linked to global temperature and therefore emission scenario, and summarise their longer term consequences beyond 2100.

The studies that are currently available use a wide range of techniques varying from assessments made on the basis of physical intuition (e.g., Pfeffer et al., 2008), through probabilistic extrapolation (Little et al., submitted) to fully-fledged process-based simulation driven by generalized changes in forcing (e.g., Bindschadler et al., submitted) or specific climate projections (Payne et al., submitted). Since the AR4, several studies have attempted to quantify plausible upper limits for SLR from the changing dynamics of the Antarctic ice sheet based on physically tenable changes to ice flow (so-called kinematic methods). Pfeffer et al. (2008) postulated a possible but extreme scenario of 615 mm SLR in which Pine Island and Thwaites Glaciers of the Amundsen Sea sector accelerate to the highest known outlet glacier velocity over the course of a decade, and the East Antarctic glaciers increase velocity by an order of magnitude on the same timescale. A more plausible scenario, based on a doubling of velocity in the next decade for the Amundsen Sea sector, generates 136 mm. Katsman et al. (2011) used a similar methodology to develop modest and severe scenarios. Their modest scenario is based on the continuation of recent trends of increasing ice velocities and generates SLR of 70 to 150 mm. Their severe scenario attempts to capture the consequences of the collapse of the West Antarctic ice sheet through the MISI and has a SLR contribution of 490 mm. These estimates thus limit the potential for contributions to no more than 615 mm by 2100; however it is difficult to place any likelihood on the postulated changes in ice flow.

Little et al. (submitted) addressed one of the limitations of kinematic studies by developing a probabilistic framework for projecting SLR. They first divided Antarctica into sectors and applied linear growth curves based on observations (Rignot, 2008). Results are then weighted according to agreement with observations of the net mass balance of Antarctica (Chen et al., 2009; Velicogna, 2009; Wu et al., 2010), with a resultant upper bound (95th percentile) for net SLR (i.e, including SMB change) of ~170 mm. If the likely change in SMB is removed (13.4.4.1, 10 to 70 mm sea level fall), this equates to a contribution from dynamics alone of 180 to 240 mm. They concluded that SLR higher than 400 mm would require either an implausibly widespread increase in discharge or the collapse of the Amundsen Sea sector.

Accurate process-based modelling of Antarctic dynamics requires both reliable projections of Antarctic climate, in particular of the temperature of coastal water masses and the likelihood of surface melt, and numerical ice flow models that can faithfully represent the physical processes leading to grounding-line migration and its effect on ice outflow. With respect to climate forcing, observations suggest two main mechanisms that may affect the outflow from the ice sheet, both of which are related to ice shelves. The first relates to the increased potential for melt ponds to form on the upper surface of the ice shelves, which may destabilize them. The second relates to increasing submarine melt experienced by ice shelves leading to their thinning and acceleration of outflow.

A recent example of the fracture-based collapse of an ice shelf caused by surface melt water is the Larsen B ice shelf; similar collapses have also occurred along the length of Antarctic Peninsula (Cook and Vaughan, 2010) which were associated with the acceleration of outflow (De Angelis and Skvarca, 2003); Rignot et al.,

2004; Scambos et al., 2004). A detailed assessment (Kuipers Munneke et al., submitted) using regional climate modelling with A1B and E1 scenarios suggests that most ice shelves in the Peninsula will be susceptible to collapse over the 21st century, whereas of the ice shelves fringing the main Antarctic ice sheet, only the small Abbott ice shelf may be affected. Using an intermediate complexity model with scenario A2, Fykes et al. (2010) find high surface melt over the ice shelves of the main Antarctic ice sheet by 2500.

Pine Island Glacier (PIG) and the neighbouring Smith and Thwaites Glaciers in the Amundsen Sea sector are the focus of current mass loss in Antarctica (Pritchard et al., 2009; Rignot et al., 2008; Shepherd and Wingham, 2007) which is associated with grounding line retreat of 19 ± 2 km between 1992 and 2011 (Park et al., submitted). Thoma et al. (2008) proposed that this mass loss was initiated by the upwelling of relatively warm Circumpolar Deep Water (CDW) on to the continental shelf between the late 1980s and early 1990s. CDW has been found under the Pine Island ice shelf in this sector (Jenkins et al., 2010) and its presence is thought to have led to increased melt and ice shelf thinning. These observations have focussed attention on the potential of warming coastal waters to trigger changes in ice flow dynamics. At present, it is not possible to assess whether the upwelling of CDW is related to global mean temperature.

Yin et al. (2011) assessed output from 19 AOGCMs under scenario A1B to determine how subsurface temperatures are projected to evolve around the ice sheets. They showed decadal-mean warming of 0.4°C–0.7°C and 0.4°C–0.9°C around Antarctica (25th to 75th percentiles of ensemble, West and East, respectively) between 1951–2000 and 2091–2100. More detailed regional modelling using scenario A1B illustrates the potential for warm water to invade the cavities underlying the large Filchner-Ronne ice shelf in the second half of the 21st century, with an associated 20-fold increase in melt (Hellmer et al., 2012). Timmermann and Hellmer (submitted) obtained compatible results with a different model for the Filchner-Ronne ice shelf, as well as finding similar increases in melt for the Ross and Amery ice shelves in the 22nd century.

Accurate modelling of grounding-line dynamics is fundamental to our ability to project Antarctica's future contribution to SLR because these dynamics are the primary control on changes in ice outflow. Accurate simulation of these dynamics presents a major challenge to ice sheet models (see Box 13.2), however, which has been addressed by either employing parameterizations of the processes at work (Pollard and DeConto, 2009) or resolving these processes at sub-kilometre model resolution (Durand et al., 2009). While the former approach is thought adequate for modelling steady states, it may be incorrect for transient behaviour on centennial timescales (Pattyn et al., submitted). Grounding line motion warrants detailed attention in models attempting to make projections and, in particular, in assessing the potential for MISI (Gudmundsson et al., submitted).

Several projections have now been made of PIG's future evolution. Joughin et al. (2010) used a high-resolution model that is potentially capable of simulating grounding line retreat accurately, although retreat is actually limited to ~25 km and a new equilibrium position established within 100 years. This retreat is associated with SLR of 27 mm with more likely melt scenarios generating <18 mm. Gladstone et al. (2012) used a flow line model forced using ocean-model output (Hellmer et al., 2012), and identified two modes of retreat: one where the grounding line stabilizes in a similar position to that identified by Joughin et al. (2010), and a second that is characterized by complete collapse from 2150 onwards. Both studies support the findings of Gudmundsson et al. (submitted) that grounding-line retreat, if triggered, is not unstoppable but may halt if local buttressing from ice rises or channel sidewalls is sufficient. These studies differ, however, with a simpler analysis based on prescribed thinning, in which ice velocity increases by approximately an order of magnitude during retreat in response to the imposed removal of PIG ice shelf (Thomas et al., 2011). Cornford et al. (submitted) illustrated the effects of model resolution on the simulated retreat of PIG by comparing experiments that differ only in their grid resolution, in which the grounding line remains motionless at 4 km resolution but retreats ~100 km in 50 years at 125 m resolution. Parizek et al. (submitted) used a flow-line model to study neighbouring Thwaites Glacier (TG) and find that, in the standardized experiments of Bindschadler et al. (submitted), ocean forcing has a limited ability to generate grounding line retreat but that catastrophic retreat is potentially possible although not in the next century. These early results for PIG and TG illustrate the complexity of modelling grounding line retreat with both numerical challenges (i.e., model resolution) and intricate physical processes (i.e., the subtle balance of stresses at the grounding line) to contend with.

An interesting consequence of likely increased snowfall over the next century (Section 13.4.4.1) may be an increase in outflow (Huybrechts and De Wolde, 1999). This is brought about by the differential mass loading of increased snowfall on grounded and floating ice, which affects the gravitational driving stress controlling ice flow. This effect is thought to compensate between 40 and 65% of the original gain in mass, which equates to an additional SLR of 3–42 mm based on the SMB range assessed in 13.4.4.1 (Winkelmann et al., accepted). Other studies (Huybrechts and De Wolde, 1999) recognise this effect but identify the compensation at only 10%. These differences are likely to be a consequence of the stress regime assumed to operate close to the grounding line. The effect is very likely to have scenario dependence because the SMB changes that cause it have this dependence.

Bindschadler et al. (submitted) and Nowicki et al. (submitted) reported an extensive model inter-comparison in which standardised experiments are used to assess the effects of changes in SMB, basal sliding and ice shelf melting on the Antarctic ice sheet. The results of this exercise are difficult to assess in terms of projections because of the simplified nature of the experiments and the level of sophistication of some models involved (two Antarctic models do not include ice shelves and one holds the grounding line fixed). Based on these results, Levermann et al. (submitted-b) used linear response functions to emulate the response to global climate change of three models that do contain ice shelves with an evolving grounding line, although the success of some of these models in a recent assessment of grounding-line migration (Pattyn et al., submitted) is limited. Relations between global mean temperature projections and coastal subsurface ocean temperatures from the CMIP5 model ensemble are then used to assess increases in ice shelf melt, which are compatible with Yin et al. (2011). This yields results for RCP6.0 of 90 mm and 240 mm SLR at 2100 (66th and 95th percentiles, respectively). Although this study is readily extendable to other emissions scenarios, it relies heavily on the assumption that the three ice sheet models adequately sample model response and that model biases compensate one another. The presence of one model with exaggerated grounding-line retreat (as shown in the inter-comparison presented by Pattyn et al., submitted), however, may introduce a bias towards high SLR, although this may be counteracted in models with unresponsive grounding lines (Winkelmann et al., 2012).

Fully process-based modelling (Payne et al., submitted) of West and parts of East Antarctica, in which the grounding line is adequately resolved, found limited grounding-line retreat by 2100 that primarily affects Pine Island and Smith Glaciers but not Thwaites Glacier. This work employs forcing from both regional atmosphere (Agosta et al., submitted; Ligtenberg et al., submitted) and ocean modelling (Hellmer et al., 2012; Timmermann and Hellmer, submitted) for scenarios A1B and E1. In all experiments, SLR by 2100 is less than ~40 mm, which increases to ~60 mm if an apparent delay between the model and observations is accounted for. Grounding line retreat is more extensive by 2200, in particular in response to the warm-water intrusion reported by Hellmer et al. (2012), however projected SLR remains low. This study only predicts SLR from WAIS and part of East Antarctica, however, because it omits much of East Antarctica and the Antarctic Peninsula. A study that includes the whole ice sheet (Winkelmann et al., 2012) reported that a SLR at 2100 of 11 mm (50th percentile) and 22 mm (66th percentile), although the relative immobility of the grounding line in this model (Pattyn et al., submitted) is likely to introduce a strong bias towards low SLR.

Barrand et al. (submitted) assessed the effect of ice shelf collapse on ice loss from the Antarctic Peninsula, which is suggested to occur over the 21st century (Kuipers Munneke et al., submitted). An ensemble of 21st century retreat chronologies and severities yield a range of SLR at 2100 between 10 and 20 mm, with a bounding maximum of 40 mm. Barrand et al. (submitted) also identified the SMB-compensation effect discussed by Winkelmann et al. (accepted), but they quantified the effect as ~15% of SMB (which itself has a range of 1–4 mm).

An alternative to fully process-based modelling of the grounding line is to investigate the effects of its retreat in a probabilistic framework. Ritz et al. (submitted) parameterised the rate of retreat and the area susceptible to retreat, and then prescribed a probabilistic, sector-based chronology for retreat being triggered based on observations (Pritchard et al., 2009) and regional climate modelling for scenario A1B (Hellmer et al., 2012; Kuipers Munneke et al., submitted). This approach introduces a bias towards high SLR because it ignores the possibility that a retreating grounding line may stabilise (Gudmundsson et al., submitted; Joughin et al., 2010). Their projections indicate SLR at 2100 of 88 mm (66th percentile) and 203 mm (90th percentile), and are dominated by mass loss from the Amundsen Sea sector. By 2200, the probability distribution develops a

substantial tail up to ~700 mm SLR with a subsidiary peak in probability at ~500 mm associated with the collapse of Thwaites Glacier.

The two principle studies to make projections suggest that SLR by 2100 is likely to be less than 88 mm (for A1B; Ritz et al., submitted) and 90 mm (for RCP6.0; Levermann et al., submitted-b). The results of these studies are compatible if scenarios A1B and RCP6.0 are assumed equivalent. The Ritz et al. (submitted) study is biased towards high SLR because of its assumption of unstable grounding-line retreat. The Payne et al. (submitted) study is biased in the opposite direction because of its omission of a large part of East Antarctica and the Antarctic Peninsula. If the latter omission is compensated using the analysis of Barrand et al. (submitted), however, the combined projection of 50–80 mm is fairly consistent with the other two studies. Considering the very likely limit to SLR at 2100, Ritz et al. (submitted) suggested 203 mm, Levermann et al. (submitted-b) suggested 240 mm, and the statistical analysis of Little et al. (submitted) suggests 180–240 mm. The study of Payne et al. (submitted) is, however, not consistent with these studies. Although it does not make probabilistic projections, it does include ocean forcing that is more severe than that used in Levermann (submitted-b) and employs a more accurate grounding-line model than the other studies. While this difference may be because of the omission of East Antarctica, SLR in Ritz et al. (submitted) and Levermann et al. (submitted-b) is largely from sectors included in Payne et al. (submitted). There is, therefore, a lack of agreement on the upper limit of the very likely range, whereas studies suggest that the likely range for scenarios RCP6.0 and A1B has an upper limit of 90 mm. In a similar manner, the lower limit of the likely range is assessed as 30 mm using the results of Levermann et al. (submitted-b) of 30 mm and Ritz et al. (submitted) of 35 mm.

Literature investigating the relation between the SLR generated by ice sheet dynamics and emission scenario is currently very limited, with only Levermann et al. (submitted-b) and Winkelmann et al. (2012) having so far attempted to do so. The former study shows a central SLR estimate varying from 80 mm to 110 mm between RCP2.6 and 8.5 at the 66th percentile. This dependency arises because of a correlation between global mean and Antarctic coastal ocean temperature change demonstrated by Winkelmann et al. (2012) within the CMIP3 ensemble. It does not include such potentially important effects as the increased likelihood of the fracture-based collapse of an ice shelves caused by increased surface melt in more severe scenarios. There is also a lack of literature on the relation between emission scenario and the intrusions of warm water into ice shelf cavities thought to be important in triggering observed mass loss (Jacobs et al., 2011) and potentially important in the future (Hellmer et al., 2012). It is therefore premature to attach a scenario-dependence to projections of ice sheet dynamics, even though such a dependency is assessed to be likely.

A further effect is the compensatory increase in outflow triggered by changes in SMB. This effect has been noted in several studies but is poorly quantified. We use likely lower and upper bounds of 3 and 42 mm, respectively, based on Winkelmann et al. (2012). This effect is not included in the projections of Levermann et al. (submitted-b) and Ritz et al. (submitted), so that the total SLR due to ice sheet dynamics has an overall likely range of 33 to 132 mm.

SLR beyond the likely range is poorly constrained and considerably larger increases are possible, however a number of factors prevent an attempt to assess their likelihood. These include the continued lack of models capable of simulating grounding-line migration robustly; uncertainty in the frequency and severity of the warm-water incursions demonstrated by Hellmer et al. (2012) and Timmermann and Hellmer (submitted); and the complexity of the relation between (often poorly known) bedrock topography and grounding-line stability (Gudmundsson et al., submitted). Studies such as Ritz et al. (submitted) suggest a long tail to the SLR probability distribution which may contain local peaks.

In summary, it is very likely that dynamic change within the Antarctic ice sheet will lead to SLR during the next century with a likely range of 33–132 mm for RCP6.0 (and A1B). Very much larger SLR is potentially possible, but its likelihood cannot yet be assessed with confidence. We are also unable to assess the equivalent SLR in other scenarios, although a dependency of SLR on scenario is likely to exist. All the available literature suggests that this dynamical contribution to sea level rise will continue well beyond 2100.

13.4.4.3 Possible Irreversibility of Ice Loss from West Antarctica

As detailed in Box 13.2 and Section 12.6.4.4, large areas of the West Antarctic Ice Sheet might be subject to potential self-accelerated ice loss via the marine ice sheet instability (Schoof, 2007a; Weertman, 1961). On West Antarctica, ice of about 3.3 m SLE is grounded below current sea level with downward sloping bedrock and thereby potentially subject to instability (Bamber et al., 2009). Paleo records suggest that such abrupt ice discharge occurred several times during warm periods of the last 5 million years (Naish et al., 2009). Currently available models are able to capture such self-accelerated discharge. Pollard and DeConto (2009) reproduced paleo-records with a forced ice sheet model at 25 km resolution and parameterized ice flow across the grounding line.

Temperatures at which past discharge occurred are reported to be 1°C–2°C above present-day temperature. These simulations showed a sea level rise of about 7 m during time spans of 1000–7000 years with approximately equal contributions from West and East Antarctica.

In East Antarctica, enough ice is grounded below sea level to cause about 13 m SLE rise and is thus potentially subject to the marine ice sheet instability. However, no available model results or paleo records have indicated the possibility of self-accelerated ice discharge from these regions.

[START BOX 13.2 HERE]

Box 13.2: History of the Marine Ice Sheet Instability Hypothesis

Marine ice sheets rest on bedrock that is submerged below sea level (often by 2–3 km). The most well-researched marine ice sheet is the West Antarctic Ice Sheet (WAIS) where approximately 75% of the ice sheet's area currently rests on bedrock below sea level. The East Antarctic ice sheet (EAIS), however, also has appreciable areas grounded below sea level (~35%) in particular around the Totten and Cook Glaciers.

These ice sheets are fringed by floating ice shelves, which are fed by flow from grounded ice across a grounding line (GL). The GL is free to migrate both seawards and landwards as a consequence of the local balance between the weight of ice and displaced ocean water. Depending on a number of factors, which include ice shelf extent and geometry, ice outflow to the ocean generally (but not always) increases with ice thickness at the grounding line. Accordingly, the ice sheet rests on a bed that deepens towards the ice sheet interior (see Box 13.2, Figure 1a), the ice outflow to the ocean will generally increase as the grounding line retreats. It is this feature that gives rise to the marine ice sheet instability (MISI), which states that a GL cannot remain stable on a landward-deepening slope. Even if snow accumulation and outflow were initially in balance (Box 13.2, Figure 1b), natural fluctuations in climate cause the GL to fluctuate slightly (Box 13.2, Figure 1c). In the case of a retreat, the new GL position is then associated with deeper bedrock and thicker ice, so that outflow increases (Box 13.2, Figure 1d). This increased outflow leads to further, self-sustaining retreat until a region of shallower, seaward-sloping bedrock is reached. Stable configurations can therefore only exist where the grounding line rests on slopes that deepen towards the ocean. A change in climate can therefore potentially force a large-scale retreat of the grounding line from a seaward-deepening slope and onto another further inland.

The MISI has a long history based on theoretical discussions that were started by Weertman (1974) and Mercer (1978), and has seen many refinements over the subsequent years. The advent of satellite-based observations has given fresh impetus to this debate, in particular work on the GL retreat and thinning of Pine Island (PIG), Thwaites (TG) and Smith Glaciers (all WAIS), which are collectively responsible for most of Antarctica's present mass loss (Rignot, 2008). These observations have highlighted the importance in understanding the MISI in order to make accurate projections of the ice sheet's future contribution to sea level rise.

Early studies of the MISI were not based on a formal derivation from the basic laws of mechanics thought to control ice sheet flow; it was therefore unclear how robust their results were. Questions were raised, for example, about the ability of changes at the grounding line to have a large-scale effect on the ice sheet (Hindmarsh, 1993). Recently, however, a more complete analysis from first principles has been developed (Schoof, 2007b; Schoof, 2011). This analysis suggests that the all-important relation between thickness and flow at the GL exists and has a power ~5 (i.e., that a 10% increase in thickness leads to a 61% increase in flux). This analysis, however, does not include ice shelves that occupy laterally constrained embayments,

which is often the case. In such situations, drag from ice shelf sidewalls reduces forces at the grounding line and can suppress the positive feedback between increasing ice thickness and ice flux (Dupont and Alley, 2005; Goldberg et al., 2009; Gudmundsson et al., submitted). Other factors that could suppress the instability include a sea level fall adjacent to the grounding line resulting from the isostatic and gravitational effects of ice loss (Gomez et al., 2010a).

Two processes that could trigger grounding line retreat are particularly relevant to contemporary polar climate change. The first is the presence of warmer ocean water under ice shelves, which should lead to enhanced submarine ice shelf melt (Jenkins et al., 2010). The second is the presence of melt water ponds on the surface of the ice shelf, which can cause stress concentrations allowing fractures to penetrate the full ice shelf thickness. This process appears to have been a primary factor in the collapse of the Larsen B Ice Shelf (LBIS) over the course of two months in 2002 (MacAyeal et al., 2003). The collapse of the LBIS provided a natural experiment that demonstrated the linkage between the structural integrity of an ice shelf and the flow of grounded ice draining into it. Following the breakup of LBIS, the speeds of the glaciers feeding the collapsed portion of the shelf increased two-to-eightfold, while the flow of glaciers draining into a surviving sector was unaltered (Rignot et al., 2004; Scambos et al., 2004). This indicates that a mechanical link does indeed exist between shelf and sheet, and has important implications for the future evolution of the far more significant PIG and TG systems of the WAIS.

The recent strides made in placing MISI on a sound analytical footing are, however, limited to the analysis of steady states. Numerical modelling is needed to simulate the GL retreat rates that are required to make accurate SLR projections. There are major challenges in designing models whose results are not controlled by the details of their numerical design. Problems arise at the GL because, in addition to flotation, basal traction is dramatically reduced as the ice loses contact with the underlying bedrock (Pattyn et al., 2006). This is a topic of active research, and a combination of more complete modelling of the GL stress regime (Morlighem et al., 2010) and the use of very high-resolution (sub kilometre) models (Cornford et al., submitted; Durand et al., 2009) shows promise towards resolving these problems.

[INSERT BOX 13.2, FIGURE 1 HERE]
Box 13.2, Figure 1: Schematic of the processes leading to the potentially unstable retreat of a grounding line.

[END BOX 13.2 HERE]

[START FAQ 13.2 HERE]

FAQ 13.2: Will the Greenland and Antarctic Ice Sheets Contribute to Sea Level Change Over the Rest of the Century?

The Greenland, West and East Antarctic ice sheets are the largest reservoirs of freshwater on the planet. As such, they have contributed to sea level change over geological and recent times. They gain mass through accumulation (snowfall) and lose it by surface ablation (mostly ice melt) and outflow at their marine boundary, either to a floating ice shelf, or directly to the ocean through iceberg calving. Increases in accumulation cause global mean sea level to fall, while increases in surface ablation and outflow cause it to rise. Fluctuations in these mass fluxes depend on a range of processes, both within the ice sheet and without, in the atmosphere and oceans. Over the course of this century, however, sources of mass loss appear set to exceed sources of mass gain, so that a continuing positive contribution to global sea level can be expected.

Over millennia, the slow horizontal flow of an ice sheet carries mass from areas of net accumulation (generally, in the high-elevation interior) to areas of net loss (generally, the low-elevation periphery and the coastal perimeter). At present, Greenland loses roughly half of its accumulated ice by surface ablation, and half by calving. Antarctica, on the other hand, loses virtually all its accumulation by outflow to ice shelves. In turn, ice shelves lose mass by calving and submarine melt. Ice shelves are floating, so their loss has only a negligible direct effect on sea level, although they can affect sea level indirectly by altering the mass budget of their parent ice sheet (see below).

In East Antarctica, some studies using satellite radar altimetry suggest that snowfall has increased, but recent atmospheric modelling and satellite gravimetric observations find no significant increase. This apparent

disagreement may be because relatively small long-term trends are masked by the strong inter-annual variability of snowfall. Projections suggest a substantial increase in 21st century Antarctic snowfall, mainly because a warmer polar atmosphere would be able to carry more moisture. Regional changes in atmospheric circulation would likely play a secondary role.

During this century, air temperatures around Antarctica are expected to remain too cold for substantial surface ablation. Field and satellite-based observations, however, indicate enhanced outflow—manifested as ice surface lowering—in a few localised coastal regions. These areas (Pine Island and Thwaites Glaciers in West Antarctica, and Totten and Cook Glaciers in East Antarctica) all lie within kilometre-deep bedrock troughs towards the edge of Antarctica's continental shelf (FAQ 13.2, Figure 1). The increase in outflow is thought to have been triggered by regional changes in ocean circulation, bringing warmer water in contact with floating ice shelves.

On the more northerly Antarctic Peninsula, there is a well-documented record of ice shelf collapse, which appears to be related to increased surface melting caused by atmospheric warming over recent decades. The subsequent thinning of glaciers draining into these ice shelves has had a positive—but minor—effect on sea level, as will any further such events on the Peninsula. Regional projections of 21st century atmospheric temperature change suggest that this process will probably not affect the stability of the large ice shelves of both the West and East Antarctica, although these ice shelves may be threatened by future oceanic change (see below).

Estimates of the contribution of the Antarctic ice sheets to sea level over the last few decades vary widely, but there are strong indications that enhanced outflow (primarily in West Antarctica) outweighs any increase in snow accumulation (mainly in East Antarctica) implying a tendency towards sea level rise, although even the sign of a future Antarctic contribution to sea level is still uncertain. Before we can project outflow over the 21st century with any confidence, we need to better simulate ice flow—especially any changes in the grounding line that separates floating ice from that resting on bedrock—and interactions between ice shelves and the ocean. The concept of 'marine ice sheet instability' is based on the idea that the outflow from an ice sheet resting on bedrock below sea level (FAQ13.2, Figure 1) increases with thicker, faster-flowing ice at the grounding line. On bedrock that slopes downward towards the ice sheet interior, this creates a vicious cycle of increased outflow, causing ice at the grounding line to thin and go afloat. The grounding line then retreats downslope into thicker ice that, in turn, drives further increases in outflow. This feedback could potentially result in the rapid loss of parts of the ice sheet, as grounding lines retreat along troughs and basins that deepen towards the ice sheet's interior. Future climate forcing could trigger such an unstable collapse, which may then continue independently of climate. That collapse might unfold over centuries in the case of individual troughs, and over millennia for West Antarctica and sectors of East Antarctica. Much research is focused on understanding how important this theoretical concept is for those ice sheets. Sea level could rise if the effects of marine instability become important, but there is not enough evidence at present to unambiguously identify the precursor of such an unstable retreat. Alternatively, enhanced snow accumulation may dominate, leading to sea level fall.

In Greenland (FAQ 13.2, Figure 1), it is unclear whether a slight observed thickening of ice in the interior supports a recent trend towards increased accumulation. Despite the large area affected, this mass gain is more than compensated by increases in mass loss through more surface ablation and outflow. Estimated mass loss due to surface ablation has doubled since the early 1990s. This trend is expected to continue over the next century as more of the ice sheet experiences surface ablation for longer periods. Indeed, projections for the 21st century suggest that increasing mass loss will dominate over weakly increasing accumulation. The refreezing of melt water within the snow pack high up on the ice sheet offers an important (though perhaps temporary) dampening effect on the relation between atmospheric warming and mass loss.

While the observed response of outlet glaciers is both complex and highly variable, iceberg calving from many of Greenland's major outlet glaciers has increased substantially over the last decade, and constitutes an appreciable additional mass loss. This seems to be related to the intrusion of warm water into the coastal seas around Greenland, but it is not clear whether this phenomenon is related to inter-decadal variability, such as the North Atlantic Oscillation, or a longer-term trend. Projecting its effect on 21st century outflow is therefore difficult, but it does highlight the apparent sensitivity of outflow to ocean warming. The effects of

more surface melt water on basal lubrication, and the ability of warmer ice to deform more easily, may lead to greater rates of flow, but the link to recent increases in outflow is presently unclear.

The Greenland ice sheet has contributed to a rise in global mean sea level over the last few decades, and this trend is expected to increase during this century. Unlike Antarctica, Greenland has no known large-scale instabilities that might generate an abrupt increase in sea level rise over the 21st century. A threshold may exist, however, so that continued shrinkage might become irreversible over multi-centennial timescales, even if the climate were to return to a pre-industrial state over centennial time scales. While mass loss through the calving of icebergs may increase in future decades, this process will eventually end when the ice margin retreats onto bedrock above sea level where the bulk of the ice sheet resides.

[INSERT FAQ 13.2, FIGURE 1 HERE]

FAQ 13.2, Figure 1: Bedrock topography of the Greenland and Antarctic ice sheets shown with 500-metre contours of ice surface elevation. Transects through the ice sheets emphasize the marine nature of West Antarctica and some of East Antarctica.

[END FAQ 13.2 HERE]

13.4.5 Anthropogenic Intervention in Water Storage on Land

Some human activities directly change water storage on land, and hence affect sea level. These activities vary with socioeconomic development, and may also be sensitive to climate change. Their potential future effects on sea level, however, have been little studied in the published peer-reviewed scientific literature.

For depletion of groundwater arising from extraction (for agriculture and other uses), we consider two possibilities. The first assumes that this contribution to sea level rise continues throughout the 21st century at the rate of 0.40 ± 0.11 mm yr^{-1} (mean ± SD) assessed for 2001–2008 by Konikow (2011), amounting to 38 [21–55, 90% confidence] mm SLE by 2081–2100 relative to 1986–2005 (an interval of 95 years between the midpoints of these time ranges). The second uses results from land surface hydrology models (Wada et al., 2012) with input from climate and socioeconomic projections for SRES scenarios, yielding 70 [51–90] mm SLE for the same time interval. This is less than Rahmstorf et al. (2011) obtained by assuming that the groundwater extraction estimates of Wada et al. (2010) can be scaled up in the future with global population, because of the improved treatment of groundwater recharge by Wada et al. (2012). These two possibilities indicate a range of about 20–90 mm for the contribution of groundwater depletion to GMSL rise.

For the rate of impoundment of water in reservoirs, we evaluate two possibilities. The first assumes it will continue throughout the 21st century (e.g., Lemperiere, 2006) at the average rate of –0.2 ± 0.05 mm yr^{-1} SLE (mean ± SD) estimated for 1971–2010 using data updated from Chao et al. (2008), giving a negative SLE change of 19 [11–27, 90% confidence] mm by 2081–2100 relative to 1986–2005. The second assumes it will be zero after 2010 (i.e., no further net impoundment), as shown for the 1990s and 2000s by Lettenmaier and Milly (2009) (see Section 13.4.4 for discussion). A zero contribution implies a balance between further construction of reservoir capacity and reduction of storage volume by sedimentation, each of which could plausibly have a rate of about 1% yr^{-1} of existing capacity (Lempérière, 2006; Lettenmaier and Milly, 2009). These two possibilities together indicate a range of about 0–30 mm of global mean sea level fall for the contribution of reservoir impoundment.

Our assessment thus leads to a range of –10 to +90 mm for the net contribution to GMSL rise from anthropogenic intervention in land water storage by 2081–2100 relative to 1986–2005. This range includes the range of 0–40 mm assumed by Katsman et al. (2008). A positive net contribution during the 21st century would arise if the rate of groundwater depletion exceeds the rate of increase in reservoir storage, whereas the reverse may have occurred during much of the 20th century. Because of the limited information on which it is based, we have low confidence in the range that we indicate, and we do not have sufficient confidence to give ranges for individual RCP scenarios.

13.5 Projections of Global Mean Sea Level Rise

13.5.1 Projections for the 21st Century

13.5.1.1 Process-Based Projections

Process-based projections for GMSL rise during the 21st century are the sum of contributions for which models are evaluated by comparison with observations in Section 13.3. In Section 13.5.1.3, we compare these process-based GMSL projections with results from other approaches and assess the level of confidence that we can place in each approach.

The process-based projections are based on results from 21 CMIP5 AOGCMs for which thermal expansion is available (see Section 13.4.1). Changes in glaciers and in ice sheet SMB are calculated from AOGCM global mean surface air temperature projections using parameterisations (see Appendix 13.A for details) derived from the results of process-based models assessed in Sections 13.4.2, 13.4.3.1 and 13.4.4.1. For all these contributions, our uncertainties are given on the basis that future changes are likely to lie within the 5–95% range of the CMIP5 projections for each RCP scenario, following the assessment of the uncertainty of global mean SAT projections in Section 12.4.1.2.

Possible ice sheet dynamical changes are assessed from the published literature (Sections 13.4.3.2 and 13.4.4.2), which does not yet provide a sufficient basis for making projections related to particular scenarios. Projections of changes in land-water storage due to human intervention are also treated as independent of emissions scenario, because we do not have sufficient confidence to give ranges for individual scenarios. Our assessment of the literature provides a likely range of each of these contributions by 2100, and we assume this contribution begins from its present-day value and interpolate between these end-points (see Appendix 13.A for details).

The likely range of GMSL rise given for each scenario combines the uncertainty in global climate change, represented by the CMIP5 ensemble (Section 12.4.1.2), with the uncertainties in modelling the contributions to GMSL. The part of the uncertainty related to the magnitude of global climate change is correlated among all the scenario-dependent contributions, while the methodological uncertainties are treated as independent (see also Appendix 13.A).

Process-based projections for GMSL rise by the end of the 21st century (over an interval of 95 years, between the 20-year mean of 2081–2100 and the 20-year mean of 1986–2005) are shown in Figure 13.8 and Table 13.5. Time series of projected GMSL and its rate of rise are shown in Figure 13.9. The central projections for GMSL in all scenarios lie within a range of 0.05 m until the middle of the century, because the divergence of the climate projections has a delayed effect owing to the time-integrating characteristic of sea level. By the end of the century, they have a spread of about 0.2 m, with RCP2.6 giving the least amount of rise (0.42 [likely range of 0.29–0.55] m) and RCP8.5 giving the most (0.64 [0.48–0.82] m). RCP4.5 and RCP6.0 are very similar at the end of the century (0.49 [0.36–0.63] m and 0.50 [0.37–0.64] m respectively), but RCP4.5 has a greater rate of rise earlier in the century than RCP6.0.

In all scenarios, the rate of rise begins from about 4 mm yr^{-1}, somewhat above the observational estimates of 3.2 [2.8–3.6] mm yr^{-1} for 1993–2010, because the AOGCMs do not reproduce the reduced rate of thermal expansion in the last decade (Section 13.4.1); instead, they simulate acceleration of sea level rise during these years. In the projections, the rate of rise initially increases. In RCP2.6 it becomes roughly constant (central projection ~5 mm yr^{-1}) before the middle of the century, and subsequently declines slightly. The rate of rise becomes roughly constant in RCP4.5 and RCP6.0 by the end of the century, whereas acceleration continues throughout the century in RCP8.5 (central projection reaching ~11 mm yr^{-1}).

In all scenarios, thermal expansion is the largest contribution, accounting for 30–50% of the total in the central projections. Glaciers are the next largest. By 2100, about a third of the present glacier volume is projected to be eliminated under RCP2.6, and about half under RCP8.5. SMB change on the Greenland ice sheet makes a positive contribution, whereas SMB change in Antarctica gives a negative contribution (see discussion in Sections 13.3.3.2 and 13.5.1.3), but in the central projections both ice sheets make positive net contributions due to dynamical changes that result in increased ice outflow. There is a relatively small positive contribution from human intervention in land-water storage, predominantly due to increasing extraction of groundwater.

[INSERT FIGURE 13.8 HERE]

Figure 13.8: Projections from process-based models with likely ranges and median values for global-mean sea level rise and its contributions in 2081–2100 relative to 1986–2005 for the four RCP scenarios and scenario SRES A1B used in the AR4. Contributions from ice sheet dynamical change and anthropogenic land water storage are included in the sum; they are independent of scenario, and are treated as having uniform probability distributions. See discussion in Sections 13.5.1.1 and 13.5.1.3 and Appendix 13.A for methods.

[INSERT FIGURE 13.9 HERE]

Figure 13.9: Projections from process-based models of **(a)** GMSL rise relative to 1986–2005 and **(b)** the rate of GMSL rise as a function of time for the four RCP scenarios and scenario SRES A1B. The solid lines show the median and the dashed lines show the likely range for each scenario.

Table 13.5: Central estimates and likely ranges for projections of global-mean sea level rise and its contributions in metres in 2081–2100 relative to 1986–2005 for the four RCP scenarios, GMSL rise at 2100, and rates of GMSL rise in mm yr^{-1} in 2081–2100. Because some of the uncertainties in modelling the contributions are treated as uncorrelated, the sum of the lower bound of contributions does not equal the lower bound of the sum, and similarly for the upper bound (see Appendix 13.A). Because of imprecision from rounding, the sum of the central estimates of contributions may not exactly equal the central estimate of the sum. The contributions from ice sheet dynamical change and anthropogenic land water storage are treated as independent of scenario, since scenario dependence cannot be evaluated on the basis of existing literature, and as having uniform probability distributions, uncorrelated with the magnitude of global climate change. Regional sea level change is expected in general to differ from the global mean (see Section 13.6).

	RCP2.6	RCP4.5	RCP6.0	RCP8.5
Thermal Expansion	0.14 [0.10 to 0.18]	0.19 [0.14 to 0.23]	0.19 [0.15 to 0.24]	0.27 [0.21 to 0.33]
Glaciers	0.13 [0.07 to 0.19]	0.16 [0.10 to 0.22]	0.16 [0.09 to 0.22]	0.20 [0.13 to 0.27]
Greenland Ice Sheet SMB	0.02 [0.00 to 0.05]	0.04 [0.00 to 0.07]	0.04 [0.00 to 0.07]	0.07 [0.01 to 0.13]
Antarctic Ice Sheet SMB	–0.02 [–0.05 to –0.00]	–0.03 [–0.06 to –0.01]	–0.03 [–0.06 to –0.01]	–0.05 [–0.09 to –0.01]
Greenland Ice Sheet Dynamics	0.04 [0.01 to 0.06]	0.04 [0.01 to 0.06]	0.04 [0.01 to 0.06]	0.04 [0.01 to 0.06]
Antarctic Ice Sheet Dynamics	0.07 [0.03 to 0.11]	0.07 [0.03 to 0.11]	0.07 [0.03 to 0.11]	0.07 [0.03 to 0.11]
Land Water Storage	0.04 [–0.01 to 0.08]	0.04 [–0.01 to 0.08]	0.04 [–0.01 to 0.08]	0.04 [–0.01 to 0.08]
Sea Level Rise	0.42 [0.29 to 0.55]	0.49 [0.36 to 0.63]	0.50 [0.37 to 0.64]	0.64 [0.48 to 0.82]
Rate of Sea Level Rise	4.7 [2.9 to 6.6]	6.4 [4.4 to 8.4]	7.8 [5.6 to 10.0]	11.4 [8.0 to 15.1]
Sea Level Rise at 2100	0.46 [0.32 to 0.61]	0.56 [0.41 to 0.71]	0.58 [0.42 to 0.74]	0.76 [0.56 to 0.96]

13.5.1.2 Semi-Empirical Projections

The semi-empirical approach regards changes in sea level as an integrated response of the entire climate system, reflecting changes in the dynamics and thermodynamics of the atmosphere, ocean and cryosphere; it explicitly does not attribute sea level rise to its individual physical components. Semi-empirical models use simple physically motivated relationships, with parameters determined from observational time series, to predict GMSL from either global mean surface air temperature (Grinsted et al., 2010; Horton et al., 2008; Rahmstorf, 2007b; Rahmstorf et al., 2011; Vermeer and Rahmstorf, 2009) or radiative forcing (Jevrejeva et al., 2009; 2010; 2011). The paleo record provides strong evidence for a relationship between GMSL and these predictors on glacial/interglacial timescales (Chapter 5). Semi-empirical models have adopted various analytical formulations for describing and projecting GMSL changes as a function of the same predictors and applied them to multidecadal timescales.

The development of semi-empirical models was motivated by two problems. First, process-based modelling was incomplete in the AR4 because of the unavailability of ice sheet dynamical models which could be used to simulate recent accelerations in ice flow and make projections with confidence (Sections 13.1.5.1, 13.3.3.2, 13.4.3.2, 13.4.4.2). Second, in the TAR (Church et al., 2001) and AR4 and previous assessments, known observed and simulated contributions to GMSL from thermal expansion, glaciers and ice sheets did not completely account for observed sea level rise during the 20th century. For example, the AR4 assessed the mean observational rate for 1961–2003 as 1.8 ± 0.5 mm yr^{-1}, and the sum of terms as 1.1 ± 0.5 mm yr^{-1}

(Bindoff et al., 2007; Hegerl et al., 2007). With the central estimates, only about 60% of observed sea level rise was thus explained, and the potential implication was that projections using process-based models which reproduce only those known contributions would underestimate future sea level rise (Grinsted et al., 2010; Jevrejeva et al., 2009; Rahmstorf, 2007b). While semi-empirical models do not solve the two problems that motivated their development, they provide an alternative approach for projecting GMSL, as well as for exploring the sensitivity of sea level to various forcing factors. Recent improvements in observational data sets for ocean warming and land ice mean that observed contributions to sea level rise since about 1970 can now account for GMSL (Church et al., 2011b; Domingues et al., 2008; Moore et al., 2011), although process-based models are not yet available for all contributions (Section 13.3).

Semi-empirical models are designed to reproduce the observed sea level record over their period of calibration, as this provides them with model parameters needed to make projections (Grinsted et al., 2010; Jevrejeva et al., 2009; Rahmstorf, 2007b; Vermeer and Rahmstorf, 2009). A test of the predictive skill of the models requires simulating a part of the observed record which has not been used for calibration. To do this, Rahmstorf (2007a) calibrated against observed GMSL rise for 1880–1940 and projected 1940–2000, obtaining results within 0.02 m of observed, while Grinsted et al. (2010), using Brohan et al. (2006) or Moberg et al. (2005) temperature for calibration up to 1990, projected a rate of rise for 1993–2006 of 2.0–4.9 mm yr^{-1} or 3.1–4.9 mm yr^{-1} respectively (5–95% ranges), compared to the altimeter estimate of 3.3 ± 0.4 mm yr^{-1}. Jevrejeva et al. (submitted) and Bittermann et al. (submitted) give examples of using various lengths of observed record for calibration. If an early portion of the instrumental record is used, the models can reproduce the remainder within uncertainties that become smaller the nearer to the present day the calibration extends.

Three kinds of issues relating to calibration of semi-empirical models have been discussed in the literature. First, the GMSL estimates used for training the models are based on the existing sparse network of long tide-gauge records, especially before the late 19th century, and are thus uncertain; these uncertainties are reflected in the observational estimates of the rate of GMSL rise (Section 3.7). There has been debate about whether the projections of Rahmstorf (2007a) may be sensitive to their statistical treatment of the temporal variability in the instrumental record of sea level change (Holgate et al., 2007; Rahmstorf, 2007a; Schmith et al., 2007). Rahmstorf et al. (2011) reported that GMSL projections for the RCP4.5 scenario for 2100 varied by ±0.04 m for values within a range of 0–25 years for the embedding dimension used for temporal smoothing during the calibration.

Second, there is some sensitivity to the choice of datasets used for calibration. For instance, the central projections of Rahmstorf et al. (2011) for 2100 under RCP4.5 lie within a range of about ±0.10 m for calibration with the GMSL datasets of Church and White (2006), Jevrejeva et al. (2008) and Kemp et al. (2011) (the last being a proxy of local sea level change regarded by its authors as possibly representative of GMSL) but they obtained projections about 0.3 m less (Table 13.6) for calibration with the Church and White (2011) dataset, although the two Church and White (2006, 2011) datasets differ at all times by less than one standard deviation. Rahmstorf et al. (2011) argued that the projection based on Church and White (2011) is less plausible because their model fits this dataset less well, and the fit suggests a global mean temperature for stable sea level which is less consistent with paleo-evidence. Grinsted et al. (2010) and Jevrejeva et al. (2010; 2011; 2011) addressed the issue of sensitivity to calibration data by using an inverse Monte-Carlo technique to determine their model parameters, effectively sampling a larger observational space determined by the uncertainty covariance matrix of their GMSL estimate, but it is unknown whether this procedure fully samples the observational space of other GMSL estimates. Grinsted et al. (2010) also investigated the sensitivity to the temperature dataset used as predictor, and Jevrejeva et al. (2010) the sensitivity to radiative forcing as predictor (Table 13.6). In the latter case, three datasets gave median projections under RCP4.5 for 2100 within a range of about ±0.20 m.

Third, Vermeer and Rahmstorf (2009) demonstrated that contributions to GMSL rise which are not caused by contemporaneous climate change or radiative forcing should be subtracted from the observational sea level record before calibrating a semi-empirical model, because otherwise they may be implicitly scaled up or down with future climate change, particularly if they correlate with the semi-empirical predictors of sea level change. Such contributions include groundwater depletion, storage of water by dams and multi-millennial adjustment of Greenland and Antarctica ice sheets to past climate change (Section 13.3.6). The terms to be excluded are time-dependent and uncertain, and this uncertainty propagates to the semi-empirical

model projections. Jevrejeva et al. (submitted) found that their median projections for 2100 were modified by 0.02–0.03 m when they allowed for land water storage of $–0.1 \pm 0.2$ mm yr^{-1} during the 20th century calibration , whereas Rahmstorf et al. (2011) found that their projections were about 0.25 m larger if they excluded reservoir storage.

Because of the above issues and structural differences between the models, projections from the semi-empirical models for the 21st century have a wide range (the spread of their central values for the A1B scenario is more than 50% of the average; Table 13.6).

Making projections with a semi-empirical model assumes that sea level change in the future will have the same relationship as it has had in the past to radiative forcing or global mean temperature change. The appropriate choice for the formulation of the semi-empirical model may depend on the nature of the climate forcing and the timescale, and could therefore differ between past and future.

Von Storch et al. (2008) analysed output from a simulation of the past millennium with the ECHO-G model in order to calibrate a relationship, of the form used by Rahmstorf (2007b), between global mean SAT and the contribution of thermal expansion to the rate of sea level rise. They found that the relationship varies with time, implying that its projections would not be reliable. In response, Vermeer and Rahmstorf (2009) argued that the sea level variations of the last millennium arise predominantly from episodic volcanic forcing and cannot be adequately simulated by the semi-empirical model of Rahmstorf (2007b) because it was intended to simulate the response to sustained forcing on multidecadal timescales. From cointegration analysis of observed SAT and GMSL change, which they interpret as a proxy for ocean heat content, Schmith et al. (2012, in press) concluded that SAT is influenced by ocean heat content (rather than vice-versa), because of the latter's role as a heat capacitor in internally generated climate variability, whereas ocean heat content is unaffected by radiative forcing. They suggested that more that 1000 years of historical data would be needed to build reliable statistical models of heat uptake.

Ice loss in Greenland during the warm period of the early 20th century could have made a positive contribution to GMSL rise (Section 13.3.3.2). Because of correlation with global mean SAT change or radiative forcing, this contribution would be included in the semi-empirical model calibration and would lead to larger projections (Jevrejeva et al., submitted). However, it is not certain to what extent this early 20th century sea level rise was causally connected to global warming or external forcing, as the calibration implicitly assumes. Schmith et al. (2012, in press) suggest from their analysis that warming early in the 20th century was at least partly due internal variability of the climate system.

Potentially non-linear physical processes may not scale in the future in ways which can be calibrated from the past (Rahmstorf et al., 2011; Vermeer and Rahmstorf, 2009; von Storch et al., 2008). Three such effects, which could lead to overestimated or underestimated projections by semi-empirical models, have been discussed in the literature.

First, AOGCMs indicate that the ocean heat uptake efficiency tends to decline as warming continues and heat penetrates more deeply (Gregory and Forster, 2008). A linear scaling of the rate of global ocean heat uptake with global SAT determined from the past will thus overestimate future time-integrated heat content change and the consequent thermosteric sea level rise on a century timescale. This is a weakness of the model of Rahmstorf (2007b), who found that the linear scaling overestimated by 0.12 m (about 30%) the thermal expansion simulated by a climate model with a 3D ocean from 1990 to 2100 under scenario SRES A1FI. The AOGCM behaviour is more accurately reproduced by taking into account the vertical profile of warming, at least by distinguishing the upper (mixed layer) and lower (thermocline) layers (Held et al., 2010; Vermeer and Rahmstorf, 2009), or by introducing a relaxation timescale for sea level rise (Jevrejeva et al., submitted).

Second, the sensitivity of glaciers to warming will tend to decrease as the area most prone to ablation and the remaining volume decrease, partly counteracted by lowering of the surface due to thinning (Huss et al., 2012; Section 13.5.2). On the other hand, glaciers at high latitudes which currently have negligible surface melting will begin to ablate as the climate becomes warmer, tending to give an increase in sensitivity (Rahmstorf et al., 2011; Section 13.5.2). Estimating the balance of these two effects will require detailed modelling of glacier SMB. The absence of an long-term acceleration in the rate of glacier mass loss in

observations of the 20th and simulations of the 21st centuries (Section 4.3,3, Marzeion et al., submitted; Radic and Hock, 2010), despite rising global temperatures, is evidence that the reduction in sensitivity may dominate (Gregory et al., submitted).

Third, future rapid dynamical changes in ice sheet dynamics could substantially increase sea level rise (Section 13.5.4). In order for large ice sheet dynamical changes to be predictable from the instrumental record, such changes must have contributed substantially to sea level rise during the period of calibration. It is likely that they have contributed only a small part of the observed sea level rise during recent decades (about 10% during 1993–2010; Section 13.3.6). This phenomenon is therefore not likely to be the reason why semi-empirical projections are larger than process-based projections.

Table 13.6: Global-mean sea level rise (m) from the year indicated to 2100 projected by semi-empirical models and compared with the IPCC AR4 projection.

	From	5%	50%	95%
Scenario SRES A1B				
IPCC AR4[c]	1990	0.22	0.37	0.50
IPCC AR4[c,d]	1990	0.22	0.43	0.65
Rahmstorf (2007b)[a]	1990	–	0.85	–
Horton et al. (2008)[b]	2000	0.62	0.74	0.88
Vermeer and Rahmstorf (2009)	1990	0.98	1.24	1.56
Grinsted et al. (2010) with Brohan et al. (2006) temperature for calibration	1990	0.32	0.83	1.34
Grinsted et al. (2010) with Moberg et al. (2005) temperature for calibration	1990	0.91	1.12	1.32
Jevrejeva et al. (2010) with Goosse et al. (2005) forcing for calibration	1990	0.60	0.75	1.15
Jevrejeva et al. (2010) with Crowley et al. (2003) forcing for calibration	1990	0.63	0.86	1.06
Jevrejeva et al. (2010) with Tett et al. (2007) forcing for calibration	1990	0.87	1.15	1.40
Scenario RCP4.5				
Rahmstorf et al. (2011) with Church and White (2006) for calibration	2000	0.84	1.01	1.28
Rahmstorf et al. (2011) with Jevrejeva et al. (2008) for calibration	2000	0.91	1.15	1.49
Rahmstorf et al. (2011) with Church and White (2011) for calibration	2000	0.62	0.73	0.91
Rahmstorf et al. (2011) with proxy data for calibration	2000	0.69	0.95	1.32
Jevrejeva et al. (2011)[e]	1990	0.52	0.74	1.10

Notes:
(a) Uncertainty range not given.
(b) The mean value and the range across the 11 GCMs are shown.
(c) Extrapolated to 2100 using the projected rates of sea level rise for 2000–2099 in Table 10.7 of Meehl et al. (2007).
(d) Including scaled-up ice sheet discharge given in Table 10.7 of Meehl et al. (2007) as an illustration of the possible magnitude of this effect.
(e) Results given are the average of three different semi-empirical models.

13.5.1.3 Confidence in Likely Ranges and Bounds

The AR4 (Meehl et al., 2007) presented model-based projections of GMSL rise for the end of the 21st century, but did not provide a best estimate principally because scientific understanding at the time was not sufficient to allow an assessment of the possibility of future rapid changes in ice sheet dynamics, that is changes on timescales of a few decades or less (Section 4.4.4). Future rapid changes in ice sheet outflow

were consequently not included in the ranges given by the AR4. For the SRES A1B scenario, the AR4 range was 0.21–0.48 m, and for the highest emissions scenario, A1FI, it was 0.26–0.59 m. The AR4 also noted that, if ice sheet outflow increased linearly with global mean surface air temperature, the AR4 maximum projections would be raised by 0.1–0.2 m. The AR4 was unable to exclude larger values or to assess their likelihood.

Since the publication of the AR4, upper bounds of between 0.9 and 2.4 m for GMSL rise by 2100 have been estimated by three other approaches (Nicholls et al., 2011), namely semi-empirical models (Section 13.6.1.2), analogues from past climates (Section 13.3.1), and physical constraints on ice sheet dynamics (Section 13.5.4). The broad range of values reflects the different methodologies for obtaining the upper bound, involving different constraining factors and sources of evidence. Moreover, an upper bound is not uniquely defined because it depends on the subjective choice of constraints that are to be tested to the limit, whereas a best estimate and a likely range are well defined in their purpose, in that they aim to equal and to encompass the true value.

The confidence that can be placed in projections by the various approaches must be considered. Confidence arises from the nature, quantity, quality and consistency of the evidence.

The first approach is based on process-based projections, which use the results from models of individual contributions (Section 13.6.1.1). Confidence in this approach comes from our understanding of the modelled physical processes, the consistency of the models with wider physical understanding of those processes as elements of the climate system, the agreement of modelled and observed contributions, and the agreement of observed and modelled GMSL (Section 13.3.6; Box 13.1; Chapters 9 and 10).

The second approach uses semi-empirical models (Section 13.6.1.2), which make projections by calibrating a physically motivated relationship between GMSL and some other parameter of the climate system in the past and applying it to the future, without quantifying the contributory physical processes. If we had no physical understanding of the causes of sea level rise, the semi-empirical approach to projections would be the only possible one, but extrapolation beyond the range of calibration implies uncertainty that is difficult to quantify. As a result, there is no consensus about the reliability of semi-empirical model projections, despite their successful calibration against the observed 20th century sea level record.

Although the semi-empirical model projections cover a wide range (Table 13.6), they all project significantly higher GMSL rise than process-based models. It is important to establish whether the semi-empirical projections are physically plausible. The only suggested explanation for the difference in terms of processes is that semi-empirical models may allow for ice sheet dynamical change on decadal timescales in response to future climate change (Grinsted et al., 2010; Little et al., submitted). However, our assessment is that this is unlikely to be the reason for the difference because our current understanding of the causes of recent dynamical changes in Greenland and Antarctica is that they have been triggered by local changes in ocean temperature (Holland et al., 2008a; Jacobs et al., 2011; Thoma et al., 2008). A link between decadal changes in ice sheet dynamics and global surface temperature or radiative forcing is therefore not likely to be strong during the 20th century. Hence we consider that ice sheet dynamical changes on decadal timescales could not be reliably extrapolated from the observed data from which semi-empirical models are calibrated.

The third approach uses paleo-records of sea level change that show rapid GMSL rise has occurred during glacial terminations, at rates of up to about 1 m century^{-1} averaged over centuries (Chapter 5), largely from ice sheets that no longer exist. Contributions from these vanished ice sheets could have continued even after sea level and climate have reached interglacial states, if the Greenland and Antarctic ice sheets contracted during the termination to smaller sizes than at present. During past interglaciations only the Greenland and Antarctic ice sheets were present. For the time interval during the LIG in which GMSL was above present, there is reliable evidence that the maximum 1000-year average rate of GMSL rise likely exceeded 4.1 m kyr^{-1} (67% probability) and was unlikely to have exceeded 5.8 m kyr^{-1} (Chapter 5, Section 13.2.1.2). Because these periods give only a limited analogy for future anthropogenic climate change, we do not consider that they provide upper bounds for GMSL rise during the 21st century.

The fourth approach uses kinematic limits on outflow from the ice sheets. Pfeffer et al. (2008) argued that scenarios of GMSL rise exceeding 2 m by 2100 are physically untenable, ruling out, for example, the

heuristic argument of Hansen et al. (2007) giving 5 m. Pfeffer et al. (2008) constructed a 'high' scenario of 2 m of sea level rise by 2100, and Katsman et al. (2011) of 1.1 m. Although Pffefer et al. (2008) and Katsman et al. (2011) considered their scenarios to be physically possible, they are unable to quantify their likelihood because these scenarios are based on assumptions, rather than being related to observations of the response of the Greenland and Antarctic ice sheets to climate change or variability on century timescales. Such scenarios involve contributions of ~0.5 m from Antarctica. This is much greater than any process-based projections of dynamical ice sheet change (Section 13.4.4.2), and would require either an implausibly high increase in outflow in all marine-based sectors or the localised collapse of the ice sheet in the Amundsen Sea sector (Little et al., submitted).

In our assessment, GMSL rise during the 21st century for each RCP scenario is likely to lie within the range given by the process-based projections (Section 13.5.1.1 and Table 13.5; see Section 13.5.2 for following centuries), which are based on the likely ranges projected for global-mean surface air temperature change (Section 12.4.1.2). Projections must be accompanied by an indication of confidence in order for them to be practically useful. We have high confidence that the time-mean rate of GMSL rise during the 21st century is very likely to exceed the rate of 2.0 [1.7–2.3] mm yr^{-1} observed during 1971–2010, because the GMSL projections indicate a significantly greater rate even under the RCP2.6 scenario, which has the lowest radiative forcing. It is more difficult to set an upper bound because there is a relationship between the level of confidence and the width of the range delimited. Extremely high bounds to GMSL rise in the 21st century could easily be set with confidence, but being physically unachievable makes them of little value. Our likely ranges are narrower, in order to be more useful, but they are consequently accompanied by lower confidence. Under the scenario with the highest radiative forcing (RCP8.5), the likely range reaches 0.84 m by 2100 relative to 1986–2005, similar to the lower estimate of Pfeffer et al. (2008).

The improved agreement of process-based models with observations and physical understanding is a basis for confidence and an advance since the AR4, but because of other factors we have only medium confidence in our likely ranges, and cannot give a definite upper bound. First, despite considerable progress in understanding, we have only medium confidence in projections of changes in ice sheet dynamics on decadal timescales; the probability of a larger dynamical ice sheet response is non-zero but poorly quantified. Second, we do not know why semi-empirical models give higher projections of GMSL rise; this difference implies either that there is some contribution which is presently unidentified or underestimated by process-based models, or that the projections of semi-empirical models are overestimates. Third, observations do not show an increase in Antarctic precipitation, which is projected by models; if this increase were entirely absent in the future, our projections would be raised by up to 0.06 m for scenario RCP8.5 (assuming uncorrelated errors). For all these reasons, larger values than given by the process-based models cannot be excluded, but the current state of scientific understanding is insufficient for evaluating their probability.

Progress has been made since the AR4, in which there was insufficient confidence to give likely ranges for 21st century GMSL rise, as we have done here. For scenario SRES A1B, which was assessed in the AR4, the likely range on the basis of science assessed in the AR5 is 0.63 [0.47–0.80] m by 2100 relative to 1986–2005, and 0.59 [0.44–0.75] m by 2090–2099 relative to 1990. Compared with the AR4 projection of 0.21–0.48 m for the same scenario and period, the largest increase is from changes in Greenland and Antarctic ice sheet dynamics on decadal timescales, for which the central projection is 0.12 m by 2090–2099. This term was largely omitted in the AR4 because a basis to make projections was not available in published literature at that time. The contribution from thermal expansion is similar to the AR4 projection and has smaller uncertainty. The contribution from glaciers is larger than in the AR4 primarily because of the greater estimate of the present glacier volume in new inventories, and the Greenland SMB contribution is larger because of recent improvement in models of relevant surface processes. Further progress on all the issues outlined above is still needed in order to attain high confidence in GMSL projections, in particular concerning the probability distribution of GMSL above the likely ranges.

13.5.2 Projections Beyond the 21st Century

The Representative Concentration Pathways (RCPs), as applied in Chapter 12, Sections 13.4 and 13.5.1, are defined up to the year 2100. The Extended Concentration Pathways (ECPs) have been introduced for the period between 2100 and 2300 (Meinshausen et al., 2011) to project long-term climate change. However, these time periods are insufficient to capture the full impact of sea level rise, since the ocean as well as

continental ice sheets respond to changes in external forcing on centennial to millennial time scales. While this section will focus on a time horizon up to the year 2500, it should be noted that sea level is very likely to continue to rise beyond 2500 unless global mean temperatures decline (e.g., Gillett et al., 2011; Huybrechts et al., 2011; Solomon et al., 2009). The sea level commitment for different levels of global warming will be discussed at the end of the section.

A number of model simulations of ice sheets and oceanic warming apply scenarios different from the ECPs. For practical reasons, sea level projections beyond the year 2100 have been grouped here into three categories: *Low scenarios* in which atmospheric GHG concentration does not exceed 500 ppm CO_2-equivalent, medium scenarios with concentrations between 500 and 700 ppm CO_2-equivalent and high scenarios above 700 ppm. The low scenarios include ECP-2.6, SRES-B1 and 0.5 and 2% yearly increase scenarios followed by no emissions after 450 ppm have been reached. The medium category contains ECP-4.5 as well as 1% yearly increase scenarios up to 560 ppm. The high scenarios are ECP-6.0 and 8.5 as well as 1120 ppm scenarios and SRES-A2. Also included are 0.5 and 2% increase scenarios as well as an SRES-A2-scenario with zero emissions after 1200 and 1120 ppm have been reached, respectively.

A synthesis of the different sea level contributions is provided in Table 13.7 and Figure 13.10 for the end of each century until the year 2500. Thermal expansion contributions were obtained from coarse-resolution coupled climate models (Gillett et al., 2011; Schewe et al., 2011; Solomon et al., 2009; Vizcaino et al., 2008). Contributions from the Greenland and Antarctic ice sheets were obtained with climate models of comparable complexity coupled to continental ice sheet models (Huybrechts et al., 2011; Vizcaino et al., 2010). Glacier projections were obtained by application of the method by Marzeion et al. (2011) to the CMIP5 model output for scenarios and models that were integrated up to the year 2300. For 2400 and 2500 the same model spread as for 2300 is shown.

[INSERT FIGURE 13.10 HERE]

Figure 13.10: Sea level projections beyond the year 2100 are grouped into three categories according to the concentration of GHG concentration (in CO_2-equivalent) in the year 2100 (upper panel: >700 ppm; middle panel: 500–700 ppm; lower panel: <500 ppm). Colored bars show the full model spread. Horizontal lines provide the specific model simulations. The range provided for the total sea level change represents the maximum possible spread that can be obtained from the four different contributions. Grey shaded bars exhibit the likely range for the 21st century projection from Figure 13.9 with the median as the horizontal line. [PLACEHOLDER FOR FINAL DRAFT: Possible slight update from revised papers.]

Due to the fact that different scenarios are used for different components and because of the relatively small number of model simulations available, the ranges provided in Figure 13.10 and Table 13.7 cannot be interpreted as uncertainty ranges but only represent the model spread. The range for the total sea level change was obtained by taking the sum of contributions that result in the lowest and the highest sea level rise, that is the largest range that can be obtained from the sum of the different contributions. This approach is adopted because of the limited number of simulations available. The underlying assumption of full correlation of the uncertainties might not always be justified which would narrow the uncertainty range.

It should be noted that apart from the models used for glaciers and ice caps, the models used here for the period beyond 2100 are different from the models used for the 21st century (Sections 13.4. and 13.5.1.). Generally, the model spread for the total sea level contribution in 2100 is lower than the likely range provided in Section 13.5.1 for the mean of 2091–2100 (grey shading in Figure 13.10). This is not due to the thermal expansion where coarse resolution model results are similar to the CMIP5 projections (light blue vertical lines in Figure 13.10, Table 13.7.). Since the glacier contribution is the same the difference arises from the ice sheets, particularly the Antarctic ice sheet.

Projections beyond 2100 show positive contributions to sea level from thermal expansion, glaciers and changes in Greenland ice sheet SMB. Due to enhanced precipitation under warming, Antarctic ice sheet SMB change makes a negative contribution to sea level in scenarios below 700 ppm CO_2-equivalent. These results were obtained with fully coupled climate-ice sheet models which need to apply a relatively low-spatial resolution. In light of the discussion in Sections 13.3.3.2 and the assessment of the 21st century changes in Section 13.4.4.1, confidence in this result is low. For scenarios above 700 ppm CO_2-equivalent, Antarctic SMB change is contributing positively to GMSL.

As discussed in Section 13.4.4.2, confidence in the ability of coupled ice sheet-climate models to project sea level contributions from dynamic ice sheet changes in Greenland and Antarctica is low, due to inadequate representation of ice shelves, ice-ocean interaction and the dynamics within fast flowing ice streams. In Greenland, dynamic mass loss is limited by topographically defined outlets regions. Solid-ice discharge induced from interaction with the ocean is furthermore self-limiting because retreat of the ice sheet results in increasingly less contact with the ocean and less mass loss by iceberg calving (Graversen et al., 2011; Pfeffer et al., 2008; Price et al., 2011).

[INSERT FIGURE 13.11 HERE]

Figure 13.11: Sea level commitment per degree of warming as obtained from physical model simulations of **(a)** ocean warming, **(b)** mountain glaciers and ice caps, **(c)** the Greenland and **(d)** the Antarctic ice sheet. **(e)** The corresponding total sea level commitment, which is consistent with paleo-estimates from past warm periods (PI = pre-industrial, LIG = last interglacial period, M11 = Marine Isotope Stage 11, Plio = Mid-Pliocene). Temperatures are relative to pre-industrial. Dashed lines provide linear approximations: (a) sea level rise for a homogeneous increase in temperature; (d) & (e) constant slopes of 1.2 and 2 m $^{\circ}C^{-1}$. Shading as well as the vertical line represents the uncertainty range as discussed in Levermann et al.(submitted-a).

By contrast, the bedrock topography of Antarctica is such that a retreating ice sheet will remain in contact with the ocean. Due to topography that is declining landward, especially in West Antarctica, this may lead to enhanced rates of mass loss as the ice retreats. While the model used by Huybrechts et al. (2011) is in principle capable of capturing this marine ice sheet instability (see Box 13.2), medium confidence is assigned to the models ability to capture the associated time scale. The model used by Vizcaino et al., (2010) does not represent the ice shelf dynamics and is thereby lacking a fundamental process that can trigger the instability. As stated by the authors, low confidence needs to be assigned to the model's ability to project future solid-ice discharge from Antarctica. It is thus likely that the contributions from Antarctica as depicted in Figure 13.11 underestimate the future contribution.

The model spread of total sea level change in 2300 ranges from 0.56 to 0.74 m for the low scenario (Table 13.8). Using a semi-empirical model Schaeffer et al. (2012) obtain a significantly larger 90%-confidence-range of 1.3–3.3 m for the ECP-2.6 scenario. The ECP-4.5 scenario for which they obtain an interval of 2.3–5.5 m is categorized here as a medium scenario for which the process-based models compute a significantly lower range of 0.39–1.16 m. Using a different semi-empirical approach, Jevrejeva et al. (submitted) obtains a 90%-confidence range of 0.13–1.74 m for ECP-2.6 in the year 2500, which encloses the model spread of 0.76–0.98 for the low scenario. For the medium and high scenarios however, the model spread of 0.35–1.71 and 1.72–5.82 is significantly lower than the intervals obtained from the semi-empirical approach of 0.72–4.3 m and 1.0–11.5 m, respectively. As discussed above and detailed in Section 13.4., it is likely that the process-based ice sheet models, used here, underestimate the sensitivity to external forcing due to missing physical processes. For a detailed discussion on the semi-empirical models see Section 13.5.1.2. In addition to this discussion, it is to be noted here that the confidence in the ability of semi-empirical methods reduces with the length of the extrapolation period and the deviation of the future forcing from the forcing of the learning period (Schaeffer et al., 2012).

For increasing GMT, sea level is virtually certain to continue to rise beyond the year 2500 as shown by available model simulations of thermal expansion and ice sheets that were computed beyond 2500 (Driesschaert et al., 2007; Gillett et al., 2011; Goelzer et al., 2011; Huybrechts et al., 2011; Mikolajewicz et al., 2007a; Rahmstorf and Ganopolski, 1999; Ridley et al., 2005; Schewe et al., 2011; Solomon et al., 2009; Swingedouw et al., 2008; Vizcaino et al., 2008; Vizcaino et al., 2010; Winguth et al., 2005) and by the semi-empirical approaches.

As detailed in Sections 13.4.3.2 and 13.4.4.2, confidence in continental scale ice sheet models to capture the temporal response to changes in external forcing on a decadal to centennial time scale is low. On multi-centennial to multi-millennial time scales these models have shown to be able to reproduce paleo-climatic records (Naish et al., 2009; Pollard and DeConto, 2009). Figure 13.11 shows the multi-millennial sea level contribution for the different components (Levermann et al., submitted-a). The thermal expansion was obtained from six coupled climate models of intermediate complexity (Figure 10.43 in Solomon et al. 2007). The contribution for glaciers was obtained with the models from Mazeion et al. (2012) and Radic and Hock (2011) by integration with fixed boundary conditions corresponding to different GMT levels for 3000 years. The contributions from the Greenland ice sheet were computed with a dynamic ice sheet model coupled to

an energy-moisture balance model for the SMB. The model parameters where constraint by paleo-data for the last interglacial (Robinson et al., 2012). The Antarctic ice sheet contribution was taken from the simulation of the last 5 million years (Pollard and Deconto, 2009) in good agreement with regional paleo-records (Naish et al., 2009). Such comparison of model results with paleo-records of past sea level and the physical basis of the different models provide medium confidence that the sea level commitment per degree of warming is about 2 m with a stepwise increase of about 6 m at the deglaciation threshold of Greenland. Current ocean- and ice sheet models indicate that such sea level rise would occur on a multi-millennial time scale (Huybrechts et al., 2011; Robinson et al., 2012), but confidence in this time-scale is low.

Table 13.7: Median and model spread of the thermal expansion of CMIP5 comprehensive climate models. ECP-2.6 belongs to the low scenarios as shown in Figure 13.11 and Table 13.8; ECP-4.5 is a 'medium scenario' and ECP-8.5 a 'high scenario'. The model spread of low and medium scenarios in Table 13.8 compare well with the ECP-2.6 and 4.5 model spread. The high scenario model spread is larger than for ECP-8.5 because by definition it includes also ECP-6.0 simulations.

	Mean 2191–2200			Mean 2291–2300		
Scenario	# of Models	Median	Model Spread	# of Models	Median	Model Spread
ECP-2.6	3	0.19	0.15–0.22	3	0.21	0.15–0.25
ECP-4.5	7	0.39	0.30–0.47	6	0.54	0.38–0.66
ECP-8.5	2	0.85	0.80–0.90	2	1.34	1.26–1.41

Table 13.8: Model spread of sea level contribution and total sea level change for low, medium and high scenarios as defined in the text and shown in Figure 13.11a.

Contribution	Scenario	2200	2300	2400	2500
Thermal Expansion	low	0.24–0.26	0.26–0.27	0.24–0.29	0.22–0.30
Glaciers	low	0.12–0.23	0.13–0.19	0.13–0.19[b]	0.13–0.19[b]
Greenland Ice Sheet	low	0.14[a]	0.25[a]	0.36[a]	0.50[a]
Antarctic Ice Sheet	low	–0.03[a]	–0.04[a]	–0.06[a]	–0.08[a]
Total	low	0.47–0.60	0.59–0.67	0.67–0.79	0.77–0.91
Thermal Expansion	medium	0.23–0.47	0.32–0.58	0.38–0.67	0.41–0.72
Glaciers	medium	0.14–0.28	0.17–0.25	0.17–0.25[b]	0.17–0.25[b]
Greenland Ice Sheet	medium	0.05–0.17	0.08–0.33	0.11–0.52	0.14–0.75
Antarctic Ice Sheet	medium	–0.17 to –0.02	–0.25 to –0.04	–0.36 to –0.05	–0.45 to –0.06
Total	medium	0.25–0.90	0.31–1.12	0.30–1.38	0.27–1.67
Thermal Expansion	high	0.36–1.07	0.52–1.49	0.62–1.76	0.71–1.97
Glaciers	high	0.22–0.34	0.25–0.35	0.25–0.35[b]	0.25–0.35[b]
Greenland Ice Sheet	high	0.13–0.50	0.31–1.19	0.51–1.94	0.73–2.57
Antarctic Ice Sheet	high	–0.04 to –0.01	0.02–0.19	0.06–0.51	0.11–0.88
Total	high	0.67–1.92	1.10–3.21	1.44–4.55	1.80–5.76

Notes:
(a) The value is based on one simulation only.
(b) Due to lack of available simulations the same interval used as for the year 2300.

13.6 Regional Sea Level Changes

Regional sea level changes may differ substantially from a global average, with complex spatial patterns resulting from ocean dynamical processes, movements of the sea floor, and changes in gravity due to water mass redistribution (land ice and other terrestrial water storage) in the climate system. In many cases, regional controls are associated with natural or anthropogenic climate modes rather than factors causing

changes in the global average value, and include such ocean processes as a dynamical redistribution of water masses, and a change of water-mass properties, caused by changes in winds and air-pressure, air-sea heat and freshwater fluxes, and ocean currents. Since the characteristic time scales of all involved processes are different, their relative contribution to net regional sea level variability or change will depend fundamentally on the time scale considered.

13.6.1 Regional Sea Level Changes, Climate Modes and Forced Sea Level Response

As discussed in Chapter 3, most of the regional sea level changes observed during the altimetry era or reconstructed during recent decades from tide gauges appear to be steric (Ishii and Kimoto, 2009; Levitus et al., 2005; Levitus et al., 2009; Lombard et al., 2005a; Lombard et al., 2005b). Moreover, steric changes observed during the altimetry era appear to be primarily thermosteric in nature, although halosteric effects, which can reduce or enhance thermosteric changes, are also important in some regions (e.g., Atlantic Ocean). Ocean models and ocean reanalysis-based results (Carton et al., 2005; Stammer et al., 2011; Wunsch and Heimbach, 2007) as well as ocean circulation models without data assimilation (Lombard et al., 2009) confirm these results.

Observations and ocean reanalysis (Stammer et al., 2011) also agree in showing that steric spatial patterns over the last half of the 20th century fluctuate in space and time as part of modes of the coupled ocean-atmosphere system such as the El Niño-Southern Oscillation (ENSO), the North Atlantic Oscillation (NAO), and the Pacific Decadal Oscillation (PDO) (Di Lorenzo et al., 2010; Levitus et al., 2005; Lombard et al., 2005b; Lozier et al., 2010), and may significantly alter (reduce or enhance) the global mean sea level rise (Becker et al., 2011). In these cases, regional sea level variability is associated with changing wind fields and resulting changes in the ocean circulation (Kohl and Stammer, 2008). For example, the large rates of sea level rise in the western tropical Pacific and the fall in the eastern Pacific over the period 1993–2010 correspond to an increase in the strength of the trade winds in the central and eastern tropical Pacific over the same period (Merrifield and Maltrud, 2011; Timmermann et al., 2010). The long-term sea level trend from 1958 to 2001 in the tropical Pacific can also be explained as the ocean's dynamical response to variations in the wind forcing (Qiu and Chen, 2006; Timmermann et al., 2010).

Spatial variations in trends in regional sea level may also be specific to a particular sea or ocean basin. For example, a sea level rise of 5.4 ± 10.3 mm yr^{-1} in the East/Japan Sea from 1993 to 2001 is about two times the GMSL trend, with more than 80% of this rise being thermosteric (Kang et al., 2005). Han et al. (2010) found that regional changes of sea level in the Indian Ocean that have emerged since the 1960s are driven by changing surface winds associated with a combined enhancement of Hadley and Walker cells.

13.6.2 CMIP5 GCM Projections/Predictions on Decadal to Centennial Time Scales

CMIP5 projections provide primarily dynamic sea level changes resulting from increased heat uptake and changes in the wind forcing. On decadal time scales, regional sea level changes identified in the CMIP5 model ensemble are associated with natural climate modes (Figure 13.12a) leading to strong interannual variability in the tropical Pacific and Indian Oceans (up to 8 cm, RMS) associated with ENSO and dynamics of the equatorial current system. Similar variability in the amplitude of sea level change is also apparent in the North Atlantic Current and in the Southern Ocean.

[INSERT FIGURE 13.12 HERE]

Figure 13.12: (a) RMS Interannual dynamic sea level variability (m) in the CMIP5 multi-model ensemble (12 models total), built from the historically forced experiments during the period 1951–2005; **(b)** Changes in the ensemble average interannual dynamic sea level variability (std. dev.; in m) evaluated over the period 2081–2100 relative to period 1986–2005. The projection data (2081–2100) is from the CMIP5 RCP4.5 experiment.

Toward the end of the 21st century, the CMIP5 results indicate it is possible that the interannual to decadal variability of dynamic sea level can weaken in some parts of the world ocean, for example the western low-latitude Pacific and parts of the Indian Ocean (Figure 13.12b), whereas it could be amplified in other parts, for example the North Pacific, the eastern tropical Pacific, the eastern subtropical Atlantic, and the Arctic. According to Han et al. (submitted) a reduction in decadal variability in the low-latitude western Pacific and

Indian Ocean might result from pattern of decadal sea level changes becoming more long-term under climate change conditions through a modified Indian Ocean-Pacific SST relationship.

Longer than decadal time scale regional sea level changes can increasingly be expected to result from long-term changes in the wind field, changes in the regional and global ocean heat and freshwater content and the associated dynamical adjustment, and (to a lesser extent) from atmospheric pressure (with associated redistribution of ocean properties). The CMIP5 projections of steric sea level changes toward the end of the 21st century reveal a clear regional pattern in dynamical sea level change, in which the Southern Ocean shows a net decline, while the remaining global ocean displays complex ridge-and-trough structures superimposed on a generally rising sea level (Slangen et al., submitted; Yin, submitted; Figure 13.13). For example, in the North Atlantic, sea level rises strongest along and north of the North Atlantic Current, but less so further to the south in the center of the warmer subtropical gyre. A similar dipole pattern was observed in CMIP3 results there due to a weakening of the AMOC which leads to a local steric sea level rise east of North America, resulting in more water on the shelf and directly impacting northeastern North America (Landerer et al., 2007; Levermann et al., 2005; Yin et al., 2010). A similar pattern can be observed in the North Pacific. Here and in other parts of the world ocean (e.g., Southern Ocean), regional sea level patterns are highly likely to be the result of changes in wind forcing, associated changes in the circulation and an associated redistribution of heat and freshwater. Some regional changes can also be expected to result from modifications in the expansion coefficient due to changes in the oceans regional heat content (Kuhlbrodt and Gregory, submitted). Suzuki et al. (2005) compared changes in mean dynamic sea level in 2080–2100 relative to 1980–2000 as obtained from a low- and a high-resolution ocean component of a coupled model and concluded that while changes are comparable between runs, the high-resolution model captures enhanced details due to resolving ocean eddy dynamics.

The 12-model ensemble indicates that regions showing an enhanced sea level toward the end of the 21st century coincide with those showing the largest uncertainty (Figure 13.13b). While this appeared also in the CMIP3 SREX A1B results, the CMPI5 results show a general reduction in the ensemble spread, especially in high latitudes. On global average this reduction is from 5.7 to 2.1 cm, rms, which at last partly, is possible to results from a better confined forcing scenario and possibly an improved high-latitude hydrological cycle in CMIP5 models.

[INSERT FIGURE 13.13 HERE]

Figure 13.13: (a) Ensemble mean projection of the time-averaged steric sea level changes for the period 2081–2100 relative to period 1986–2005, computed from 12 CMIP5 climate models (in m), using the RCP4.5 scenario. The figure includes the globally averaged steric sea level increase of 0.17 ± 0.05 m. **(b)** RMS spread (deviation) of the individual model result around the ensemble mean (m).

The contribution of changes of global ocean heat storage to regional steric sea level anomalies is virtually certain to increase with time as the climate-warming signal increasingly penetrates into the deep ocean (Pardaens et al., 2011a). For the last three decades of the 21st century, the AR4 climate model ensemble mean shows a significant heat storage increase (Yin et al., 2010), about half of which is stored in the ocean below 700 m depth (Section 13.5). Recent detection of ongoing changes in the ocean salinity structure (Durack and Wijffels, 2010) may also contribute to future regional steric sea level changes. Halosteric effects can dominate in some regions, especially in regions of high-latitude water mass formation where long-term heat and freshwater changes are expected to occur (e.g., in the subpolar North Atlantic, the Arctic, the Southern Ocean; Pardaens et al., 2011a; Yin et al., 2010). Because of an anticipated increased atmospheric moisture transport from low to high latitudes (Pardaens et al., 2003), future halosteric anomalies are likely to be negative in the North Atlantic basin and partly compensate the thermosteric sea level increase there. However, they are positive in the Arctic Ocean and dominate regional sea level anomalies (Yin et al., 2010). It is likely that future thermosteric changes will dominate the steric variations in the Southern Ocean, and strong compensation between thermosteric and halosteric change will characterise the Atlantic (Pardaens et al., 2011a).

13.6.3 Response to Atmospheric Pressure Changes

Regional sea level also adjusts to regional changes in atmospheric sea level pressure relative to its instantaneous mean over the ocean. Over time scales longer than a few days, the adjustment is nearly

isostatic (i.e., inverted barometer effect). Sea level pressure is projected to increase over the subtropics and mid-latitudes (depressing sea level) and decrease over high latitudes (raising sea level), especially over the Arctic (order several millibars by the end of the 21st century) associated with a poleward expansion of the Hadley Circulation and a poleward shift of the storm tracks of several degrees latitude (Held and Soden, 2006). The atmospheric inverse barometer effect may therefore contribute positively to the sea level rise in the Arctic (Yin et al., 2010). Air pressure may also influence regional sea level elsewhere, as demonstrated by sea level changes in the Mediterranean in the second half of the 20th century (Tsimplis et al., 2005).

13.6.4 Response to Freshwater Forcing

Enhanced freshwater fluxes derived from an increase in ice sheet melt water at high latitudes results in a regional pattern of sea level rise originating from adjustments in ocean dynamics and in the solid earth. Both effects are presently not included in CMPI5 models although the latter adjustment is computed off line here.

13.6.4.1 Dynamic Ocean Response to Cryospheric Freshwater Forcing

The addition of freshwater from glaciers and ice sheets to the ocean leads to an instantaneous increase in global mean sea level. But because it is communicated around the ocean basins via a dynamical adjustment, it is not instantaneously globally uniform (e.g., Cane, 1989; Kawase, 1987). The addition of mass is communicated barotropically within days (Gower, 2010; Lorbacher et al., 2012). The addition of freshwater to the ocean from Greenland melting results in an additional basin-wide steric response of the North Atlantic within months and is communicated to the global ocean via boundary waves, equatorial Kelvin waves, and westward propagating baroclinic Rossby waves on decadal time scales (Stammer, 2008). A similar response but with a different pattern can be observed from Antarctic meltwater input. In both cases, an associated complete baroclinic adjustment of the global ocean might take as long as several centuries. The adjustment of the ocean to high-latitude meltwater input also involves atmospheric teleconnections which, such as in response to Greenland meltwater pulses, could lead to sea level changes in the Pacific within months (e.g., Stammer et al., 2011). On longer-than-decadal time scales, the freshwater input to the North Atlantic raises sea level in the Arctic Ocean and reverses the Bering Strait throughflow, transporting colder, fresher water from the Arctic Ocean into the North Pacific (Hu et al., 2010) and causing North Pacific cooling (Okumura et al., 2009).

Meltwater forcing in the subpolar North Atlantic also causes changes of the AMOC, which in turn causes dynamic changes of sea level in the North Atlantic, particularly in its northwestern region (Lorbacher et al., 2010). The combination of this dynamic sea level rise and the global mean sea level makes the northeastern North American coast vulnerable to some of the fastest and largest sea level rises during this century (Yin et al., 2009).

13.6.4.2 Earth and Gravitational Response to Contemporary Surface Water Mass Redistribution

Ice sheet and glacier mass loss and corresponding water mass redistribution between the cryosphere, the land and the oceans causes solid Earth and rotational responses to the varying loads and distinctive regional changes in the gravity field and sea level (‘fingerprints’; Gomez et al., 2010b; Mitrovica et al., 2009; Mitrovica et al., 2001; Riva et al., 2010; see FAQ 13.1). Most existing studies of these effects have not defined a specific rate of ice sheet mass loss (Mitrovica et al., 2001) or are based on end-member scenarios of ice retreat, such as from the West Antarctic ice sheet (Bamber et al., 2009; Gomez et al., 2010b; Mitrovica et al., 2009) and marine-based parts of the East Antarctic ice sheet (Gomez et al., 2010b). Bamber and Riva (2010) calculated the relative sea level fingerprint of all contemporary land-ice melt and each of its major components.

All of these studies demonstrate that the sea level response to these events includes large regional departures from the mean value, whereby regions adjacent to the source of the mass loss are subject to relative sea level fall up to several times the global average rise from these mass contributions, whereas in the far field the sea level rise is larger (up to about 30%) than the global average rise (Gomez et al., 2010b; Mitrovica et al., 2009; Mitrovica et al., 2001). Gomez et al. (2010b) and Mitrovica et al. (2011) showed that differences in the maximum predicted rise (relative to the global mean) between published results is due to the accuracy with which water expulsion from the deglaciated marine basins is calculated. These changes are in addition to the

ongoing response to past changes (e.g., glacial isostatic adjustment in response to the last deglaciation). While the ice sheet fingerprints have not yet been detected in the observations, it is likely that with further ice sheet melting they will begin to dominate the regional patterns of sea level change toward the end of the 21st century, especially under strong climate forcing conditions (RCP8.5, Kopp et al., 2010).

Water mass redistributions associated with land hydrology changes other than those from land ice may also produce spatially variable 'fingerprints' in sea level (Fiedler and Conrad, 2010). In particular, regional changes in the terrestrial storage of water can lead to a sea level response on interannual and longer time scales, specifically near large river basins (Riva et al., 2010).

13.6.5 Net Regional Sea Level Changes

Over the next decades, net regional sea level changes are likely to be dominated by dynamical changes (mass redistribution and steric components) resulting from natural variability. However, toward the end of the 21st century, regional patterns in sea level from all other contributions will progressively emerge and eventually dominate over the natural variability (Church et al., 2011a; Katsman and van Oldenborgh, 2011; Slangen et al., 2011).

Slangen et al. (submitted) presented ensemble mean estimates of relative sea level change during the period 2081–2100 relative to 1986–2000 resulting from GIA and from glacier and ice sheet melting for RCP4.5 and RCP8.5 scenarios[1]. Their results (Figure 13.14) suggest that for the 21st century, past, present and future loss of land ice is likely to remain an important contributor to spatial patterns in sea level change, leading to rates of maximum rise at low to mid latitudes due ice-melt fingerprints. Locally, sea level rise can also partly be compensated by vertical land movement resulting from GIA, especially in some formerly glaciated high-latitudes regions where high rates of land uplift may lead to a decrease of relative sea level.

[INSERT FIGURE 13.14 HERE]

Figure 13.14: Ensemble mean regional sea level contributions to sea level change (m) from GIA (upper panel), glaciers (middle panel) and ice sheets (lower panel). The lower two panels are based on information from scenario RCP4.5 and all panels represent changes between the periods 1986–2000 and 2081–2100 (from Slangen et al., submitted).

The ensemble mean net sea level anomaly pattern (Figure 13.15a; not including the dynamic ocean contribution in response to the influx of freshwater associated with land-ice loss, the change of atmospheric loading and changes in terrestrial ground water) reveals that under the RCP4.5 scenario, many regions are likely to experience regional sea level changes that differ substantially from the global mean. Local sea level changes deviate more than 10% and 25% from the global mean projection for as much as 45% and 12% of the ocean area, respectively, indicating that spatial variations can be very large: regional changes in sea level reach values of up to 30% above the global mean value in equatorial regions, in the southern Ocean and around North America, and up to 50% below the global mean in the Arctic region Figure 13.15b).

[INSERT FIGURE 13.15 HERE]

Figure 13.15: (a) Ensemble mean regional sea level change (m) evaluated from 12 models of the CMIP5 scenario RCP4.5 between 1986–2005 and 2081–2100 (Slangen et al., submitted). Global mean = 0.35 ± 0.06 m; range = –0.68 to +0.73 m. **(b)** Percentage of the deviation of the ensemble mean regional sea level change between 1986–2005 and 2081–2100 from the global mean value.

Shown in Figure 13.16a are the probability distribution functions (PDF's) of sea level changes along coastlines above and below the global mean value resulting from an RCP4.5 and RPC8.5 scenario between 1986–2005 and 2081–2100. The figure shows substantially skewed non-Gaussian distributions revealing significant coastal deviations of sea level changes from the global mean. For a comparison, similar PDFs but excluding the coastlines around Antarctica and Greenland are shown in the lower panel of the figure. Although most negative changes disappear, the general structures of the PDF remain, revealing changes along the coastlines ranging from about 20 to 50 cm for an RCP4.5 scenario, peaking near 40 cm, and from about 40 cm to more than 80 cm under a RCP8.5 scenario, peaking near 75 cm.

[1] We note here that the Slangen et al. (submitted) results used for the regional projections differ from the ice-sheet projections presented in Section 13.4, although they agree within uncertainties. In the final draft, the Slangen et al. analyses will be redone in a consistent manner.

[INSERT FIGURE 13.16 HERE]

Figure 13.16: (top) PDF of the deviation of the ensemble mean regional sea level change along all coastlines between 1986–2005 and 2081–2100 from the global mean value. Shown are results for RCP4.5 (blue) and ROC8.5 (pink), respectively. (bottom) Same as in the top panel, but excluding Antarctic and Greenland coastlines.

The combination of the natural variability (annual mean) and the projected sea level rise from the AR5 are shown for a number of locations distributed around the world (Figure 13.17). For example, in Pago Pago (14°S, 195°E) in the western equatorial Pacific, the available historical record indicates that annual variability in mean sea level has been about 21 cm (5–95% range). In Palermon (38°N, 13°E), the annual variability in the historic sea level record is 5.1 cm. Projections by individual climate models indicate that it is likely that a similar range of natural variability will continue through the 21st century (Figure 13.15b). However, by 2100, the average projected sea level for the RCP4.5 scenario of 35 cm (with a 5–95% range of 28.7–41.3 cm) is greater than any observations of annual mean sea level in the instrumental record. Of course, monthly variability and extreme sea levels from winds and waves associated with weather phenomena (Section 13.8) need to be considered in addition to these projections of mean sea level.

[INSERT FIGURE 13.17 HERE]

Figure 13.17: Observed and projected relative sea level change near nine representative stations. The observed *in situ* relative sea level records from tide gauges (since the late 1970s) are plotted in yellow, and the satellite record (since 1993) is provided as purple lines. The projected range from 12 CMPI5 RCP4.5 scenario runs (5–95% uncertainty range) are shown by the shaded region for the period 2000–2100, with the bold line showing the ensemble mean. Colored lines represent individual climate model realizations drawn from three different climate models.

Grinsted et al. (submitted) estimated a 21st century relative sea level rise of about 50 cm for the southern Baltic, and a relative sea level drop of about 30 cm in the Bay of Bothnia. Hu et al. (2011) and Sallanger Jr. et al. (2012) suggested that steric and dynamical sea- level changes can potentially increase the sea level increase near the northeastern coast of North America and in the western Pacific; however, considerable uncertainties remain in both the sea level budget and in the regional expression of sea level rise.

13.6.6 Uncertainties and Sensitivity to Ocean/Climate Model Formulations and Parameterizations

Sea level is a property of the ocean connected to nearly all dynamical and thermodynamical processes over the full ocean column, from the surface fluxes to the ocean bottom. While many of the processes are to first order correctly simulated in climate models, differences between models indicate that uncertainties in simulated and projected steric sea level remain poorly understood (Figure 13.18). Moreover, the ocean heat uptake efficiency differs between models leading to a spread of 50% in heat storage changes (Kuhlbrodt and Gregory, submitted). In addition, some processes are not yet properly simulated, such as the dynamical response of the ocean to melt-water input or processes in the solid Earth associated with this ice mass loss. In addition, Stammer and Hüttemann (2008) showed that coupled climate models that do not include the effect of changes in atmospheric moisture content on sea level pressure will underestimate future regional atmospheric pressure loading effects by up to 2 cm. Other uncertainties result form GIA/rotational/gravitational effects as well as from uncertainties in air-sea fluxes.

[INSERT FIGURE 13.18 HERE]

Figure 13.18: Projected relative sea level change patterns (m) from the combined global steric plus dynamic topography and glacier contributions for RCP4.5 over the period from 1986–2005 to 2081–2100 for each individual climate model used in the production of Figure 13.15a.

Improvements in the skill of a sea level projection require (1) better parameterizations of unresolved physical processes, (2) improved numerical algorithms for such processes as tracer advection, (3) refined grid resolution to better represent such features as boundary currents and mesoscale eddies, and (4) the elimination of obsolete assumptions that have a direct impact on sea level (e.g., rigid lid and virtual tracer fluxes). Among the many limiting approximations made in ocean models, the Boussinesq approximation has been found to only marginally impact regional patterns (i.e., deviations from global mean) when directly compared to non-Boussinesq simulations (Losch et al., 2004), thus lending greater confidence in Boussinesq models for addressing questions of regional sea level change. Furthermore, for global sea level, the now

standard *a posteriori* adjustment of Greatbatch (1994) accurately incorporates the missing global steric effect.

Coarse-resolution ocean-climate simulations require a parameterization of mesoscale and smaller eddies, but the parameterizations as well as the details of their numerical implementations can greatly impact the simulation. As shown by Farneti et al. (2010), coarse-resolution climate models may be over-estimating the ACC response to wind changes. Better implementations of eddy parameterizations reduce such biases (Farneti and Gent, 2011; Gent and Danabasoglu, 2011), and they form the basis for some, but not all, of the CMIP5 simulations. Moreover, Vinogradov and Ponte (2011) suggested that as one considers regional sea level variability and its relevant dynamics and forcing, mesoscale ocean features become important factors on a sub-decadal time scale.

Even with a perfect ocean model, skill in sea level projections depends on skill of the coupled climate model in which errors impacting sea level may originate from non-ocean components. Furthermore, initialization is fundamental to the prediction problem, particularly for simulation of low-frequency climate variability modes (Meehl et al., 2010). Projections of land-ice melting and the resultant sea level rise patterns also have large uncertainties, with additional uncertainties arising from GIA models such as the mantle viscosity structure. Each of the many uncertainties and errors results in considerable spread in the projected patterns of sea level changes in the CMIP3 models used as part of AR4, which is similar to the spread seen in the TAR models (Pardaens et al., 2011a; Slangen et al., 2011). In addition to ocean/climate model formulations and parameterizations, uncertainty (in predictions of sea level change) may be associated with specified freshwater forcing. Whether or not an ocean model is coupled with an ice sheet model, the forcing should distinguish between runoff and iceberg flux. Martin and Adcroft (2010) reported the only attempt thus far to explicitly represent iceberg drift and melting in a fully coupled climate model.

13.6.7 Summary Assessment

During the 20th century, sea level relative to the coast has varied as a result of natural variability in the climate system, longterm trends in ocean height and vertical land motion. These variations will continue during the 21st century.

For much of the coastline, the largest sea level changes over the next few decades will continue to be associated with natural (dynamical) climate modes superimposed on the long term trends (high confidence), with good correspondence between regional sea level variability, and changes in ocean currents and upper-ocean heat and salt content. It is *very likely* (high confidence) that toward the end of the 21st century sea level change will remain to have a strong regional pattern, with significant deviations of local and regional sea level change from the global mean change. The dynamical variability of sea level will continue and will be critical component of sea level impacts and extreme events (Section 13.8). However, on those longer time scales, regional sea level changes will result increasingly from mass changes of the ocean from glaciers and ice sheets, including the regional patterns from both contemporary and past changes in land ice, changes in atmospheric loading, and vertical land motions, with relative contributions from each varying significantly around the Earth.

It is *very likely* (high confidence) that over about 95% of the world ocean, regional sea level rise will be positive with mostly regions near current and former glaciers and ice sheets experiencing a sea level fall. About 72% and 77% of the coastline will experience a sea level change within ±20% of the GMSL change for RCP4.5 and 8.5, respectively. In both cases the maximum of the PDF is larger than the GMSL, however, the arithmetic mean is lower than the global mean (0.3 m vs. 0.37 m for RCP4.5; 0.56 m vs. 0.68 m for RCP8.5, respectively). Only some coastlines will experience a sea level rise of up to 50% above the GMSL change.

13.7 21st Century Projections of Sea Level Extremes and Waves

Climate change will affect extreme sea levels and ocean waves in two principal ways. First, because extra-tropical and tropical storms are the key drivers of extreme wave and sea level events, future changes in intensity, frequency, duration, and path of these storms will have impacts on wave and sea level extremes. Second, sea level rise adds to the heights of sea level extremes, regardless of how the storm-related

component evolves. MSL change may also change the threat of coastal inundation due to changes in wave runup. Observational evidence on changes in extreme sea level and waves is discussed in Chapter 3. Extreme sea levels at the coast occur mainly in the form of storm surges and tsunamis, but because the latter is not a climatic event, it is not considered. Here we assess projections for extreme sea levels and waves based on estimates of future storminess and MSL change.

13.7.1 Changes in Sea Level Extremes

As discussed in the AR4 (Bindoff et al., 2007) and confirmed by more recent studies (Menéndez and Woodworth, 2010), statistical analyses of tide-gauge observations have shown an increase in observed sea level extremes worldwide that are caused primarily by an increase in MSL (Chapter 3). Dominant modes of climate variability, particularly the El Niño–Southern Oscillation (ENSO) and the North Atlantic Oscillation (NAO), also have a measureable influence on extreme sea levels in many regions (Lowe et al., 2010; Walsh et al., 2011). These impacts are due to sea level anomalies associated with the climate mode, as well as mode-related changes in storminess.

13.7.2 Projections of Extreme Sea Levels

13.7.2.1 Recent Projection Assessments

The AR4 assessed projections of storm surges for a few regions (Europe, Australia, the Bay of Bengal) based on a limited number of dynamical modeling studies (Christensen et al., 2007). Although their results generally indicated higher magnitude surges in future scenarios, there was low confidence in these projections because of the wide spread in AOGCM and RCM projections. Lowe et al. (2010) completed a comprehensive review of changes in observed extremes and their driving forces and future projections, and concluded that the increases in the observed sea level extremes in the 20th century occurring primarily through an increase in MSL apply to projections for the 21st century as well.

Studies since the AR4 have also considered extreme sea levels in other regions, including the relative contributions of sea level rise and storminess on projected extremes. The SREX (Seneviratne et al., 2012) assessment concluded that it is very likely that MSL rise will contribute to upward trends in future extreme sea level. It notes that changes in storminess may also affect extreme sea levels but the limited geographical coverage of studies and uncertainties associated with storminess changes prevented a general assessment. It also noted that the global tropical cyclone frequency will likely decrease or remain roughly constant, but there is medium confidence that the frequency of the most intense storms will increase in some ocean basins (Seneviratne et al., 2012). Uncertainties in projections of the frequency and track of cyclones make it difficult to project how these changes will impact particular regions. Similarly, while the SREX and the current assessment (Chapter 14) find that it is likely that there has been a poleward shift in the main northern and southern extra-tropical cyclone tracks during the last 50 years, and that regional changes may be substantial, there is only low confidence in region-specific projections.

13.7.2.2 Projections Based on Dynamical and Statistical Approaches

Projected changes in storminess have been assessed by directly applying climate-model forcing to a storm-surge model. Using three regionally downscaled GCMs for A2, B2 and A1B scenarios, Debernard and Roed (2008) found statistically significant changes between 1961–1990 and 2071–2100 of an 8–10% increase in the 99th percentile surge heights, mainly during the winter season, along the coastlines of the eastern North Sea and the northwestern British Isles, and decreases south of Iceland. Using a downscaled GCM under an A1B scenario, Wang et al. (2008) projected a significant increase in wintertime storm surges around most of Ireland between 1961–1990 and 2031–2060. Sterl et al. (2009) concatenated the output from a 17-member ensemble of A1B simulations from a GCM over the model periods 1950–2000 and 2050–2100 into a single longer time series to estimate 10,000-year return values of surge heights (relative to mean sea level) along the Dutch coastline. No statistically significant change in this value was projected for the 21st century because projected wind-speed changes were not associated with the maximum surge-generating northerlies. Using an ensemble of three climate models under A2 simulations, Colberg and McInnes (2012) found changes in 95th percentile sea level height across the southern Australian coast in 2081–2100 compared to 1981–2000 were small (±0.1 m), mostly negative, and resembled the changes in wind patterns simulated by

the climate models to some degree (McInnes et al., 2011) although inter-model differences were apparent. These studies demonstrate that the results are sensitive to the particular choice of GCM or RCM, therefore indicating uncertainties associated with the projections. Unnikrishnan et al. (2011) used RCM simulations to force a storm-surge model for the Bay of Bengal and found that the combined effect of sea level rise and RCM projections for the A2 scenario (2071–2100) gave an increase in 100-year return levels of total sea level (including tides) varying between 0.40 and 0.67 m (about 15–20%) along the northern part of the east coast of India, except around the head of the bay, compared to those in the base line (1961–1990) scenario.

Several regional storm surge studies have considered the relative contribution of the two main causative factors, MSL rise and changes in projected atmospheric fields, on changes in future sea level extremes (e.g., McInnes et al., 2009, for the southeastern coast of Australia; Brown et al., 2010, for the eastern Irish Sea; and Woth et al., 2006, for the North Sea). They concluded that sea level rise has a greater potential than meteorological changes to increase extreme sea levels by the end of the 21st century in these locations. Similarly, for the tropical east coast of Australia, Harper et al. (2009) found that a 10% increase in tropical cyclone intensity led to increases in the 1-in-100 year total sea level (including tides) that were considerably smaller than for a 0.3 m sea level rise.

Using six hypothetical hurricanes that produced approximate 100-year return sea levels, Smith et al. (2010) found that on the southeastern Louisiana coast in the regions of large surges, the effect of mean sea level rise on simulated surges was linear. However, in the regions of moderate surges (2–3 m), particularly in wetland-fronted areas, the increase in surges was larger by 1–3 m than the present values. The study showed that sea level rise alters the speed of propagation of surges and their amplification varied in different regions of the coast. For the Gulf of Mexico, Mousavi et al. (2011) developed a simple relationship between hurricane-induced storm surges, sea level rise and hurricane intensification through increased SSTs for three modeled major historical cyclones, and found that the dynamic interaction of surge and sea level rise lowered or amplified the surge at different points within a shallow coastal bay.

Higher mean sea levels can significantly decrease the return period for exceeding given threshold levels. For a network of 198 tide gauge sites covering much of the globe, Hunter (2012) determined the Gumbel scale parameter to estimate the factor by which the frequency of flooding events at a given height would increase for a MSL rise of 0.5 m (Figure 13.19). The factor depends exponentially on the inverse of the Gumbel scale parameter, which is a measure of the variability of sea level extremes (caused by a combination of tides and storm surges). The scale parameter is generally large where tides and/or storm surges are large, leading to a small amplification factor. Conversely, locations that have small overall sea level range have a small scale parameter and consequently a large multiplication factor. This implies that for many locations a 0.5 m MSL rise would likely result in the 100-year return period event shifting to a 10-year or even 1-year return period. Large increases in the frequency of extreme sea levels for 2050 were found for a network of sites around the USA coastline based on semi-empirical MSL rise projections and 20th century statistics of extremes (Tebaldi et al., 2012). Cayan et al. (2008) obtained a similar finding for the California coast, in which they used projected time series of tides, MSL rise, components for sea level fluctuations from projected MSLP and wind stress fields and a contribution for ENSO variability through projected SSTs for the 21st century, to show that for high-end scenarios of MSL rise, the frequency and magnitude of extremes increases considerably relative those experienced in the 20th century.

[INSERT FIGURE 13.19 HERE]

Figure 13.19: The estimated factor (shown in red circles) at 198 tide gauge stations over the globe by which the frequency of flooding events of a given height increase for a mean sea level rise of 0.5 metre.

13.7.3 Projections of Ocean Waves

Wave-field variability is determined by changes in the major wind systems, especially in the main tropical and extra-tropical storm tracks. Prevailing wind and storm characteristics are known to vary with natural modes of climate variability (see Chapter 14), and a number of studies have related changes in wind wave climatologies to ENSO (Adams et al., 2008; Allan and Komar, 2006; Menéndez et al., 2008), the NAO (Izaguirre et al., 2010; Woolf et al., 2002), and SAM (Hemer et al., 2010; Izaguirre et al., 2011). Therefore, the primary challenge for wind-wave projection efforts is to down-scale information regarding future wind states based on coarse resolution climate models into regional and global wave model predictions.

13.7.3.1 Storm Projections and Ocean Waves

The AR4 assessment, the SREX assessment (Seneviratne et al., 2012), and the current assessment (Chapter 3) have reviewed evidence for positive, as well as negative, wave-height trends based on *in situ* observations. Trends and variability in wave heights since the early 1990s have been described using satellite altimeter data (Hemer et al., 2010; Izaguirre et al., 2011; Young et al., 2011). Based on *in situ* and altimeter observations, it is likely that wave heights have increased in the North Pacific over the past century, in the North Atlantic since the 1950s, and in the Southern Ocean over the last two decades (Chapter 3). Nevertheless, the observational wave record is sparse in space and time, which makes the separation of long-term change from natural variability uncertain. Wang et al. (2009) concluded that the effects of anthropogenic forcing are detectable during winter months at high latitudes, particularly in the northeastern North Atlantic; however, biases in their simulations raise the uncertainty of this finding.

For long-term wind projections, the SREX (Seneviratne et al., 2012) and current (Chapter 14) assessments report a likely poleward shift in mid-latitude winter storm tracks, with less certainty regarding future changes in tropical cyclones. In the Southern Hemisphere, this shift is likely to be associated with a trend toward a positive SAM phase, with an increase in wind speeds. In general, there is low confidence in region-specific projections of tropical cyclones. As noted in Chapter 14, projections for ENSO remain uncertain, and model projections show that the NAO tends toward a more positive phase in late 21st century projections, but the amplitude change is slight.

13.7.3.2 Wave Projections Based on Climate Models

Although uncertainties remain regarding future storm patterns, there has been continued progress in translating climate model outputs into wind-wave projections. In the AR4, projected changes in global SWHs were based on a single statistical model (Wang and Swail, 2006). The projected conditions were consistent with increased wind speeds associated with mid-latitude storms, but considered only a limited five-member ensemble for a single future emission scenario (SRES A2), and wave parameters other than SWH were not considered.

Since the AR4, global wave-climate projections for the end of the 21st century have been made by dynamically downscaling CMIP3 AOGCM results. A multi-model ensemble based on dynamical models forced with various greenhouse gas emission scenarios (SRES A1B; Mori et al., 2010; Semedo et al., submitted; Fan et al., submitted; SRES A2; Hemer et al., submitted-b), as well as the statistical model of Wang and Swail (2006; emission scenarios IS92a and SRES A2 and B2) has been constructed as part of the Coordinated Ocean Wave Climate Project (COWCLIP) Hemer et al. (submitted-a). In general, the ensemble projected changes of annual mean SWH (Figure 13.20a) are similar to the statistical projections of Wang and Swail (2006) discussed in the AR4 (under an SRES A2 scenario). The region with the largest projected change is the Southern Ocean, where mean SWHs at the end of the 21st century are approximately 5–10% higher than the present-day mean. SWH increase in this region reflects the projected strengthening of the westerlies over the Southern Ocean, particularly during austral winter (Figure 13.20b). Another notable region of SWH increase in the ensembles is in the tropical South Pacific associated with a projected strengthening of austral winter easterly trade winds in the CMIP3 multi-model dataset (Figure 13.20c). A consistent mean SWH decrease is projected for all other ocean basins, notably in the trade wind region of the North Pacific, below the mid-latitude westerlies in all basins, and in the trade and monsoon wind regions of the Indian Ocean. Three of the model projections (Hemer et al., submitted-b; Mori et al., 2010; Fan et al., submitted) were used to intercompare projections of wave direction and period. Wave direction (Figure 13.20d) exhibits clockwise rotation in the tropics, consistent with a higher contribution from swell from the Southern Ocean. Wave period (Figure 13.20e) shows an increase over the eastern Pacific, which also is attributed to enhanced generation in the Southern Ocean and northward propagation. A decrease in wave periods in the North Atlantic and western and central North Pacific is symptomatic of weaker projected wind forcing in these regions. The ensemble model results are starting to identify robust features of wave model projections, however, model uncertainties remain high due to uncertainties regarding future wind states, particularly storm wind tendencies, and to the different methodologies used to downscale climate model results to regional scales (Hemer et al., submitted-a).

A number of dynamical wave-projection studies have been carried out with a regional focus. For the Mediterranean Sea, Lionello et al. (2008; 2010) projected a widespread shift of the wave-height distribution to lower values by the mid-21st century under an SRES A1B scenario, implying a decrease in mean and extreme wave heights. Several studies have developed wave-climate projections in the North Sea using statistical and dynamical approaches. Despite several of these being derived from the same GCM and emission scenarios (SRES B2 and A2), projected changes in wave height over the 21st century span a broad range from a 21 cm (4%) decrease in extreme heights (Leake et al., 2009) through an insignificant change in SWH (Caires et al., 2008; Debernard and Røed, 2008) to a 35 cm (5–8%) increase in extreme wave heights with greater/less contribution of westerly directed waves in the eastern/western North Sea (Grabemann and Weisse, 2008). The range of uncertainty observed in projected conditions results from different regional dynamical downscaling models and different approaches to developing wave projections.

Dynamical wave-climate projection studies have also been carried out for open coasts of the North Atlantic. Charles et al. (2012) projected a general decrease in wave heights in the Bay of Biscay, accompanied by clockwise rotations in winter swell (attributed to a projected northward shift in North Atlantic storm tracks) and summer sea and intermediate waves (attributed to a projected slackening of westerly winds). Under the A2, B2 and A2B scenarios, Leake et al. (2009) projected larger waves at the end of the 21st century south of the UK, but smaller waves to the north. Along the Portuguese coast, Andrade et al. (2007) found little projected change in SWH and a tendency for a more northerly wave direction than present under the SRES A2 scenario.

In the Pacific, Graham et al. (submitted) used multi-model projections under the SRES A2 scenario and found a decrease in boreal winter significant wave heights over the mid-latitude North Pacific associated with a projected decrease in westerly wind speeds, and a tendency for higher extreme waves at higher latitudes. On the Australian east coast, Hemer et al. (submitted-c) reported a small projected decrease in mean SWH (<5cm) and a shift to a more southerly wave direction under SRES A2 and B1 scenarios, consistent with a projected southward shift of the sub-tropical ridge in the forcing fields.

[INSERT FIGURE 13.20 HERE]

Figure 13.20: Projected changes in wind-wave conditions derived from the Coordinated Ocean Wave Climate Projection (COWCLIP) Project (Hemer et al., submitted-a). **(a)** Percentage difference between projected future (~2075–2100) and historical (~1980–2009) annual mean significant wave height. **(b)** Percentage difference between projected future (~2075–2100) and historical (~1980–2009) January-March mean significant wave height. **(c)** Percentage difference between projected future (~2075–2100) and historical (~1980–2009) July-September mean significant wave height. Hashed regions indicate projected change is greater than the 5-member ensemble standard deviation. **(d)** As for a), but displaying absolute changes in mean wave direction, with positive values representing projected clockwise rotation relative to displayed vectors, and colours shown only where ensemble members agree on sign of change. **(e)** As for a), but displaying absolute changes in mean wave period.

13.7.4 Summary Assessment

Dynamical and statistical methods on regional scales show that it is very likely that there will be an increase in the occurrence of future extreme sea level and flooding events. The impact on exceedence probabilities is likely to be high, for example with current 100-year return period events changing to 10-year and possibly 1-year events by the end of the 21st century. The combined effects of MSL rise and changes in storminess will decide future extremes. There is high confidence that extremes will increase with MSL rise, however, there is low confidence in region-specific projections in storminess and storm surges.

Dynamical and statistical techniques for wave projections are improving, and ensemble assessments of wave-model projections are beginning to quantify uncertainties. Significant uncertainties are involved in the specification and downscaling of future winds, particularly storm winds. Accordingly, wave projections are presented with low confidence, with medium confidence assigned to wave-field changes associated with stronger winds over the Southern Ocean.

13.8 Synthesis and Key Uncertainties

Paleo sea level data clearly indicate that past climates with higher greenhouse gas concentrations or warmer surface temperatures have been accompanied by substantially higher sea levels. These observations, together

with our current scientific understanding and projections of future climate and sea level, means that is *virtually certain* that higher sea level will be experienced during the 21st century and beyond. While the paleo data provide valuable analogues for future sea level, finding appropriate paleo analogues to realistically constrain 21st century rates of sea level rise is more challenging. The large rate of sea level rise, in excess of 1 m century^{-1}, during the transition from the Last Glacial Maximum to the Holocene is not a robust guide to the 21st century because of the very different distribution and much larger volume of the ice sheets at that time, and there is little understanding of the reasons for sea level change during the last interglacial period.

Paleo and instrumental observations (Figure 13.21) together clearly indicate that the rate of sea level rise has increased significantly from a few tenths of a mm yr^{-1} over previous centuries to rates of almost 2 mm yr^{-1} averaged over the 20th century, and over 3 mm yr^{-1} since 1993. While significant uncertainties remain, understanding of sea level rise, particularly over recent decades but also for the 20th century as a whole, has improved significantly and it is now possible to account for much of the observed global mean sea level rise using both observations and process-based models of ocean thermal expansion and the melting of glaciers and the Greenland Ice Sheet. These models simulate the observed increase in the rate of rise during the last two decades and project a continuing rise during the 21st century and beyond, with the amount dependent of greenhouse gas scenarios (Figure 13.21).

[INSERT FIGURE 13.21 HERE]

Figure 13.21: Compilation of paleo sea level data, tide gauge data, altimeter data (from Figure 13.3), and central estimates and likely ranges for projections of global-mean sea level rise for RCP2.6 (blue) and RCP8.5 (red) scenarios (Section 13.5.1.1), all relative to pre-industrial values.

Contributions from ice sheets to sea level are thought to have been small for most of the 20th century. However, recent observations highlight a significant acceleration in the surface melting of Greenland and the solid ice discharge from both Antarctica and Greenland. Warmer ocean waters in the immediate vicinity of the outlet glaciers are a major trigger for this increased discharge but the evolution of these warmer regional ocean temperatures and of the ice sheet response are only just beginning to be understood. Improved ice sheet models that are beginning to simulate these recent ice sheets changes project a 21st century response of centimetres to a few tens of centimetres. However, coupled ocean ice sheet models are incomplete and inadequately tested and larger rates of rise cannot be excluded. Indeed, some of these models indicate the possibility of larger ice sheet contributions but there is insufficient understanding to quantify their likelihood. Semi-empirical models also project larger rates of rise than process-based models but the reason for these larger projections is inadequately understood, and there is little consensus about the reliability of semi-empirical model projections. Given this incomplete understanding it will be important to continue carefully monitoring changes in sea level and contributions to that change.

Sea level will continue to rise for centuries, even if greenhouse gas concentrations are stabilised, with the amount of sea level rise dependent on future greenhouse gas emissions. For higher emission scenarios, surface melting of the Greenland Ice Sheet is projected to exceed accumulation, leading to its long-term decay and a sea level rise of metres, consistent with paleo sea level data. However, the timing when such a critical threshold might be crossed and the accompanying contribution from Antarctica is uncertain. While the loss of the Greenland Ice Sheet is not inevitable, a significant decay of the ice sheet may be irreversible on millennial time scales.

The rates of sea level rise projected for the end of the 21st century for the RCP8.5 scenario approach average rates experienced during the deglaciation of the Earth after the Last Glacial Maximum. These rates imply a significant transfer of mass from the ice sheets to the oceans and thus a change in the gravitational field of the Earth and regional departures of sea level rise from the global average. In addition, ocean and atmosphere dynamics lead to a non-uniform distribution of sea level rise. However, there is little understanding of the regional sea level rise projection patterns.

Despite incomplete understanding of a number of aspects of sea level rise, it is clear there will be a significant impact on the intensity and frequency of high coastal sea levels. Multi-model projections of changes in surface wave conditions necessary for understanding some of the impacts of sea level change are beginning to become available but there is as yet low confidence in these projections.

References

Ablain, M., Cazenave, A., Valladeau, G. and Guinehut, S., 2009. A new assessment of the error budget of global mean sea level rate estimated by satellite altimetry over 1993–2008. Ocean Science, **5**(2): 193-201.

Adams, P.N., Inman, D.L. and Graham, N.E., 2008. Southern California deep-water wave climate: characterization and application to coastal processes. Journal of Coastal Research, **24**(4): 1022–1035.

Agosta, C., Favier, V., Krinner, G., Gallee, H. and Genthon, C., submitted. High-resolution modelling of the Antarctic surface mass balance, application for the 20th, 21st and 22nd centuries. Climate Dynamics.

Allan, J.C. and Komar, P.D., 2006. Climate controls on US West Coast erosion processes. Journal of Coastal Research, **22**(3): 511-529.

Allen, M., Frame, D., Huntingford, C., Jones, C., Lowe, J., Meinshausen, M. and Meinshausen, N., 2009. Warming caused by cumulative carbon emissions towards the trillionth tonne. Nature, **458**(7242): 1163–1166.

Amundson, J.M., Fahnestock, M., Truffer, M., Brown, J., M. P. Luthi, M.P. and Motyka, R.J., 2010. Ice melange dynamics and implications for terminus stability, Jakobshavn Isbræ, Greenland. Journal of Geophysical Research - Earth Surface, **115**: F01005.

Andrade, C., Pires, H.O., Taborda, R. and Freitas, M.C., 2007. Projecting future changes in wave climate and coastal response in Portugal by the end of the 21st century. Journal of Coastal Research, **SI 50**: 263-257.

Anschütz, H., Müller, K., Isaksson, E., McConnell, J.R., Fischer, H., Miller, H., Albert, M. and Winther, J.G., 2009. Revisiting sites of the South Pole Queen Maud Land Traverses in East Antarctica: accumulation data from shallow firn cores. Journal of Geophysical Research-Atmospheres, **114**: D012204.

Arendt, A., T. Bolch, J.G. Cogley, A. Gardner, J.-O. Hagen, R. Hock, G. Kaser, W.T. Pfeffer, G. Moholdt, F. Paul, V. Radić, L. Andreassen, S. Bajracharya, M. Beedle, E. Berthier, R. Bhambri, A. Bliss, I. Brown, E. Burgess, D. Burgess, F. Cawkwell, T. Chinn, L. Copland, B. Davies, H. de Angelis, E. Dolgova, K. Filbert, R. Forester, A. Fountain, H. Frey, B. Giffen, N. Glasser, S. Gurney, W. Hagg, D. Hall, U.K. Haritashya, G. Hartmann, C. Helm, S. Herreid, I. Howat, G. Kapustin, T. Khromova, C. Kienholz, M. Koenig, J. Kohler, D. Kriegel, S. Kutuzov, I. Lavrentiev, R. LeBris, J. Lund, W. Manley, C. Mayer, E. Miles, X. Li, B. Menounos, A. Mercer, N. Moelg, P. Mool, G. Nosenko, A. Negrete, C. Nuth, R. Pettersson, A. Racoviteanu, R. Ranzi, P. Rastner, F. Rau, J. Rich, H. Rott, C. Schneider, Y. Seliverstov, M. Sharp, O., Sigurðsson, C. Stokes, R. Wheate, S. Winsvold, G. Wolken, F. Wyatt and Zheltyhina, N., 2012. Randolph Glacier Inventory [v2.0]: A Dataset of Global Glacier Outlines. Global Land Ice Measurements from Space, Boulder Colorado, USA. Digital Media.

Arthern, R., Winebrenner, D.P. and Vaughan, D.G., 2006. Antarctic snow accumulation mapped using polarization of 4.3-cm wavelength microwave emission. Journal of Geophysical Research-Atmospheres, **111**: D06107.

Bahr, D.B., Dyurgerov, M. and Meier, M.F., 2009. Sea-level rise from glaciers and ice caps: A lower bound. Geophysical Research Letters, **36**(L03501): 4.

Bahr, D.B. and Radic, V., 2012. Significant contribution to total mass from very small glaciers. The Cryosphere Discussions, **6**: 763-770.

Bales, R.C., Guo, Q.H., Shen, D.Y., McConnell, J.R., Du, G.M., Burkhart, J.F., Spikes, V.B., Hanna, E. and Cappelen, J., 2009. Annual accumulation for Greenland updated using ice core data developed during 2000-2006 and analysis of daily coastal meteorological data. Journal of Geophysical Research-Atmospheres, **114**: D06116.

Bamber, J. and Riva, R., 2010. The sea level fingerprint of recent ice mass fluxes. Cryosphere, **4**(4): 621-627.

Bamber, J.L., Riva, R.E.M., Vermeersen, B.L.A. and LeBrocq, A.M., 2009. Reassessment of the potential sea-level rise from a collapse of the West Antarctic Ice Sheet. Science, **324**(5929): 901-903.

Barrand, N.E., submitted. Computing the volume response of the Antarctic Peninsula ice sheet to warming scenarios to 2200. Journal of Glaciology.

Bartholomew, I., Nienow, P., Mair, D., Hubbard, A., King, M.A. and Sole, A., 2010. Seasonal evolution of subglacial drainage and acceleration in a Greenland outlet glacier. Nature Geoscience, **3**(6): 408-411.

Bartholomew, I.D., Nienow, P., Sole, A., Mair, D., Cowton, T., King, M.A. and Palmer, S., 2011. Seasonal variations in Greenland Ice Sheet motion: Inland extent and behaviour at higher elevations. Earth and Planetary Science Letters, **307**(3-4): 271-278.

Becker, M., Meyssignac, B., Llovel, W., Cazenave, A. and Delcroix, T., 2011. Sea level variations at tropical pacific islands since 1950. Global and Planetary Change, **80-81**(2012): 85-98.

Beckley, B.D., Zelensky, N.P., Holmes, S.A., Lemoine, F.G., Ray, R.D., Mitchum, G.T., Desai, S.D. and Brown, S.T., 2010. Assessment of the Jason-2 Extension to the TOPEX/Poseidon, Jason^{-1} sea-surface height time series for global mean sea level monitoring. Marine Geodesy, **33**(S1): 447-471.

Bengtsson, L., Koumoutsaris, S. and Hodges, K., 2011. Large-scale surface mass balance of land ices from a comprehensive atmosphere model. Surveys in Geophysics, **32**(4-5): 459-474.

Benn, D.I., Warren, C.R. and Mottram, R.H., 2007. Calving processes and the dynamics of calving glaciers. Earth-Science Reviews, **82**(3-4): 143–179.

Bindoff, N.L., Willebrand, J., Artale, V., Cazenave, A., Gregory, J., Guley, S., Hanawa, K., Le Quéré, C., Levitus, S., Nojiri, Y., Shum, C.K., Talley, L.D. and Unnikrishnan, A., 2007. Observations: Oceanic climate change and sea level. In: S. Solomon and D. Qin (Editors), Climate change 2007: the physical science basis. Cambridge University Press, Cambridge, UK, pp. 385-432.

Bindschadler, R.A., Nowicki, S., Abe-Ouchi, A., Aschwanden, A., Choi, H., Fastook, J., Granzow, G., Greve, R., Gutowski, G., Herzfeld, U., Jackson, C., Johnson, J., Khroulev, C., Levermann, A., Lipscomb, W.H., Martin, M.A., Morlighem, M., Parizek, B.R., Pollard, D., Price, S.F., Ren, D., Saito, F., Sato, T., Seddik, H., Seroussi, H., Takahashi, K., Walker, R. and Wang, W.L., submitted. Ice-Sheet Model Sensitivities to Environmental Forcing and Their Use in Projecting Future Sea-Level (The SeaRISE Project). Journal of Glaciology.

Bittermann, K., Rahmstorf, S., Perrette, M. and Vermeer, M., submitted. Predictability of 20th century sea-level rise from past data. Nature Climate Change.

Bjork, A.A., Kjaer, K.H., Korsgaard, N.J., Kham, A.A., Kjeldsen, K.K., Andresen, C.S., Box, J.E., Larsen, N.K. and Funder, F., 2012. An aerial view of 80 years of climate-related glacier fluctuations in southeast Greenland. Nature Geoscience, **5**(6): 427-432.

Blum, M.D. and Roberts, H.H., 2009. Drowning of the Mississippi Delta due to insufficient sediment supply and global sea-level rise. Nature Geoscience, **2**: 488-491.

Boening, C., Willis, J.K., Landerer, F.W., Nerem, R.S. and Fasullo, J., submitted. The 2011 La Niña: so strong, the oceans fell. Geophysical Research Letters.

Bougamont, M., Bamber, J.L., Ridley, J., Gladstone, R.M., Greuell, W., Hanna, E., Payne, A.J. and Rutt, I., 2007. The impact of model physics on estimating the surface mass balance of the Greenland Ice Sheet. Geophysical Research Letters, **34**(17): L17501.

Bouttes, N., Gregory, J.M. and Lowe, J.A., submitted. The Reversibility of Sea-Level Rise. Journal of Climate.

Box, J., Yang, L., Bromwich, D. and Bai, L., 2009. Greenland Ice Sheet Surface Air Temperature Variability: 1840-2007. Journal of Climate, **22**(14): 4029-4049.

Box, J.E., submitted-a. Greenland ice sheet mass balance reconstruction. Part II: Surface mass balance (1840-2010). Journal of Climate.

Box, J.E., submitted-b. Greenland ice sheet mass balance reconstruction. Part III: Marine ice loss and total mass balance (1840-2010). Journal of Climate.

Box, J.E., Cressie, N., Bromwich, D.H., Jung, J., van den Broeke, M., van Angelen, J.H., Forster, R.R., Miège, C., Mosley-Thompson, E., Vinther, B. and McConnell, J.R., submitted. Greenland ice sheet mass balance reconstruction. Part I: net snow accumulation (1600-2009). Journal of Climate.

Bracegirdle, T.J., Connolley, W.M. and Turner, J., 2008. Antarctic climate change over the twenty first century. Journal of Geophysical Research-Atmospheres, **113**: D03103.

Broerse, D.B.T., Vermeersen, L.L.A., Riva, R.E.M. and van der Wal, W., 2011. Ocean contribution to co-seismic crustal deformation and geoid anomalies: Application to the 2004 December 26 Sumatra-Andaman earthquake. Earth and Planetary Science Letters, **305**(3-4): 341-349.

Brohan, P., Kennedy, J.J., Harris, I., Tett, S.F.B. and Jones, P.D., 2006. Uncertainty estimates in regional and global observed temperature changes: A new data set from 1850. Journal of Geophysical Research-Atmospheres, **111**: D12106.

Bromwich, D.H., Fogt, R.L., Hodges, K.I. and Walsh, J.E., 2007. A tropospheric assessment of the ERA-40, NCEP, and JRA-25 global reanalyses in the polar regions. Journal of Geophysical Research-Atmospheres, **112**: D10111.

Bromwich, D.H., Nicolas, J.P. and Monaghan, A.J., 2011. An assessment of precipitation changes over Antarctica and the Southern Ocean since 1989 in contemporary global reanalyses. Journal of Climate, **24**(16): 4189-4209.

Brown, J., Souza, A. and Wolf, J., 2010. Surge modelling in the eastern Irish Sea: present and future storm impact. Ocean Dynamics, **60**(2): 227-236.

Burgess, E.W., Forster, R.R., Box, J.E., Mosley-Thompson, E., Bromwich, D.H., Bales, R.C. and Smith, L.C., 2010. A spatially calibrated model of annual accumulation rate on the Greenland Ice Sheet (1958-2007). Journal of Geophysical Research-Earth Surface, **115**: F02004.

Caires, S., Groeneweg, J. and Sterl, A., 2008. Past and future changes in North Sea extreme waves, 31st International Conference on Coastal Engineering 2008, Hamburg, pp. 547-559.

Cane, M.A., 1989. A mathmatical note on Kawase study of deep ocean. Journal of Physical Oceanography, **19**(4): 548-550.

Carton, J.A., Giese, B.S. and Grodsky, S.A., 2005. Sea level rise and the warming of the oceans in the Simple Ocean Data Assimilation (SODA) ocean reanalysis. Journal of Geophysical Research - Oceans, **110**: C09006.

Cayan, D., Bromirski, P., Hayhoe, K., Tyree, M., Dettinger, M. and Flick, R., 2008. Climate change projections of sea level extremes along the California coast. Climatic Change, **87**(Supplement 1): 57-73.

Cazenave, A., Dominh, K., Guinehut, S., Berthier, E., Llovel, W., Ramillien, G., Ablain, M. and Larnicol, G., 2009. Sea level budget over 2003-2008: A reevaluation from GRACE space gravimetry, satellite altimetry and Argo. Global and Planetary Change, **65**(1-2): 83-88.

Cazenave, A., Henry, O., Munier, S., Delcroix, T., Gordon, A.L., Meyssignac, B., Llovel, W., Palanisamy, H. and Becker, M., Accepted. Estimating ENSO influence on the global mean sea level over 1993-2010. Marine Geodesy Special Issue.

Chambers, D., Merrifield, M.A. and Nerem, R.S., submitted. Is there a 60-year oscillation in global mean sea level? Geophysical Resarch Letters.

Chambers, D.P., 2006. Evaluation of new GRACE time-variable gravity data over the ocean. Geophys. Res. Lett., **33**(L17603).

Chambers, D.P., Wahr, J. and Nerem, R.S., 2004. Preliminary observations of global ocean mass variations with GRACE. Geophys. Res. Lett., **31**(L13310): doi:10.1029/2004GL020461.
Chambers, D.P., Wahr, J.M., Tamisiea, M. and Nerem, R.S., 2010. Ocean mass from GRACE and glacial isostatic adjustment. Journal of Geophysical Research, **115**: B11415.
Chao, B.F., Wu, Y.H. and Li, Y.S., 2008. Impact of artificial reservoir water impoundment on global sea level. Science, **320**(5873): 212-214.
Charbit, S., Paillard, D. and Ramstein, G., 2008. Amount of CO(2) emissions irreversibly leading to the total melting of Greenland. Geophysical Research Letters, **35**: L12503.
Charles, E.D., Idier, D., Delecluse, P., Deque, M. and Le Cozannet, G., 2012. Climate change impact on waves in the Bay of Biscay, France. Ocean Dynamics, **62**(6): 831-848.
Chen, J.L., Wilson, C.R., Blankenship, D. and Tapley, B.D., 2009. Accelerated Antarctic ice loss from satellite gravity measurements. Nature Geoscience, **2**(12): 859-862.
Christensen, J.H., Hewitson, B., Busuioc, A., Chen, A., Gao, X., Held, R., Jones, R., Kolli, R.K., Kwon, W.K., Laprise, R., Magana Rueda, V., Mearns, L., Menendez, C.G., Räisänen, J., Rinke, A., Sarr, A., Whetton, P., Arritt, R., Benestad, R., Beniston, M., Bromwich, D., Caya, D., Comiso, J., de Elia, R. and Dethloff, K., 2007. Regional climate projections, Climate Change, 2007: The Physical Science Basis. Cambridge University Press, Cambridge, pp. 849-925.
Christoffersen, P., Mugford, R.I., Heywood, K.J., Joughin, I., Dowdeswell, J.A., Syvitski, J.P.M., Luckman, A. and Benham, T.J., 2011. Warming of waters in an East Greenland fjord prior to glacier retreat: mechanisms and connection to large-scale atmospheric conditions. Cryosphere, **5**(3): 701-714.
Church, J.A., Gregory, J.M., Huybrechts, P., Kuhn, M., Lambeck, K., Nhuan, M.T., Qin, D. and Woodworth, P.L., 2001. Changes in sea level, Climate change 2001: The scientific basis. Contribution of Working Group I to the Third Assessment Report of the Intergovernmental Panel on Climate Change. Cambridge University Press, pp. 639-693.
Church, J.A., Gregory, J.M., White, N.J., Platten, S.M. and Mitrovica, J.X., 2011a. Understanding and projecting sea level change. Oceanography, **24**(2): 130^{-1}43.
Church, J.A. and White, N.J., 2006. A 20th century acceleration in global sea-level rise. Geophysical Research Letters, **33**: L01602.
Church, J.A. and White, N.J., 2011. Sea-level rise from the late 19th to the early 21st century. Surveys in Geophysics, **32**(4-5): 585-602.
Church, J.A., White, N.J. and Arblaster, J.M., 2005. Significant decadal-scale impact of volcanic eruptions on sea level and ocean heat content. Nature, **438**(7064): 74-77.
Church, J.A., White, N.J., Konikow, L.F., Domingues, C.M., Cogley, J.G., Rignot, E., Gregory, J.M., van den Broeke, M.R., Monaghan, A.J. and Velicogna, I., 2011b. Revisiting the Earth's sea-level and energy budgets from 1961 to 2008. Geophysical Research Letters, **38**: L18601.
Church, J.A., Woodworth, P.L., Aarup, T. and Wildon, W.S. (Editors), 2010. Understanding sea-level rise and variability. Wiley-Blackwell, 428 pp.
Chylek, P., Box, J.E. and Lesins, G., 2004. Global warming and the Greenland ice sheet. Climatic Change, **63**(1-2): 201-221.
Clark, J.A. and Lingle, C.S., 1977. Future sea-level changes due to West Antarctic ice sheet fluctuations. Nature, **269**(5625): 206-209.
Clarke, P.J., Lavallee, D.A., Blewitt, G., van Dam, T.M. and Wahr, J.M., 2005. Effect of gravitational consistency and mass conservation on seasonal surface mass loading models. Geophysical Research Letters, **32**: L08306.
Cogley, J.G., 2009. A more complete version of the World Glacier Inventory. Annals of Glaciology, **50**(53): 32-38.
Colberg, F. and McInnes, K.L., 2012. The impact of future changes in weather patterns on extreme sea levels over southern Australia. Journal of Geophysical Research - Oceans, **117**: C08001.
Committee on Sea Level Rise in California, Oregon and Washington, Board on Earth Sciences and Resources, Ocean Studies Board, Division on Earth and Life Studies and National Research Council, 2012. Sea-Level Rise for the Coasts of California, Oregon, and Washington: Past, Present, and Future. National Academies Press.
Conrad, C.P. and Hager, B.H., 1997. Spatial variations in the rate of sea level rise caused by the present-day melting of glaciers and ice sheets. Geophysical Research Letters, **24**(12): 1503^{-1}506.
Cook, A.J. and Vaughan, D.G., 2010. Overview of areal changes of the ice shelves on the Antarctic Peninsula over the past 50 years. The Cryosphere, **4**: 77-98.
Cornford, S.L., Martin, D.F., Graves, D.T., Ranken, D.F., le Brocq, A.M., Gladstone, R.M., Payne, A.J., Ng, E.G., and Lipscomb, W.H., submitted. Adaptive mesh, finite volume modeling of marine ice sheets. Journal of Computational Physics.
Crowley, T., 2000. Causes of climate change over the past 1000 years. Science, **289**(5477): 270-277.
Crowley, T.J., Baum, S.K., Kim, K.-Y., Hegerl, G.C. and Hyde, W.T., 2003. Modeling ocean heat content changes during the last millennium. Geophys. Res. Lett., **30**(18).
Das, S.B., Joughin, I., Behn, M.D., Howat, I.M., King, M.A., Lizarralde, D. and Bhatia, M.P., 2008. Fracture propagation to the base of the Greenland Ice Sheet during supraglacial lake drainage. Science, **320**(5877): 778-781.
De Angelis, H. and Skvarca, P., 2003. Glacier surge after ice shelf collapse. Science, **299**(5612): 1560^{-1}562.

Debernard, J.B. and Røed, L.P., 2008. Future wind, wave and storm surge climate in the Northern Seas: a revisit. Tellus A, **60**(3): 427-438.
Delworth, T.L., Ramaswamy, V. and Stenchikov, G.L., 2005. The impact of aerosols on simulated ocean temperature and heat content in the 20th century. Geophysical Research Letters, **32**(24): L24709.
Di Lorenzo, E., Cobb, K.M., Furtado, J.C., Schneider, N., Anderson, B.T., Bracco, A., Alexander, M.A. and Vimont, D.J., 2010. Central Pacific El Nino and decadal climate change in the North Pacific Ocean. Nature Geoscience, **3**(11): 762-765.
Domingues, C.M., Church, J.A., White, N.J., Gleckler, P.J., Wijffels, S.E., Barker, P.l.M. and Dunn, J.R., 2008. Improved estimates of upper-ocean warming and multi-decadal sea-level rise. Nature, **453**(7198): 1090–1093.
Douglas, B.C., 2001. Sea level change in the era of the recording tide gauge. In: B.C. Douglas, M.S. Kearney and S.P. Leatherman (Editors), Sea level rise, history and consequences. Academic Press, San Diego, pp. 37-64.
Driesschaert, E., Fichefet, T., Goosse, H., Huybrechts, P., Janssens, I., Mouchet, A., Munhoven, G., Brovkin, V. and Weber, S.L., 2007. Modeling the influence of Greenland ice sheet melting on the Atlantic meridional overturning circulation during the next millennia. Geophysical Research Letters, **34**(10): L10707.
Dufresne, J.L. and Bony, S., 2008. An assessment of the primary sources of spread of global warming estimates from coupled atmosphere-ocean models. Journal of Climate, **21**(19): 5135-5144.
Dupont, T.K. and Alley, R.B., 2005. Assessment of the importance of ice-shelf buttressing to ice-sheet flow. Geophysical Research Letters, **32**(L04503): doi:10.1029/2004GL022024.
Durack, P.J. and Wijffels, S.E., 2010. Fifty-Year Trends in Global Ocean Salinities and Their Relationship to Broad-Scale Warming. Journal of Climate, **23**(16): 4342-4362.
Durand, G., Gagliardini, O., Zwinger, T., Le Meur, E. and Hindmarsh, R.C.A., 2009. Full Stokes modeling of marine ice sheets: influence of the grid size. Annals of Glaciology, **50**(52): 109–114.
Dutton, A. and Lambeck, K., 2012. Ice volume and sea level during the last interglacial. Science, **337**(6091): 216-219.
Easterling, D.R. and Wehner, M.F., 2009. Is the climate warming or cooling? Geophysical Research Letters, **36**(8): L08706.
Ericson, J.P., Vorosmarty, C.J., Dingman, S.L., Ward, L.G. and Meybeck, M., 2006. Effective sea-level rise and deltas: Causes of change and human dimension implications. Global and Planetary Change, **50**(1-2): 63-82.
Ettema, J., van den Broeke, M.R., van Meijgaard, E., van de Berg, W.J., Bamber, J.L., Box, J.E. and Bales, R.C., 2009. Higher surface mass balance of the Greenland ice sheet revealed by high-resolution climate modeling. Geophysical Research Letters, **36**(12): L12501
Fan, Y., Held, I.M. and Lin, S.J., Submitted. Global ocean wave climate change scenarios for the end of the 21st century. Journal of Climate.
Farneti, R., Delworth, T.L., Rosati, A.J., Griffies, S.M. and Zeng, F., 2010. The Role of Mesoscale Eddies in the Rectification of the Southern Ocean Response to Climate Change. Journal of Physical Oceanography, **40**(7): 1539–1557.
Farneti, R. and Gent, P.R., 2011. The effects of the eddy-induced advection coefficient in a coarse-resolution coupled climate model. Ocean Modelling, **39**(1-2): 135–145.
Farrell, W.E. and Clark, J.A., 1976. On postglacial sea level. Geophysical Journal of the Royal Astronomical Society, **46**(3): 647-667.
Fausto, R.S., Ahlstrom, A.P., van As, D., Johnsen, S.J., Langen, P.L. and Steffen, K., 2009. Improving surface boundary conditions with focus on coupling snow densification and meltwater retention in large-scale ice-sheet models of Greenland. Journal of Glaciology, **55**(193): 869-878.
Fettweis, X., Belleflame, A., Erpicum, M., Franco, B. and Nicolay, S., 2011. Estimation of the sea level rise by 2100 resulting from changes in the surface mass balance of the Greenland ice sheet. In: J. Blanco and H. Kheradmand (Editors), Climate Change - Geophysical Foundations and Ecological Effects. Intech, Croatia, pp. 503-520.
Fettweis, X., Franco, B., Tedesco, M., van Angelen, J.H., Lenaerts, J.T.M., van den Broeke, M.R. and Gallee, H., Submitted. Estimating Greenland ice sheet surface mass balance contribution to future sea level rise using the regional atmospheric model MAR. The Cryosphere.
Fettweis, X., Hanna, E., Gallee, H., Huybrechts, P. and Erpicum, M., 2008. Estimation of the Greenland ice sheet surface mass balance for the 20th and 21st centuries. Cryosphere, **2**(2): 117–129.
Fiedler, J.W. and Conrad, C.P., 2010. Spatial variability of sea level rise due to water impoundment behind dams. Geophysical Research Letters, **37**(12): L12603.
Fluckiger, J., Knutti, R. and White, J.W.C., 2006. Oceanic processes as potential trigger and amplifying mechanisms for Heinrich events. Paleoceanography, **21**(2): PA2014.
Forster, P., Ramaswamy, V., Artaxo, P., Berntsen, T., Betts, R., Fahey, D.W., Haywood, J., Lean, J., Lowe, D.C., Myhre, G., Nganga, J., Prinn, R., Raga, G., Schulz, M. and Van Dorland, R., 2007. Changes in Atmospheric Constituents and in Radiative Forcing, Climate Change 2007: The Physical Science Basis. Contribution of Working Group I to the Fourth Assessment Report of the Intergovernmental Panel on Climate Change. Cambridge University Press, Cambridge, United Kingdom and New York, NY, USA.
Franco, B., Fettweis, X., Erpicum, M. and Nicolay, S., 2011. Present and future climates of the Greenland ice sheet according to the IPCC AR4 models. Climate Dynamics, **36**(9–10): 1897–1918.
Fürst, J.J., Goelzer, H. and Huybrechts, P., Submitted. Ice-dynamic projections of the Greenland ice sheet to future atmosphere and ocean warming. Nature Climate Change.

Fyke, J.G., Carter, L., Mackintosh, A., Weaver, A.J. and Meissner, K.J., 2010. Surface Melting over Ice Shelves and Ice Sheets as Assessed from Modeled Surface Air Temperatures. Journal of Climate, **23**(7): 1929–1936.
Gehrels, R. and Woodworth, P.L., submitted. When did modern rates of sea-level rise start? Global and Planetary Change.
Gent, P.R. and Danabasoglu, G., 2011. Response to Increasing Southern Hemisphere Winds in CCSM4. Journal of Climate, **24**(19): 4992-4998.
Genthon, C., Krinner, G. and Castebrunet, H., 2009. Antarctic precipitation and climate-change predictions: horizontal resolution and margin vs plateau issues. Annals of Glaciology, **50**(50): 55-60.
Geoffroy, O., Saint-Martin, D., Olivie, D.J.L., Voldoire, A., Belon, G. and Tyteca, S., submitted-a. Transient climate response in a two-box energy-balance model. Part I: analytical solution and parameter calibration using CMIP5. Journal of Climate.
Geoffroy, O., Saint-Martin, D. and Ribes, A., submitted-b. Quantifying the source of spread in climate change experiments. Geophysical Research Letters.
Gillett, N., Arora, V., Zickfeld, K., Marshall, S. and Merryfield, A., 2011. Ongoing climate change following a complete cessation of carbon dioxide emissions. Nature Geoscience: 83-87.
Gladstone, R.M., Lee, V., Rougier, J., Payne, A.J., Hellmer, H., Le Brocq, A., Shepherd, A., Edwards, T.L., Gregory, J.M. and Cornford, S.L., 2012. Calibrated prediction of Pine Island Glacier retreat during the 21st and 22nd centuries with a coupled flowline model. Earth and Planetary Science letters, **333-334**: 191–199.
Gladstone, R.M., Lee, V., Vieli, A. and Payne, A.J., 2010a. Grounding line migration in an adaptive mesh ice sheet model. Journal of Geophysical Research-Earth Surface, **115**(19): F04014.
Gladstone, R.M., Payne, A.J. and Cornford, S.L., 2010b. Parameterising the grounding line in flow-line ice sheet models. Cryosphere, **4**(4): 605-619.
Gleckler, P.J., AchutaRao, K., Gregory, J.M., Santer, B.D., Taylor, K.E. and Wigley, T.M.L., 2006a. Krakatoa lives: The effect of volcanic eruptions on ocean heat content and thermal expansion. Geophysical Research Letters, **33**(17): L17702.
Gleckler, P.J., Santer, B.D., Domingues, C.M., Pierce, D.W., Barnett, T.P., Church, J.A., Taylor, K.E., AchutaRao, K.M., Boyer, T.P., Ishii, M. and Caldwell, P.M., 2012. Human-induced global ocean warming on multidecadal timescales. Nature Climate Change, **2**(7): 524-529.
Gleckler, P.J., Wigley, T.M.L., Santer, B.D., Gregory, J.M., AchutaRao, K. and Taylor, K.E., 2006b. Krakatoa's signature persists in the ocean. Nature, **439**(7077): 675-675.
Goelzer, H., Huybrechts, P., Fürst, J.J., Andersen, M.L., Edwards, T.L., Fettweis, X., Nick, F.M., Payne, A.J. and Shannon, S., Submitted. Sensitivity of Greenland ice sheet projections to model formulations. The Cryosphere.
Goelzer, H., Huybrechts, P., Loutre, M., Goosse, H., Fichefet, T. and Mouchet, A., 2011. Impact of Greenland and Antarctic ice sheet interactions on climate sensitivity. Climate Dynamics, **37**(5-6): 1005–1018.
Goldberg, D., Holland, D.M. and Schoof, C., 2009. Grounding line movement and ice shelf buttressing in marine ice sheets. Journal of Geophysical Research-Earth Surface, **114**: F04026.
Gomez, N., Mitrovica, J.X., Huybers, P. and Clark, P.U., 2010a. Sea level as a stabilizing factor for marine-ice-sheet grounding lines. Nature Geoscience, **3**(12): 850-853.
Gomez, N., Mitrovica, J.X., Tamisiea, M.E. and Clark, P.U., 2010b. A new projection of sea level change in response to collapse of marine sectors of the Antarctic Ice Sheet. Geophysical Journal International, **180**(2): 623-634.
Good, P., Gregory, J.M. and Lowe, J.A., 2011. A step-response simple climate model to reconstruct and interpret AOGCM projections. Geophysical Research Letters, **38**: L01703.
Good, P., Gregory, J.M., Lowe, J.A. and Andrews, T., Submitted. Abrupt CO2 experiments as tools for predicting and understanding CMIP5 representative concentration pathway projections. Climate Dynamics.
Goosse, H., Renssen, H., Timmermann, A. and Bradley, R.S., 2005. Internal and forced climate variability during the last millennium: a model-data comparison using ensemble simulations. Quaternary Science Reviews, **24**(12–13): 1345–1360.
Gornitz, V., 2001. Impoundment, groundwater mining, and other hydrologic transformations: Impacts on global sea level rise. In: B.C. Douglas, M.S. Kearney and S.P. Leatherman (Editors), Sea Level Rise, History and Consequences. Int. Geophys. Series. Academic Press, San Diego, pp. 97–119.
Gouretski, V. and Koltermann, K.P., 2007. How much is the ocean really warming? Geophysical Research Letters, **34**(1): L01610.
Gower, J.F.R., 2010. Comment on "Response of the global ocean to Greenland and Antarctic ice melting" by D. Stammer. Journal of Geophysical Research-Oceans, **115**: C10009.
Grabemann, I. and Weisse, R., 2008. Climate change impact on extreme wave conditions in the North Sea: an ensemble study. Ocean Dynamics, **58**(3-4): 199-212.
Graham, N.E., Cayan, D.R., Bromirski, P. and Flick, R., submitted. Multi-model projections of 21st century North Pacific winter wave climate under the IPCC A2 scenario. Climate Dynamics.
Graversen, R.G., Drijfhout, S., Hazeleger, W., van de Wal, R., Bintanja, R. and Helsen, M., 2011. Greenland's contribution to global sea level rise by the end of the 21st century. Climate Dynamics, **37**: 1427–1442.
Greatbatch, R.J., 1994. A note on the representation of steric sea-levels in models that conserve volume rather than mass. Journal of Geophysical Research-Oceans, **99**(C6): 12767–12771.

Gregory, J.M., 2000. Vertical heat transports in the ocean and their effect an time-dependent climate change. Climate Dynamics, **16**(7): 501-515.
Gregory, J.M., 2010. Long-term effect of volcanic forcing on ocean heat content. Geophysical Research Letters, **37**: L22701.
Gregory, J.M. and Forster, P.M., 2008. Transient climate response estimated from radiative forcing and observed temperature change. Journal of Geophysical Research - Atmospheres, **113**: D23105.
Gregory, J.M. and Huybrechts, P., 2006. Ice-sheet contributions to future sea-level change. Philosophical Transactions of the Royal Society a-Mathematical Physical and Engineering Sciences: 1709–1731.
Gregory, J.M. and Lowe, J.A., 2000. Predictions of global and regional sea-level rise using AOGCMs with and without flux adjustment. Geophysical Research Letters, **27**(19): 3069-3072.
Gregory, J.M., Lowe, J.A. and Tett, S.F.B., 2006. Simulated global-mean sea-level changes over the last half-millennium. Journal of Climate, **19**(18): 4576-4591.
Gregory, J.M., White, N.J., Church, J.A., Bierkens, M.F.P., Box, J.E., van den Broeke, M.R., Cogley, J.G., Fettweis, X., Hanna, E., Huybrechts, P., Konikow, L.F., Leclercq, P.W., Marzeion, B., Oerlemans, J., Tamisiea, M.E., Wada, Y., Wake, L.M. and van de Wal, R.S.W., submitted. Twentieth-century global-mean sea level rise: is the whole greater than the sum of the parts? Journal of Climate.
Greve, R., 2000. On the response of the Greenland ice sheet to greenhouse climate change. Climatic Change: 289-303.
Grinsted, A., Jevrejeva, S. and Riva, R.E.M., submitted. 21st century sea level rise projections for northern Europe.
Grinsted, A., Moore, J.C. and Jevrejeva, S., 2010. Reconstructing sea level from paleo and projected temperatures 200 to 2100 ad. Climate Dynamics, **34**(4): 461-472.
Gudmundsson, G.H., Krug, J., Durand, G., L., F. and Gagliardini, O., Submitted. The stability of grounding lines on retrograde slopes. The Cryosphere.
Han, W., Meehl, G.A., Hu, A., Yamagata, T., Alexander, M.A., Deser, C., Yuan, D., Ishii, M., Quan, X.W., Zheng, J., Hamlington, B.D. and Leben, R.R., submitted. Pacific Decadal Sea Level Change Patterns associated with a Warming Indo-Pacific Warm Pool. Nature Geoscience.
Han, W.Q., Meehl, G.A., Rajagopalan, B., Fasullo, J.T., Hu, A.X., Lin, J.L., Large, W.G., Wang, J.W., Quan, X.W., Trenary, L.L., Wallcraft, A., Shinoda, T. and Yeager, S., 2010. Patterns of Indian Ocean sea-level change in a warming climate. Nature Geoscience, **3**(8): 546-550.
Hanna, E., Huybrechts, P., Cappelen, J., Steffen, K., Bales, R.C., Burgess, E., McConnell, J.R., Steffensen, J.P., van den Broeke, M., Wake, L., Bigg, G., Griffiths, M. and Savas, D., 2011. Greenland Ice Sheet surface mass balance 1870 to 2100 based on Twentieth century reanalysis, and links with global climate forcing. Journal of Geophysical Research, **116**: D24121.
Hanna, E., Huybrechts, P., Janssens, I., Cappelen, J., Steffen, K. and Stephens, A., 2005. Runoff and mass balance of the Greenland ice sheet: 1958-2003. Journal of Geophysical Research-Atmospheres, **110**: D13108.
Hanna, E., Huybrechts, P., Steffen, K., Cappelen, J., Huff, R., Shuman, C., Irvine-Fynn, T., Wise, S. and Griffiths, M., 2008. Increased runoff from melt from the Greenland Ice Sheet: A response to global warming. Journal of Climate, **21**(2): 331-341.
Hansen, J., Nazarenko, L., Ruedy, R., Sato, M., Willis, J., Genio, A.D., Koch, D., Lacis, A., Lo, K., Menon, S., Novakov, T., Perlwitz, J., Russell, G., Schmidt, G.A. and Tausnev, N., 2005. Earth's energy imbalance: confirmation and implications. Science, **308**(5727): 1431–1435.
Hansen, J., Sato, M., Kharecha, P., Russell, G., Lea, D. and Siddall, M., 2007. Climate change and trace gases. Philosophical Transactions of the Royal Society a-Mathematical Physical and Engineering Sciences: 1925–1954.
Harper, B., Hardy, T., Mason, L. and Fryar, R., 2009. Developments in storm tide modelling and risk assessment in the Australian region. Natural Hazards, **51**(1): 225-238.
Hegerl, G.C., Zwiers, F.W., Braconnot, P., Gillett, N.P., Luo, Y., Orsini, J.A.M., Nicholls, N., Penner, J.E. and Stott, P.A., 2007. Understanding and attributing climate change, Climate Change 2007: The Physical Science Basis. Contribution of Working Group I to the Fourth Assessment Report of the Intergovernmental Panel on Climate Change. Cambridge University Press, United Kingdom.
Held, I.M. and Soden, B.J., 2006. Robust responses of the hydrological cycle to global warming. Journal of Climate, **19**(21): 5686-5699.
Held, I.M., Winton, M., Takahashi, K., Delworth, T., Zeng, F.R. and Vallis, G.K., 2010. Probing the fast and slow components of global warming by returning abruptly to preindustrial forcing. Journal of Climate, **23**(9): 2418-2427.
Hellmer, H.H., Kauker, F., Timmermann, R., Determann, J. and Rae, J., 2012. Twenty-first-century warming of a large Antarctic ice-shelf cavity by a redirected coastal current. Nature, **485**(7397): 225-228.
Hemer, M.A., Church, J.A. and Hunter, J.R., 2010. Variability and trends in the directional wave climate of the Southern Hemisphere. International Journal of Climatology, **30**(4): 475-491.
Hemer, M.A., Fan, Y., Mori, N., Semedo, A. and Wang, X.L., submitted-a. Projected future changes in wind-wave climate in a multi-model ensemble. Nature Climate Change.
Hemer, M.A., Katzfey, J. and Trenham, C., submitted-b. Global dynamical projections of surface ocean wave climate for a future high greenhouse gas emission scenario. Ocean Modelling.
Hemer, M.A., McInnes, K.L. and Ranasinghe, R., submitted-c. Exploring uncertainty in regional East Australian wave climate projections. International Journal of Climatology.

Hewitt, I.J., 2011. Modelling distributed and channelized subglacial drainage: the spacing of channels. Journal of Glaciology, **57**(202): 302-314.
Hindmarsh, R.C.A., 1993. Qualitative dynamics of marine ice sheets. **I 12**: 68-99.
Holgate, S., Jevrejeva, S., Woodworth, P. and Brewer, S., 2007. Comment on "A semi-empirical approach to projecting future sea-level rise". Science, **317**(5846): 2.
Holgate, S.J., 2007. On the decadal rates of sea level change during the twentieth century. Geophysical Research Letters, **34**(1): L01602.
Holland, D.M., Thomas, R.H., De Young, B., Ribergaard, M.H. and Lyberth, B., 2008a. Acceleration of Jakobshavn Isbrae triggered by warm subsurface ocean waters. Nature Geoscience, **1**(10): 659-664.
Holland, P.R., Jenkins, A. and Holland, D.M., 2008b. The response of ice shelf basal melting to variations in ocean temperature. Journal of Climate, **21**(11): 2558-2572.
Horton, R., Herweijer, C., Rosenzweig, C., Liu, J.P., Gornitz, V. and Ruane, A.C., 2008. Sea level rise projections for current generation CGCMs based on the semi-empirical method. Geophysical Research Letters, **35**(2): L02715.
Hu, A., Meehl, G.A., Han, W. and Yin, J., 2011. Effect of the potential melting of the Greenland Ice Sheet on the Meridional Overturning Circulation and global climate in the future. Deep-Sea Research Part Ii-Topical Studies in Oceanography, **58**(17^{-1}8): 1914^{-1}926.
Hu, A.X., Meehl, G.A., Otto-Bliesner, B.L., Waelbroeck, C., Han, W.Q., Loutre, M.F., Lambeck, K., Mitrovica, J.X. and Rosenbloom, N., 2010. Influence of Bering Strait flow and North Atlantic circulation on glacial sea-level changes. Nature Geoscience, **3**(2): 118^{-1}21.
Huber, M. and Knutti, R., 2012. Anthropogenic and antural warming inferred from changes in earth's energy balance. Nature Geoscience, **5**(1): 31-36.
Hunter, J., 2012. A simple technique for estimating an allowance for uncertain sea-level rise. Climatic Change, **113**(2): 239-252.
Huntington, T.G., 2008. Can we dismiss the effect of changes in land-based water storage on sea-level rise? Hydrological Processes, **22**(5): 717-723.
Huss, M., Hock, R., Bauder, A. and Funk, M., 2012. Conventional versus reference-surface mass balance. Journal of Glaciology, **58**(208): 278-286.
Huybrechts, P., 2002. Sea-level changes at the LGM from ice-dynamic reconstructions of the Greenland and Antarctic ice sheets during the glacial cycles. Quaternary Science Reviews, **21**(1-3): 203-231.
Huybrechts, P. and De Wolde, J., 1999. The Dynamic Response of the Greenland and Antarctic ice sheets to multiple-century climatic warming. Journal of Climate, **12**(8 Part 1): 2169-2188.
Huybrechts, P., Goelzer, H., Janssens, I., Driesschaert, E., Fichefet, T., Goosse, H. and Loutre, M.F., 2011. Response of the Greenland and Antarctic ice sheets to multi-millennial greenhouse warming in the earth system model of intermediate complexity LOVECLIM. Surveys in Geophysics, **32**(4-5): 397-416.
Ishii, M. and Kimoto, M., 2009. Reevaluation of historical ocean heat content variations with time-varying XBT and MBT depth bias corrections. Journal of Oceanography, **65**(3): 287-299.
Izaguirre, C., Méndez, F.J., Menéndez, M. and Losada, I.J., 2011. Global extreme wave height variability based on satellite data. Geophysical Research Letters, **38**(10): L10607.
Izaguirre, C., Mendez, F.J., Menendez, M., Luceño, A. and Losada, I.J., 2010. Extreme wave climate variability in southern Europe using satellite data. Journal of Geophysical Research - Oceans, **115**(C4): C04009.
Jacobs, S.S., Jenkins, A., Giulivi, C.F. and Dutrieux, P., 2011. Stronger ocean circulation and increased melting under Pine Island Glacier ice shelf. Nature Geoscience, **4**(8): 519-523.
Jenkins, A., Dutrieux, P., Jacobs, S.S., McPhail, S.D., Perrett, J.R., Webb, A.T. and White, D., 2010. Observations beneath Pine Island Glacier in West Antarctica and implications for its retreat. Nature Geoscience, **3**(7): 468-472.
Jevrejeva, S., Grinsted, A. and Moore, J.C., 2009. Anthropogenic forcing dominates sea level rise since 1850. Geophysical Research Letters, **36**(20): L20706.
Jevrejeva, S., Grinsted, A., Moore, J.C. and Holgate, S., 2006. Nonlinear trends and multiyear cycles in sea level records. Journal of Geophysical Research-Oceans, **111**(9): C09012.
Jevrejeva, S., Moore, J.C. and Grinsted, A., 2010. How will sea level respond to changes in natural and anthropogenic forcings by 2100? Geophysical Research Letters, **37**(7): L07703.
Jevrejeva, S., Moore, J.C. and Grinsted, A., 2011. Sea level projections to AD 2500 with a new generation of climate change scenarios. Global and Planetary Change, **80-81**: 14-20.
Jevrejeva, S., Moore, J.C. and Grinsted, A., submitted. Are we overestimating sea level projections by2100 with semi-empirical models. Journal of Geophysical Research.
Jevrejeva, S., Moore, J.C., Grinsted, A. and Woodworth, P.L., 2008. Recent global sea level acceleration started over 200 years ago? Geophysical Research Letters, **35**(8): L08715.
Johnson, G.C. and Gruber, N., 2007. Decadal water mass variations along 20 degrees W in the Northeastern Atlantic Ocean. Progress in Oceanography, **73**(3-4): 277-295.
Johnson, G.C., Mecking, S., Sloyan, B.M. and Wijffels, S.E., 2007. Recent bottom water warming in the Pacific Ocean. Journal of Climate, **20**(21): 5365-5375.
Joughin, I., Das, S.B., King, M.A., Smith, B.E., Howat, I.M. and Moon, T., 2008. Seasonal speedup along the western flank of the Greenland Ice Sheet. Science, **320**(5877): 781-783.

Joughin, I., Smith, B.E. and Holland, D.M., 2010. Sensitivity of 21st century sea level to ocean-induced thinning of Pine Island Glacier, Antarctica. Geophysical Research Letters, **37**: L20502.

Kang, S.K., Cherniawsky, J.Y., Foreman, M.G.G., Min, H.S., Kim, C.H. and Kang, H.W., 2005. Patterns of recent sea level rise in the East/Japan Sea from satellite altimetry and in situ data. Journal of Geophysical Research-Oceans, **110**: C07002.

Kato, S., 2009. Interannual variability of the global radiation budget. Journal of Climate, **22**(18): 4893-4907.

Katsman, C., Hazeleger, W., Drijfhout, S., Oldenborgh, G. and Burgers, G., 2008. Climate scenarios of sea level rise for the northeast Atlantic Ocean: a study including the effects of ocean dynamics and gravity changes induced by ice melt. Climatic Change, **91**(3-4): 351-374.

Katsman, C.A., Sterl, A., Beersma, J.J., van den Brink, H.W., Church, J.A., Hazeleger, W., Kopp, R.E., Kroon, D., Kwadijk, J., Lammersen, R., Lowe, J., Oppenheimer, M., Plag, H.P., Ridley, J., von Storch, H., Vaughan, D.G., Vellinga, P., Vermeersen, L.L.A., van de Wal, R.S.W. and Weisse, R., 2011. Exploring high-end scenarios for local sea level rise to develop flood protection strategies for a low-lying delta - the Netherlands as an example. Climate Dynamics, **109**(3-4): 617-645.

Katsman, C.A. and van Oldenborgh, G.J., 2011. Tracing the upper ocean's missing heat. Geophysical Research Letters, **38**(14): L14610.

Kawase, M., 1987. Establishment of deep ocean circulation driven by deep-water. Journal of Physical Oceanography, **17**(12): 2294-2317.

Kemp, A.C., Horton, B.P., Donnelly, J.P., Mann, M.E., Vermeer, M. and Rahmstorf, S., 2011. Climate related sea-level variations over the past two millennia. Proceedings of the National Academy of Sciences of the United States of America, **108**(27): 11017^{-1}1022.

Kendall, R.A., Mitrovica, J.X. and Milne, G.A., 2005. On post-glacial sea level - II. Numerical formulation and comparative results on spherically symmetric models. Geophysical Journal International, **161**(3): 679-706.

Khan, S.A., Wahr, J., Bevis, M., Velicogna, I. and Kendrick, E., 2010. Spread of ice mass loss into northwest Greenland observed by GRACE and GPS. Geophysical Research Letters, **37**: L06501.

Knutti, R. and Tomassini, L., 2008. Constraints on the transient climate response from observed global temperature and ocean heat uptake. Geophys. Res. Lett., **35**: L09701.

Kohl, A. and Stammer, D., 2008. Decadal sea level changes in the 50-year GECCO ocean synthesis. Journal of Climate, **21**(9): 1876^{-1}890.

Konikow, L.F., 2011. Contribution of global groundwater depletion since 1900 to sea-level rise. Geophysical Research Letters, **38**: L17401.

Konikow, L.F., submitted. Comment on "Model estimates of sea-level change due to anthropogenic impacts on terrestrial water storage" by Pokhrel et al. Nature Geoscience.

Kopp, R.E., Mitrovica, J.X., Griffies, S.M., Yin, J.J., Hay, C.C. and Stouffer, R.J., 2010. The impact of Greenland melt on local sea levels: a partially coupled analysis of dynamic and static equilibrium effects in idealized water-hosing experiments A letter. Climatic Change, **103**(3-4): 619-625.

Kopp, R.E., Simons, F.J., Mitrovica, J.X., Maloof, A.C. and Oppenheimer, M., 2009. Probabilistic assessment of sea level during the last interglacial stage. Nature, **462**(7275): 863-868.

Körper, J., Höschel, I., Lowe, J.A., Hewitt, C.D., Salas-Melia, D., Roeckner, E., Huebener, H., Royer, J.F., Dufresne, J.L., Pardaens, A., Giorgetta, M.A., Sanderson, M.G., Otterå, O.H., Tjiputra, J. and Denvil, S., submitted. The effect of aggressive mitigation on sea level rise and sea ice changes. Climate Dynamics.

Kouketsu, S., Doi, T., Kawano, T., Masuda, S., Sugiura, N., Sasaki, Y., Toyoda, T., Igarashi, H., Kawai, Y., Katsumata, K., Uchida, H., Fukasawa, M. and Awaji, T., 2011. Deep ocean heat content changes estimated from observation and reanalysis product and their influence on sea level change. Journal of Geophysical Research-Oceans, **116**: C03012.

Krinner, G., Magand, O., Simmonds, I., Genthon, C. and Dufresne, J.L., 2007. Simulated Antarctic precipitation and surface mass balance at the end of the twentieth and twenty-first centuries. Climate Dynamics, **28**(2-3): 215-230.

Kuhlbrodt, T. and Gregory, J.M., submitted. Ocean heat uptake and its consequences for the magnitude of sea level rise and climate change. Geophysical Research Letters.

Kuipers Munneke, P., Ligtenberg, S.R.M., van den Broeke, M.R. and Vaughan, D.G., submitted. Firn air depletion as a trigger for Antarctic ice-shelf collapse. Science.

Lambeck, K. and Nakiboglu, S.M., 1984. Recent global changes in sea level. Geophysical Research Letters, **11**(10): 959-961.

Lambeck, K., Smither, C. and Ekman, M., 1998. Tests of glacial rebound models for Fennoscandinavia based on instrumented sea- and lake-level records. Geophysical Journal International, **135**(2): 375-387.

Landerer, F.W., Jungclaus, J.H. and Marotzke, J., 2007. Regional dynamic and steric sea level change in response to the IPCC-A1B scenario. Journal of Physical Oceanography, **37**(2): 296-312.

Landerer, F.W., Jungclaus, J.H. and Marotzke, M., 2008. El Niño–Southern Oscillation signals in sea level, surface mass redistribution, and degree-two geoid coefficients. Journal of Geophysical Research, **113**: C08014.

Langden, P.L., Solgaard, A.M. and Hiviberg, C.S., 2012. Self-inhibiting growth of the Greenland Ice Sheet. Geophysical Research Letters, **39**: L12502.

Leake, J., Wolf, J., Lowe, J., Hall, J. and Nicholls, R., 2009. Response of marine climate to future climate change: application to coastal regions, 31st International Conference on Coastal Engineering, 5. World Scientific Publishing, Singapore, Hamburg, pp. 4354-4364.

Leclercq, P.W., Oerlemans, J. and Cogley, J.G., 2011. Estimating the glacier contribution to sea-level rise for the period 1800-2005. Surveys in Geophysics, **32**(4-5): 519-535.

Lemieux-Dudon, B., Blayo, E., Petit, J.R., Waelbroeck, C., Svensson, A., Ritz, C., Barnola, J.M., Narcisi, B.M. and Parrenin, F., 2010. Consistent dating for Antarctic and Greenland ice cores. Quaternary Science Reviews, **29**(1-2): 8-20.

Lemperiere, F., 2006. The role of dams in the XXI century. International Journal on Hydropower and Dams, **3**.

Lenaerts, J.T.M., van den Broeke, M.R., van de Berg, W.J., van Meijgaard, E. and Munneke, P.K., 2012. A new high-resolution surface mass balance map of Antarctica (1989-2009) based on regional atmospheric climate modeling. Geophysical Research Letters, **39**(L04501).

Lettenmaier, D.P. and Milly, P.C.D., 2009. Land waters and sea level. Nature Geoscience, **2**(7): 452-454.

Leuliette, E.W. and Miller, L., 2009. Closing the sea level rise budget with altimetry, Argo, and GRACE. Geophysical Research Letters, **36**: L04608.

Leuliette, E.W. and Willis, J.K., 2011. Balancing the sea level budget. Oceanography, **24**(2): 122–129.

Levermann, A., Clark, P.U., Marzeion, B., Pollard, D., Radic, V. and Robinson, A., submitted-a. Closing the budget of future sea-level commitment. Science.

Levermann, A., Griesel, A., Hofmann, M., Montoya, M. and Rahmstorf, S., 2005. Dynamic sea level changes following changes in the thermohaline circulation. Climate Dynamics: 347-354.

Levermann, A., Winkelmann, R., Nowicki, S., Fastook, J.L., Frieler, K., Greve, R., Hellmer, H.H., Martin, M.A., Mengel, M., Payne, A.J., Pollard, D., Sato, T., Timmermann, R., Wang, W.L. and Bindschadler, R.A., submitted-b. Projecting Antarctic ice discharge using response functions from SeaRise ice-sheet models. The Cryosphere Discussions.

Levitus, S., Antonov, J. and Boyer, T., 2005. Warming of the world ocean, 1955-2003. Geophysical Research Letters, **32**(2): L02604.

Levitus, S., Antonov, J.I., Boyer, T.P., Locarnini, R.A., Garcia, H.E. and Mishonov, A.V., 2009. Global ocean heat content 1955-2008 in light of recently revealed instrumentation problems. Geophysical Research Letters, **36**: L07608.

Levitus, S., Antonov, J.I., Wang, J.L., Delworth, T.L., Dixon, K.W. and Broccoli, A.J., 2001. Anthropogenic warming of Earth's climate system. Science, **292**(5515): 267-270.

Ligtenberg, S.R.M., van de Berg, W.J., van den Broeke, M.R., Rae, J.G.L. and van Meijgaard, E., Submitted. Four scenarios for the future surface mass balance of the Antarctic ice sheet: a contribution to ice2sea. Climate Dynamics.

Lionello, P., Cogo, S., Galati, M.B. and Sanna, A., 2008. The Mediterranean surface wave climate inferred from future scenario simulations. Global and Planetary Change, **63**(2-3): 152–162.

Lionello, P., Galati, M.B. and Elvini, E., 2010. Extreme storm surge and wind wave climate scenario simulations at the Venetian littoral. Physics and Chemistry of the Earth, Parts A/B/C, **40-41**: 86-92.

Little, C.M., Oppenheimer, M. and Urban, N.M., submitted. A probabilistic assessment of upper bounds on 21st century Antarctic ice loss. Nature Climate Change.

Llovel, W., Becker, M., Cazenave, A., Cretaux, J.F. and Ramillien, G., 2010a. Global land water storage change from GRACE over 2002-2009; Inference on sea level. Comptes Rendus Geoscience, **342**(3): 179–188.

Llovel, W., Becker, M., Cazenave, A., Jevrejeva, S., Alkama, R., Decharme, B., Douville, H., Ablain, M. and Beckley, B., 2011. Terrestrial waters and sea level variations on interannual time scale. Global and Planetary Change, **75**(1-2): 76-82.

Llovel, W., Guinehut, S. and Cazenave, A., 2010b. Regional and interannual variability in sea level over 2002-2009 based on satellite altimetry, Argo float data and GRACE ocean mass. Ocean Dynamics, **60**(5): 1193–1204.

Loeb, N.G., Wielicki, B.A., Doelling, D.R., Smith, G.L., Keyes, D.F., Kato, S., Manalo-Smith, N. and Wong, T., 2009. Toward optimal closure of the earth's top-of-atmosphere radiation budget. Journal of Climate, **22**(3): 748-766.

Lombard, A., Cazenave, A., DoMinh, K., Cabanes, C. and Nerem, R.S., 2005a. Thermosteric sea level rise for the past 50 years; comparison with tide gauges and inference on water mass contribution. Global and Planetary Change, **48**(4): 303-312.

Lombard, A., Cazenave, A., Le Traon, P.Y. and Ishii, M., 2005b. Contribution of thermal expansion to present-day sea-level change revisited. Global and Planetary Change, **47**(1): 1–16.

Lombard, A., Garric, G. and Penduff, T., 2009. Regional patterns of observed sea level change: insights from a 1/4A degrees global ocean/sea-ice hindcast. Ocean Dynamics, **59**(3): 433-449.

Lorbacher, K., Dengg, J., Boning, C.W. and Biastoch, A., 2010. Regional patterns of sea level change related to interannual variability and multidecadal trends in the atlantic meridional overturning circulation. Journal of Climate, **23**(15): 4243-4254.

Lorbacher, K., Marsland, S.J., Church, J.A., Griffies, S.M. and Stammer, D., 2012. Rapid barotrophic sea-level rise from ice-sheet melting scenarios. Journal of Geophysical Research, **117**: C06003.

Losch, M., Adcroft, A. and Campin, J.M., 2004. How sensitive are coarse general circulation models to fundamental approximations in the equations of motion? Journal of Physical Oceanography, **34**(1): 306-319.

Lowe, J.A. and Gregory, J.M., 2006. Understanding projections of sea level rise in a hadley centre coupled climate model. Journal of Geophysical Research-Oceans, **111**(C11): C11014.

Lowe, J.A., Woodworth, P.L., Knutson, T., McDonald, R.E., McInnes, K.L., Woth, K., von Storch, H., Wolf, J., Swail, V., Bernier, N.B., Gulev, S., Horsburgh, K.J., Unnikrishnan, A.S., Hunter, J.R. and Weisse, R., 2010. Past and future changes in extreme sea levels and waves. Understanding Sea-Level Rise and Variability. Wiley-Blackwell, Oxford, UK, 326-375 pp.

Lozier, M.S., Roussenov, V., Reed, M.S.C. and Williams, R.G., 2010. Opposing decadal changes for the North Atlantic meridional overturning circulation. Nature Geoscience, **3**(10): 728-734.

Luthcke, S.B., Zwally, H.J., Abdalati, W., Rowlands, D.D., Ray, R.D., Nerem, R.S., Lemoine, F.G., McCarthy, J.J. and Chinn, D.S., 2006. Recent Greenland ice mass loss by drainage system from satellite gravity observations. Science, **314**(5803): 1286–1289.

MacAyeal, D.R., Scambos, T.A., Hulbe, C.L. and Fahnestock, M.A., 2003. Catastrophic ice-shelf break-up by an ice-shelf-fragment- capsize mechanism. Journal of Glaciology, **49**(164): 22-36.

Marcelja, S., 2010. The timescale and extent of thermal expansion of the global ocean due to climate change. Ocean Science, **6**(1): 179–184.

Martin, T. and Adcroft, A., 2010. Parameterizing the fresh-water flux from land ice to ocean with interactive icebergs in a coupled climate model. Ocean Modelling, **34**(3-4): 111–124.

Marzeion, B., Hofer, M., Jarosch, A.H., Kaser, G. and Mölg, T., 2011. A minimal model for reconstructing interannual mass balance variability of glaciers in the European Alps. The Cryosphere Discuss., **5**(5): 2799-2839.

Marzeion, B., Jarosch, A.H. and Hofer, M., submitted. Past and future sea-level changes from the surface mass balance of glaciers. The Cryosphere Discuss.

Masters, D., Nerem, R.S., Choe, C., Leuliette, E., Beckley, B., White, N. and Ablain, M., submitted. Comparison of global mean sea level time series from TOPEX/Poseidon, Jason 1 and Jason 2. Marine Geodesy.

Matsuo, K. and Heki, K., 2010. Time-variable ice loss in Asian high mountains from satellite gravimetry. Earth and Planetary Science Letters, **290**(1-2): 30-36.

McInnes, K., Macadam, I., Hubbert, G. and O'Grady, J.G., 2011. An assessment of current and future vulnerability to coastal inundation due to sea level extremes in Victoria, southeast Australia. International Journal of Climatology, **Published on line November 2011**.

McInnes, K., Macadam, I., Hubbert, G. and O'Grady, J., 2009. A modelling approach for estimating the frequency of sea level extremes and the impact of climate change in southeast Australia. Natural Hazards, **51**(1): 115–137.

Meehl, G.A., Arblaster, J.M., Fasullo, J.T., Hu, A. and Trenberth, K.E., 2011. Model-based evidence of deep-ocean heat uptake during surface-temperature hiatus periods. Nature Climate Change, **1**(7): 360-364.

Meehl, G.A., Hu, A.X. and Tebaldi, C., 2010. Decadal Prediction in the Pacific Region. Journal of Climate, **23**(11): 2959-2973.

Meehl, G.A., Stocker, T.F., Collins, W.D., Friedlingstein, P., Gaye, A.T., Gregory, J.M., Kitoh, A., Knutti, R., Murphy, J.M., Noda, A., Raper, S.C.B., Watterson, I.G., Weaver, A.J. and Zhao, Z., 2007. Global climate projections, Climate Change 2007: The Physical Science Basis. Contribution of Working Group I to the Fourth Assessment Report of the Intergovernmental Panel on Climate Change. Cambridge University Press, United Kingdom, pp. 755-828.

Meehl, G.A., Washington, W.M., Collins, W.D., Arblaster, J.M., Hu, A.X., Buja, L.E., Strand, W.G. and Teng, H.Y., 2005. How much more global warming and sea level rise? Science, **307**(5716): 1769–1772.

Meier, M.F., Dyurgerov, M.B., Rick, U.K., O'Neel, S., Pfeffer, W.T., Anderson, R.S., Anderson, S.P. and Glazovsky, A.F., 2007. Glaciers dominate eustatic sea-level rise in the 21st century. Science, **317**(5841): 1064–1067.

Meinshausen, M., Smith, S., Calvin, K., Daniel, J., Kainuma, M., Lamarque, J., Matsumoto, K., Montzka, S., Raper, S., Riahi, K., Thomson, A., Velders, G. and van Vuuren, D., 2011. The RCP greenhouse gas concentrations and their extensions from 1765 to 2300. Climatic Change, **109**(1-2): 213-241.

Menéndez, M., Méndez, F.J., Losada, I.J. and Graham, N.E., 2008. Variability of extreme wave heights in the northeast Pacific Ocean based on buoy measurements. Geophysical Research Letters, **35**(22): L22607.

Menéndez, M. and Woodworth, P.L., 2010. Changes in extreme high water levels based on a quasi-global tide-gauge data set. Journal of Geophysical Research - Oceans, **115**(C10): C10011.

Mercer, J.H., 1978. West Antarctic ice sheet and CO2 greenhouse effect: a threat of disaster. Nature, **271**: 321-325.

Mernild, S.H., Hanna, E., Yde, J.C., Cppelen, J. and Malmros, J.K., Submitted. Extreme Greenland air temperatures in a warming climate, 1890-2010, and impacts on the Greenland Ice Sheet surface mass balance. Journal of Geophysical Research.

Mernild, S.H. and Liston, G.E., submitted. Greenland freshwater runoff. Part II: Distribution and trends, 1960-2010. Journal of Climate.

Mernild, S.H., Liston, G.E., Hiemstra, C.A. and Christensen, J.H., 2010. Greenland Ice Sheet Surface Mass-Balance Modeling in a 131-Yr Perspective, 1950-2080. Journal of Hydrometeorology, **11**(1): 3-25.

Merrifield, M.A. and Maltrud, M.E., 2011. Regional sea level trends due to a Pacific trade wind intensification. Geophysical Research Letters, **38**: L21605.

Mikolajewicz, U., Groger, M., Maier-Reimer, E., Schurgers, G., Vizcaino, M. and Winguth, A., 2007a. Long-term effects of anthropogenic CO2 emissions simulated with a complex earth system model. Climate Dynamics: 599-631.

Mikolajewicz, U., Vizcaino, M., Jungclaus, J. and Schurgers, G., 2007b. Effect of ice sheet interactions in anthropogenic climate change simulations. Geophysical Research Letters, **34**: L18706.
Miller, L. and Douglas, B.C., 2007. Gyre-scale atmospheric pressure variations and their relation to 19th and 20th century sea level rise. Geophysical Research Letters, **34**(16): L16602.
Milly, P.C.D., Cazenave, A. and Gennero, M.C., 2003. Contribution of climate-driven change in continental water storage to recent sea-level rise. Proceedings of the National Academy of Sciences of the United States of America, **100**(23): 13158–13161.
Milne, G.A., Gehrels, W.R., Hughes, C.W. and Tamisiea, M.E., 2009. Identifying the causes of sea-level change. Nature Geoscience, **2**(7): 471-478.
Milne, G.A. and Mitrovica, J.X., 1998. Postglacial sea-level change on a rotating Earth. Geophysical Journal International, **133**(1): 1–19.
Mitrovica, J.X., Gomez, N. and Clark, P.U., 2009. The Sea-Level Fingerprint of West Antarctic Collapse. Science, **323**(5915): 753-753.
Mitrovica, J.X., Gomez, N., Morrow, E., Hay, C., Latychev, K. and Tamisiea, M.E., 2011. On the robustness of predictions of sea-level fingerprints. Geophysical Journal International, **187**(2): 729-742.
Mitrovica, J.X. and Milne, G.A., 2003. On post-glacial sea level: I. general theory. Geophysical Journal International, **154**(2): 253-267.
Mitrovica, J.X. and Peltier, W.R., 1991. On postglacial geoid subsidence over the equatorial oceans. Journal of Geophysical Research-Solid Earth, **96**(B12): 20053-20071.
Mitrovica, J.X., Tamisiea, M.E., Davis, J.L. and Milne, G.A., 2001. Recent mass balance of polar ice sheets inferred from patterns of global sea-level change. Nature, **409**(6823): 1026–1029.
Mitrovica, J.X., Wahr, J., Matsuyama, I. and Paulson, A., 2005. The rotational stability of an ice-age earth. Geophysical Journal International, **161**(2): 491-506.
Moberg, A., Sonechkin, D.M., Holmgren, K., Datsenko, N.M. and Karlen, W., 2005. Highly variable Northern Hemisphere temperatures reconstructed from low- and high-resolution proxy data. Nature, **433**(7026): 613-617.
Monaghan, A.J., Bromwich, D.H., Fogt, R.L., Wang, S.H., Mayewski, P.A., Dixon, D.A., Ekaykin, A., Frezzotti, M., Goodwin, I., Isaksson, E., Kaspari, S.D., Morgan, V.I., Oerter, H., Van Ommen, T.D., Van der Veen, C.J. and Wen, J.H., 2006. Insignificant change in Antarctic snowfall since the International Geophysical Year. Science, **313**(5788): 827-831.
Moore, J.C., Jevrejeva, S. and Grinsted, A., 2011. The historical global sea level budget. Annals of Glaciology, **52**(59): 8–14.
Mori, N., Yasuda, T., Mase, H., Tom, T. and Oku, Y., 2010. Projection of extreme wave climate change under global warming. Hydrological Research Letters, **4**: 15–19.
Morlighem, M., Rignot, E., Seroussi, H., Larour, E. and Ben Dhia, H., 2010. Spatial patterns of basal drag inferred using control methods from a full-stokes and simpler models for Pine Island Glacier, West Antarctica. Geophysical Research Letters, **37**: L14502.
Moucha, R., Forte, A.M., Mitrovica, J.X., Rowley, D.B., Quere, S., Simmons, N.A. and Grand, S.P., 2008. Dynamic topography and long-term sea-level variations: there is no such thing as a stable continental platform. Earth and Planetary Science Letters, **271**(1-4): 101–108.
Mousavi, M., Irish, J., Frey, A., Olivera, F. and Edge, B., 2011. Global warming and hurricanes: the potential impact of hurricane intensification and sea level rise on coastal flooding. Climatic Change, **104**(3): 575-597.
Murphy, D.M., Solomon, S., Portmann, R.W., Rosenlof, K.H., Forster, P.M. and Wong, T., 2009. An observationally based energy balance for the Earth since 1950. Journal of Geophysical Research - Oceans, **114**(D17): D17107.
Naish, T., Powell, R., Levy, R., Wilson, G., Scherer, R., Talarico, F., Krissek, L., Niessen, F., Pompilio, M., Wilson, T., Carter, L., DeConto, R., Huybers, P., McKay, R., Pollard, D., Ross, J., Winter, D., Barrett, P., Browne, G., Cody, R., Cowan, E., Crampton, J., Dunbar, G., Dunbar, N., Florindo, F., Gebhardt, C., Graham, I., Hannah, M., Hansaraj, D., Harwood, D., Helling, D., Henrys, S., Hinnov, L., Kuhn, G., Kyle, P., Laufer, A., Maffioli, P., Magens, D., Mandernack, K., McIntosh, W., Millan, C., Morin, R., Ohneiser, C., Paulsen, T., Persico, D., Raine, I., Reed, J., Riesselman, C., Sagnotti, L., Schmitt, D., Sjunneskog, C., Strong, P., Taviani, M., Vogel, S., Wilch, T. and Williams, T., 2009. Obliquity-paced Pliocene West Antarctic ice sheet oscillations. Nature, **458**: 322-328.
Nerem, R.S., Chambers, D.P., Choe, C. and Mitchum, G.T., 2010. Estimating mean sea level change from the TOPEX and Jason altimeter missions. Marine Geodesy, **33**(S1): 435-446.
Ngo-Duc, T., Laval, K., Polcher, J., Lombard, A. and Cazenave, A., 2005. Effects of land water storage on global mean sea level over the past half century. Geophysical Research Letters, **32**(9): L09704.
Nicholls, R.J., Marinova, N., Lowe, J.A., Brown, S., Vellinga, P., De Gusmao, D., Hinkel, J. and Tol, R.S.J., 2011. Sea-level rise and its possible impacts given a 'beyond 4 degrees C world' in the twenty-first century. Philosophical Transactions of the Royal Society a-Mathematical Physical and Engineering Sciences, **369**(1934): 161–181.
Nick, F.M., Luckman, A., Vieli, A., Van Der Veen, C.J., Van As, D., Van De Wal, R.S.W., Pattyn, F., Hubbard, A.L. and Floricioiu, D., 2012. The response of Petermann Glacier, Greenland, to large calving events, and its future stability in the context of atmospheric and oceanic warming. Journal of Glaciology, **58**(208): 229-239.
Nick, F.M., van der Veen, C.J., Vieli, A. and Benn, D.I., 2010. A physically based calving model applied to marine outlet glaciers and implications for the glacier dynamics. Journal of Glaciology, **56**(199): 781-794.

Nick, F.M., Vieli, A., Howat, I.M. and Joughin, I., 2009. Large-scale changes in Greenland outlet glacier dynamics triggered at the terminus. Nature Geoscience, **2**(2): 110–114.
Nick, F.M., Vieli, A., Langer Andersen, M., Joughin, I., Payne, A.J., Edwards, T.L., Pattyn, F. and van de Wal, R., Submitted. Future sea-level rise from Greenland's major outlet glaciers in a warming climate. Nature.
Nowicki, S., Submitted. Spatial Sensitivities of the Greenland Ice Sheet to Environmental Changes (The SeaRISE Project). Journal of Geophysical Research.
Okumura, Y.M., Deser, C., Hu, A., Timmermann, A. and Xie, S.P., 2009. North Pacific Climate Response to Freshwater Forcing in the Subarctic North Atlantic: Oceanic and Atmospheric Pathways. Journal of Climate, **22**(6): 1424–1445.
Palmer, M.D., McNeall, D.J. and Dunstone, N.J., 2011. Importance of the deep ocean for estimating decadal changes in Earth's radiation balance. Geophysical Research Letters, **38**: L13707.
Pardaens, A., Gregory, J.M. and Lowe, J., 2011a. A model study of factors influencing projected changes in regional sea level over the twenty-first century. Climate Dynamics, **36**(9–10): 2015-2033.
Pardaens, A.K., Banks, H.T., Gregory, J.M. and Rowntree, P.R., 2003. Freshwater transports in HadCM3. Climate Dynamics, **21**(2): 177–195.
Pardaens, A.K., Lowe, J.A., Brown, S., Nicholls, R.J. and de Gusmao, D., 2011b. Sea-level rise and impacts projections under a future scenario with large greenhouse gas emission reductions. Geophysical Research Letters, **38**: L12604.
Parizek, B.R., Christianson, K., Anandakrishnan, S., Alley, R.B., Walker, R.T., Edwards, R.A., Wolfe, D.S., Bertini, G.T., Rinehart, S.K., Bindschadler, R.A. and Nowicki, S.M.J., Submitted. Dynamic (In)stability of Thwaites Glacier, West Antarctica. Journal of Geophysical Research.
Park, J.W., Gourmelen, N., Shepherd, A., Kim, S.W., Vaughan, D.G. and Wingham, D.J., submitted. Sustained retreat of the Pine Island Glacier through accelerated 1 ocean melting. Geophysical Research Letters.
Pattyn, F., Huyghe, A., De Brabander, S. and De Smedt, B., 2006. Role of transition zones in marine ice sheet dynamics. Journal of Geophysical Research-Earth Surface, **111**(F2): 10.
Pattyn, F., Perichon, L., Durand, G., Favier, L., Gagliardini, O., Hindmarch, R.C.A., Zwinger, T., Albrecht, T., Cornford, S., Docquier, D., Furst, J.J., Goldberg, D., Gudmundsson, G.H., Humbert, A., Hutten, M., Huybrechts, P., Jouvet, G., Kleiner, T., Larour, E., Martin, D., Morlighem, M., Payne, A.J., Pollard, D., Ruckamp, M., Rybak, O., Seroussi, H., Thoma, M. and Wilkens, N., submitted. Grounding-line migration in plan-view marine ice-sheet models: results of the ice2sea MISMIP3d intercomparison. The Cryosphere.
Paulson, A., Zhong, S.J. and Wahr, J., 2007. Inference of mantle viscosity from GRACE and relative sea level data. Geophysical Journal International, **171**(2): 497-508.
Payne, A.J., Cornford, S.L., Martin, D.F., Agosta, C., van den Broeke, M.R., Edwards, T.L., Gladstone, R.M., H.H. Hellmer, H.H., G. Krinner, G., Le Brocq, A.M., Ligtenberg, S.R.M., Lipscomb, W.H., Ng, E.G., Shannon , S.R., Timmerman, R. and Vaughan, D.G., submitted. Impact of uncertain climate forcing on projections of the West Antarctic ice sheet over the 21st and 22nd centuries. Earth and Planetary Science Letters.
Peltier, W.R., 1974. Impulse response of a Maxwell Earth. Reviews of Geophysics, **12**(4): 649-669.
Peltier, W.R., 2004. Global glacial isostasy and the surface of the ice-age earth: The ice-5G (VM2) model and grace. Annual Review of Earth and Planetary Sciences, **32**: 111–149.
Peltier, W.R., 2009. Closure of the budget of global sea level rise over the GRACE era: the importance and magnitudes of the required corrections for global glacial isostatic adjustment. Quaternary Science Reviews, **28**(17–18): 1658–1674.
Peltier, W.R. and Tushingham, A.M., 1991. Influence of glacial isostatic-adjustment on tide gauge measurements of secular sea-level change. Journal of Geophysical Research-Solid Earth and Planets, **96**(B4): 6779-6796.
Pfeffer, W.T., 2007. A simple mechanism for irreversible tidewater glacier retreat. Journal of Geophysical Research-Earth Surface, **112**: F03S25.
Pfeffer, W.T., Harper, J.T. and O'Neel, S., 2008. Kinematic constraints on glacier contributions to 21st-century sea-level rise. Science, **321**(5894): 1340–1343.
Phillips, T., Rajaram, H. and Steffen, K., 2010. Cryo-hydrologic warming: A potential mechanism for rapid thermal response of ice sheets. Geophysical Research Letters, **37**: L20503.
Pokhrel, Y.N., Hanasaki, N., Yeh, P.J.F., Yamada, T.J., Kanae, S. and Oki, T., 2012. Model estimates of sea-level change due to anthropogenic impacts on terrestrial water storage. Nature Geoscience, **5**(6): 389-392.
Pollack, H.N., Hurter, S.J. and Johnson, J.R., 1993. Heat flow from the Earth's interior: Analysis of the global data set. Rev. Geophys., **31**(3): 267-280.
Pollard, D. and DeConto, R.M., 2009. Modelling West Antarctic ice sheet growth and collapse through the past five million years. Nature, **458**: 329-332.
Polvani, L.M., Previdi, M. and Deser, C., 2011. Large cancellation, due to ozone recovery, of future Southern Hemisphere atmospheric circulation trends. Geophysical Research Letters, **38**: L04707.
Price, S.F., Payne, A.J., Howat, I.M. and Smith, B.E., 2011. Committed sea-level rise for the next century from Greenland ice sheet dynamics during the past decade. Proceedings of the National Academy of Sciences of the United States of America, **108**(22): 8978-8983.
Pritchard, H.D., Arthern, R.J., Vaughan, D.G. and Edwards, L.A., 2009. Extensive dynamic thinning on the margins of the Greenland and Antarctic ice sheets. Nature, **461**(7266): 971-975.

Purkey, S.G. and Johnson, G.C., 2010. Warming of global abyssal and deep southern ocean waters between the 1990s and 2000s: contributions to global heat and sea level rise budgets. Journal of Climate, **23**(23): 6336-6351.
Qiu, B. and Chen, S.M., 2006. Decadal variability in the large-scale sea surface height field of the South Pacific Ocean: observations and causes. Journal of Physical Oceanography, **36**(9): 1751–1762.
Quinn, K.J. and Ponte, R.M., 2010. Uncertainty in ocean mass trends from GRACE. Geophysical Journal International, **181**(2): 762-768.
Radic, V., Bliss, A., Beedlow, C.D., Hock, R., Miles, E. and Cogley, J.G., submitted. Regional and global projections of the 21st century glacier mass changes in response to climate scenarios from GCMs. Climate Dynamics.
Radic, V. and Hock, R., 2010. Regional and global volumes of glaciers derived from statistical upscaling of glacier inventory data. Journal of Geophysical Research-Earth Surface, **115**: F01010.
Radic, V. and Hock, R., 2011. Regionally differentiated contribution of mountain glaciers and ice caps to future sea-level rise. Nature Geoscience, **4**(2): 91-94.
Rae, J.G.L., Adalgeirsdottir, G., Edwards, T.L., Fettweis, X., Gregory, J.M., Hewitt, H.T., Lowe, J.A., Lucas-Picher, P., Mottram, R.H., Payne, A.J., Ridley, J.K., Shannon, S.R., van de Berg, W.J., van de Wal, R.S.W. and van den Broeke, M.R., submitted. Greenland ice sheet surface mass balance: evaluating simulations and making projections with regional climate models. The Cryosphere Discussions.
Rahmstorf, S., 2007a. Response to comments on "A semi-empirical approach to projecting future sea-level rise". Science, **317**(5846).
Rahmstorf, S., 2007b. A semi-empirical approach to projecting future sea-level rise. Science, **315**(5810): 368-370.
Rahmstorf, S., Cazenave, A., Church, J., Hansen, J., Keeling, R., Parker, D. and Somerville, R., 2007. Recent climate observations compared to projections. Science, **316**(5825): 709-709.
Rahmstorf, S., Foster, G. and Cazenave, A., submitted. Comparing climate projections to observations up to 2011. Environmental Research Letters.
Rahmstorf, S. and Ganopolski, A., 1999. Long-term global warming scenarios computed with an efficient coupled climate model. Climatic Change, **43**(2): 353-367.
Rahmstorf, S., Perrette, M. and Vermeer, M., 2011. Testing the robustness of semi-empirical sea level projections. Climate Dynamics, **39**(3-4): 861-875.
Ramillien, G., Famiglietti, J.S. and Wahr, J., 2008. Detection of Continental Hydrology and Glaciology Signals from GRACE: A Review. Surveys in Geophysics, **29**(4-5): 361-374.
Raper, S.C.B. and Braithwaite, R.J., 2005. The potential for sea level rise: New estimates from glacier and ice cap area and volume distributions. Geophysical Research Letters, **32**(5): L05502.
Raper, S.C.B., Gregory, J.M. and Stouffer, R.J., 2002. The role of climate sensitivity and ocean heat uptake on AOGCM transient temperature response. Journal of Climate, **15**(1): 124–130.
Ray, R.D. and Douglas, B.C., 2011. Experiments in reconstructing twentieth-century sea levels. Progress in Oceanography, **91**(4): 495-515.
Ridley, J., Gregory, J.M., Huybrechts, P. and Lowe, J., 2010. Thresholds for irreversible decline of the Greenland ice sheet. Climate Dynamics, **35**(6): 1065–1073.
Ridley, J.K., Huybrechts, P., Gregory, J.M. and Lowe, J.A., 2005. Elimination of the Greenland ice sheet in a high CO2 climate. Journal of Climate, **18**(17): 3409-3427.
Rignot, E., 2008. Changes in West Antarctic ice stream dynamics observed with ALOS PALSAR data. Geophysical Research Letters, **35**(12): L12505.
Rignot, E., Bamber, J.L., Van Den Broeke, M.R., Davis, C., Li, Y.H., Van De Berg, W.J. and Van Meijgaard, E., 2008. Recent Antarctic ice mass loss from radar interferometry and regional climate modelling. Nature Geoscience, **1**(2): 106–110.
Rignot, E., Casassa, G., Gogineni, P., Krabill, W., Rivera, A. and Thomas, R., 2004. Accelerated ice discharge from the Antarctic Peninsula following the collapse of Larsen B ice shelf. Geophysical Research Letters, **31**(18): L18401.
Rignot, E., Velicogna, I., van den Broeke, M.R., Monaghan, A. and Lenaerts, J., 2011. Acceleration of the contribution of the Greenland and Antarctic ice sheets to sea level rise. Geophysical Research Letters, **38**: L05503.
Ritz, C., Durand, G., Edwards, T.L., Payne, A.J., Peyaud, V. and Richard C.A. Hindmarsh, R.C.A., Submitted. Bimodal probability of the dynamic contribution of Antarctica to future sea level. Nature.
Riva, R.E.M., Bamber, J.L., Lavallee, D.A. and Wouters, B., 2010. Sea-level fingerprint of continental water and ice mass change from GRACE. Geophysical Research Letters, **37**: L19605.
Robinson, A., Calov, R. and Ganopolski, A., 2012. Multistability and critical thresholds of the Greenland ice sheet. Nature Climate Change, **2**(6): 429-432.
Russell, G.L., Gornitz, V. and Miller, J.R., 2000. Regional sea-level changes projected by the NASA/GISS atmosphere-ocean model. Climate Dynamics, **16**(10–11): 789-797.
Sahagian, D., 2000. Global physical effects of anthropogenic hydrological alterations: sea level and water redistribution. Global and Planetary Change, **25**(1-2): 39-48.
Sallenger, A.H., Doran, K.S. and Howd, P.A., 2012. Hotspot of accelerated sea-level rise on the Atlantic coast of North America. Nature Climate Change, **Advanced on line publication**.
Sasgen, I., van den Broeke, M., Bamber, J.L., Rignot, E., Sørensen, L.S., Wouters, B., Martinec, Z., Velicogna, I. and Simonsen, S.B., 2012. Timing and origin of recent regional ice-mass loss in Greenland. **333-334**: 293-303.

Scambos, T.A., Bohlander, J.A., Shuman, C.A. and Skvarca, P., 2004. Glacier acceleration and thinning after ice shelf collapse in the Larsen B embayment, Antarctica. Geophysical Research Letters, **31**(18): L18402.

Schaeffer, M., Hare, W., Rahmstorf, S. and Vermeer, M., 2012. Long-term sea-level rise implied by 1.5 °C and 2 °C warming levels. Nature Climate Change, **advance online publication**.

Schewe, J., Levermann, A. and Meinshausen, M., 2011. Climate change under a scenario near 1.5 °C of global warming: monsoon intensification, ocean warming and steric sea level rise. Earth Syst. Dynam., **2**(1): 25-35.

Schmith, T., Johansen, S. and Thejll, P., 2007. Comment on "A semi-empirical approach to projecting future sea-level rise". Science, **317**(5846): 1866.

Schmith, T., Johansen, S. and Thejll, P., 2012, in press. Statistical analysis of global surface temperature and sea level using cointegration methods. Journal of Climate.

Schoof, C., 2007a. Ice sheet grounding line dynamics: steady states, stability, and hysteresis. Journal of Geophysical Research-Earth Surface, **112**: F03S28.

Schoof, C., 2007b. Marine ice-sheet dynamics. Part 1. the case of rapid sliding. Journal of Fluid Mechanics, **573**: 27-55.

Schoof, C., 2010. Ice-sheet acceleration driven by melt supply variability. Nature, **468**(7325): 803-806.

Schoof, C., 2011. Marine ice sheet dynamics. Part 2. A Stokes flow contact problem. Journal of Fluid Mechanics, **679**: 122–155.

Seddik, H., Greve, R., Zwinger, T., Gillet-Chaulet, F. and Gagliardini, O., 2012. Simulations of the Greenland ice sheet 100 years into the future with the full Stokes model Elmer/Ice. Journal of Glaciology, **58**(209): 427-440.

Semedo, A., Bengtson, L., Gunther, H., Weisse, R., Beherens, A. and Sterl, A., submitted. Impact of a warmer climate on the global wave field. Journal of Climate.

Seneviratne, S. and others, 2012. Changes in Climate Extremes and their impacts on the natural Physical Environment, Managing the Risks of Extreme Events and Disasters to Advance Climate Change Adaptation (SREX). IPCC, Cambridge, pp. 109-230.

Shannon, S.R., Payne, A.J., Bartholomew, I.D., van den Broeke, M.R., Edwards, T.L., Fettweis, X., Gagliardini, F., Gillet-Chaulet, F., Goelzer, H., Hoffman, M.J., Huybrechts, P., Mair, D., Nienow, P., Perego, M., Price, S.F., Smeets, C.J.P.P., Sole, A.J., van de Wal, R.S.W. and Zwinger, T., submitted. Enhanced basal lubrication and the contribution of the Greenland ice sheet to future sea level rise. Proceedings of the National Academy of Science.

Shepherd, A. and Wingham, D., 2007. Recent sea-level contributions of the Antarctic and Greenland ice sheets. Science, **315**(5818): 1529–1532.

Slangen, A.B.A., Carson, M., Katsman, C.A., van deWal, R.S.W., Kohl, A., Vermeersen, L.L.A. and Stammer, D., submitted. Projecting twenty-first century regional sea-level changes. Nature.

Slangen, A.B.A., Katsman, C.A., van de Wal, R.S.W., Vermeersen, L.L.A. and Riva, R.E.M., 2011. Towards regional projections of twenty-first century sea-level change based on IPCC SRES scenarios. Climate Dynamics, **38**(5-6): 1191–1209.

Smith, J.M., Cialone, M.A., Wamsley, T.V. and McAlpin, T.O., 2010. Potential impact of sea level rise on coastal surges in southeast Louisiana. Ocean Engineering, **37**(1): 37-47.

Sokolov, A.P., Forest, C.E. and Stone, P.H., 2010. Sensitivity of climate change projections to uncertainties in the estimates of observed changes in deep-ocean heat content. Climate Dynamics, **34**(5): 735-745.

Sole, A., Payne, T., Bamber, J., Nienow, P. and Krabill, W., 2008. Testing hypotheses of the cause of peripheral thinning of the Greenland Ice Sheet: is land-terminating ice thinning at anomalously high rates? Cryosphere, **2**(2): 205-218.

Solomon, S., Plattner, G.-K., Knutti, R. and Friedlingstein, P., 2009. Irresversible climate change due to carbon dioxide emissions. Proceedings of the National Academy of Science, **106**(6): 1704–1709.

Solomon, S., Qin, D., Manning, M., Chen, Z., Marquis, M., Averyt, K.B., Tignor, M. and Miller, H.L. (Editors), 2007. Climate Change 2007: The Physical Science Basis. Cambridge University Press, Cambridge, 940 pp.

Stackhouse Jr, P.W., Wong, T., Loeb, N.G., Kratz, D.P., Wilber, A.C., D.R. Doelling, a. and Nguyen, L.C., 2010. Earth Radiation Budget at top-of-atmosphere [in "State of the Climate in 2009"]. Bulletin of the American Meteorological Society - Special Supplement, **91**(7): S41.

Stammer, D., 2008. Response of the global ocean to Greenland and Antarctic ice melting. Journal of Geophysical Research - Oceans, **113**: C06022.

Stammer, D., Agarwal, N., Herrmann, P., Kohl, A. and Mechoso, C.R., 2011. Response of a coupled ocean-atmosphere model to greenland ice melting. Survey in Geophysics, **32**(4-5): 621-642.

Stammer, D. and Huttemann, S., 2008. Response of regional sea level to atmospheric pressure loading in a climate change scenario. Journal of Climate, **21**(10): 2093-2101.

Stenni, B., Buiron, D., Frezzotti, M., Albani, S., Barbante, C., Bard, E., Barnola, J.M., Baroni, M., Baumgartner, M., Bonazza, M., Capron, E., Castellano, E., Chappellaz, J., Delmonte, B., Falourd, S., Genoni, L., Iacumin, P., Jouzel, J., Kipfstuhl, S., Landais, A., Lemieux-Dudon, B., Maggi, V., Masson-Delmotte, V., Mazzola, C., Minster, B., Montagnat, M., Mulvaney, R., Narcisi, B., Oerter, H., Parrenin, F., Petit, J.R., Ritz, C., Scarchilli, C., Schilt, A., Schuepbach, S., Schwander, J., Selmo, E., Severi, M., Stocker, T.F. and Udisti, R., 2011. Expression of the bipolar see-saw in Antarctic climate records during the last deglaciation. Nature Geoscience, **4**(1): 46-49.

Sterl, A., van den Brink, H., de Vries, H., Haarsma, R. and van Meijgaard, E., 2009. An ensemble study of extreme North Sea storm surges in a changing climate. Ocean Science Discussions, **6**(2): 1031–1059.

Straneo, F., Hamilton, G.S., Sutherland, D.A., Stearns, L.A., Davidson, F., Hammill, M.O., Stenson, G.B. and Rosing-Asvid, A., 2010. Rapid circulation of warm subtropical waters in a major glacial fjord in East Greenland. Nature Geoscience, **3**(3): 182–186.

Sundal, A.V., Shepherd, A., Nienow, P., Hanna, E., Palmer, S. and Huybrechts, P., 2011. Melt-induced speed-up of Greenland ice sheet offset by efficient subglacial drainage. Nature, **469**(7331): 522-U83.

Suzuki, T., Hasumi, H., Sakamoto, T.T., Nishimura, T., Abe-Ouchi, A., Segawa, T., Okada, N., Oka, A. and Emori, S., 2005. Projection of future sea level and its variability in a high-resolution climate model: Ocean processes and Greenland and Antarctic ice-melt contributions. Geophysical Research Letters, **32**(19): L19706.

Suzuki, T. and Ishii, M., 2011. Regional distribution of sea level changes resulting from enhanced greenhouse warming in the Model for Interdisciplinary Research on Climate version 3.2. Geophysical Research Letters, **38**: L02601.

Swingedouw, D., Fichefet, T., Huybrechts, P., Goosse, H., Driesschaert, E. and Loutre, M.F., 2008. Antarctic ice-sheet melting provides negative feedbacks on future climate warming. Geophysical Research Letters, **35**: L17705.

Syvitski, J.P.M. and Kettner, A., 2011. Sediment flux and the Anthropocene. Philosophical Transactions of the Royal Society a-Mathematical Physical and Engineering Sciences, **369**(1938): 957-975.

Syvitski, J.P.M., Kettner, A.J., Overeem, I., Hutton, E.W.H., Hannon, M.T., Brakenridge, G.R., Day, J., Vorosmarty, C., Saito, Y., Giosan, L. and Nicholls, R.J., 2009. Sinking deltas due to human activities. Nature Geoscience, **2**(10): 681-686.

Tamisiea, M.E., 2011. Ongoing glacial isostatic contributions to observations of sea level change. Geophysical Journal International, **186**(3): 1036–1044.

Tamisiea, M.E., Hill, E.M., Ponte, R.M., Davis, J.L., Velicogna, I. and Vinogradova, N.T., 2010. Impact of self attraction and loading on the annual cycle in sea level. Journal of Geophysical Research, **115**: C07004.

Tebaldi, C., Strauss, B.H. and Zervas, C.E., 2012. Modelling sea level rise impacts on storm surges along US coasts. Environmental Research Letters, **7**(1): 2–11.

Tett, S.F.B., Betts, R., Crowley, T.J., Gregory, J., Johns, T.C., Jones, A., Osborn, T.J., Oestroem, E., Roberts, D.L. and Woodage, M.J., 2007. The impact of natural and anthropogenic forcings on climate and hydrology since 1550. Climate Dynamics, **28**(1): 3-34.

Thoma, M., Jenkins, A., Holland, D. and Jacobs, S., 2008. Modelling circumpolar deep water intrusions on the Amundsen Sea continental shelf, Antarctica. Geophysical Research Letters, **35**: L18602.

Thomas, R., Frederick, E., Li, J., Krabill, W., Manizade, S., Paden, J., Sonntag, J., Swift, R. and Yungel, J., 2011. Accelerating ice loss from the fastest Greenland and Antarctic glaciers. Geophysical Research Letters, **38**: L10502.

Timmermann, A., McGregor, S. and Jin, F.F., 2010. Wind effects on past and future regional sea level trends in the Southern Indo-Pacific. Journal of Climate, **23**(16): 4429-4437.

Timmermann, R. and Hellmer, H.H., submitted. Southern Ocean warming and increased ice shelf basal melting in the 21st and 22nd centuries based on coupled ice-ocean finite-element modelling. Ocean Dynamics.

Trenberth, K.E., 2009. An imperative for climate change planning: tracking Earth's global energy. Current Opinion in Environmental Sustainability, **1**(1): 19-27.

Trenberth, K.E., 2010. Global change: The ocean is warming, isn't it? Nature, **465**(7296): 304-304.

Trenberth, K.E. and Fasullo, J.T., 2010. Tracking Earth's Energy. Science, **328**(5976): 316-317.

Trenberth, K.E., Fasullo, J.T. and Kiehl, J., 2009. Earth's Global Energy Budget. Bulletin of the American Meteorological Society, **90**(3): 311-323.

Tsimplis, M., Alvarez-Fanjul, E., Gomis, D., Fenoglio-Marc, L. and Perez, B., 2005. Mediterranean Sea level trends: Atmospheric pressure and wind contribution. Geophysical Research Letters, **32**(20).

Unnikrishnan, A.S., Kumar, M.R.R. and Sindhu, B., 2011. Tropical cyclones in the Bay of Bengal and extreme sea-level projections along the east coast of India in a future climate scenario. Current Science (India), **101**(3): 327-331.

Uotila, P., Lynch, A.H., Cassano, J.J. and Cullather, R.I., 2007. Changes in Antarctic net precipitation in the 21st century based on Intergovernmental Panel on Climate Change (IPCC) model scenarios. Journal of Geophysical Research-Atmospheres, **112**: D10107.

van Angelen, J.H., Lenaerts, J.T.M., Lhemitte, S., Fettweis, X., Kuipers Munneke, P., van den Broeke, M.R., van Meijgaard, E. and Greuell, W., 2012. Sensitivity of Greenland ice sheet surface mass balance to surface albedo parameterization: a study with a regional climate model. The Cryosphere Discuss., **6**: 1531–1562.

van Angelen, J.H., Lenaerts, J.T.M., van den Broeke, M.R., Fettweis, X. and van Meijgaard, E., submitted. Loss of refreezing capacity accelerates 21st century Greenland mass loss. Nature.

van de Wal, R.S.W., Boot, W., van den Broeke, M.R., Smeets, C., Reijmer, C.H., Donker, J.J.A. and Oerlemans, J., 2008. Large and rapid melt-induced velocity changes in the ablation zone of the Greenland Ice Sheet. Science, **321**(5885): 111–113.

van den Broeke, M., Bamber, J., Ettema, J., Rignot, E., Schrama, E., van de Berg, W.J., van Meijgaard, E., Velicogna, I. and Wouters, B., 2009. Partitioning Recent Greenland Mass Loss. Science, **326**(5955): 984-986.

van den Broeke, M., van de Berg, W.J. and van Meijgaard, E., 2006. Snowfall in coastal West Antarctica much greater than previously assumed. Geophysical Research Letters, **33**(2): L02505.

Van Ommen, T.D., Morgan, V. and Curran, M.A.J., 2004. Deglacial and Holocene changes in accumulation at Law Dome, East Antarctica. Annals of Glaciology, **39**(1): 395-365.

Vaughan, D.G., 2008. West Antarctic Ice Sheet collapse - the fall and rise of a paradigm. Climatic Change, **91**(1-2): 65-79.
Velicogna, I., 2009. Increasing rates of ice mass loss from the Greenland and Antarctic ice sheets revealed by GRACE. Geophysical Research Letters, **36**: L19503.
Vellinga, M. and Wood, R., 2008. Impacts of thermohaline circulation shutdown in the twenty-first century. Climatic Change, **91**(1-2): 43-63.
Vermeer, M. and Rahmstorf, S., 2009. Global sea level linked to global temperature. Proceedings of the National Academy of Science, **106**: 21527-21532.
Vieli, A. and Nick, F.M., 2011. Understanding and Modelling Rapid Dynamic Changes of Tidewater Outlet Glaciers: Issues and Implications. Surveys in Geophysics, **32**(4-5): 437-458.
Vinogradov, S.V. and Ponte, R.M., 2011. Low-frequency variability in coastal sea level from tide gauges and altimetry. Journal of Geophysical Research-Oceans, **116**.
Vizcaino, M., Mikolajewicz, U., Groger, M., Maier-Reimer, E., Schurgers, G. and Winguth, A., 2008. Long-term ice sheet-climate interactions under anthropogenic greenhouse forcing simulated with a complex Earth System Model. Climate Dynamics: 665-690.
Vizcaino, M., Mikolajewicz, U., Jungclaus, J. and Schurgers, G., 2010. Climate modification by future ice sheet changes and consequences for ice sheet mass balance. Climate Dynamics, **34**(2-3): 301-324.
von Schuckmann, K. and Le Traon, P.Y., 2011. How well can we derive Global Ocean Indicators from Argo data? Ocean Science, **7**(6): 783-791.
von Storch, H., Zorita, E. and Gonzalez-Rouco, J.F., 2008. Relationship between global mean sea-level and global mean temperature in a climate simulation of the past millennium. Ocean Dynamics, **58**(3-4): 227-236.
Wada, Y., van Beek, L.P.H., van Kempen, C.M., Reckman, J.W.T.M., Vasak, S. and Bierkens, M.F.P., 2010. Global depletion of groundwater resources. Geophysical Research Letters, **37**: L20402.
Wada, Y., van Beek, L.P.H., Weiland, F.C.S., Chao, B.F., Wu, Y.H. and Bierkens, M.F.P., 2012. Past and future contribution of global groundwater depletion to sea-level rise. Geophysical Research Letters, **39**: L09402.
Wake, L.M., Huybrechts, P., Box, J.E., Hanna, E., Janssens, I. and Milne, G.A., 2009. Surface mass-balance changes of the Greenland ice sheet since 1866. Annals of Glaciology, **50**(50): 178–184.
Walsh, K.J.E., McInnes, K. and McBride, J.L., 2011. Climate change impacts on tropical cyclones and extreme sea levels in the South Pacific – a regional assessment. Global and Planetary Change, **80-81**: 149–164.
Wang, S., McGrath, R., Hanafin, J., Lynch, P., Semmler, T. and Nolan, P., 2008. The impact of climate change on storm surges over Irish waters. Ocean Modelling, **25**(1-2): 83-94.
Wang, X. and Swail, V., 2006. Climate change signal and uncertainty in projections of ocean wave heights. Climate Dynamics, **26**(2): 109–126.
Wang, X., Swail, V., Zwiers, F., Zhang, X. and Feng, Y., 2009. Detection of external influence on trends of atmospheric storminess and northern oceans wave heights. Climate Dynamics, **32**(2): 189-203.
Wang, X.L., Swail, V.R. and Cox, A., 2010. Dynamical versus statistical downscaling methods for ocean wave heights. International Journal of Climatology, **30**(3): 317-332.
Warrick, R.A., Le Provost, C., Meier, M.F., Oerlemans, J. and Woodworth, P.L., 1996. Changes in sea level. In: J.T. Houghton, L.G. Meira Filho, B.A. Callander, N. Harris, A. Klattenberg and K. Maskell (Editors), Climate Change 1995, The Science of Climate Change. Cambridge University Press, Cambridge, pp. 359-405.
Warrick, R.A. and Oerlemans, J., 1990. Sea level rise. In: J.T. Houghton, G.J. Jenkins and J.J. Ephraums (Editors), Climate Change, The IPCC Scientific Assessment. Cambridge University Press, Cambridge, pp. 260-281.
Washington, W.M., Knutti, R., Meehl, G.A., Teng, H., Tebaldi, C., Lawrence, D., Buja, L. and Strand, W.G., 2009. How much climate change can be avoided by mitigation? Geophys. Res. Lett., **36**(L08703).
Watson, C., Burgette, R., Tregoning, P., White, N., Hunter, J., Coleman, R., Handsworth, R. and Brolsma, H., 2010. Twentieth century constraints on sea level change and earthquake deformation at Macquarie Island. Geophysical Journal International, **182**(2): 781-796.
Watts, A.B., 2001. Isostasy and Flexure of the Lithosphere. Cambridge University Press, 458 pp.
Weertman, J., 1961. Stability of Ice-Age ice sheets. Journal of Geophysical Research, **66**(11): 3783-3792.
Weertman, J., 1974. Stability of the junction of an ice sheet and an ice shelf. Journal of Glaciology, **13**(67): 3–11.
White, N.J., Church, J.A. and Gregory, J.M., 2005. Coastal and global averaged sea level rise for 1950 to 2000. Geophysical Research Letters, **32**(1): L01601.
Winguth, A., Mikolajewicz, U., Groger, M., Maier-Reimer, E., Schurgers, G. and Vizcaino, M., 2005. Centennial-scale interactions between the carbon cycle and anthropogenic climate change using a dynamic Earth system model. Geophysical Research Letters: -.
Winkelmann, R., Levermann, A., Frieler, K. and Martin, M.A., 2012. Uncertainty in future solid ice discharge from Antarctica. The Cryosphere Discuss., **6**(1): 673-714.
Winkelmann, R., Levermann, A., Martin, M.A. and Frieler, K., Accepted. Snowfall increases future ice discharge from Antarctica. Nature.
Wong, T., Wielecki, B.A., Lee, R.B.I., Smith, G.L., Bush, K.A. and Willis, J.K., 2006. Reexamination of the observed decadal variability of the earth radiation budget using altitude-corrected ERBE/ERBS nonscanner WFOV data. Journal of Climate, **19**(16): 4028-4040.

Woolf, D.K., Challenor, P.G. and Cotton, P.D., 2002. Variability and predictability of the North Atlantic wave climate. Journal of Geophysical Research-Oceans, **107**: C103145.

Woth, K., Weisse, R. and von Storch, H., 2006. Climate change and North Sea storm surge extremes: an ensemble study of storm surge extremes expected in a changed climate projected by four different regional climate models. Ocean Dynamics, **56**(1): 3–15.

Wouters, B., Chambers, D. and Schrama, E.J.O., 2008. GRACE observes small-scale mass loss in Greenland. Geophysical Research Letters, **35**(20): 5.

Wu, X.P., Heflin, M.B., Schotman, H., Vermeersen, B.L.A., Dong, D.A., Gross, R.S., Ivins, E.R., Moore, A. and Owen, S.E., 2010. Simultaneous estimation of global present-day water transport and glacial isostatic adjustment. Nature Geoscience, **3**(9): 642-646.

Wunsch, C. and Heimbach, P., 2007. Practical global oceanic state estimation. Physica D-Nonlinear Phenomena, **230**(1-2): 197-208.

Wunsch, C. and Stammer, D., 1997. Atmospheric loading and the oceanic "inverted barometer" effect. Reviews of Geophysics, **35**(1): 79–107.

Yin, J., submitted. Century to multi-century sea level rise projections from CMIP5 models. Geophysical Research Letters.

Yin, J.J., Griffies, S.M. and Stouffer, R.J., 2010. Spatial Variability of Sea Level Rise in Twenty-First Century Projections. Journal of Climate, **23**(17): 4585-4607.

Yin, J.J., Overpeck, J.T., Griffies, S.M., Hu, A.X., Russell, J.L. and Stouffer, R.J., 2011. Different magnitudes of projected subsurface ocean warming around Greenland and Antarctica. Nature Geoscience, **4**(8): 524-528.

Yin, J.J., Schlesinger, M.E. and Stouffer, R.J., 2009. Model projections of rapid sea-level rise on the northeast coast of the United States. Nature Geoscience, **2**(4): 262-266.

Yoshimori, M. and Abe-Ouchi, A., 2012. Sources of spread in multi-model projections of the Greenland ice-sheet surface mass balance. Journal of Climate, **25**(4): 1157–1175.

Young, I.R., Zieger, S. and Babanin, A.V., 2011. Global trends in wind speed and wave height. Science, **332**(6028): 451-455.

Zhong, S.J., Paulson, A. and Wahr, J., 2003. Three-dimensional finite-element modelling of Earth's viscoelastic deformation: effects of lateral variations in lithospheric thickness. Geophysical Journal International, **155**(2): 679-695.

Zickfeld, K., Eby, M., Matthews, H. and Weaver, A., 2009. Setting cumulative emissions targets to reduce the risk of dangerous climate change. Proceedings of the National Academy of Sciences of the United States of America, **106**(38): 16129–16134.

Appendix 13.A: Methods of Sea Level Projections for the 21st Century

This appendix summarises the methods used to produce the projections shown in Section 13.5.1.1 for the RCP scenarios and scenario SRES A1B. Annual time series for change in global-mean surface air temperature and GMSL rise due to thermal expansion in the historical period and during the 21st century under RCP scenarios (Section 13.4.1) were obtained from a set of 21 CMIP5 AOGCMs. These were all those for which thermal expansion was available, including from a parallel pre-industrial control experiment, which is required to remove the effect on thermal expansion of climate model spin-up drift in deep-ocean temperatures. Where CMIP5 results were not available for a particular AOGCM and scenario, they were estimated by the method of Good et al. (2011) and Good et al. (submitted) using the response of that AOGCM to an instantaneous quadrupling of CO_2 concentration. The same method was used to estimate the CMIP5 projections for scenario SRES A1B. Uncertainties were derived from the CMIP5 ensemble by treating the model spread as a normal distribution, and following Section 12.4.1.2 it was assumed that the 5–95% interval of CMIP5 projections for each RCP scenario can be interpreted as a likely range with high confidence for the 21st century. As in the AR4, the temperature and expansion timeseries were chosen from their distributions in a perfectly correlated way, but all other uncertainties were assumed independent and combined by Monte Carlo. The global mean surface air temperature anomaly $T(t)$ as a function of time was calculated from CMIP5 results relative to the time-mean of 1986–2005 and used to estimate land ice contributions to GMSL rise, as follows.

Changes in glacier mass from 2006 onwards were projected using a parametrised scheme which was fitted to results from the global glacier models of Marzeion et al. (submitted), Radic et al. (submitted) and Slangen et al. (submitted), all of which have been used to make projections for RCP scenarios using output from several CMIP5 AOGCMs. The glacier contribution to GMSL rise is estimated in millimetres as $6.62\ I^{0.667}$, where $I(t)$ is the time-integral of T from 2006 to time t in °C year. The global glacier models on which this formula is based have different treatments of glacier SMB and the evolution of hypsometry, and their spread of results around the prediction of this formula has a coefficient of variation (standard deviation divided by mean) of 15%, which was taken to be the normally distributed methodological uncertainty in the glacier projection. Because the time-integration began in 2006, a constant 9.5 mm was added to the projections to account for the glacier contribution from 1996 (the centre of the reference period for projections) to 2005; this is the mean result from the model of Marzeion et al. (2011) using input from CMIP5 AOGCM historical experiments. The formula is not applicable beyond 2100 because it does not represent the tendency of global glacier mass to reach a new steady value when global climate stabilises, although the global glacier models on which it is based can predict this as a consequence of the evolution of hypsometry.

Changes in Greenland ice sheet SMB were computed from T using the cubic polynomial formula of Fettweis et al. (submitted), which predicts the Greenland SMB anomaly as a function of T, and was obtained by fitting results from an RCM using input from several CMIP5 AOGCMs. The projection of the formula was multiplied by 1.1 and a normally distributed methodological uncertainty of 40% (standard deviation divided by mean) was assumed, in order to obtain a spread which includes the projections of Greenland SMB by other methods assessed in Section 13.4.3.1, especially the range of results obtained for CMIP5 AOGCMs by the models of Gregory and Huybrechts (2006) and Yoshimori and Abe-Ouchi (2012).

Changes in Antarctic ice sheet SMB were assumed to be due to increase in accumulation, which was estimated using the results of Gregory and Huybrechts (2006) from CMIP3 AOGCMs. Accumulation was taken to increase at 5.1 ± 1.5% $°C^{-1}$ of warming in Antarctica, and the ratio of warming in Antarctic to T was taken to be 1.1 ± 0.2. Both of these uncertainties (standard deviations) were treated as normally distributed methodological uncertainties in the projections. The resulting spread of projections is very close to the spread of the results from the high-resolution Antarctic SMB models of Krinner et al. (2007), Bengtsson et al. (2011), and Ligtenberg et al. (submitted) assessed in Section 13.4.4.1.

The contributions from ice sheet dynamics at the start of the projections were taken to be half of the observed rate of loss for 2005–2010 from Greenland and all of that for Antarctica (Section 13.3.6). The contributions reach 0.016–0.074 m at 2100 from Greenland and 0.033–0.132 m from Antarctica; these are the likely ranges from our assessment of existing studies (Section 13.4.3.2 and 13.4.4.2). For each ice sheet, a quadratic function of time was fitted which begins at the minimal initial rate and reaches the minimum final amount, and another for the maxima. Time series for the dynamic contribution lying between these

extremes were constructed as combinations of the extreme time series using a random and uniform linear weight. The same method was followed for the anthropogenic land water storage contribution (initial rates from Section 13.3.6 and final amounts from Section 13.4.5). The projections of these contributions are the same for all scenarios, since insufficient information is available to assess scenario dependence.

Chapter 13: Sea Level Change

Coordinating Lead Authors: John A. Church (Australia), Peter U. Clark (USA)

Lead Authors: Anny Cazenave (France), Jonathan Gregory (UK), Svetlana Jevrejeva (UK), Anders Levermann (Germany), Mark Merrifield (USA), Glenn Milne (Canada), R. Steven Nerem (USA), Patrick Nunn (Australia), Antony Payne (UK), W. Tad Pfeffer (USA), Detlef Stammer (Germany), Alakkat Unnikrishnan (India)

Contributing Authors: David Bahr (USA), Jason E. Box (USA), David H. Bromwich (USA), Mark Carson (Germany), William Collins (UK), Xavier Fettweis (Belgium), Piers Forster (UK), Alex Gardner (USA), Peter Good (UK), Rune Grand Graversen (Sweden), Ralf Greve (Japan), Stephen Griffies (USA), Edward Hanna (UK), Mark Hemer (Australia), Regine Hock (USA), Simon J. Holgate (UK), John Hunter (Australia), Philippe Huybrechts (Belgium), Gregory Johnson (USA), Ian Joughin (USA), Georg Kaser (Austria), Caroline Katsman (Netherlands), Leonard Konikow (USA), Gerhard Krinner (France), Jan Lanaerts (Netherlands), Ben Marzeion (Austria), Kathleen L. McInnes (Australia), Sebastian Mernild (USA), Didier Monselesan (Australia), Ruth Mottram (Denmark), Tavi Murray (UK), Gunnar Myhre (Norway), J.P. Nicholas (USA), David Pollard (USA),Valentina Radić (Canada), Jamie Rae (UK), Christian Schoof (Canada), Aimée Slangen (Netherlands), Jan H. van Angelen (Netherlands), Willem Jan van de Berg (Netherlands), Michiel van den Broeke (Netherlands), Miren Vizcaíno (Netherlands), Yoshihide Wada (Netherlands), Jianjun Yin (USA), Masakazu Yoshimori (Japan)

Review Editors: Jean Jouzel (France), Roderik van de Wal (Netherlands), Philip L. Woodworth (UK), Cunde Xiao (China)

Date of Draft: 5 October 2012

Notes: TSU Compiled Version

Figures

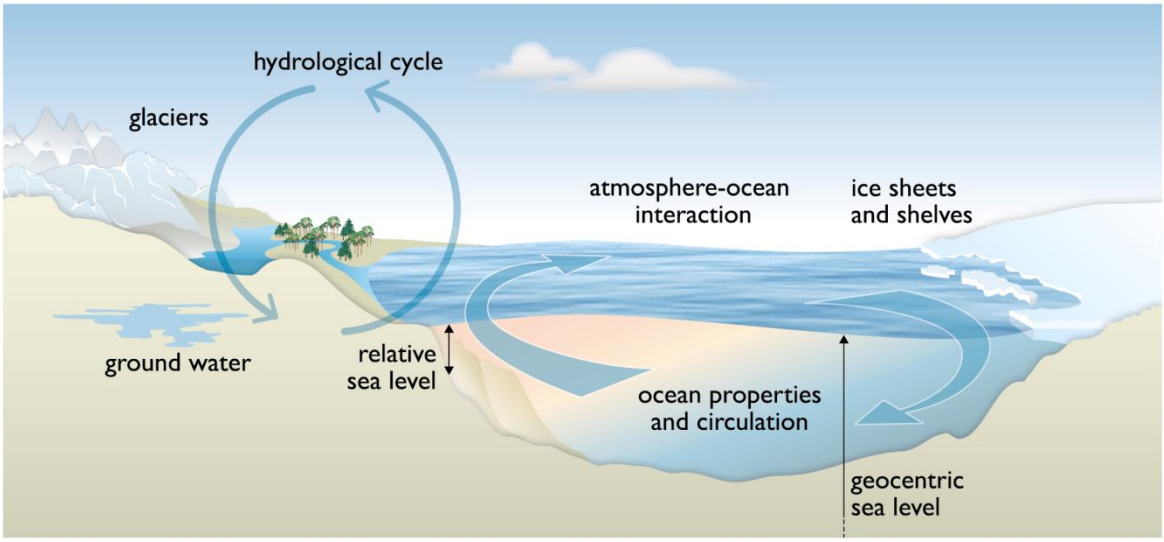

Figure 13.1: Climate sensitive processes and components that can influence sea level and are considered in this chapter. Changes in any one of the components or processes shown will result in a sea level change. The term 'ocean properties' refers to ocean temperature, salinity and density, which influence and are dependent on ocean circulation.

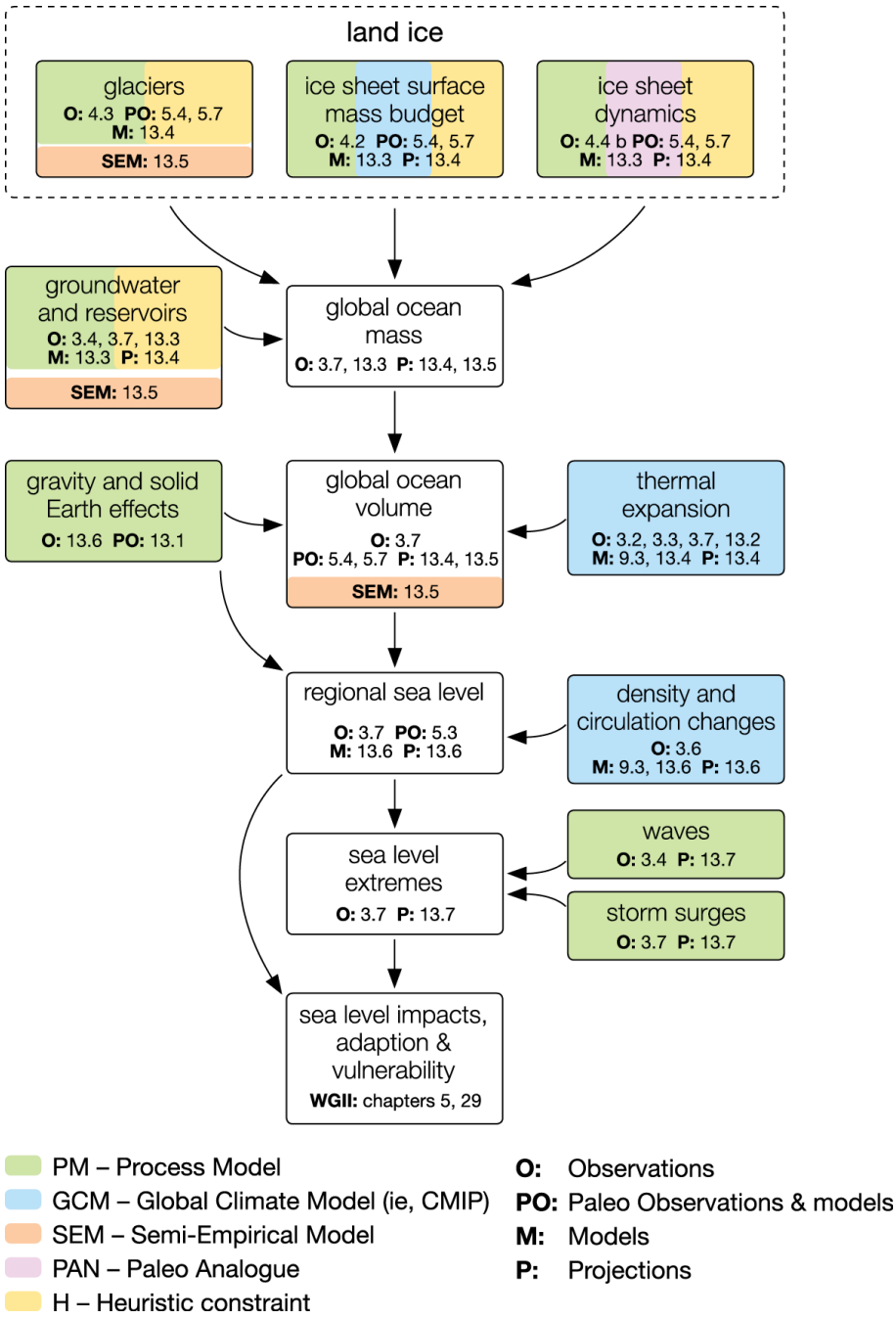

Figure 13.2: Schematic representation of key processes and components that contribute to sea level change and are considered in this report. Colouring of individual boxes indicates the types of models and approaches used in projecting the contribution of each process or component to future sea level change. The diagram also serves as an index to the sections in this report that are relevant to the assessment of sea level projections via the section numbers given at the bottom of each box. Note gravity and solid Earth effects change the shape of the ocean floor hence global mean sea level.

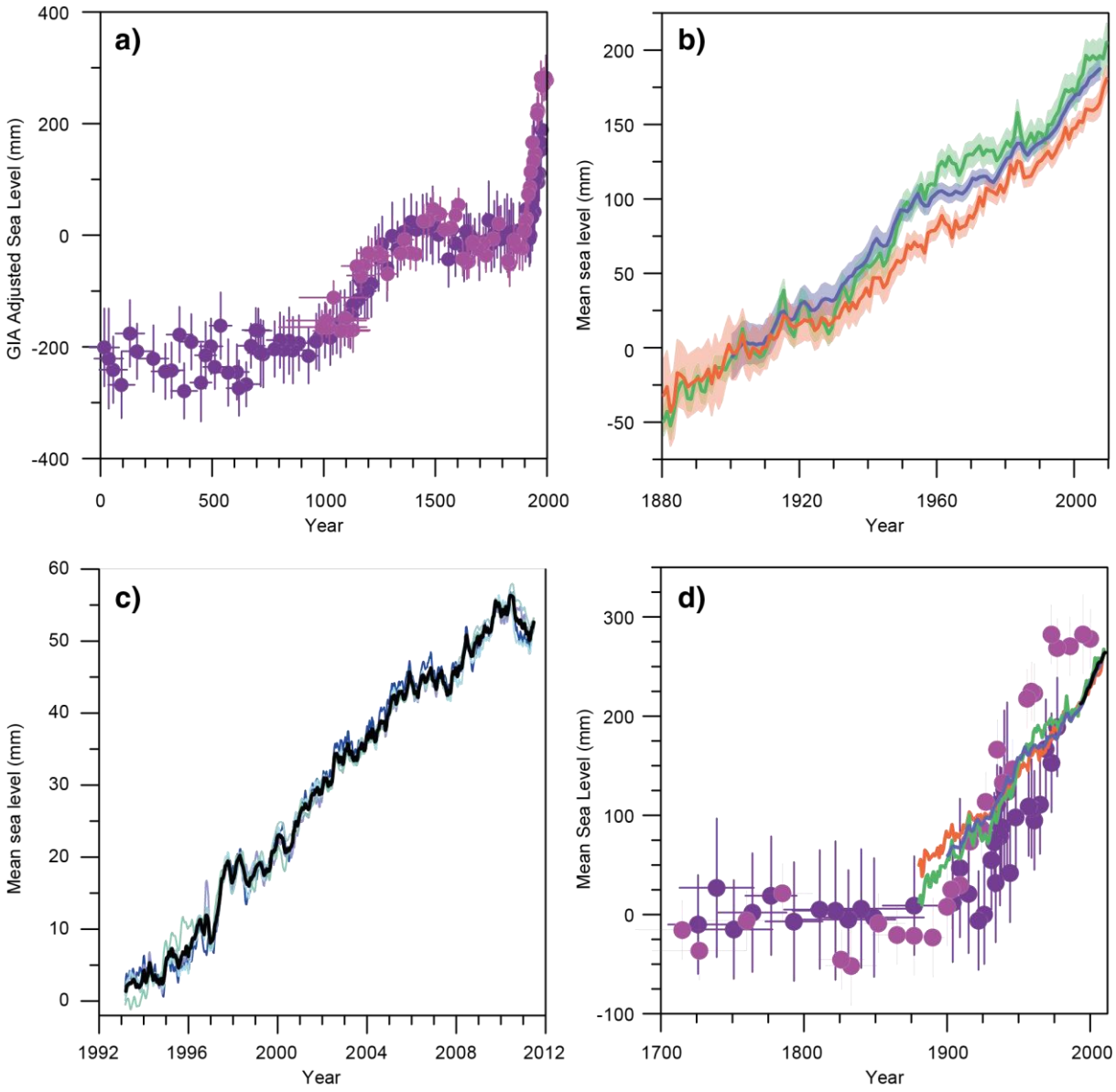

Figure 13.3: (a) Paleo sea level data from salt-marsh reconstructions from two sites in North Carolina (purple symbols is Sand Point, magenta symbols is Tump Point), with corrections for long-term subsidence attributed to glacial isostatic adjusment (Kemp et al., 2011). Values are relative to a preindustrial average for AD 1400–1800. **(b)** Tide gauge reconstructions from Ray and Douglas (2011) (twilight blue), Church and White (2011) (autumn orange), and Jevrejeva et al. (submitted) (light green line), relative to the mean for 1900–1905. Uncertainties are one standard deviation as reported by the authors. **(c)** Altimetry data sets from five groups (CU, NOAA, GSFC, AVISO, CSIRO) with mean of the five shown as black line. **(d)** Comparison of the paleo, tide gauge, and altimetry data sets (same symbol and line colors as in panels a-c. All tide gauge time series have been centered so that their individual mean is zero over their common period (1900–2007). The altimeter time series has been shifted so that is mean value over the 1993–2007 period is equal to the mean value of the average of all three tide gauge time series over the same period. The tide gauge and altimeter time series were then shifted vertically up by 150 mm in order to align with the paleo data.

a)

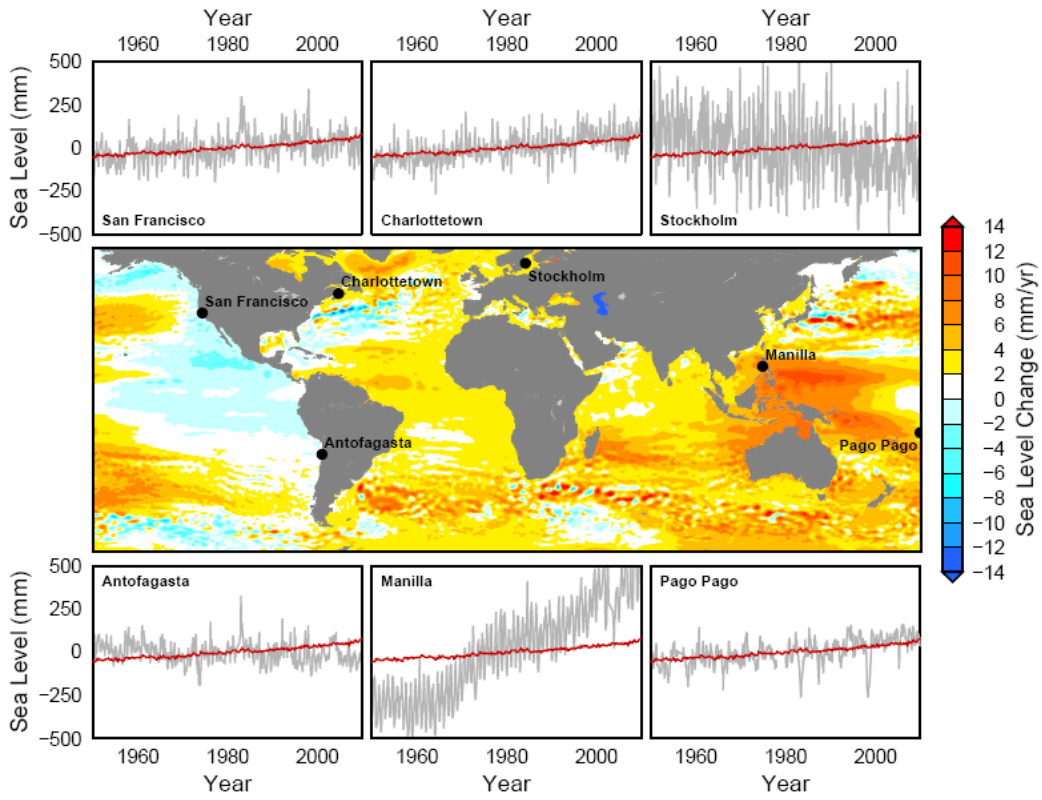

b)

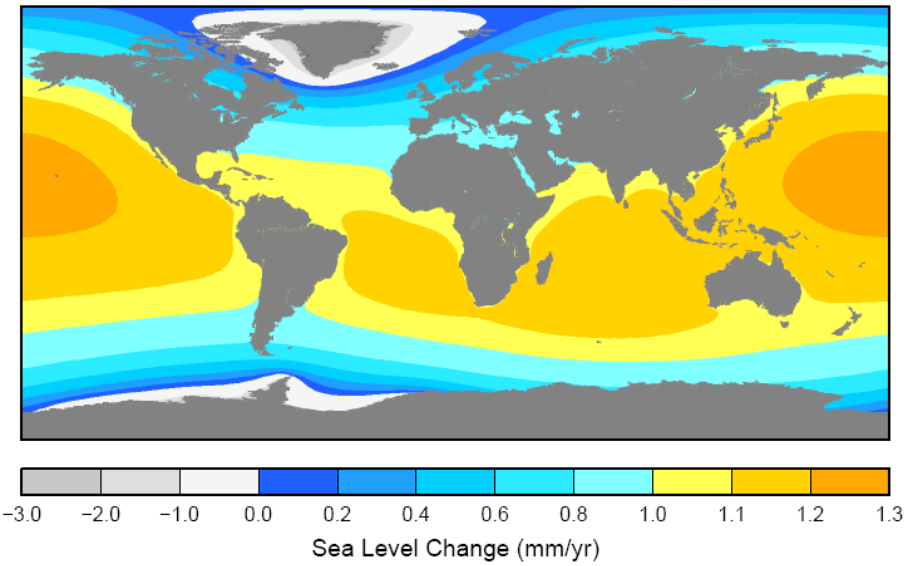

FAQ13.1, Figure 1: (a) Mean rates of change in sea surface height (geocentric sea level) for the period 1993–2010 from satellite altimetry. Also shown are relative sea level changes (grey lines) from selected tide gauge stations for the period 1950–2010. For comparison, an estimate of global mean sea level change is also shown (red lines) with each tide gauge time series. (b) Model output, showing relative sea level change due to melting of the Greenland ice sheet and the West Antarctic ice sheet at rates of 0.5 mm yr^{-1} each (giving a global mean value of 1 mm yr^{-1}).

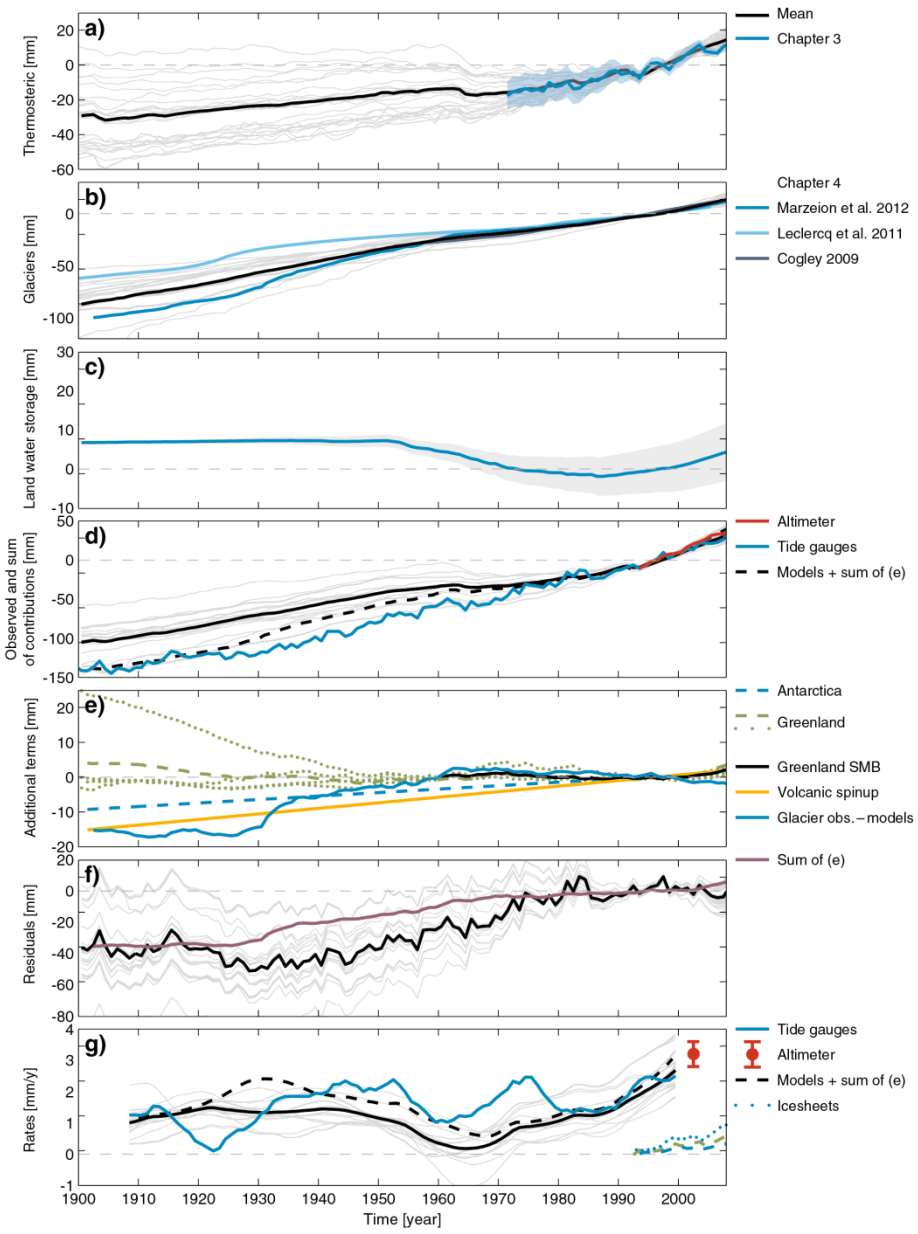

Figure 13.4: Modeled and observed global-mean sea level contributions and total sea level from 1900 to 2008. All curves have an arbitrary offset and are set to zero in the time-mean of 1986–2005 (the reference period for the projections). The grey lines are derived from individual AOGCM simulations and the black line from the average of the AOGCM-based results. **(a)** Thermal expansion, with the observations since 1971 in blue and the 5–95% uncertainty shaded. **(b)** Glacier melting, with the observations of Marzeion et al. (submitted), Leclercq et al. (2011) and Cogley (2009). **(c)** Estimated changes in land water storage due to human intervention. **(d)** Observed sea level (blue - tide gauges; red - altimeter) and modeled sea level (black, the sum of terms in a to c, and black dashed also including the terms in e). **(e)** Additional terms: modeled Greenland SMB changes since 1900 (dashed green, the average of four individual estimates in dotted green, and for comparison the modeled Greenland SMB changes from the results shown in Figure 13.5 in black), a possible long term Antarctic ice sheet contribution (dashed blue), the possible underestimate of thermal expansion due to AOGCM preindustrial simulations not including volcanic forcing (orange), and the possible greater mass loss by glaciers in high northern latitudes prior to 1950. The two ice sheet series are joined to the observed changes in Greenland and Antarctica (from Chapter 4) in 1992. **(f)** The residual (black, observed GMSL rise – modelled expansion – modelled glaciers – land water, the difference between blue and black in d), and the sum of the additional terms (purple, from e). **(g)** Trends in sea level calculated over 18 year periods (the length of the altimeter record), from tide-gauges (blue; Church and White, 2011), altimetry (red dot), and models (black and dashed black, as in d); also the observed rates of the contributions from the Greenland (green dashed) and Antarctic (blue dashed) ice sheets and their sum (blue dots) since 1992.

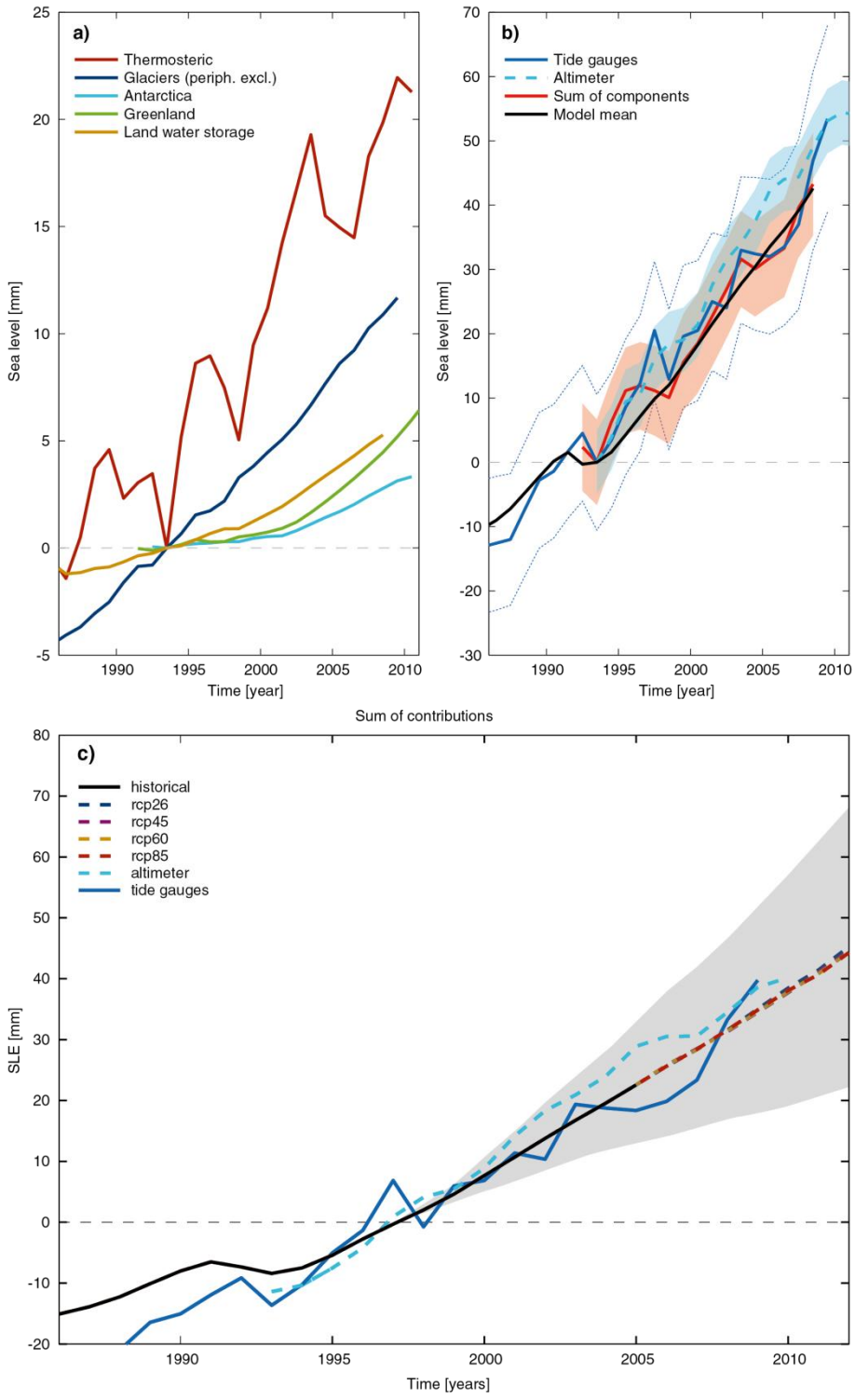

Figure 13.5: Observed global-mean sea level contributions and observed and projected total sea level from 1993 to 2010. **(a)** Observed contributions to GMSL from 1993 (ocean thermal expansion, red, Chapter 3; Glaciers, dark blue and Ice Sheets, light blue and green, Chapter 4; Land water storage, brown, Section 13.4). **(b)** Observed GMSL from satellites (light blue dashed) and estimated from tide gauges (dark blue solid) and the sum of contributions from (a, red). The shading indicates 5–95% confidence limits. The mean sea level from modeled thermal expansion, modeled glaciers and land water storage from Figure 13.4 is shown in black. **(c)** The projected sea level rise (Section 13.5) relative to the 1986–2005 average (black and coloured lines for the four scenarios, with shading indicating the likely range). Also shown is the observed sea level from (b), set to have the same value as the projections over 1993 to 2001.

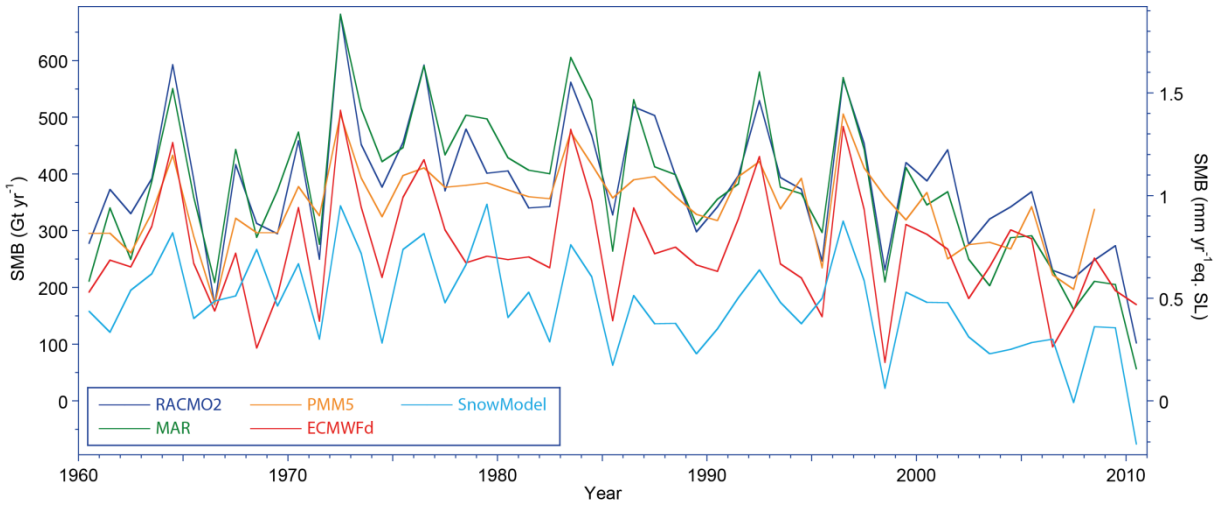

Figure 13.6: Annual-mean surface mass balance (accumulation minus ablation) for the Greenland Ice Sheet, simulated by regional climate models for the period 1960–2010.

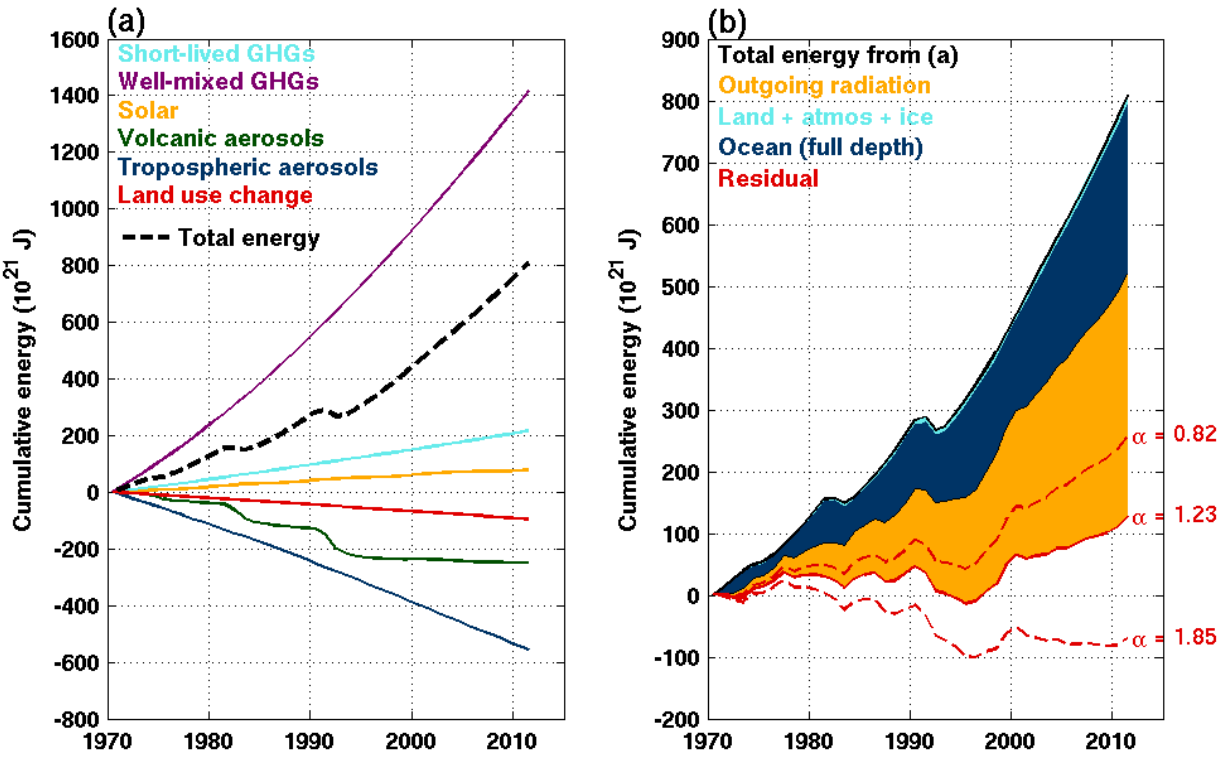

Box 13.1, Figure 1: The Earth's energy budget from 1970 through 2010. **(a)** The cumulative energy flux into the Earth system from changes in solar forcing, well-mixed and short-lived greenhouse gases, changes in surface albedo, volcanic forcing and tropospheric aerosol forcing are shown by the coloured lines and these are added to give the total energy changes (dashed black line). **(b)** The cumulative total energy change from (a), with an expanded scale, is balanced by the warming of the Earth system (energy absorbed in the melting of ice and warming the atmosphere, the land and the ocean) and an increase in outgoing radiation inferred from temperature change of a warming Earth. These terms are represented by the time-varying thicknesses of the coloured regions. The residuals in the cumulative energy budget are indicated by the difference between the red lines and the horizontal zero line. The full-drawn line is for a climate feedback parameter α of 1.23 W m^{-2} $^{o}C^{-1}$, equivalent to a radiative forcing for a doubled CO_2 concentration of 3.7 W m^{-2} (Forster et al., Chapter 2, AR4) combined with an equilibrium climate sensitivity of 3.0°C (assessed in Box 12.1 to be the most likely value). Following Box 12.1, the climate feedback parameter α is likely to be in the range from 0.82 W m^{-2} $^{o}C^{-1}$ (corresponding to an equilibrium climate sensitivity of 4.5ºC) to 1.85 W m^{-2} $^{o}C^{-1}$ (corresponding to an equilibrium climate sensitivity of 2.0 ºC).

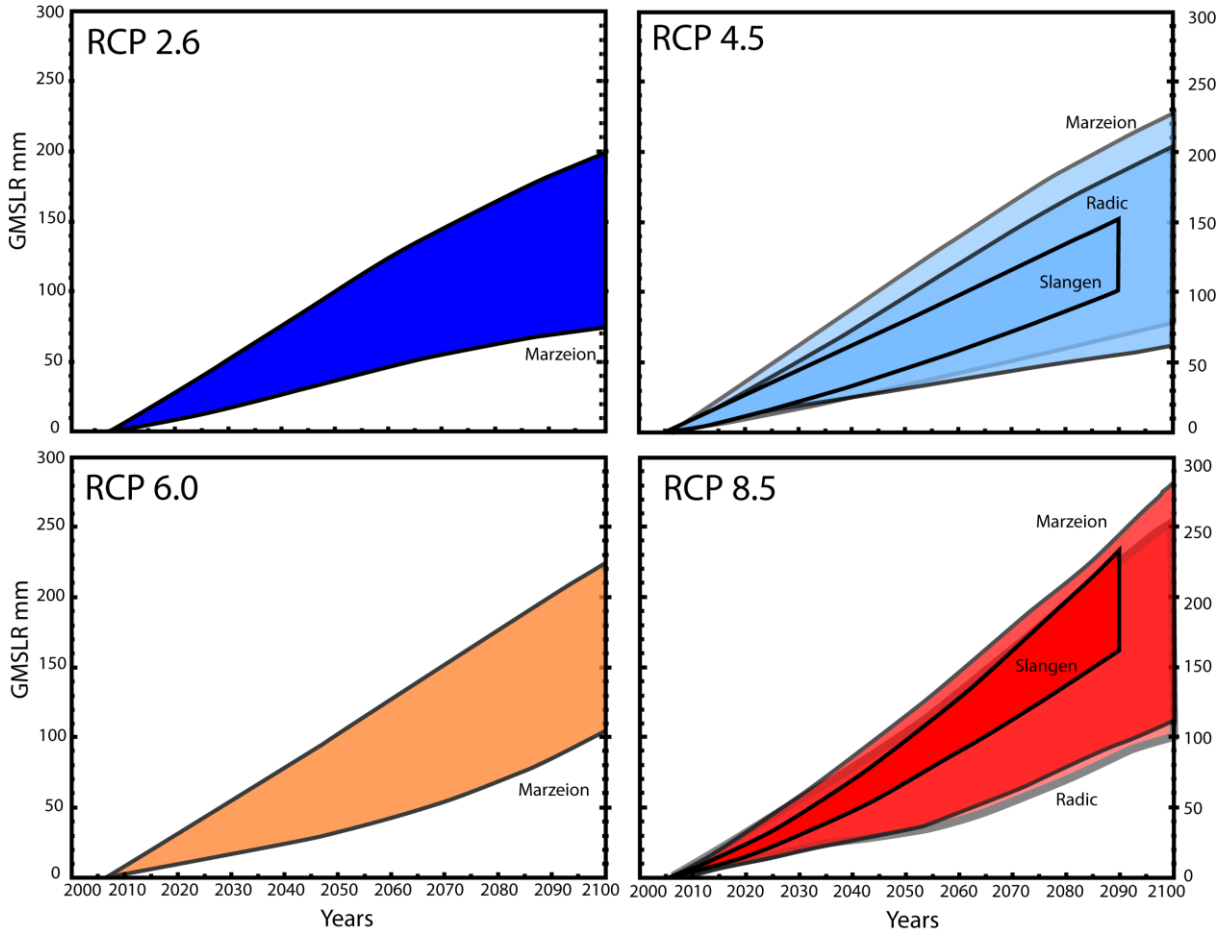

Figure 13.7: Modeled glacier contributions to sea level from glaciers (including peripheral glaciers surrounding the Greenland and Antarctic ice sheets), from models of Marzeion et al. (submitted), Radic et al. (submitted), and Slangen et al. (submitted).

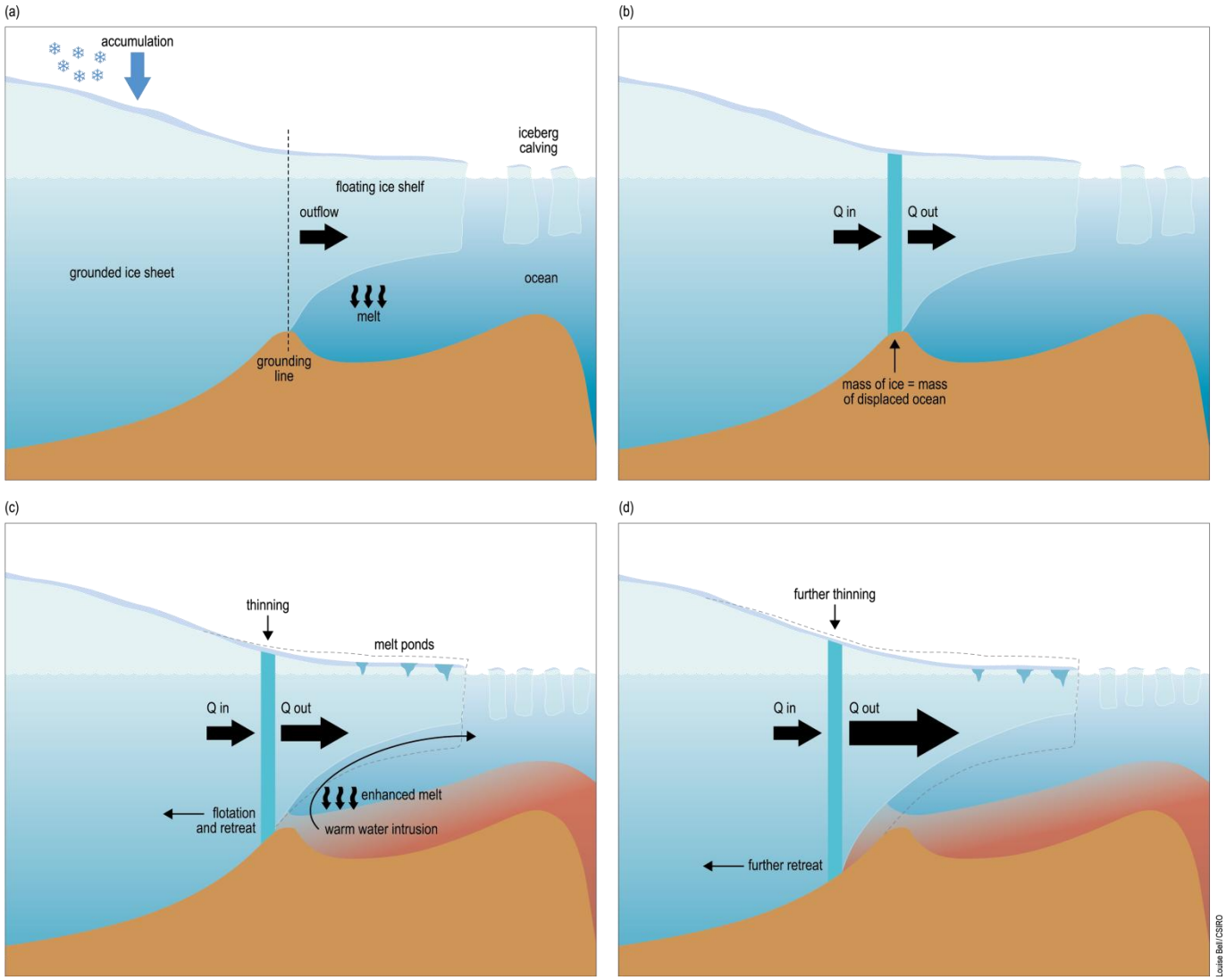

Box 13.2, Figure 1: Schematic of the processes leading to the potentially unstable retreat of a grounding line.

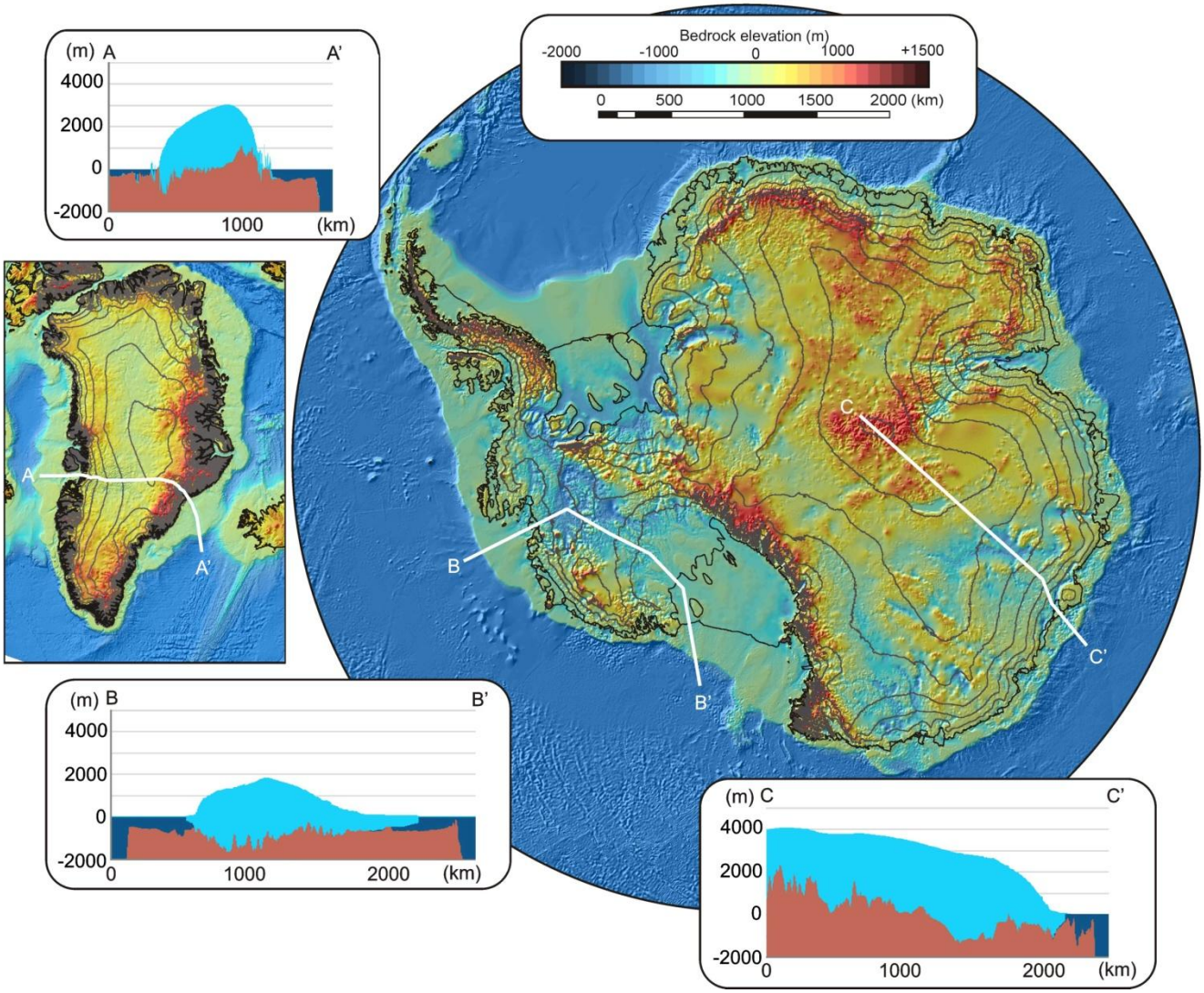

FAQ 13.2, Figure 1: Bedrock topography of the Greenland and Antarctic ice sheets shown with 500-metre contours of ice surface elevation. Transects through the ice sheets emphasize the marine nature of West Antarctica and some of East Antarctica.

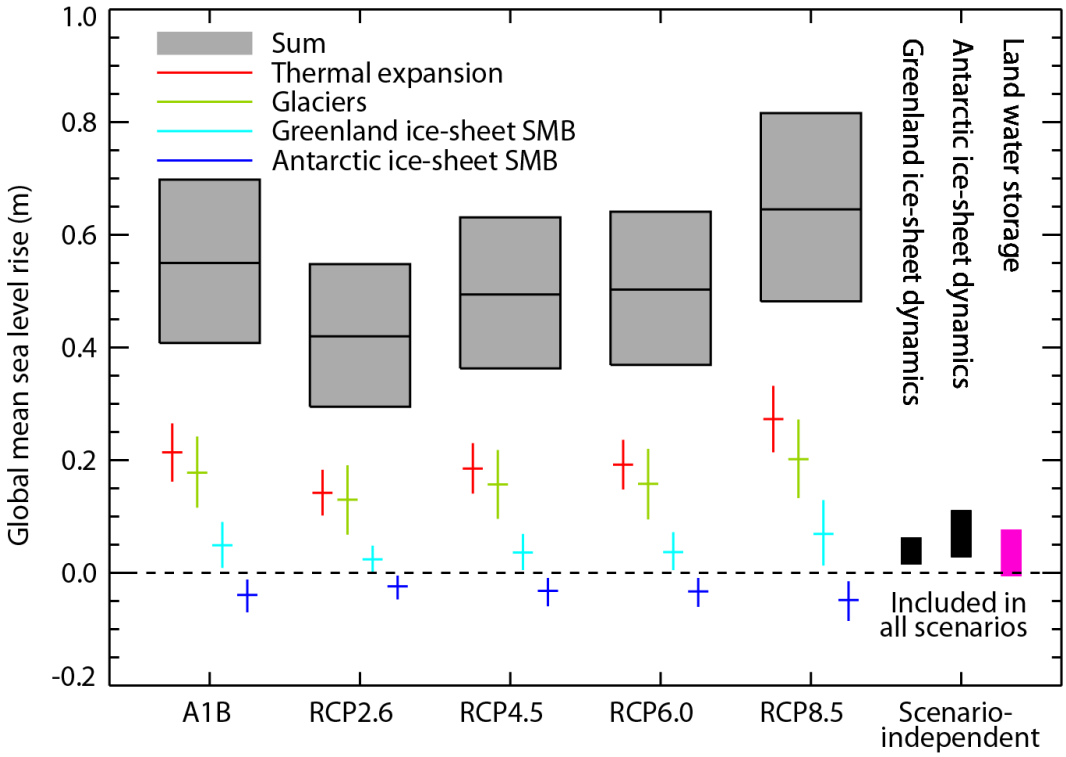

Figure 13.8: Projections from process-based models with likely ranges and median values for global-mean sea level rise and its contributions in 2081–2100 relative to 1986–2005 for the four RCP scenarios and scenario SRES A1B used in the AR4. Contributions from ice sheet dynamical change and anthropogenic land water storage are included in the sum; they are independent of scenario, and are treated as having uniform probability distributions. See discussion in Sections 13.6.1.1 and 13.6.1.3 and Appendix 13.A for methods.

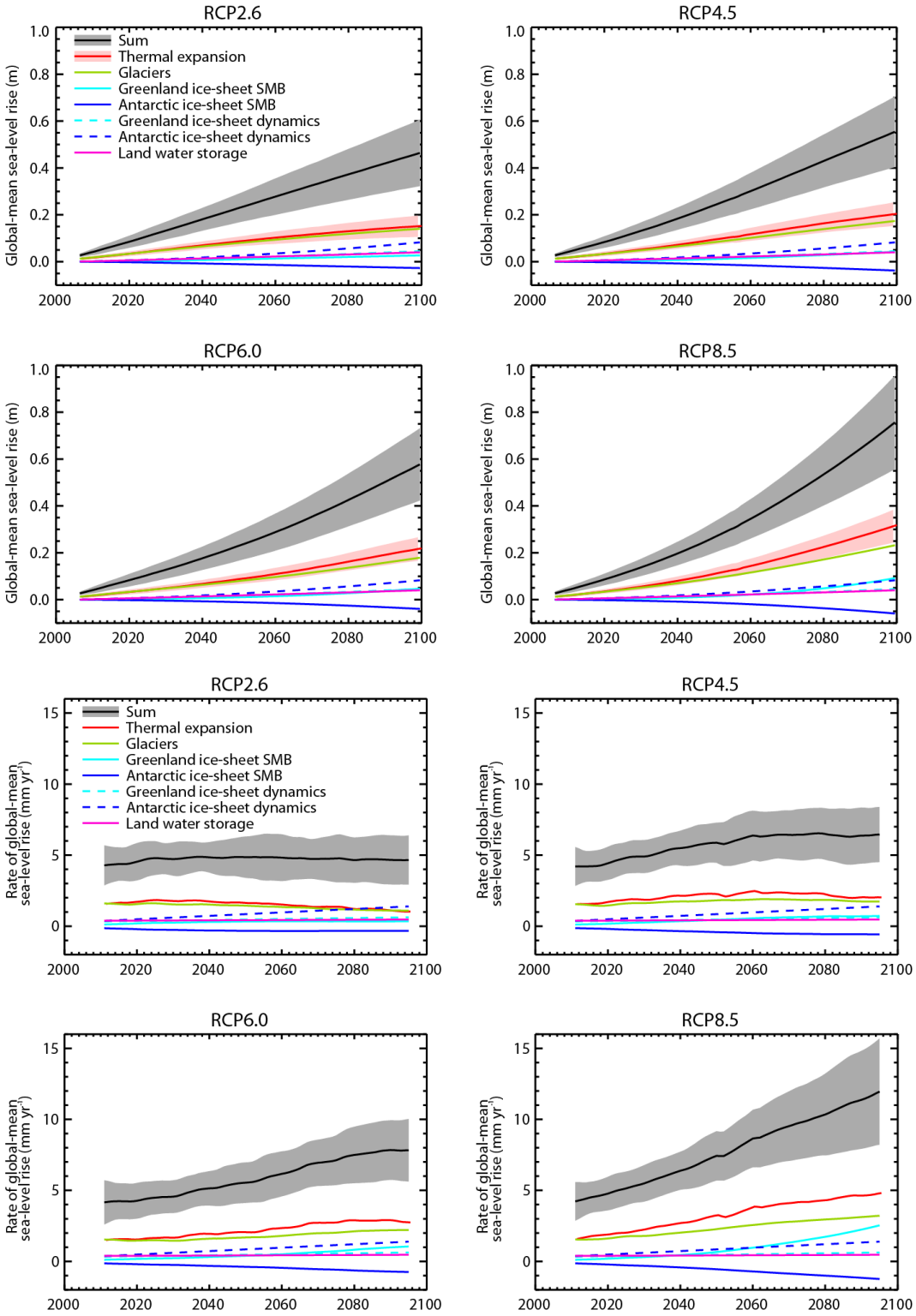

Figure 13.9: Projections from process-based models of **(a)** GMSL rise relative to 1986–2005 and **(b)** the rate of GMSL rise as a function of time for the four RCP scenarios and scenario SRES A1B. The solid lines show the median and the dashed lines show the likely range for each scenario.

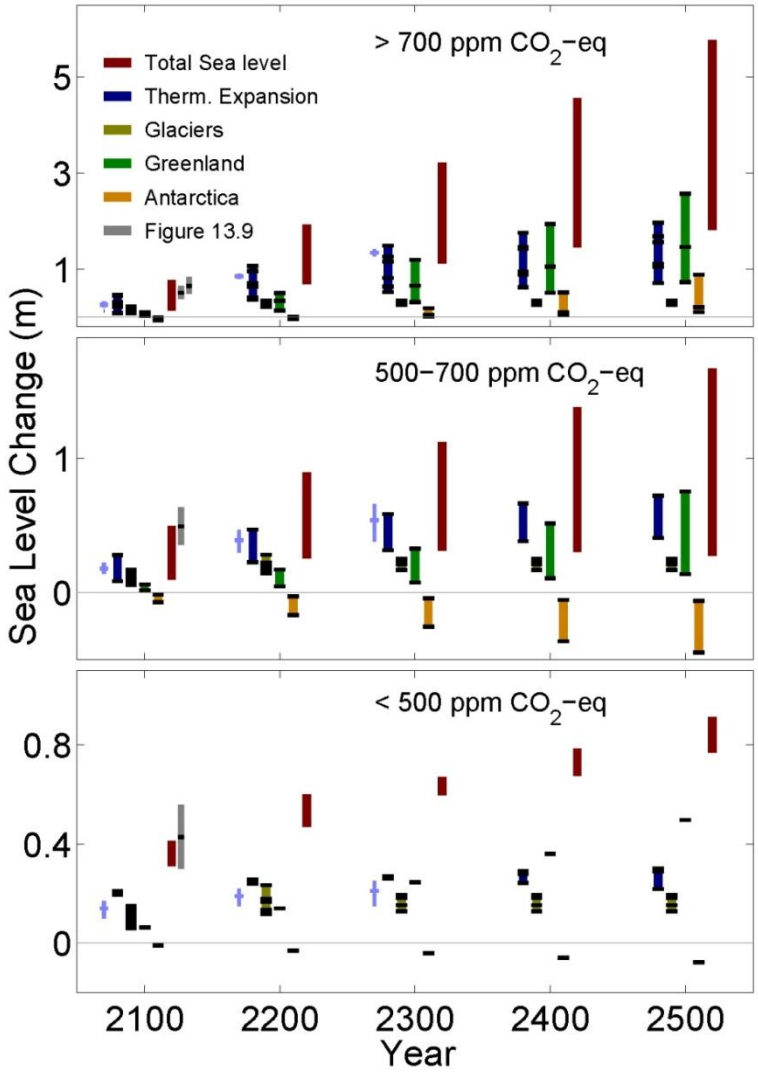

Figure 13.10: Sea level projections beyond the year 2100 are grouped into three categories according to the concentration of GHG concentration (in CO_2-equivalent) in the year 2100 (upper panel: >700 ppm; middle panel: 500–700 ppm; lower panel: <500 ppm). Colored bars show the full model spread. Horizontal lines provide the specific model simulations. The range provided for the total sea level change represents the maximum possible spread that can be obtained from the four different contributions. Grey shaded bars exhibit the likely range for the 21st century projection from Figure 13.9 with the median as the horizontal line. [PLACEHOLDER FOR FINAL DRAFT: Possible slight update from revised papers.]

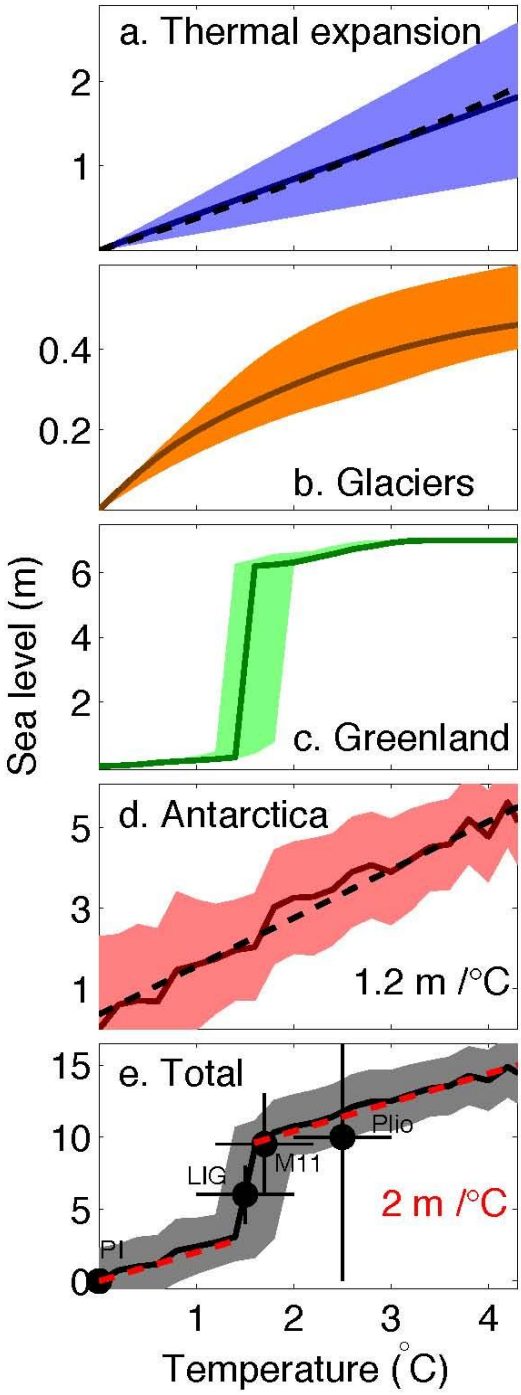

Figure 13.11: Sea level commitment per degree of warming as obtained from physical model simulations of **(a)** ocean warming, **(b)** mountain glaciers and ice caps, **(c)** the Greenland and **(d)** the Antarctic ice sheet. **(e)** The corresponding total sea level commitment, which is consistent with paleo-estimates from past warm periods (PI = pre-industrial, LIG = last interglacial period, M11 = Marine Isotope Stage 11, Plio = Mid-Pliocene). Temperatures are relative to pre-industrial. Dashed lines provide linear approximations: (a) sea level rise for a homogeneous increase in temperature; (d) & (e) constant slopes of 1.2 and 2 m $^{o}C^{-1}$. Shading as well as the vertical line represents the uncertainty range as discussed in Levermann et al.(submitted).

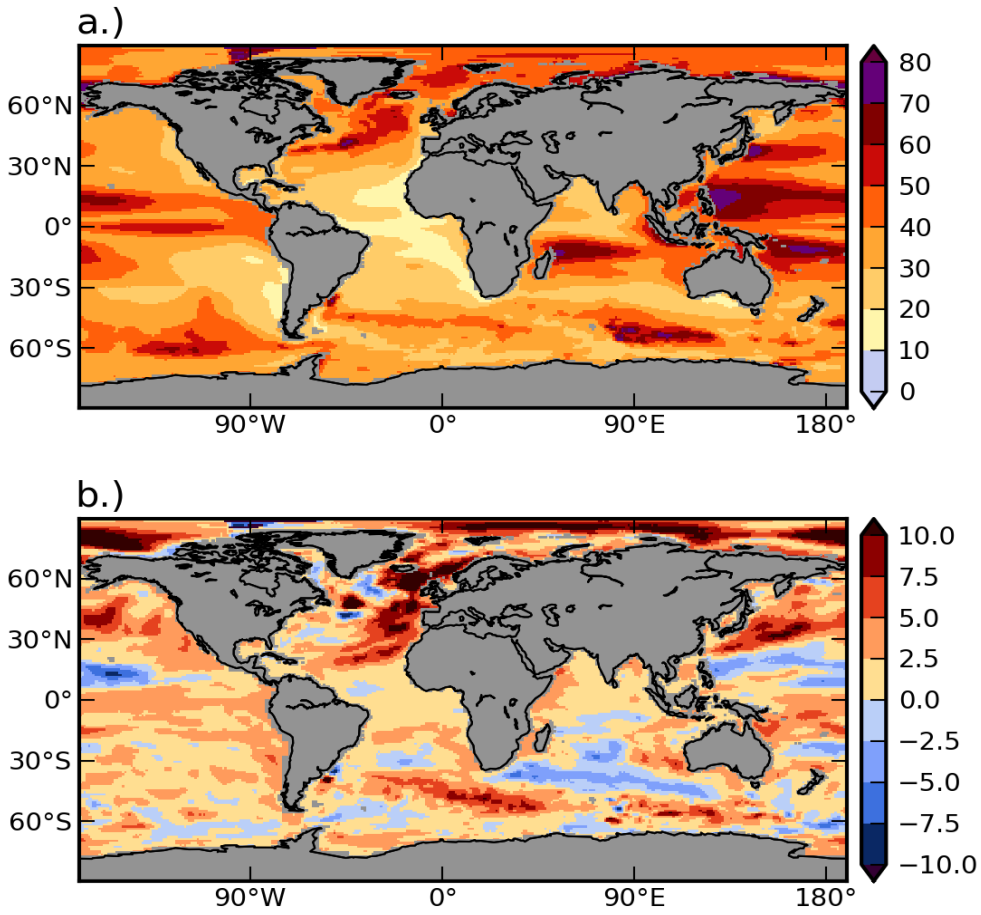

Figure 13.12: (a) RMS Interannual dynamic sea level variability (m) in the CMIP5 multi-model ensemble (12 models total), built from the historically forced experiments during the period 1951–2005; **(b)** Changes in the ensemble average interannual dynamic sea level variability (std. dev.; in m) evaluated over the period 2081–2100 relative to period 1986–2005. The projection data (2081–2100) is from the CMIP5 RCP4.5 experiment.

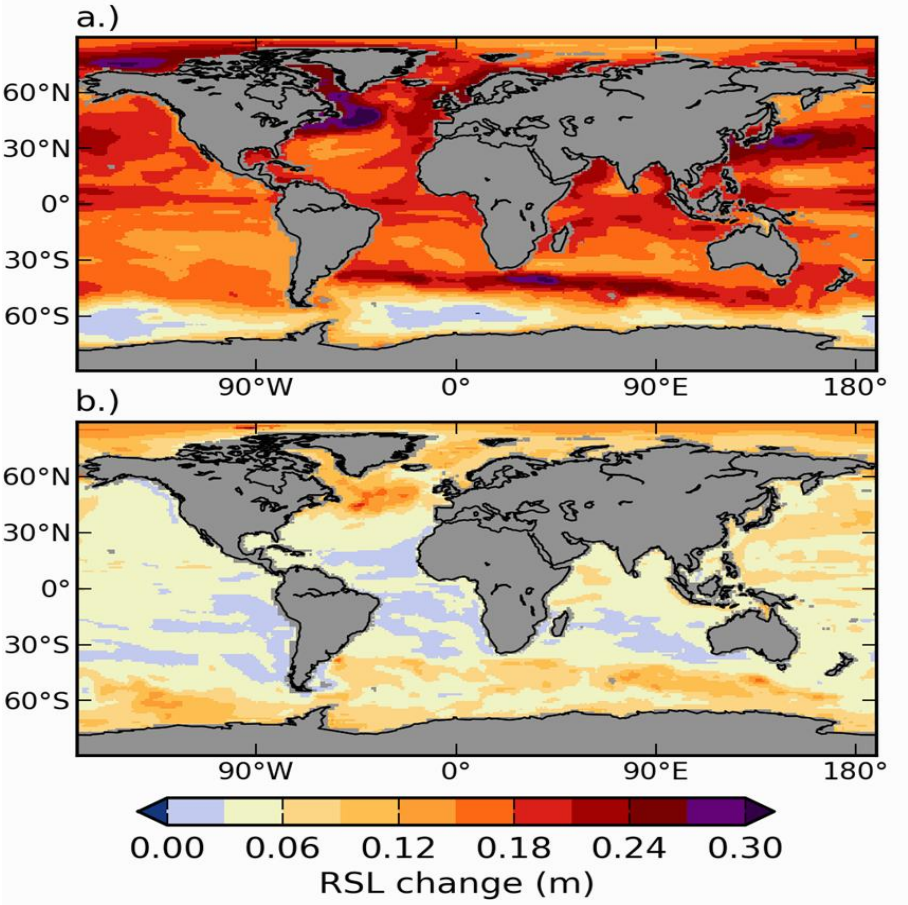

Figure 13.13: (a) Ensemble mean projection of the time-averaged steric sea level changes for the period 2081–2100 relative to period 1986–2005, computed from 12 CMIP5 climate models (in m), using the RCP4.5 scenario. The figure includes the globally averaged steric sea level increase of 0.17 ± 0.05 m. **(b)** RMS spread (deviation) of the individual model result around the ensemble mean (m).

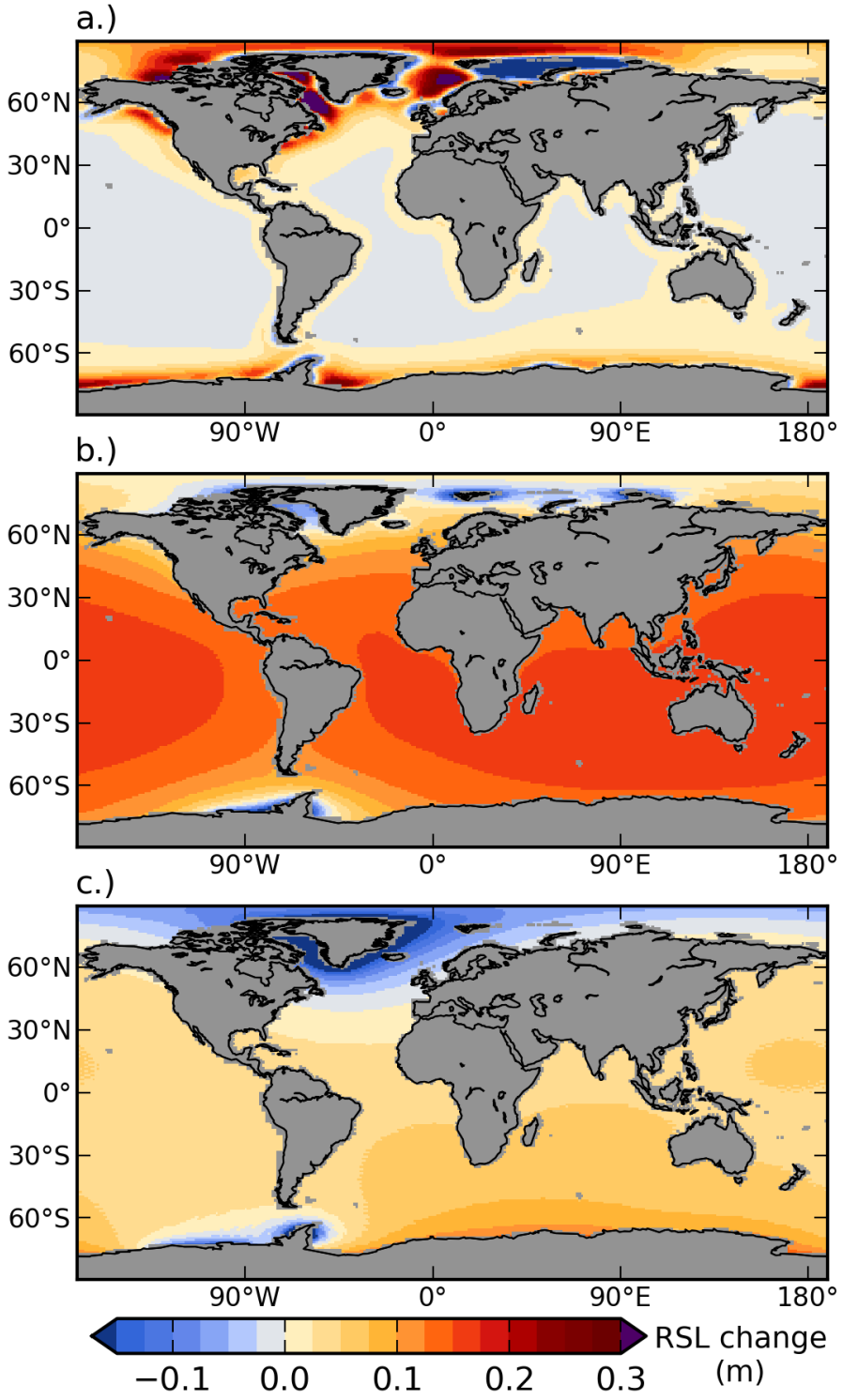

Figure 13.14: Ensemble mean regional sea level contributions to sea level change (m) from GIA (upper panel), glaciers (middle panel) and ice sheets (lower panel). The lower two panels are based on information from scenario RCP4.5 and all panels represent changes between the periods 1986–2000 and 2081–2100 (from Slangen et al., submitted).

a)

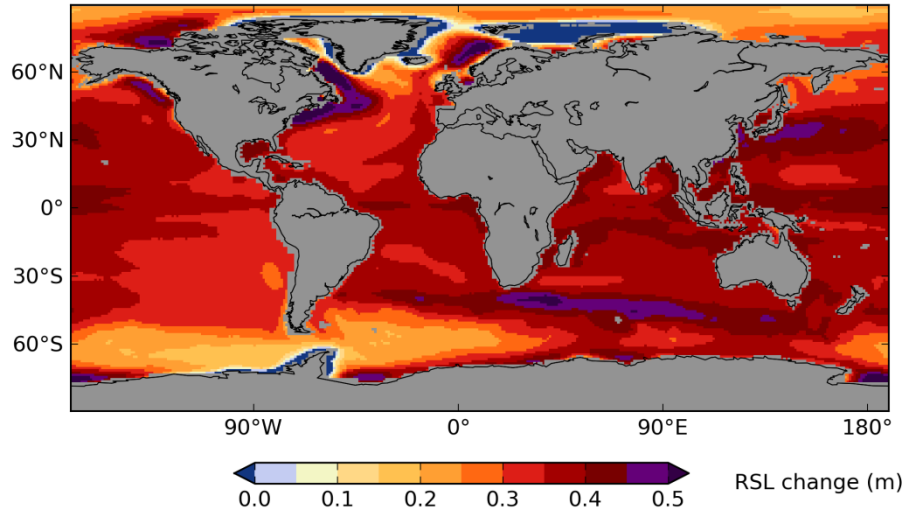

b)

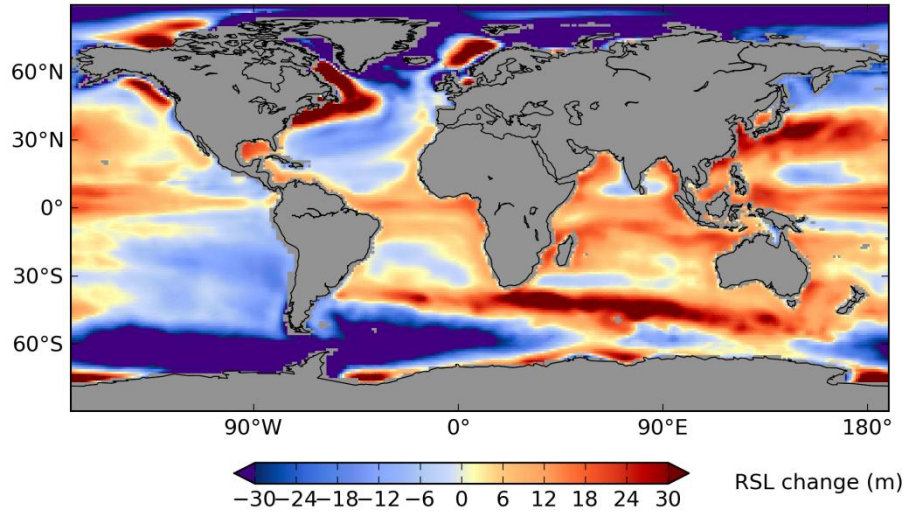

Figure 13.15: (a) Ensemble mean regional sea level change (m) evaluated from 12 models of the CMIP5 scenario RCP4.5 between 1986–2005 and 2081–2100 (Slangen et al., submitted). Global mean = 0.35 ± 0.06 m; range = –0.68 to +0.73 m. **(b)** Percentage of the deviation of the ensemble mean regional sea level change between 1986–2005 and 2081–2100 from the global mean value.

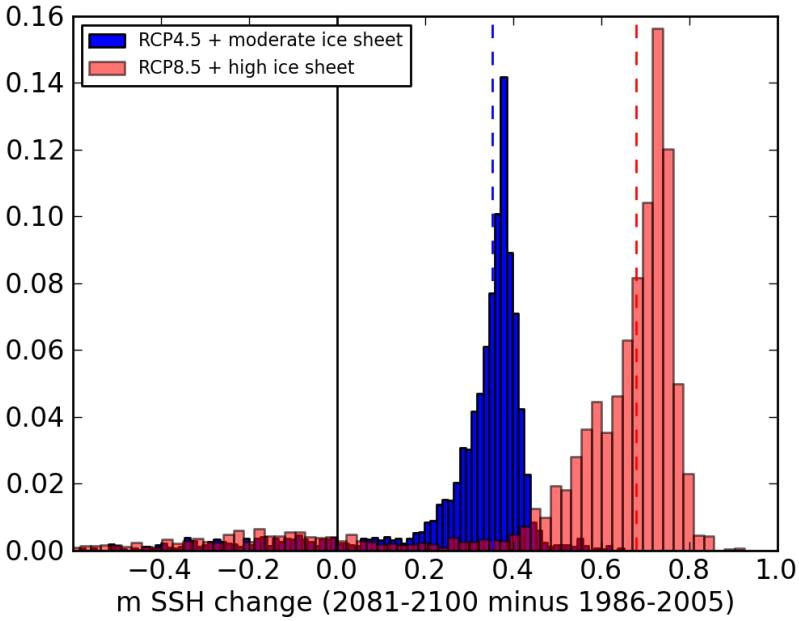

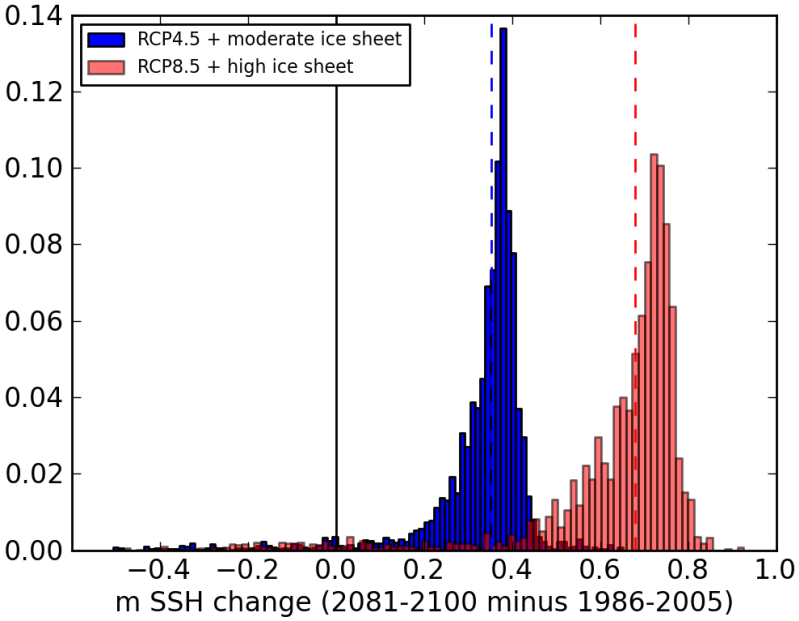

Figure 13.16: (top) PDF of the deviation of the ensemble mean regional sea level change along all coastlines between 1986–2005 and 2081–2100 from the global mean value. Shown are results for RCP4.5 (blue) and ROC8.5 (pink), respectively. (bottom) Same as in the top panel, but excluding Antarctic and Greenland coastlines.

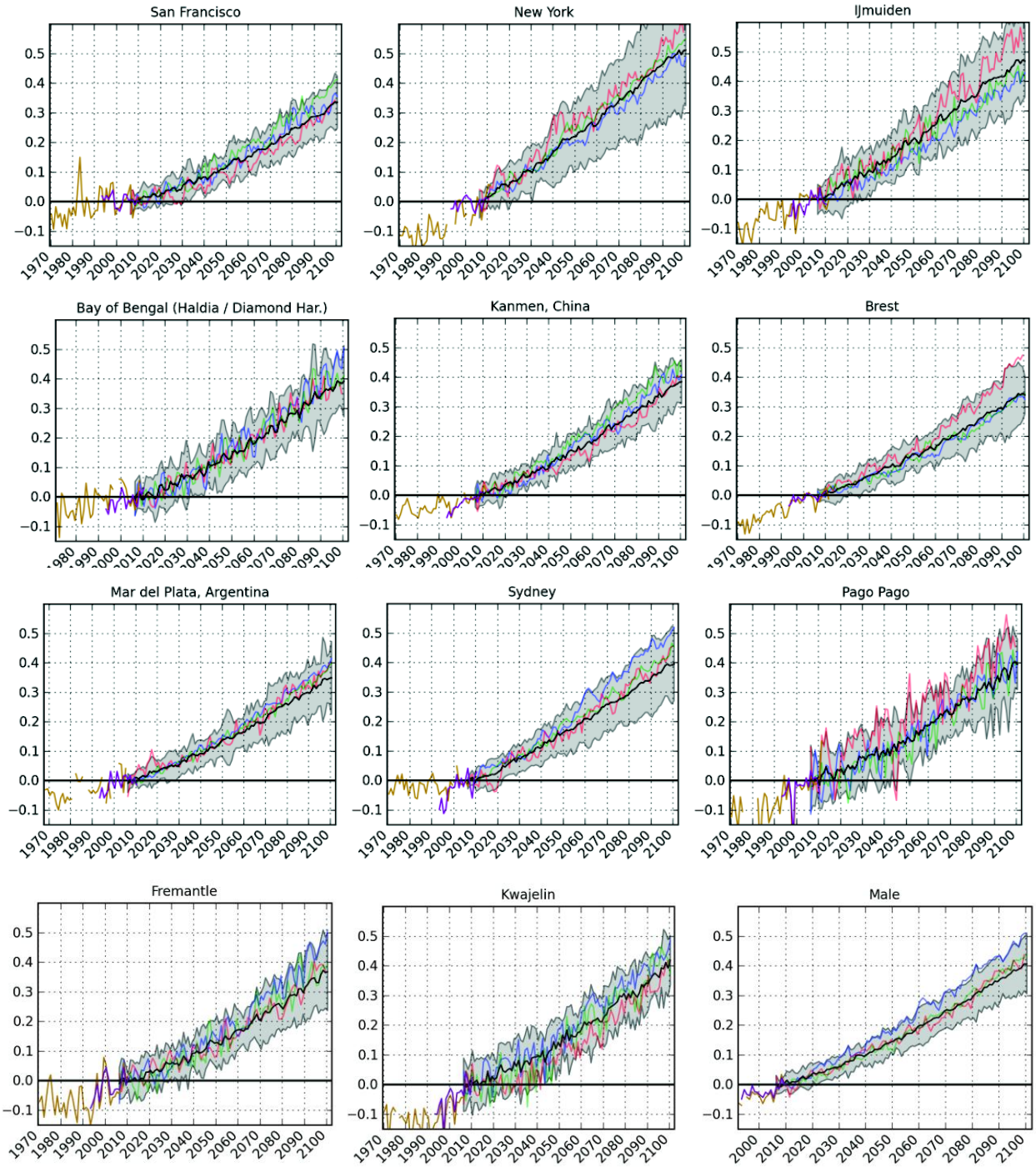

Figure 13.17: Observed and projected relative sea level change near nine representative stations. The observed *in situ* relative sea level records from tide gauges (since the late 1970s) are plotted in yellow, and the satellite record (since 1993) is provided as purple lines. The projected range from 12 CMPI5 RCP4.5 scenario runs (5–95% uncertainty range) are shown by the shaded region for the period 2000–2100, with the bold line showing the ensemble mean. Colored lines represent individual climate model realizations drawn from three different climate models.

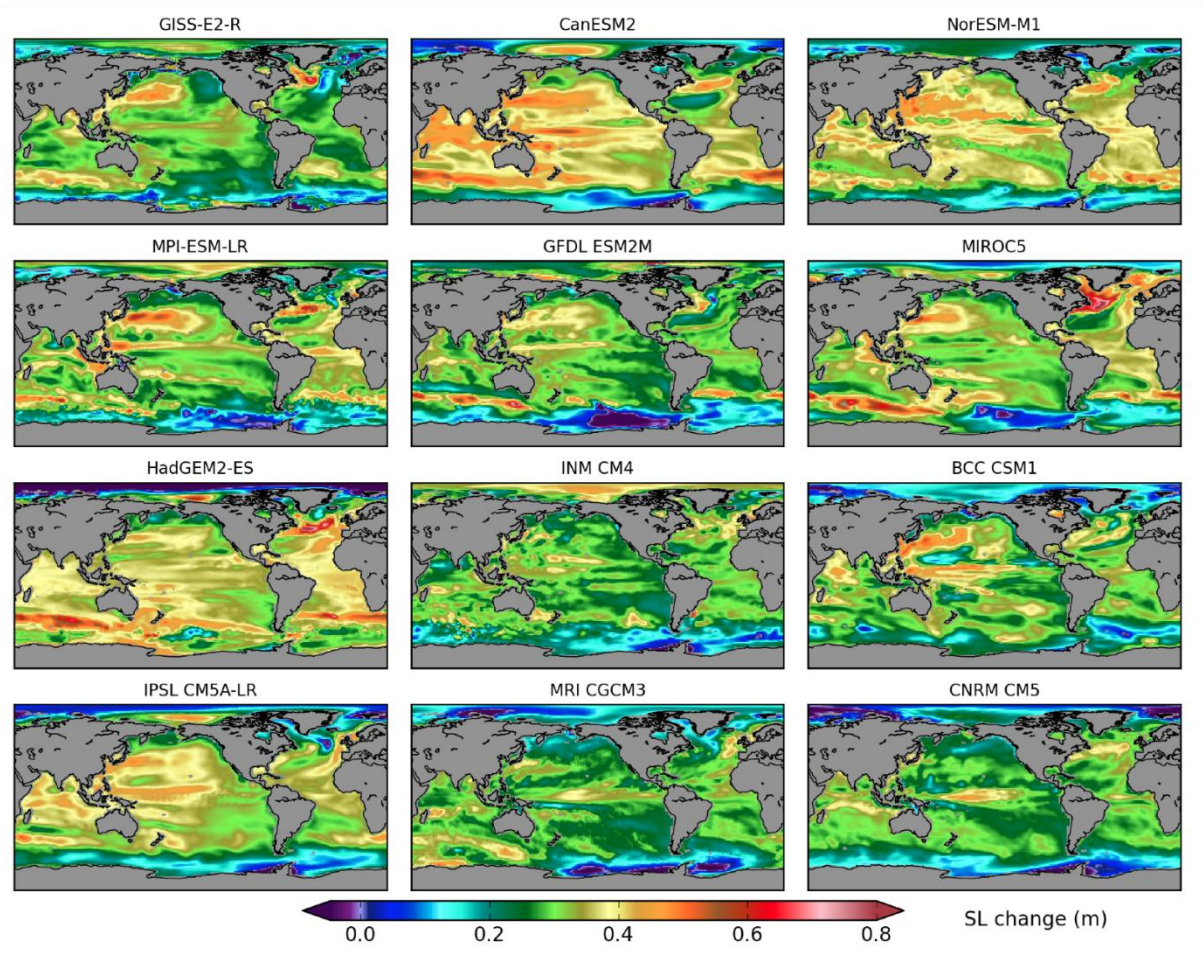

Figure 13.18: Projected relative sea level change patterns (m) from the combined global steric plus dynamic topography and glacier contributions for RCP4.5 over the period from 1986–2005 to 2081–2100 for each individual climate model used in the production of Figure 13.15a.

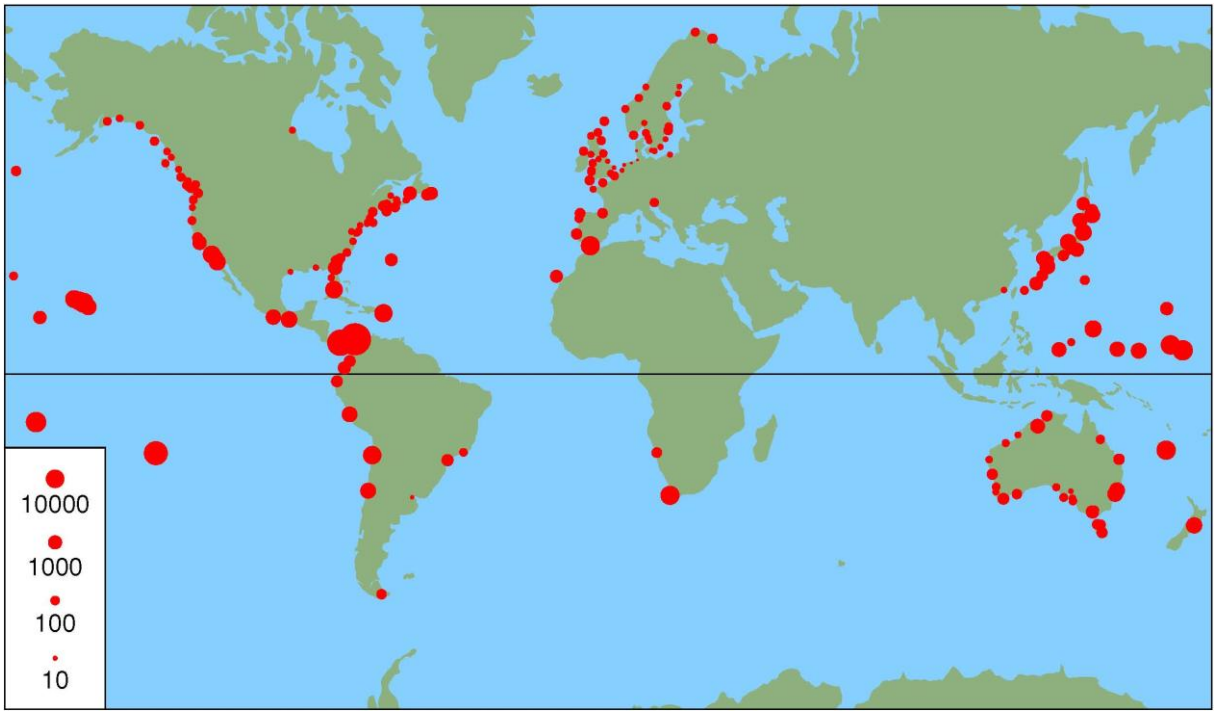

Figure 13.19: The estimated factor (shown in red circles) at 198 tide gauge stations over the globe by which the frequency of flooding events of a given height increase for a mean sea level rise of 0.5 metre.

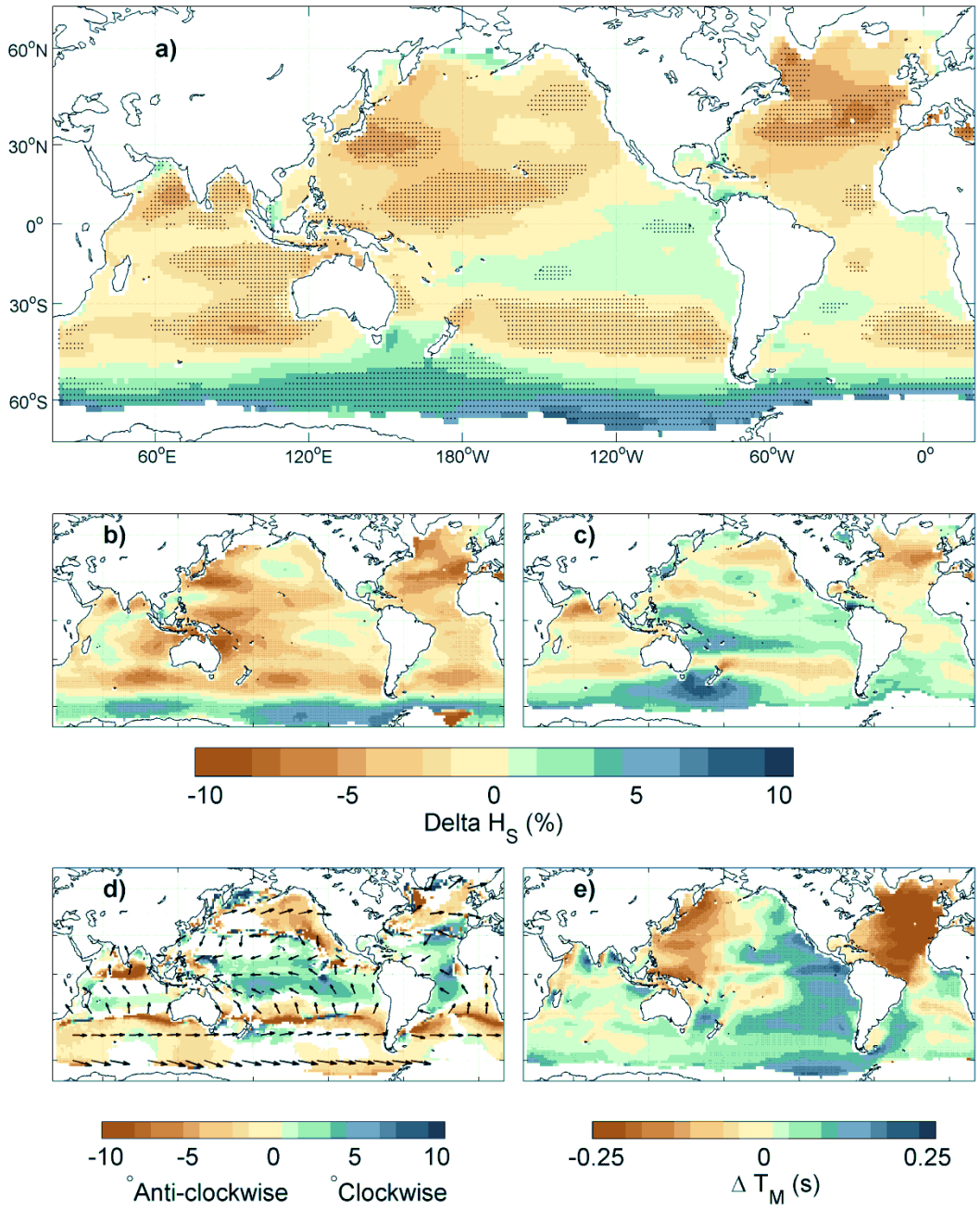

Figure 13.20: Projected changes in wind-wave conditions derived from the Coordinated Ocean Wave Climate Projection (COWCLIP) Project (Hemer et al., submitted). **(a)** Percentage difference between projected future (~2075–2100) and historical (~1980–2009) annual mean significant wave height. **(b)** Percentage difference between projected future (~2075–2100) and historical (~1980–2009) January-March mean significant wave height. **(c)** Percentage difference between projected future (~2075–2100) and historical (~1980–2009) July-September mean significant wave height. Hashed regions indicate projected change is greater than the 5-member ensemble standard deviation. **(d)** As for a), but displaying absolute changes in mean wave direction, with positive values representing projected clockwise rotation relative to displayed vectors, and colours shown only where ensemble members agree on sign of change. **(e)** As for a), but displaying absolute changes in mean wave period.

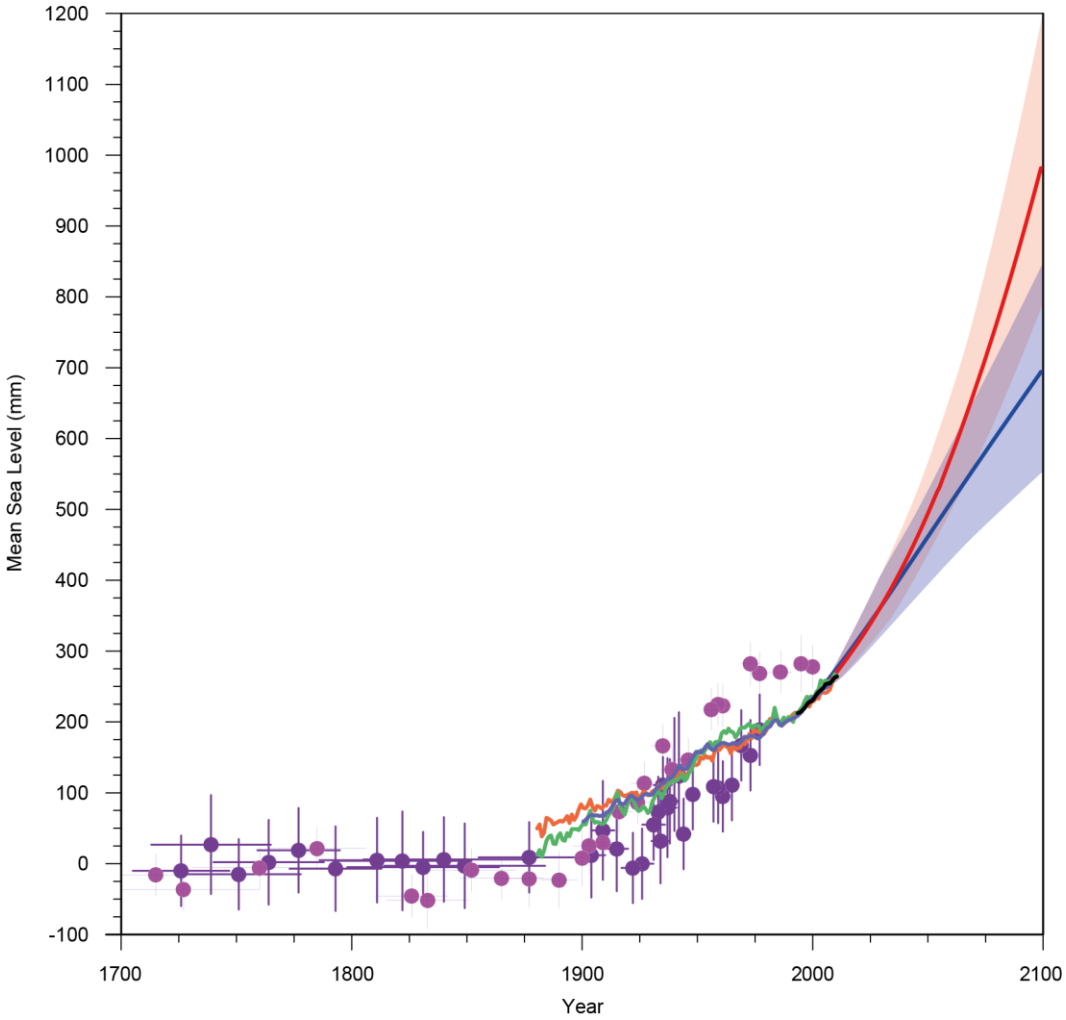

Figure 13.21: Compilation of paleo sea level data, tide gauge data, altimeter data (from Figure 13.3), and central estimates and likely ranges for projections of global-mean sea level rise for RCP2.6 (blue) and RCP8.5 (red) scenarios (Section 13.5.1.1), all relative to pre-industrial values.